CRANFIELD UNIVERSITY

Silsoe College

Ph.D Thesis

SEAWATER GREENHOUSE FOR ARID LANDS

by

Abdelkrim Raoueche, Engineer, M.Sc.

Supervisors Mr B.C. Stenning

Dr B.J. Bailey

September 1997

This thesis is submitted for the degree of Doctor of Philosophy

Abstract

The growth of the world's population and the consequent food shortage, requires the expansion of agriculture into arid zones which constitute about 60 % of the earth's land area and are characterized by high levels of solar radiation and shortage of freshwater. The objective of the seawater greenhouse for arid lands was to develop and demonstrate a cost effective means of producing both crops and pure water in hot, arid coastal regions. The project exploited both the high solar radiation and prevailing wind to drive most of the energy exchange processes in the greenhouse. In addition to a crop grown inside the greenhouse, a shade tent provided shelter for nursery plants and an outdoor planting scheme was maintained with the supply of freshwater as well as protected by the structure of the greenhouse itself.

The greenhouse is cooled with an evaporative cooling pad (Celdek™) through which an air flow is promoted by the prevailing wind. The water vapour transpired by the plants combines with the cooled and humidified ventilation air stream to generate a high relative humidity in the exhaust air. A second evaporation pad (Celdek™) is used to further humidify the exhaust air which passes through a condenser cooled by seawater to produce fresh water. The wind also promotes an air flow through a roof cavity in the greenhouse where more seawater is evaporated and the humid air passes through the condenser.

A computer program was modified to describe the greenhouse, which at first was triangular in plan, and models were written to describe the evaporative cooling systems, the selectively absorbing roof, the humidification of the air in

the roof and the seawater condenser. These models were incorporated into the existing greenhouse model.

Analytical techniques were used to create the hourly values of solar radiation, air temperature, humidity, cloud cover and wind speed required by the simulation model.

This simulation model was used to predict system performance and determine the sensitivity of the greenhouse environment and fresh water output to air and water flowrates and the climatic conditions. The sensitivity analysis showed that adding the second (rear pad) evaporative cooling pad increased the fresh water production compared to using only the front evaporative cooling pad. The use of cooling water at the wet bulb temperature gave a lower condenser output than using surface seawater. The results showed that an effective desalination system would consist of an evaporating cooling pad coupled directly to the seawater condenser.

Data were recorded in the greenhouse in Tenerife in order to determine the heat and mass transfer coefficients of the second Celdek™; these established the program of the system and provided data for validating the model.

The experiments performed on a prototype Celdek™ heat exchanger in the laboratory were used to design the Celdek™ condenser.

The validity of the seawater greenhouse simulation model was checked using experimental data recorded on the prototype seawater greenhouse in Tenerife, in December 1994 and June 1995. The model was revised as a result of the validation exercise.

The model was then used to assess the performance of the different systems of the seawater greenhouse. Using meteorological data for the Tenerife island (Canaries Islands, Spain) and with a cooling water temperature of 10 °C, the simulations showed the complete system could have an annual net water output of 350 kg m^{-2} greenhouse, and the conditions created inside the greenhouse would be suitable for protected crop production. The simulations showed that the major sources of vapour were both evaporative pads (90 %) followed by the roof cavity (9.5 %) and plant transpiration (0.5 %) in December, while in June the two pads contributed 80 %, the plant transpiration 13 % and the roof cavity 7 % of the total water evaporated.

The model was suitable for designing and establishing the performance of the Greenhouse and fresh water condensing system for other locations given appropriate meteorological data.

Acknowledgments

I am particularly grateful and thankful to Dr B.J. Bailey and Mr B.C Stenning for their advice and encouragement during the supervision of this work. Appreciation is expressed to Dr C.S. Parkin for charing my thesis committee and supervision throughout the research period.

I also wish to express my appreciation for the financial assistance of the JNICT, Programa Ciencia, Portugal.

My sincere thanks go to professor Ana Maria Silva of the Univiversity of Evora, Physics Department, Portugal and Eng° Joao M. Marques, Unesul, Portugal, for their interest throughout and wise advice at a crucial phase of the project.

My thanks also go to Charlie Paton of Light Works Ltd for allowing the experiments, on the prototype CELdek™ condenser, to be done in the premises of the company .

Reference is made to the invaluable support of Cristina Alberto, my wife, in the dedication to this thesis. As a Ph.D student and wife, her constant interest and great assistance with many aspects of this work, was of immeasurable value.

Many others people provided assistance during this project, and they too are thanked: Tony Lockwood, David Wilkinson, Simon Reavell and Allan Hilton.

Content of the thesis

ABSTRACT ..... **II**

ACKNOWLEDGMENTS ..... **V**

NOTATION ..... **X**

LIST OF FIGURES ..... **XV**

LIST OF TABLES ..... **XIX**

CHAPTER 1 INTRODUCTION **1**

1.1 DEFINITION OF THE PROBLEM 1
1.2 MODEL 4
1.3 SENSITIVITY ANALYSIS 5
1.4 OBJECTIVES OF THE RESEARCH 5
1.5 OVERVIEW OF THIS THESIS 6

CHAPTER 2 LITERATURE SURVEY **8**

INTRODUCTION **8**

2.1 METHODS OF DESALINATION 8
2.1.1 Processes using a phase change of water *9*
2.1.1.1 Distillation 9
2.1.1.2 Freeze separation 14
2.1.1.3 Hydrate separation 16
2.1.2 Process utilising properties of membranes *17*
2.1.2.1 Electrodialysis 17
2.1.2.2 Reverse osmosis 18
2.1.3 Processes utilising ion selective properties of solids *19*
2.1.3.1 Ion exchange 19

CONCLUSIONS **20**

2.2 GREENHOUSE 22

INTRODUCTION **22**

2.2.1 Selective absorber *24*
2.2.1.1 Water film 26
2.2.2 Air temperature, air humidity and crop temperature *28*
2.2.3 Methods of cooling *29*
2.2.3.1 Shading 31
2.2.3.2 Ventilation 31
2.2.3.3 Evaporative cooling with natural ventilation 32
2.2.3.4 Evaporative cooling with forced ventilation 33
2.2.3.5 Refrigerated air conditioning 35
2.2.3.6 Other methods 35
2.2.3.7 Combined methods 36

CONCLUSIONS **36**

2.2.4 Greenhouse models *37*

CHAPTER 3 GREENHOUSE DESIGN **40**

INTRODUCTION **40**

3.1 GREENHOUSE DESCRIPTION 40
3.1.1 Roof cavity *42*
3.1.1.1 Experimental method 43
3.2 SENSITIVITY ANALYSIS 51
3.2.1 Results and discussion *51*
3.2.1.1 Effect of efficiency of the selective solar radiation absorber 52
3.2.1.2 Effect of cooling water flow rate through condenser 52
3.2.1.3 Effect of the condenser cooling temperature 54
3.2.1.4 Effect of the efficiency of the outlet humidification pad 56
3.2.1.5 Cooling the condenser using deep seawater 56
3.2.1.6 Cooling the condenser using water at air wet bulb temperature 58

CHAPTER 4. MODEL **61**

INTRODUCTION **61**

4.1 GREENHOUSE MODEL 61
4.1.1 Flow of air through the greenhouse *62*
4.1.2 Convective heat transfer *65*
4.1.2.1 Roof heat transfer 68
4.1.2.2 Leaf heat transfer 70
4.1.3 Thermal radiation *71*
4.1.3.1 Sky temperature 72
4.1.4 Conduction *73*
4.1.5 Latent heat *73*
4.1.6 Solar energy *74*
4.2 EVAPORATIVE COOLER 75
4.2.1 Evaporative cooling potential *76*
4.3 CONDENSER 78
4.4 THERMAL AND MASS BALANCE EQUATIONS 81
4.4.1 Thermal balance equations *82*
4.4.2 Moisture Balance Equation *83*
4.4.3 Solution of thermal and mass balance equations *84*

CHAPTER 5 MATERIALS AND METHODS **85**

5.1 GREENHOUSE 85
5.1.1 Location *85*
5.1.2 Physical description *85*
5.1.2.1 Greenhouse 85
5.1.2.2 Roof cavity 85
5.1.2.3 Control flap and control vents 87
5.1.2.4 Spray nozzles in roof cavity 89
5.1.2.5 Evaporative cooling pads 89
5.1.2.6 Heat pump 89
5.1.2.7 Condenser 91
5.1.3 Horticulture *91*
5.2 MEASUREMENT SYSTEM 93

5.2.1 Variables *93*
5.2.2 Sensors *93*
5.2.2.1 Temperature 93
5.2.2.2 Humidity 95
5.2.2.3 Solar radiation 97
5.2.2.4 Net Radiation 97
5.2.2.5 Wind speed 98
5.2.2.6 Wind direction 99
5.2.2.7 External conditions 99
5.2.2.8 Data recording 99
5.3 EXPERIMENTS 102
5.3.1 December *102*
5.3.2 June *104*

CHAPTER 6 EVAPORATIVE COOLER REAR PAD 108

INTRODUCTION 108

6.1 THEORY 108
6.1.1 CELdek™ evaporator *108*
6.1.2 CELdek™ prototype condenser *113*
6.2 EXPERIMENTS 121
6.2.1 Experiments in Tenerife *121*
6.2.1.1 Results and discussions 121
6.2.2 CELdek™ condenser experiments *122*
6.2.2.1 Results and discussions 124

CHAPTER 7 MEASUREMENTS AND VALIDATION OF SIMULATION MODEL 126

INTRODUCTION 126

7.1 MEASUREMENTS 126
7.1.1 Solar radiation *126*
7.1.2 Wind *128*
7.1.3 Evaporative cooling pad *131*
7.1.4 Roof cavity *136*
7.1.5 Greenhouse *139*
7.2 MODEL VALIDATION 143
7.2.1 Roof cavity *145*
7.2.2 Evaporative cooling pad *145*
7.2.3 Greenhouse *150*
7.2.3.1 Inside air and crop temperatures 150
7.2.3.2 Humidity 150
7.2.4 Condenser *152*

CONCLUSIONS 154

CHAPTER 8 SEAWATER GREENHOUSE PERFORMANCE 157

8.1 INTRODUCTION .....
8.2 PERFORMANCE OF EACH SYSTEM OF THE GREENHOUSE 157
8.2.1 Evaporative cooling pad *157*
8.2.2 Greenhouse *159*
8.2.3 Roof cavity *159*
8.3 GREENHOUSE PERFORMANCE IN TENERIFE AND CAPE VERDE 160

8.3.1 Effect of solar radiation *160*
8.3.2 Effect of outside air temperature *164*
8.3.3 Effect of wind speed *164*
8.3.4 Effect of seawater temperature *168*
8.4 ECONOMICS OF SEAWATER GREENHOUSE 168
8.4.1 Desalination plants *171*
8.4.2 Solar distillation *172*
8.4.3 Seawater greenhouse *172*
8.4.3.1 Tenerife prototype 174
8.4.3.2 Oman and Gaza schemes 174
8.4.3.3 Investment analysis 175

CONCLUSIONS **180**

CHAPTER 9 CONCLUSIONS AND FURTHER WORKS **182**

GENERAL DISCUSSION **182**

CONCLUSIONS **185**

RECOMMENDATION FOR FURTHER WORK **186**

APPENDIX A **188**

A1. METEOROLOGICAL DATA 188
A.1.1 Global radiation *188*
A.1.2 Air temperature *190*
A.1.2.1 Mathematical model for air temperature 191
A.1.3 Humidity *194*

APPENDIX B **199**

B.1 GREENHOUSE PARAMETERS 199
B.2 TEMPERATURE DEPENDENT PROPERTIES OF AIR 201

APPENDIX C **203**

APPENDIX D **204**

REFERENCES **206**

In memory of my father

To the beloved ones

Cristina, Luisa and Yosef

Notation

A	*area through which heat flows, (m^2)*
A'	*area of distiller on which yields are based, (m^2)*
a	*coefficient in a differential equation*
a_h, a_m	*air-water interfacial contact surface area per unit CELdek™ volume,(m^{-1})*
a_i	*absorbtivity of node i*
b	*coefficient in a differential equation*
C	*heat capacity at constant pressure, tube-fluid, (W kg^{-1} K^{-1})*
Cw	*cost of water (pounds per m^3)*
C'	*operating labour wage (pounds per man hours)*
c	*heat capacity at constant pressure, spray water, (W kg^{-1} K^{-1})*
cld	*cloud cover (0 <= cld <= 1)*
c_s	*heat capacity of a vapour-gas mixture per unit mass of dry gas content, (W kg^{-1} K^{-1})*
D	*tube diameter, D_i for inside, D_0 for outside, D_m for mean, (m)*
d	*differential coefficient*
e	*vapour pressure (mbar)*
F	*shape , angle or configuration factor*
G_m	*superficial mass velocity of dry air, (kg m^{-2} s^{-1})*
Gr	*Grashof number (dimensionless)*
Gr'	*equivalent Grashof number (dimensionless)*
G'	*air flow loading (mass flow rate/unit cross-sectional area of the evaporator) , (kg m^{-2} s^{-1})*
g	*acceleration of gravity (m s^{-1})*
H	*enthalpy of moist air (reference conditions: air and saturated liquid water at 0° C, (W kg^{-1} dry air)*
Hs	*average monthly global radiation received at the surface of the earth, (kJ m^{-2} day^{-1})*
Ho	*mean values for the monthly extra-terrestrial radiation on a horizontal surface, (kJ m^{-2} day^{-1})*
H^*	*enthalpy of a saturated water-air mixture, in equilibrium with the bulk liquid, (W kg^{-1} dry air)*
h	*heat transfer coefficient (W m^{-2}. K^{-1})*
h_i	*film coefficient for heat transfer between the fluid inside the tubes and the inside surface*

	of the tubes, ($W\ m^{-2}\ K^{-1}$)
h_L	*film coefficient for heat transfer between bulk spray water and the air-water interface in an evaporative cooler, ($W\ m^{-2}\ K^{-1}$)*
h_{LEC}	*film coefficient for heat transfer between the outer tube surface and bulk spray water in an evaporative cooler, ($W\ m^{-2}\ K^{-1}$)*
h_{LF}	*film coefficient for heat transfer between the outer tube surface and bulk spray water in a falling-film cooler, ($W\ m^{-2}\ K^{-1}$)*
I	*average hourly global radiation received on a horizontal surface*
I'	*total capital investment (pounds)*
Ia_m	*annual interest and amortisation rate (percentage of investment)*
I_{SC}	*solar constant (1353 $W\ m^{-2}$)*
K	*overall mass transfer coefficient, (kg water transferred $m^{-2}\ s^{-1}$)*
K_l	*long wave radiation extinction coefficients of the crop, (m^{-1})*
K_s	*short wave radiation extinction coefficients of the crop, (m^{-1})*
k	*thermal conductivity,($W\ m^{-1}.K^{-1}$)*
k_y	*mass transfer coefficient,(kg water transferred $m^{-2}\ s^{-1}$)*
L	*thickness of tube, (m)*
l	*thickness of the layer, (m)*
l'	*characteristic dimension of the system, (m)*
M	*mass rate of fluid flow, ($kg\ s^{-1}$)*
MR_m	*annual maintenance and repair labour and materials (percentage of investment)*
M_i	*integration constant (i=1,2)*
m'	*mass transfer coefficient, ($kg\ m^{-2}\ s^{-1}$)*
m''	*mass rate , ($kg\ s^{-1}$)*
m	*slope of the saturation curve on the enthalpy-temperature diagram for moist air, ($W\ kg^{-1}$ dry air)*
N	*Julian day number*
Nu	*Nusselt number, (dimensionless)*
NTU	*number of transfer units, (dimensionless)*
N_i	*integration constant (i=1,2), ($W\ kg^{-1}$ dry air)*
O'	*annual operating labour (man hours)*
P	*atmospheric pressure,(kPa)*

Pr	*Prandl number, (dimensionless)*
Q	*rate of heat transfer, (W)*
Q_w	*rate of heat transfer based upon spray-water measurements, (W)*
r_i	*roots of characteristic equation (i=1,2)*
Re	*Reynolds number, (dimensionless)*
RH	*relative humidity*
S	*number sunshine hours for the month (h)*
S'	*total cost (fixed and operating) of salt-water supply*
T	*temperature of fluid inside tube, (° C)*
Ta	*temperature of the air, (° C)*
Ti_m	*annual taxes and insurance charges (percentage of investment)*
t	*temperature of spray water, (° C)*
tn	*time of minimum temperature, (s)*
tr	*sunrise time, (s)*
ts	*sunset time, (s)*
tx	*time of maximum temperature, (s)*
t'	*time, (s)*
U	*overall coefficient for heat transfer, ($W\ m^{-2}\ K^{-1}$)*
V_{al}	*air leakage rate, ($m\ s^{-1}$)*
W_T	*rate of flow, tube fluid, ($kg\ s^{-1}$)*
W_s	*rate of flow, dry air, ($kg\ s^{-1}$)*
w	*rate of flow, spray water, ($kg\ s^{-1}$)*
Y	*absolute humidity,(kg water-vapour kg^{-1} dry air)*
Y_D	*annual unit yield of distilled water (liter m^{-2})*
Y_R	*annual unit yield of collected water (liter m^{-2})*
y	*temperature difference (T - t),(° C)*
Z	*length or height of active part of equipment, (m)*
Z'	*day length, (h)*
z	*fraction of surface traverse, measured in the direction of air flow*
Γ	*mass rate of spray water per tube per tube length, ($kg\ m^{-1}\ s^{-1}$)*
$Ó$	*heat exchanger efficiency*
Δ	*prefix indicating difference*
$\tilde{n}$	*density of the fluid ($kg\ m^{-3}$)*

λ_0 *latent heat of evaporation, (kJ kg $^{-1}$)*

ë *latitude, (rad)*

α_a *resistance coefficients for the evaporative cooling pads, (dimensionless)*

α_c *resistance coefficients for the inside greenhouse shape, (dimensionless)*

ö *effectiveness of the evaporative cooling pad, (%)*

γ *psychometric constant, (mbar °C $^{-1}$)*

θ *thermal capacity, (J m $^{-2}$ K $^{-1}$)*

τ *length of the day, (s)*

α *time difference between the occurrence of tx and midday, (s)*

β_0 *time difference between tn and sunrise, (s)*

γ_0 *decay parameter*

ω *angle relative to solar noon, (rad)*

ω_s *sunset hour angle, (rad)*

ν *velocity of the fluid, (kg m $^{-1}$ s $^{-1}$)*

η *dynamic viscosity of the fluid, (m ^{2} s $^{-1}$)*

β *coefficient of cubical expansion, , (K $^{-1}$)*

β' *ratio of greenhouse or roof air speed over wind speed*

ó *Stefan's constant, W m $^{-2}$ K $^{-4}$)*

ä *solar declination, (rad)*

ε *emissivity of a clear sky, (dimensionless)*

ε_s *emissivity of a cloudy sky, (dimensionless)*

ñ *density of the fluid, (kg m $^{-3}$)*

Subscripts

1, 2 *air inlet, air outlet (successive estimates when used with U and K)*

aep1 *air entering pad1*

aep2 *air entering pad2*

alp1 *air leaving pad1*

alp2 *air leaving pad2*

alr *air leaving roof cavity*

avg *average*

c	*crop*
c'	*convective*
cl	*cold fluid*
f	*ground*
g	*dry air (gas)*
h	*hot fluid*
i	*interface*
ia	*inside*
k	*conduction*
l	*liquid water*
l'	*latent*
m	*mean*
min	*minimum*
max	*maximum*
p	*pad*
oa	*outside air*
ri	*inner roof*
ro	*outer roof*
r	*radiative*
s	*sensible*
su	*surface*
s'	*saturation*
sky	*sky*
sol	*solar*
w	*water vapour*
w'	*wet bulb temperature of the outside air*
wec	*water entering condenser*
wlc	*water leaving condenser*
wep2	*water entering pad2*
wlp2	*water leaving pad2*
wind	*wind speed*

List of figures

Figures **Page**

Fig. 1. 1 General layout of the seawater greenhouse (Paton et al., 1996) 3

Fig. 2. 1 Multi-stage flash and reverse osmosis desalinalination plants in Cape Verde (Light WorkLtd,1993) 15

Fig. 2. 2 Schematic sketch of ''still on roof'' system, (after Sodha et al., 1980b) 12

Fig. 2. 3 Schematic diagram of Thinau's greenhouse, (Malik, 1970) 12

Fig. 2. 4 Photosynthetically active solar radiation (after Luft and Froechtenight, 1981) 13

Fig. 2. 5 Greenhouse design for hot climates with PAR glazing filter and solar still (afterLuft and Froechtenight, 1981) 14

Fig. 2. 6 Greenhouse design for hot climates with double glazing and PAR liquidfilter and solar still

Fig. 2. 7 Cost of water/1000 gallons for solar still plant and for humidification-dehumidification plant (after Garg. et al., 1966) 21

Fig. 2. 8 Cooling pad at winward side of greenhouse (afterBreuer et al., 1996) 30

Fig. 2. 9 Fans at leeward side of greenhouse (afterBreuer et al., 1996) 30

Fig. 2.10 Pattens of air flow during operation of fan and pad cooling systems (Mastalerz, 1977) 34

Fig. 3. 1 Air circulation of the Seawater greenhouse (Light works ltd,1994) 41

Fig. 3. 2 Light transmission of a thick plastic film 45

Fig. 3. 3 Light transmission of a flat GRP sheet with shallow channels

Fig. 3. 4 Light transmission of a corrugated GRP sheet

Fig. 3. 5 Solar radiation in overcast sky 49

Fig. 3. 6 Transmitivity to PAR variations in overcast sky 49

Fig. 3. 7 Solar radiation in clear sky 50

Fig. 3. 8 Transmitivity to PAR in clear sky 50

Fig. 3. 9 Effect of the selective solar absorberefficiency 53

Fig. 3. 10 Effect of the condenser mass flow rate 53

Fig. 3. 11 Effect of seawater temperature 55

Fig. 3. 12 Effect of the evaporative cooling pad efficiency 55

Fig. 3. 13 Effect of the air ventilation on the freshwater production for the months of December and June when using deep seawater to cool the condenser (1 pad) 57
Fig. 3. 14 Effect of the air ventilation on the freshwater production for the months of December and June when using deep seawater to cool the condenser (2 pads) 57
Fig. 3. 15 Effect of the air ventilation on the freshwater production for the months of December and June when using water at the air wet bulb temperature to cool the condenser 59
Fig. 3. 16 Effect of the air ventilation on the freshwater productionfor the months of December and June when using water at the air wet bulb temperature to cool the condenser 59

Fig. 4. 1 Energy fluxes included in the model 63
Fig. 4. 2 Convective heat transfer at the outside of a multispan glasshouse roof (Bot, 1983) 69
Fig. 4. 3 Reduction in air temperature obtainable with evaporative cooling
Fig. 4. 4 Air temperature with evaporative cooling

Fig. 5. 1 Greenhouse location (light works ltd, 1995) 86
Fig. 5. 2 Control flap and control vents (light works ltd, 1995) 88
Fig. 5. 3 Seawater circuit
Fig. 5. 4 Planting area 92
Fig. 5. 5 Crop and soil temperature thermistors 96
Fig. 5. 6 Weather stations in december 1994 and june 1995
Fig. 5. 7 Sensors position in December 1994 103
Fig. 5. 8 Sensors position in June1995 107

Fig. 6. 1 Evaporator CELdec™ 110
Fig. 6. 2 Evaporation mathematical model 111
Fig. 6. 3 Experimental celdek™ condenser 115
Fig. 6. 4 Temperature and enthalpy gradient (Parker and Treybal, 1960) 116
Fig. 6. 5 Effect of air mass velocity on the heat transfer coefficient 122
Fig. 6. 6 Effect of air mass velocity on the mass transfer coefficient 122

Fig. 7. 1 Radiation variations in December 128
Fig. 7. 2 Radiation variations in June 128
Fig. 7. 3 Light transmission variations 130

Fig. 7. 4 Wind direction variations 130
Fig. 7. 5 Fluctuations of the wind speed and air speed after pad1 and pad2 131
Fig. 7. 6 Fluctuations of the wind speed and air speed in the roof cavity and greenhouse 131
Fig. 7. 7 Variations of the rating of the air speed in the greenhouse, or the roof cavity to the wind speed 133
Fig. 7. 8 Fluctuations of evaporative cooling pad efficiency in December 133
Fig. 7. 9 Fluctuations of evaporative cooling pad efficiency in June 134
Fig. 7. 10 Variations of the air temperature entering and leaving pad1 134
Fig. 7. 11 Variations of the air temperature entering and leaving pad2 135
Fig. 7. 12 Variations of the air temperature entering and leaving pad1
Fig. 7. 13 Variations of the air temperature entering and leaving pad2 136
Fig. 7. 14 Variations of the relative humidity of the air outside the greenhouse, the air entering and leaving roof and pad2 136
Fig. 7. 15 Variations of the water entering and leaving pad2 138
Fig. 7. 16 Variations of air speed with distance from ground (height)
Fig. 7. 17 Variations of the water temperature entering and leaving the roof cavity 139
Fig. 7. 18 Variations of the air temperature entering and leaving the roof cavity, December 141
Fig. 7. 19 Variations of the air temperature entering and leaving the roof cavity, June 141
Fig. 7. 20 Measured crop temperature at different distance from inlet pad 141
Fig. 7. 21 Measured inside air temperature at different heights 143
Fig. 7. 22 Comparison of the measurements of the inside air temperature with a thermistor and a psychrometer 143
Fig. 7. 23 Predicted and measured air temperature leaving the roof cavity 145
Fig. 7. 24 Predicted and measured air temperature leaving the roof cavity 147
Fig. 7. 25 Predicted and measured inside cover temperature 147
Fig. 7. 26 Predicted and measured outside cover temperature 148
Fig. 7. 27 Predicted and measured air temperature leaving pad1 148
Fig. 7. 28 Predicted and measured air temperature leaving pad1 149
Fig. 7. 29 Predicted and measured air temperature leaving pad2 149
Fig. 7. 30 Predicted and measured air temperature leaving pad2 150
Fig. 7. 31 Predicted and measured crop temperature 150
Fig. 7. 32 Predicted and measured inside air temperature 152
Fig. 7. 33 Predicted and measured inside air relative humidity 152
Fig. 7. 34 Predicted and measured relative humidity of the air leaving pad2 154

Fig. 7. 32 Predicted and measured inside air temperature 152
Fig. 7. 33 Predicted and measured inside air relative humidity 152
Fig. 7. 34 Predicted and measured relative humidity of the air leaving pad2 154
Fig. 7. 35 Predicted and measured relative humidity of the air leaving the condenser 154
Fig. 7. 36 Variations of the freshwater production 156

Fig. 8. 1 Contribution of system components to vapour production and water output of the condenser for the month of December 158
Fig. 8. 2 Contribution of system components to vapour production and water output of the condenser for the month of June 158
Fig. 8. 3 Influence of solar radiation on water evaporated, condensed and crop transpiration in December 162
Fig. 8. 4 Influence of solar radiation on water evaporated, condensed and crop transpiration in June 162
Fig. 8. 5 Influence of solar radiation on water evaporated, condensed and crop transpiration in December 163
Fig. 8. 6 Influence of solar radiation on water evaporated, condensed and crop transpiration in June 163
Fig. 8. 7 Effect of the outside air temperature on the condenser output in December,Tenerife 165
Fig. 8. 8 Effect of the outside air temperature on evaporation, transpiration and condensation rates in June, Tenerife 165
Fig. 8. 9 Effect of the outside air temperature on the condenser output in December,CapeVerde 166
Fig. 8. 10 Effect of the outside air temperature on evaporation, transpiration and condensation rates in June, Tenerife 166
Fig. 8. 11 Effect of the wind speed on water evaporation, water condensation and transpiration in Tenerife 167
Fig. 8. 12 Effect of the wind speed on water evaporation, water condensation and transpiration in Cape Verde 167
Fig. 8. 13 Annual freshwater production using seawater temperature at different depths, Tenerife 169
Fig. 8. 14 Monthly water production using seawater temperature at different depths, Tenerife 169
Fig. 8. 15 Annual freshwater production using seawater temperature at different depths 170
Fig. 8. 16 Monthly water production using seawater temperature at different depths 170
Fig. 8. 17 Water cost comparison for different techniques of desalination (after Gomkale, 1968) 173
Fig. 8. 18 Sensitivity study of the seawater greenhouse reference scheme (ODA, 1996) 178

Chapter 1 Introduction

1.1 Definition of the problem

Water is a basic necessity of man along with food and air; the importance of supplying fresh water can be hardly over stressed. Man has been dependent on rivers, lakes and underground water reservoirs for fresh water requirements in domestic life, industry and agriculture.

However, use of untreated water from such sources is not always possible or desirable on account of the presence of large amount of salts and harmful organisms. Further, the rapid industrial growth and population explosion all over the world has resulted in a large escalation of demand for fresh water. Besides this there are several regions on the earth, e.g. the deserts and remote arid regions, which have inhospitable climatic conditions and have only brackish water sources. In such places fresh water will have to be provided not only for domestic use, but also for agricultural needs.

Numerous processes have been proposed for the desalination of water, and a few of these have attained important commercial status. Distillation, electrodialysis, and reverse osmosis are already applied to a variety of practical installations. Solvent extraction, ion exchange, freeze separation, and hydrate separation have been less developed, and are limited to special cases. Of the methods that are of current importance, electrodialysis and reverse osmosis are best adapted to the desalination of brackish waters while distillation is applicable to the entire range of salinity. Most of the conventional water distillation processes are energy-intensive and often require scarce electric power for operation.

The main efforts in solar desalination have been directed to basin solar stills. Even for the best of these stills, the required intercepted solar energy per kg of

distillate is equal to several times the latent heat of evaporation. On the other hand, the energy required for other desalination systems represents only a fraction of the latent heat. This fact limits the utilisation of solar basins to very small capacities.

With the development of greenhouses and water conservation techniques in agriculture, it is possible to have small-scale agricultural activity in places where only saline or brackish water is available. Solar distillation may in most cases be able to provide the rather modest demand for fresh water, consistent with clever choice of crops, suitable thermal environment provided by the greenhouse and efficient water conservation technology [Malik *et al.*, 1982].

Although solar distillation have been studied in detail, little attention has been paid to the use of solar stills for controlling the environment combined with distilled water production; the work has been restricted to greenhouses.

Greenhouses are used because in general they provide a more favourable environment for the growth of the plants than when plants are grown in the open. The solar irradiance inside a greenhouse is typically 60-70 % of that outside but only 2-3 % of the solar radiation absorbed by plants is used in photosynthesis. The remainder is reflected or transferred to surrounding surfaces by thermal radiation, to the greenhouse air by convection or is used as latent heat to evaporate water in transpiration from leaves. However, the water vapour produced raises the moisture content of the greenhouse atmosphere above the value in the external air. Regions with mild winter climates often experience high summer temperatures. During high radiation periods, high greenhouse air temperature is a major problem in arid lands, this limits the effective production of crops in greenhouses cooled by natural or forced ventilation. If the high external air temperatures are

associated with low absolute humidity, evaporative cooling can provide an effective way of reducing the thermal and water stresses on greenhouse plants.

In the light of the above considerations, a study of a seawater greenhouse was proposed. This offered the means of avoiding the problem of high temperatures during periods of strong insolation and also of providing a supply of fresh water. It consists of a greenhouse with an evaporative cooling pad through which an air flow is promoted by the prevailing wind. The water vapour transpired by the plants combines with the cooled and humidified ventilation air stream to generate a high relative humidity in the exhaust air. A second evaporative cooling pad is used to further humidify the exhaust air and to increase the water production. The roof consists of two layers, the inner forms a selective solar radiation absorber. The solar radiation absorbed evaporates seawater flowing through the cavity; the wind promotes an air flow through the roof cavity and the air emerges saturated with water vapour. The humid greenhouse and roof air streams pass through a heat exchanger cooled by cold seawater in which pure water is condensed (Fig. 1.1).

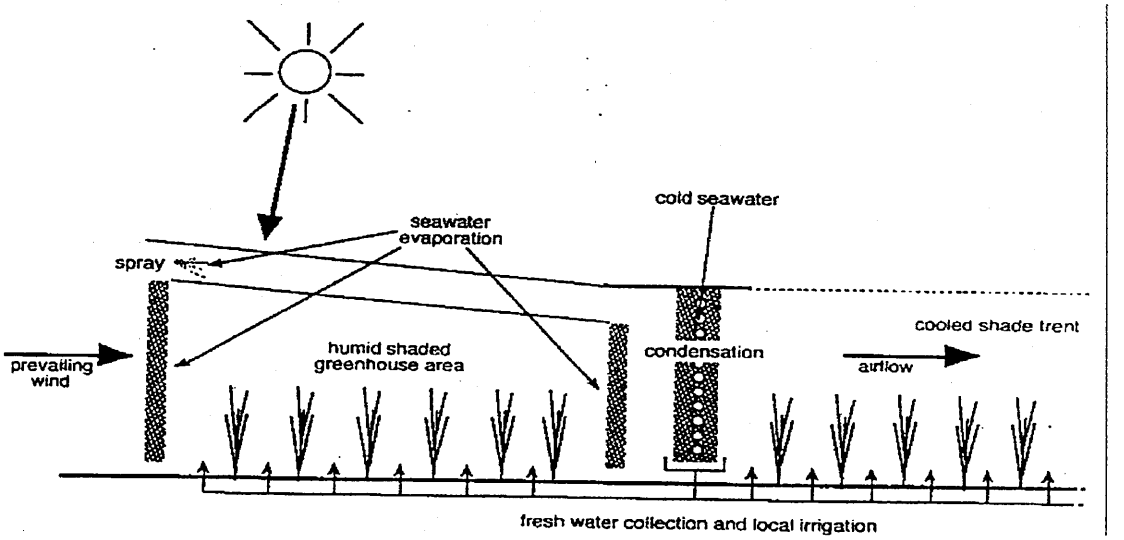

Fig. 1. 1 General layout of the seawater greenhouse (Paton *et al.*, 1996)

1.2 Model

The thermodynamic model of the greenhouse was based on one developed by Chalabi and Bailey [1991]. It consists of energy and mass balances described by a set of coupled non-linear first order differential equations driven by external processes specified at the boundary nodes: outside air temperature, sky temperature, deep ground temperature, outside moisture content, wind speed and solar radiation. It is parameterised by a set of constants relating to the thermal, optical and geometrical properties of the seawater greenhouse.

The model was modified to describe the greenhouse, which at first was triangular in plan, and thermodynamic submodels were developed to describe the thermal and mass balances of the direct contact condenser, the roof cavity, and the front and rear evaporation pad. Condenser efficiency was first taken as 70%, this was a simplification and then was modeled more precisely using the condenser effectiveness for a cross flow heat exchanger with mixed flow on the air side.

A mathematical model was developed to estimate relationships between the overall volumetric heat transfer coefficient and the overall mass transfer coefficient based on the mass velocity of the air with a fixed mass velocity of water.

From experiments performed on a prototype condenser, film coefficients for heat and mass transfer were deduced for the following: (i) tube surface to water for sensible heat transfer to the water only, (ii) condensation of water from the air.

1.3 Sensitivity analysis

The simulation model was developed to describe the thermal and mass balance of the air, crop, floor, inside roof, outside roof, the inlet evaporative cooling pad, the outlet humidification pad and the direct contact heat exchanger. A sensitivity analysis was used to identify those parameters which had an important influence on the system performance. The model was then used to determine the expected rate of fresh water produced during June and December.

1.4 Objectives of the research

The objectives of the research were

1. To determine design parameters of the seawater greenhouse using the existing simulation model developed at Silsoe Research Institute. The sensitivity of the rate of fresh water production to the following parameters was determined:
    i) Efficiency of the outlet humidification pad
    ii) Cooling water flow rate
    iii) Seawater temperature
    iv) Efficiency of selective solar absorber in roof
    v) Air flow rate through the greenhouse and roof cavity, and through the roof alone

2. To modify the model to describe the seawater greenhouse and to incorporate submodels to describe the evaporative cooling of the air in the greenhouse, the humidification of air in the roof cavity, and the performance of the seawater condenser.

Mathematical models to describe the film coefficients for heat and mass transfer of a prototype condenser, and to describe the heat and mass transfer coefficients of the rear evaporation pad were developed and used in the model.

3. To validate the performance of the seawater greenhouse model under the conditions of Tenerife.

4. To optimise the design of the seawater greenhouse.

5. To predict the overall performance of the seawater greenhouse in Tenerife and at another location (Cape Verde).

1.5 Overview of this thesis

The following chapter presents the background for this research; it examines the different methods of desalination and which process is more economic. Different methods of ventilation for controlling greenhouse temperatures in summer were also examined. Chapter 3 presents the investigation of optical transmission of different materials used to design the roof cavity of the greenhouse. A sensitivity analysis on the influence of different variables (efficiency of the selective solar radiation absorber, cooling water flow rate, condenser cooling water temperature, efficiency of the outlet humidification pad, and cooling the condenser using deep seawater and water at the wet bulb temperature) on the water production by the condenser was determined; this shows the implications of this analysis for the design of the greenhouse.
Chapter 4 presents the physical description of the greenhouse, the theory of the model used as well as of the submodels developed in this study. Chapter 5

describes the measurement system and the set up of the experiments carried out in Tenerife (Spain). Chapter 6 presents the mathematical model developed to estimate relationships between the volumetric overall heat and mass transfer coefficients of the CELdek™ evaporator; it also presents a study on a prototype CELdek™ heat exchanger which concludes with the design of the condenser. The next two chapters describe the measurements and validation of the simulation model (Chapter 7), and the performance of each system of the greenhouse and the performance of the greenhouse in Tenerife and Cape Verde (Chapter 8). The latter concludes with an economic comparison between desalination plants and the seawater greenhouse.

Chapter 9 presents the conclusions of the thesis, describes how the research's contributions met its objectives and possible future work.

Chapter 2 Literature survey

Introduction

Desalination has become increasingly important because of the tendency in recent years for the world 's swelling population to dwell in areas where local supplies of high quality fresh water are less than adequate. Since, in many of these areas, there are saline sources of considerable extent close at hand, the use of desalination is becoming an attractive possibility. The basic need for the desalination of water arises because of the essential role of water in all organic life. It is the solvent portion of the fluid in plants and animals which carries nutrients from cell to cell.

The separation of pure liquid water from a mineral solution will not occur spontaneously. In those areas of the earth where demineralised water is needed for drinking and irrigation, it is necessary to create a controlled regime of space- usually containing an interface- at which the separation may be forced to occur. To force the separation, resources outside the controlled region must be used [Howe, 1974]. Solar energy may be used to generate heat or power which can be used for operating a desalination process.

2.1 Methods of desalination

Numerous processes have been proposed for the desalination of water and a few of these have attained an important commercial status. Distillation, electrodialysis and reverse osmosis [Spiegler *et al.*, 1980] are already applied to a variety of

practical installations. Solvent extraction, ion exchange, freeze separation, and hydrate separation have been less developed, and are limited to special cases [Howe, 1974]. Of the methods that are of current importance, electrodialysis and reverse osmosis are best adapted to the desalination of brackish waters while distillation is applicable to the entire range of salinity. The several processes for desalination have been grouped according to the phenomena involved, those involving phase change of water, those utilising surface properties of membranes and those utilising ion-selective properties of solids and liquids.

2.1.1 Processes using a phase change of water

2.1.1.1 Distillation

Distillation is the oldest of all desalting technologies. Distillation is the process in which a portion of a solution is first made to evaporate and the vapour is subsequently condensed. It is an effective process of desalination because most of the chemical materials found in saline waters are non-volatile at the temperatures normally employed, and hence remain in the unevaporated brine.

A critical review of new developments in desalination by distillation processes, with the multistage flash evaporation process as the reference (Fig. 2.1), was presented by Veenman [1978]. Other work and reviews [Aussenac *et al.*, 1978] include production of fresh water from seawater by multiple effect distillation, flash evaporation and vapour compression.

Solar distillation is particularly applicable to isolated desert and island areas where saline water may present problems and small production rates are required [Malik *et al.*, 1982]. The classical basin type solar still is simple and suitable for

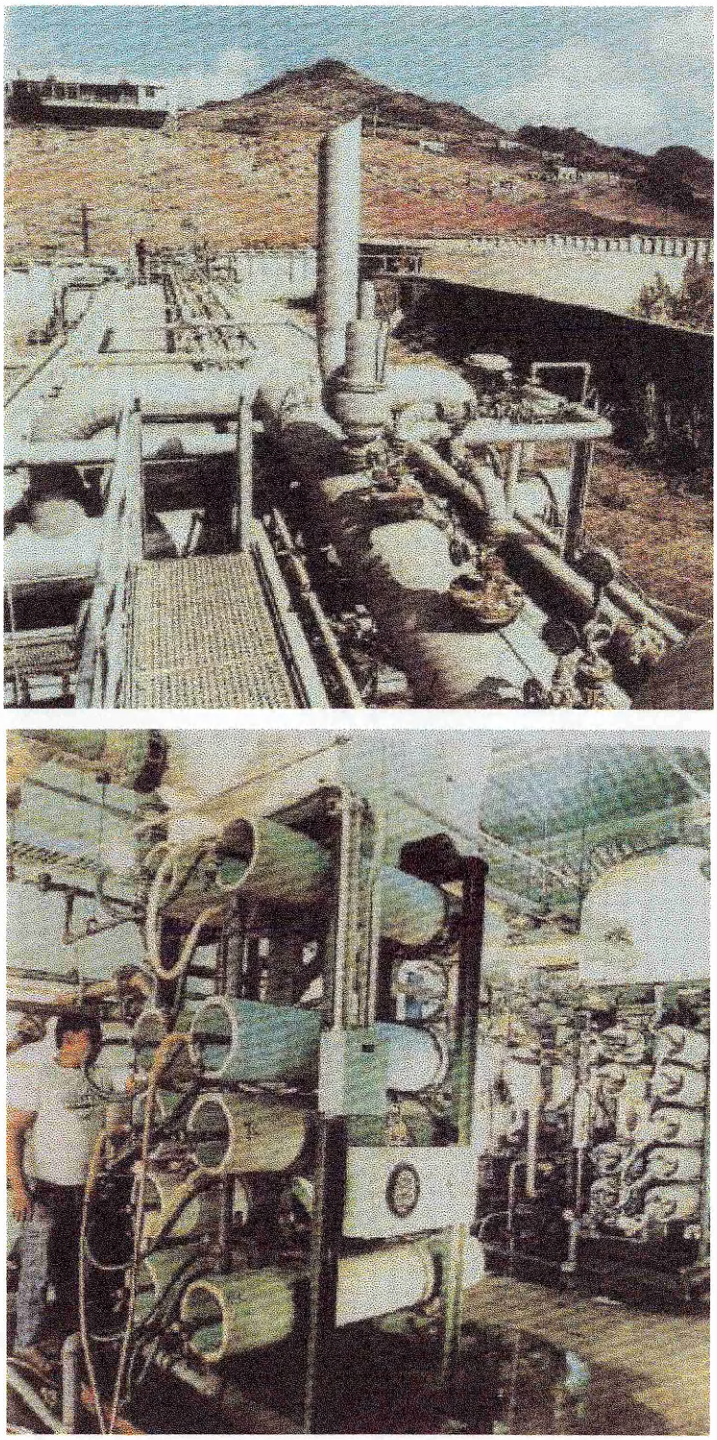

Fig. 2. 1 Multi-stage flash and reverse osmosis desalination plants in Cape Verde (Light Works Ltd, 1994)

small capacities. Tabor [1978] concluded that for larger yields, conventional desalination processes, using solar energy, are more appropriate and give a cost of water lower by an order of magnitude. The overall efficiency of a typical basin type solar desalination plant is 30 % or lower. Moustafa *et al.* [1979] showed that the major design factors affecting energy utilisation are basin, condensing surface and ambient air temperatures. The efficiency of a solar desalination plant can be improved by controlling radiation from the plant basin and by the reuse of the latent heat of condensation.

Selcuk [1970, 1971] has analysed the thermal performance of a greenhouse whose roof is covered with a solar still. Sodha *et al.* [1980b] proposed that a still can be placed on the roof of a building (Fig. 2.2) for producing distilled water and, at the same time assisting in air conditioning of the building.

A solar still with a cover made from polyethylene and an area of 50 m^2 gave an output of 3.3 to 3.6 l m^{-2} day^{-1} [Norov *et al.*, 1978]. Akhtamov *et al.* [1978] presented and correlated the annual operating data with meteorological factors for stepped-oblique solar stills. Output varied from 0.6 l m^{-2} day^{-1} in January to 4.75 l m^{-2} day^{-1} in June. The efficiency varies from 18.0 % in January to 46.1 % in June.

Tinaut *et al.* [1978] constructed a solar-still greenhouse, shown in Fig. 2.3, to study the application of spectrum cut-off by a semi-transparent plastic still basin. In theory, the semi-transparent still basin should ideally absorb only the thermal radiation and transmit the Photosynthetically Active Radiation (PAR), see Fig. 2.4. Such a still basin would also serve as a thermal blanket during the night for the greenhouse, absorbing the thermal radiation emitted by the greenhouse and storing the heat in the water, reducing nocturnal cooling. They tested red and blue methacrylates and blue polyethylene and found that the relative photosynthetic activity under the red methacrylate was about twice that of the blue methacrylate

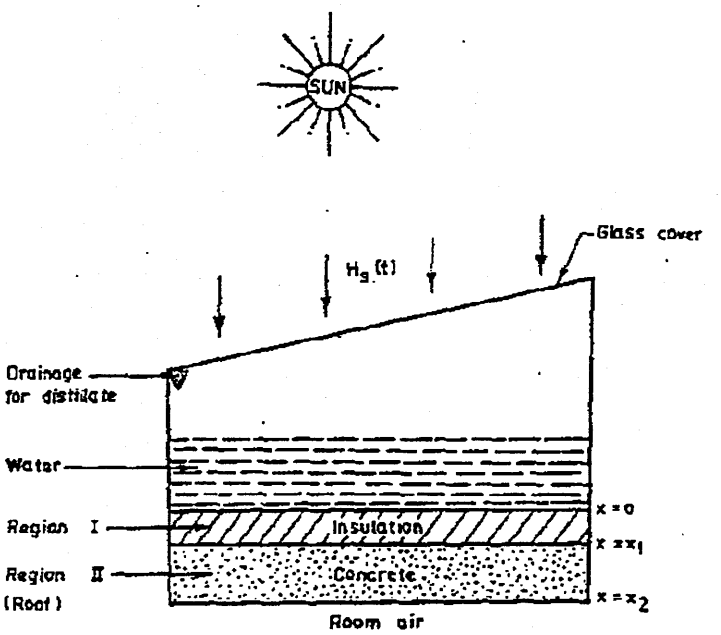

Fig. 2. 2 Schematic sketch of ˝ still on roof ˝ system, (After Sodha *et al.*, 1980b)

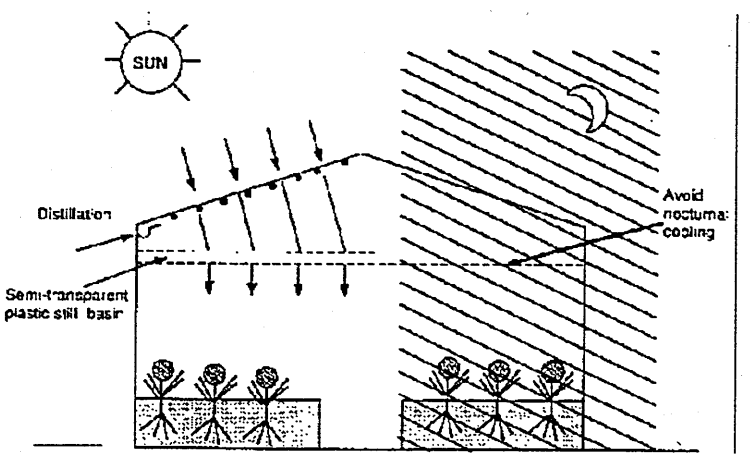

Fig. 2. 3 Schematic diagram of Tinaut ´s greenhouse, (Tinaut *et al.*, 1978)

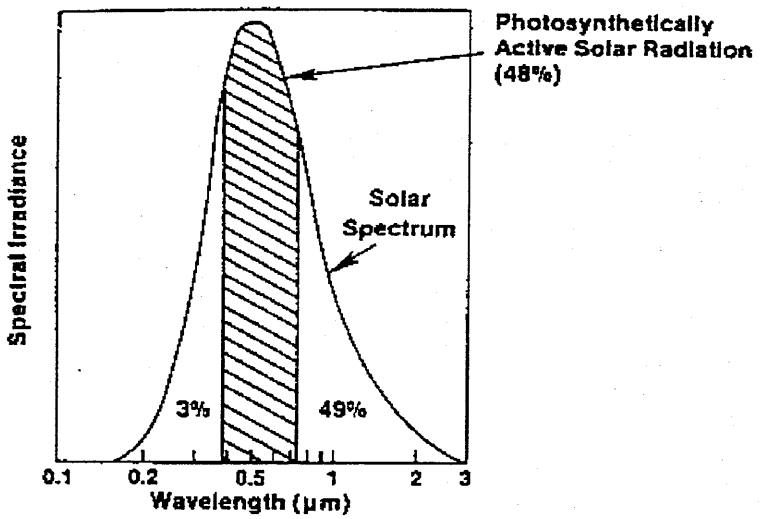

Fig. 2. 4 Photosynthetically active solar radiation (After Luft and Froechtenight, 1981)

and polyethylene. In such a design it is also possible to control the amount or spectrum of the solar radiation entering the greenhouse by adjusting the water depth in the basin or by the addition of dyes to the water. Luft and Froechtenigt [1981] have described two designs that take advantage of the fact that only 48% of the solar spectrum is PAR, namely the spectrum from 0.39 to 0.72 μm in wavelength. The first design, shown in Fig. 2.5, used an absorbing filter (the inner glazing) to absorb the thermal radiation and provide the energy to distil the saline water flowing between the double glazing. This type of design has the added advantage of reducing the heat load within the greenhouse, which is critical in hot climates where it is necessary to ventilate the greenhouse during the summer. The second design, see Fig. 2.6, utilised a PAR liquid filter, which flowed between the double glazing. In this case the solar still was external to the greenhouse. The thermal energy absorbed by the liquid filter was transferred to the saline solution by means of a heat exchanger, which may be placed in the basin of a single-basin-type solar still or used to preheat the feedstock.

2.1.1.2 Freeze separation

Freezing is a separation process related to the solid-liquid change phenomenon. When the temperature of salt water, of limited salinity, is reduced to its freezing point, which is function of salinity, ice crystals of pure water are formed within the salt solution. These ice crystals can be mechanically separated from the concentrated salt solution and remelted to obtain pure water.

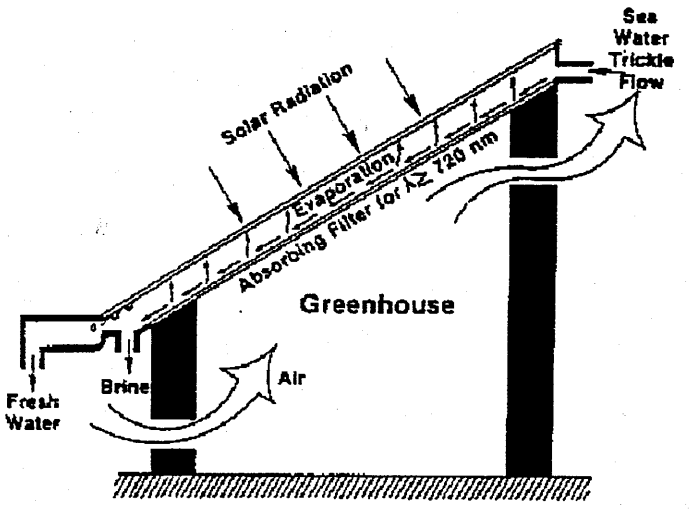

Fig. 2. 5 Greenhouse design for hot climates with PAR glazing filter and solar still (After Luft and Froechtenight, 1981)

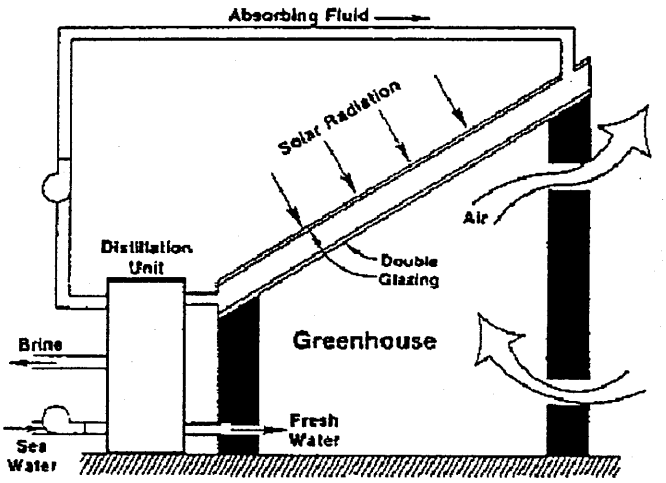

Fig. 2. 6 Greenhouse design for hot climates with double glazing and PAR liquid filter and solar still (After Luft and Froechtenight, 1981)

Hendrickson and Moulton [1956] found that freeze separation was attractive because the low temperatures involved greatly reduced the problems of scale formation and corrosion, which are troublesome in all forms of distillation. Stubstad *et al.* [1978] studied the performance characteristics of a scale model annular flow ice-water heat sink. Comparisons were made between experimental results and computer predictions of outlet water temperature and melting time. The computer program gave a reasonable simulation of actual behaviour and could be used as the basis for design calculations.

Data on the ice formation rate were presented by Bustany *et al.* [1979] for a salt water drop suspended by drag forces in a flowing cold organic liquid. The effects of refrigerant under cooling, salt concentration, drop size and time were studied. Ice formation rates in drops of 3 % NaCl solution by weigh twere two to three time lower than in pure water drops.

An experimental determination was made of the velocity profiles which resulted from the free convective melting of a vertical ice sheet into fresh water at temperatures in the range from 2.0 °C to 7.0 °C. The results suggested that upward flows exist for water temperatures below 4.7 °C. Entirely downward flowing boundary layers were suggested for temperatures above 7.0 °C. For intermediate temperatures, an oscillatory dual flow regime was indicated [Wilson et *al.*, 1979].

2.1.1.3 Hydrate separation

The process of desalting seawater by hydrate formation can be looked upon as a freezing process in which water solidifies and precipitates at higher temperatures and pressures than does pure ice.

Hydrate separation was thought possibly to be superior to freeze separation because crystalline hydrates are formed at temperatures closer to ambient than those at which ice is formed [Garrison *et al.*, 1968] and [Williams *et al.*, 1968].
The desalination of seawater, based on the formation of a solid crystalline H_2S hydrate, requires a considerable expenditure of energy, which can theoretically be obtained from a reverse cycle operating on the difference in temperature of the surface and lower water layers [Kleshchunov *et al.*, 1976].
Water contents for methane, ethane, and propane hydrates were calculated and were found to be temperature dependent. The maximum value was attained at the quadruple point where liquid water, ice, gas and hydrate coexist [Byk, 1978].

2.1.2 Processes utilising properties of membranes

It is important before describing the individual membrane processes, to define the terms osmosis and dialysis. Both terms refer to situations where a membrane serves as barrier separating two aqueous solutions of different concentrations. Osmosis is the transmission of water through a membrane from the less concentrated solution to the more concentrated one. Dialysis is the diffusion through the membrane of dissolved salt, the diffusion transferring ions from the more concentrated solution to the less concentrated one.
The two processes that utilise membranes for desalination, electrodialysis and reverse osmosis, have become more practical in recent years due to the continuing development of plastic membranes.

2.1.2.1 Electrodialysis

Zubets *et al.* [1976] found that the energy consumption required for decreasing the salinity of 1 m^3 of seawater from 26 to 1 g l^{-1} was 29.5 kWh. The capacity of the device working 8 hours a day for 3 months without a substantial change of parameters was 30 l h^{-1}.

Kinetic equations describing desalination processes in a potentiostatic electrodialysis device were derived by Zubets *et al.* [1976]. They calculated current-time and concentration-time curves which were in good agreement with corresponding experimental data.

Korolev *et al.* [1976] determined the optimum operating parameters, e.g., current, pH, salinity, and dialysis time for an apparatus producing 1 m^3 day^{-1} of drinking water by electrodialysis desalination of seawater.

The performance of an electrodialysis unit depends greatly upon the structure of spacers which are inserted between ion-exchange membranes. Of the various net-type spacers as turbulence promoters studied, a honeycomb-type spacer and laminated thin nets exhibited higher limiting current densities, less current shadowing and less fouling than a single net, although some rise in pressure drop was observed [Ichiki *et al.*, 1978].

The capital cost of an electrodialysis plant is proportional to the number of stacks involved, so that the multiplicity of stacks needed in series for the desalting of highly saline water increases the cost quite rapidly. The electrodialysis method can be cheaper than distillation when the source water has a total salinity of about 4000 or 5000 ppm, but is more costly than distillation when used with seawater [Howe, 1974].

2.1.2.2 Reverse osmosis

Important progress has been made in synthetic semi-permeable membranes, leading to a wider scope of reverse osmosis applications, including the purification of used water and saline water for drinking, the supply of ultra-pure water for the pharmaceutical and electronic industries and for feeding boilers [Crowe *et al.*, 1977].

Stability of the membrane to high and low pH and to oxidation by Cl was examined for various types of membrane material by Spatz *et al.* [1978]. They concluded that membrane flux rates decreased as NaCl rejection increased and pore size decreased.

Leung [1979] simulated the time variation of filtration-system variables, e.g. concentration, volume and permeation rate. Rigorous mathematical solutions, were formulated for a physical model.

2.1.3 Processes utilising ion selective properties of solids

2.1.3.1 Ion exchange

Development of modern techniques made it possible to use ion exchangers not only for the preparation of demineralised water, but also for the recuperation of materials from waste water and solutions.

Skvortsov *et al.* [1978] defined a method for calculating the performance of settling filters based on the theory of dynamic sorption of ions on granular particles; this required a knowledge of the ion exchange velocity constant, resin

exchange capacity, grain size and the kinetic characteristics of the filter. They found that the theoretical and experimental results for a horizontal settling filter containing H-ion type cation resin were in good agreement.

Thermally regenerable ion exchange resins were used to partially demineralise water containing up to 3000 ppm of dissolved salts. They were used for treatment of brackish underground and surface waters, and for effluent treatment [Bolto *et al.*, 1978].

Conclusions

The first significant economic analysis of solar distillation systems was made by Lof [1962]. In this study the cost of production of distilled water from seawater by solar distillation was compared with that by vapour compression and multiple-stage flash distillation techniques. It was shown that for plant capacities of less than 227 $m^3 d^{-1}$, solar distillation was the cheapest among the three techniques. Similar conclusions have been arrived at by Bloemer *et al.* [1965a] in their cost analysis based on solar energy-supply rate of 23 000 kJ m^{-2} day and $ 0.50 per man hour, typical of developing countries. Gomkale [1968] made comparison for different techniques of desalination in Rajasthan (India). Figure 2.7 shows the relative performance of a solar still and a humidification-dehumidification plant, proposed by Garg *et al.* [1966]. From these figures also it is clear that for water requirements less than 90 $m^3 d^{-1}$ it is better to install a solar desalination plant.

Solar stills in their current form cannot compete with the large distillation plants. On the contrary for water requirements less than 227 $m^3 d^{-1}$ the multi-stage flash distillation or the vapour compression process cannot compete with solar distillation. Perhaps, the only competitors could be electrodialysis and reverse

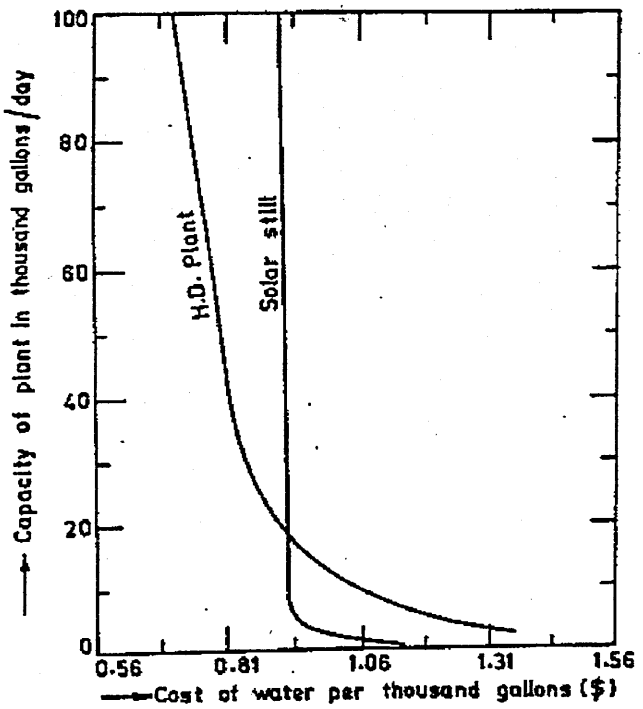

Fig. 2. 7 Cost of water/1000 gallons for solar still plant and for humidification-dehumidification plant (After Garg *et al.*, 1966)

osmosis, but the cost of water in this case would depend on the salinity of the available water and also on the availability of electric power.

The cost of desalting water by means of electrodialysis has become competitive with distillation in situations where the initial salinity of the water supply is less than about 5 000 ppm (seawater averages 35 000 ppm of total dissolved salt while brackish water are counted in the range from 2 000 ppm upwards). Reverse osmosis is more economic than distillation when used for waters with low salinity, and has promise of being successful with even seawater. It is competitive with electrodialysis, but is in a much earlier stage of development than the latter.

2.2 Greenhouse

Introduction

The cultivation of horticultural crops under cover is practised in nearly every country of the world. Greenhouses are plant shelters which prevent the free exchange of internal air with the exterior. The greenhouse is a huge solar collector, and during sunny days large amounts of heat are dissipated by ventilation in order to keep the air temperature at an acceptable level. Greenhouse ventilation is a key function in the control of the greenhouse climate and in the control of crop growth and development.

Numerous environmental parameters are important for good crop production. Each species has its own requirements, although many common floricultural crops are grown using similar conditions. The main environmental parameters are air temperature, light and relative humidity [Parker, 1991].

The use of solar energy in greenhouses would appear to be an energy benefit to our ecosystem, if not a financially profitable enterprise at this time. A desert environment tends to have extreme temperature differences between night and day, and it is particularly expensive to protect the system against small peaks of dry heat in summer, using only solar energy [Brownell, 1983].

For plant growth a special portion of the spectrum in the visible region between 400 and 700 nm is of interest, this part is called Photosynthetic Active Radiation (PAR), only a small part of the PAR energy absorbed by the crop is directly converted in the photosynthesis process. The remainder is converted into heat. Solar radiation is the driving force of the greenhouse; it supplies not only the light necessary for plant growth, but also the heat necessary to maintain a growing environment. Solar energy enters the greenhouse as short-wave radiation, or light, but when it is absorbed by the plants and other surfaces inside the greenhouse, the light is changed to thermal energy or heat. Visible light constitutes a source of energy for plants. Light energy, carbon dioxide and water all enter into the process of photosynthesis.

There is also a wealth of evidence to show that the yield of most greenhouse crops is dependent on irradiance, though there is not agreement on the form of the relationship. Verhaegh [1980] and Goldseels *et al.* [1986] show a response of 3% increase in yield of tomatoes and cucumbers for a 1% increase of light in the winter and spring in the Netherlands, but less sensitivity in the summer. Cockshull and Hughes [1971] showed 1 % for 1 % for the weight of chrysanthemum flowers, and in a direct experiment in which tomatoes were partially shaded.

Plant growth and development are directly related to water status, either in the form of liquid within plant tissue or in the form of vapour in the surrounding air.

Transpiration plays a very important role in the hydraulic cycle of crops. According to Rosenberg *et al.* [1983], only 1 % of the available liquid water taken by the plants is actually involved in metabolic activities. Most of the water passes through the plants and is vaporised into the air.

2.2.1 Selective absorber

Interest in protected crop cultivation has increased over recent years in many countries. Glass has been the traditional covering material for many years but over the last decade there has been a widespread move toward the use of plastic covers.

A number of researchers [Trickett *et al.*, 1958, Bailey, 1975 and Abbott and Brundett, 1981] have investigated the transmission of light into glasshouses. Critten [1983] developed a model which calculated the daily light integral and transmissivity of a greenhouse, including multiple reflections and attenuation by glazing bars; he measured the transmission in a four-span Venlo house under overcast conditions and found that between 65 and 70 % of the incident light was transmitted.

The amount of radiation present inside a glasshouse as a function of its shape, orientation and cladding material was modelled by Kirsten [1973]. He found that glasshouses positioned in the east-west direction had the greatest transmissivity and saddle or shed roofed structures also had a small advantage in this respect. Kozai, and Kimura [1977], also investigated the light transmission of glasshouses, finding that the east-west orientation gave a greater flux, whereas the north-south orientation gave an overall reduced flux but more even radiation distribution.

For many years glass has held an unchallenged place as the material for the protection of plants against unfavourable climatic conditions. This protection is afforded in three ways: from wind, from heat loss by natural convection, and from heat loss by radiation to the cold sky. The amount of short-wave solar radiation present inside the greenhouse is affected by the type of cladding and amount of structural material present. The solar radiation flux is extremely important for photosynthesis and it is desirable to ensure that the internal downward flux is maximised.

Measurements made by Agarwal and Verna [1977] show that heat absorbing glass absorbs 53 % of incident radiation, transmits 41 % and reflects the remainder. Nisen [1979] gives transmission values of 0.92 for 0.1 mm PVC, 0.91 for 3 mm horticultural glass and 0.9 for 1.1 mm layered polyester. Kirsten [1973] states that for silicate glass, 86 % of radiation between the wavelengths 0.35-2.8 μm is transmitted, but he does mention the important problem of soiling. As an average, he assumed that about 10 % of the light incident on the outer surface of the covering was blocked by dirt deposits.

The work of McCree [1971] showed that only the radiant energy between 350 and 700 nm can be utilised by common green plants. In view of the spectral energy distribution of solar radiation, we can conclude that only half of it is useful for plant growth.

Silverstein [1980] concluded that the glass substrate in the thickness range of 0.32-0.64 cm will absorb 33-50 % of the insolation. The heated glass will then transfer its thermal energy partially to the interior and partially to the exterior. The heat transfer in both directions is composed of convective and radiative components. There is preferential convective cooling to the exterior partially due to natural convection but predominately due to wind induced forced convection.

He also described and analysed the optical and thermal properties of a group of energy conserving-heat absorbing greenhouse glasses which exhibit selective transmittance of photosynthesis active radiation (PAR). He concluded that the inexpensive iron doped, heat absorbing soda lime glasses have selective transmittance of photosynthesis active radiation while substantially absorbing the near IR at wavelengths greater than ~ 750 nm. These materials when covered on the interior side by selective IR mirror films such as SnO2:F, serve in a dual energy conserving capacity of saving substantially on both summer solar heat and winter space heating losses.

Trickett *et al.* [1958] studied the radiation transmission properties of a number of plastic materials and concluded that the data for transmission at 600 nm showed that all the materials tested were highly transparent to visible radiation. There were important differences in the infra-red transmission spectra of the materials tested.

Damagnez [1976] studied a novel solar greenhouse with a double cover. Copper chloride solution was circulated between the covers, absorbing solar energy and was then returned to a thermal store under the greenhouse. The active greenhouse cover absorbed the near infra-red (IR) radiation which did not contribute to photosynthesis. Often IR radiation causes overheating and excessive transpiration of plants. At night the heated fluid was recirculated in the roof to provide greenhouse heating.

2.2.1.1 Water film

Since about 1939 water films have been used [Marshall, 1948] and [Brown, 1939] to limit the maximum temperature in glasshouses and it has been generally

considered that the absorption of infra-red radiation was the main means by which this was achieved. The most important effects of the water film on the sloping roof are to lower the surface temperature of the glass and to increase the overall heat transfer coefficient due to the high heat transfer coefficient from glass to water. Both have the effect of increasing the rate of heat removal from the greenhouse, particularly if the water is chilled [Morris, 1958].

Morris *et al.* [1970] showed that it was not possible to maintain a sufficiently thick film of water on a traditional glasshouse roof to absorb a significant amount of solar radiation. Cohen *et al.* [1983] found the roof temperature of a greenhouse containing plants could be reduced by up to 8 °C by maintaining a water film of 0.024 mm on the roof, if the external vapour pressure deficit was high. However, if the deficit was low the resulting reduction in internal air temperature could be less than 1 °C. They considered this method was less effective than wetting the foliage and greenhouse floor.

This method can be made more effective by adding a selective absorber such as copper chloride to the water. A 3 % solution absorbs weakly in the visible part of the solar spectrum but strongly in the infrared region. The problem of containing the fluids, which can be phytotoxic, have resulted in the development of selectively absorbing glasses [Silverstein, 1980]. However the light transmission of these is invariably less than normal glass and so the light transmittance of the greenhouse is permanently reduced.

Van Bavel and Damagnez [1978] compared a fluid-roof solar greenhouse and an ordinary greenhouse and concluded that while the amount of solar energy absorbed by the fluid-roof was greater than that of the material roof, the storage of this energy moderated the roof temperature and, in consequence, the crop temperature. Heating and ventilation were substantially reduced and, water use

rates and daytime depression of leaf water potential were significantly lowered. Van Bavel and Sadler [1981] concluded in another study that the fluid-roof design was more advantageous in regard to forced ventilation requirements and water use, although at the expense of a 10 % loss in photosynthetic radiation.

2.2.2 Air temperature, air humidity and crop temperature

The air inside a greenhouse is usually warmer than outside. The increase in air temperature above that outside depends primarily upon the type of structure, the type of cladding material, and the air tightness of the greenhouse. Variation of temperature also depends upon factors such as the orientation and shape of the greenhouse, and the number of cladding layers. In addition, the inside air temperature is affected by the temperatures of all the other interior glasshouse components.

The inside air humidity differs significantly from that of the open air. The variation in the absolute humidity inside the glasshouse is closely related to the soil temperature [Albright, 1991].

Solar radiation or radiation from heating systems will tend to raise the plant temperature above that of the surrounding air, while transpiration will tend to bring the temperature down. If transpiration is hindered by high inside relative humidity or water stress then damage may be caused if the plant temperature rises too high.

High levels of air humidity favours the incidence of fungal diseases and affect crop growth [Hand, 1988]. The most common humidity regulation strategy is to maintain air humidity levels below fixed threshold values (one for the daytime and another for night-time). It was reported [Stanghellini *et al.*, 1992], that this

approach to humidity control, which often amounts to preserving a low humidity at any cost, can be expensive. If optimal climate control strategies are to be developed for humidity, it will be necessary to quantify and predict the effect of humidity on yield and the various plant processes.

Authors generally point out that the main objective pursued with humidity control is to maintain a certain rate of transpiration. Various models linking transpiration to climatic parameters have been proposed. Most of these models [Stanghellini, 1987], [Jolliet and Bailey, 1990], [Chalabi and Bailey, 1989] are based on a thermal balance of the canopy and are variants of the Penman-Monteith equation [Monteith, 1973]. In these models, transpiration is mainly affected by radiation and by the air vapour deficit inside the greenhouse.

Modern greenhouses offer great potential for the production of high-value crops. They make use of sophisticated equipment such as thermal or shading screens, fogging systems, cooling pads, proportional heating and ventilation and computerised control.

2.2.3 Methods of cooling

Ventilation alone is often not sufficient to maintain the desired temperature during hot summer days, so some form of cooling is advantageous. The methods of controlling the greenhouse temperature in summer can be divided into those that restrict the heat input by limiting the entry of solar radiation, and those that dissipate the internal energy by some means of heat removal. Sometimes a combination of both is used.

Many greenhouses in sunny areas are cooled by using fans and wet pads (Figs. 2.8 and 2.9). In 1970 Morris [1970] concluded that this form of evaporative cooling

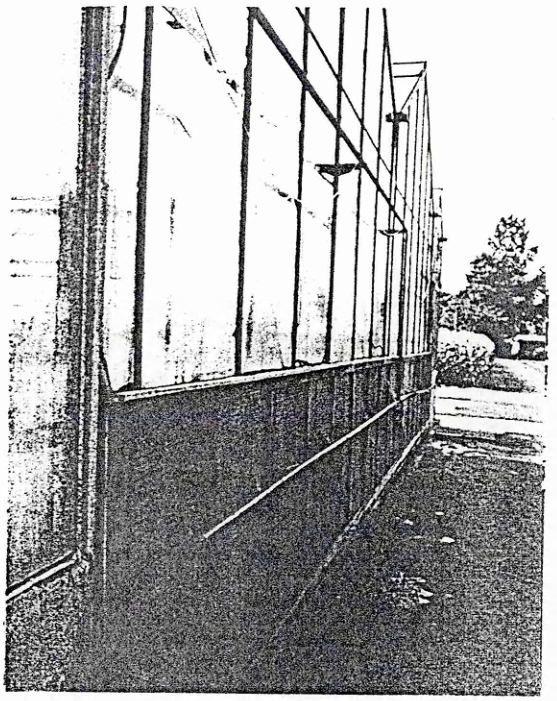

Fig. 2. 8 Cooling pad at winward side of greenhouse (After Breuer *et al.*, 1996)

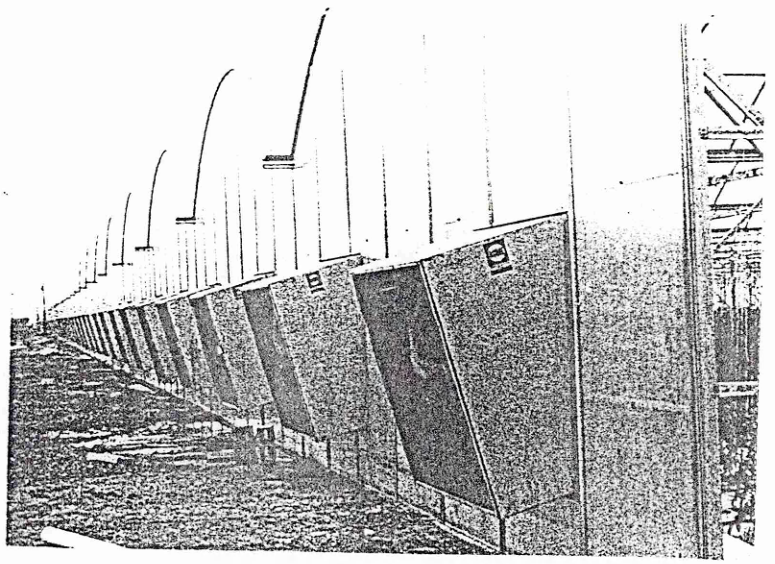

Fig. 2. 9 Fans at leeward side of greenhouse (After Breuer *et al.*, 1996)

2.2.3.1 Shading

Shading consists of cutains and white-wash or some other suitable liquid, sprayed over the outside surface of the greenhouse, thereby increasing the reflectivity of the surface and so reducing the transmission of solar radiation [Garzoli, 1971].
Gray [1948] reported that a 50 % reduction in light intensity reduced the internal temperature by at least 3 °C. The materials used for this purpose include ground lime in water, dilute white emulsion paint and a number of proprietary compounds such as Arocoat and Varishade.
Shading can also be used inside the greenhouse [Bailey, 1978]. An advantage is that the shading system is protected from the weather conditions outside the greenhouse. However, as the solar radiation is absorbed internally, ventilation is required for its removal. This need can be minimised by using a shading material which has a high reflectance for solar radiation. It is generally preferable to apply the shading material in stages to avoid the restriction of solar radiation during the dull, cool weather in summer. This practice is useful when it is desired to maintain a generally high level of illumination while obscuring all direct sunlight.

2.2.3.2 Ventilation

Two types of ventilation can be distinguished: natural and forced. In the case of natural ventilation, the pressure difference across the openings, the driving force for ventilation, is caused by wind effects and by a difference in temperature between the inside and outside air. Energy for the forced ventilation process is supplied by fans.

The use of fans to increase both the rates of evaporation and ventilation has been found very useful. The process of evaporation consists of the state change of water from liquid to gas which requires a significant amount of energy known as the latent heat of evaporation. However all evaporative cooling systems are limited by the moist air properties of the environment [Garzoli, 1971].

2.2.3.3 Evaporative cooling with natural ventilation

Carpenter and Willis [1957] and Leach [1959] found some cooling effect by introducing mist and fog into the greenhouse. While the actual cooling effect depended on the condition of the outside air, some worthwhile temperature reductions were generally obtained.

Misting and fogging rely on producing a fine dispersion of water droplets which evaporate and cool the greenhouse air. The droplets can be generated at a number of positions within the greenhouse so very uniform cooling can be obtained when combined with either natural ventilation through the roof, or forced ventilation using fans. The most common form of misting system uses a disc spinning at between 3,000 and 10,000 rpm which is supplied with water at its centre and produces the droplets around its circumference. The advantages of this method are that it is not dependent on the quality of the water, and droplet size is not strongly dependent on the water flow, so the cooling rate can be varied.

Fogging systems produce water droplets in the range 15-20 μm which have a typical terminal velocity of 0.15 m s^{-1} and evaporate within 3 s in air at 20 °C, and 80 % relative humidity. They were developed primarily to maintain a humid atmosphere for plant propagation. As with the misting they can provide very

uniform conditions, but the nozzles are susceptible to being blocked by salts if the water quality is poor.

Giacomelli *et al.* [1985] compared two methods of evaporative cooling, a wetted overhead energy-saving blanket and fog nozzles on a movable boom; they concluded that there was a reduction of 4 °C when using the blanket method and the fog produced by nozzles on the movable boom showed a greater evaporation rate and a reduction up to 10 °C was achieved.

Spoelstra [1975] compared fan and pad cooling with plant wetting on the basis of changes in transpiration rate. He reported that transpiration decreased by 54 % when fan and pad cooling was switched on, and by 27 % when the plant canopy was sprayed with water.

Boulard *et al.* [1991] presented experimental results on the combined effects of aeration, fogging and shading on greenhouse climate and on crop temperature and transpiration. It was shown that the coupling between air humidity and temperature on one hand and between crop temperature and transpiration on the other, depends on the ventilation rate and on the intensity of the evaporative cooling.

2.2.3.4 Evaporative cooling with forced ventilation

The effectiveness of both mist and fog treatments are approximately doubled by the use of exhaust fans in the greenhouse [Carpenter *et al.*, 1959] and [Leach, 1959]. In fan and pad system (Fig. 2.10) air is drawn through the pad where adiabatic cooling takes place and the temperature of the air entering the greenhouse is reduced by 80 % of the wet bulb depression. Disadvantages of fan and pad cooling are fouling and growth of algae on the pad and the occurrence of

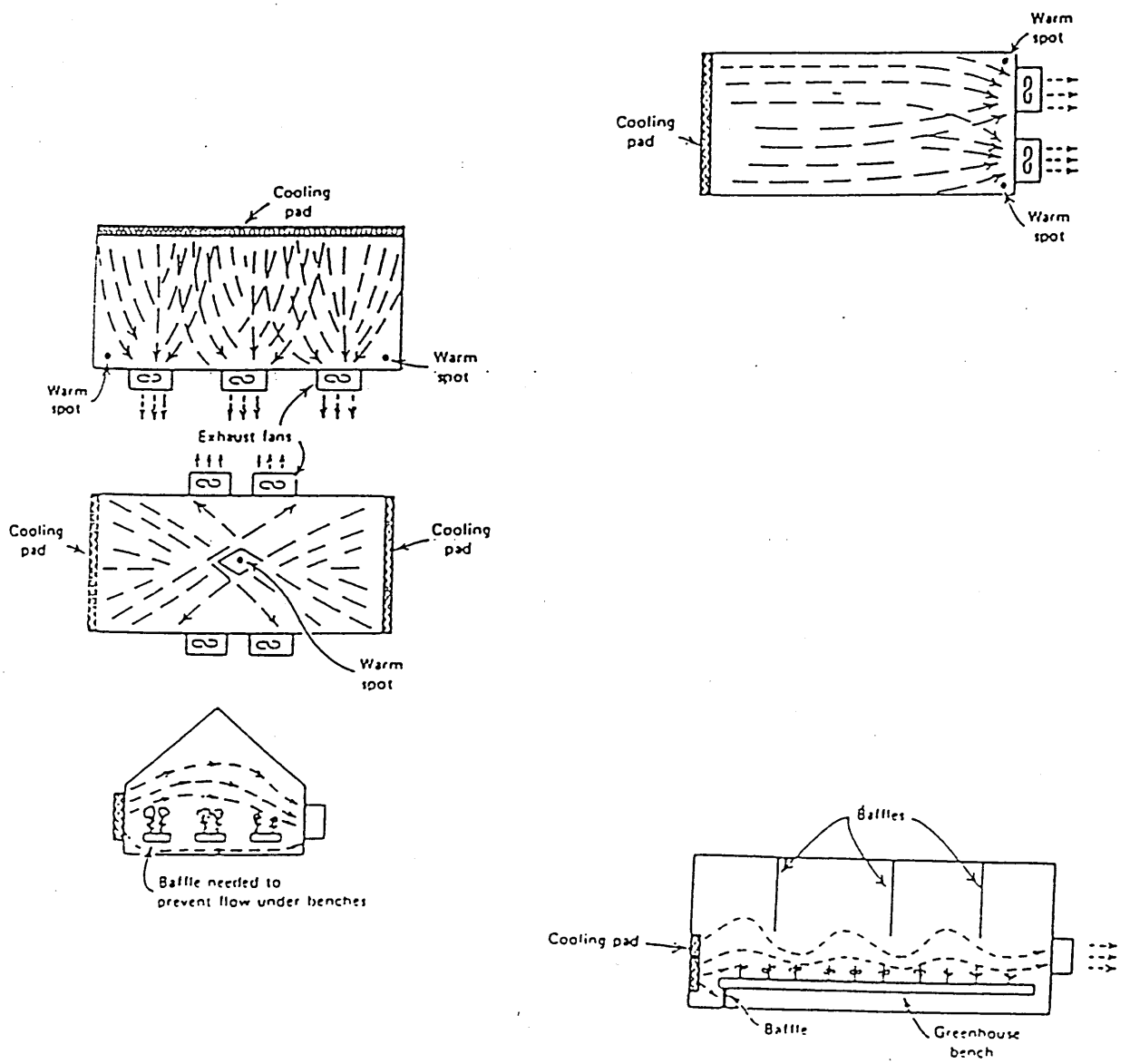

Fig. 2. 10 Patterns of air flow during operation of fan and pad cooling systems (Mastalerz, 1977)

unacceptable temperature and humidity gradients in the greenhouse if the systems are not designed correctly.

2.2.3.5 Refrigerated air conditioning

Temperature control can be achieved under all conditions only with refrigerated air conditioning. The equipment is very expensive and is used only in the better equipped research laboratories [Garzoli, 1971].

2.2.3.6 Other methods

Montero *et al.* [1981] studied the influence of 3 methods of evaporative cooling (evaporative cooling pad, sonic humidifier and electric humidifier) on the greenhouse environment. The evaporative cooling pad did not cool the greenhouse uniformly. This system reduced leaf temperature near the pad to 3 degrees below outside air temperature, but its effectiveness decreased significantly as the distance from the cooling pad increased. The electric spinner humidifier, which consisted of a mechanical atomiser with a one kW electric motor turning at 3600 r.p.m., reached 100 % relative humidity and decreased leaf and greenhouse temperature to 0.9 and 3.3 degrees below the outside air temperature respectively. The sonic humidifier, which used sound-waves to disperse liquids into a fine mist, was highly efficient and lowered air temperature as much as the electric humidifier. Leaf temperature was 2 °C lower on average than the outside temperature.

2.2.3.7 Combined methods

MacNeill [1962] described a greenhouse in which both slatted and fabric blinds were used, together with water nozzles on the roof which produced both a continuous film of water running over the glass and an evaporative spray above the roof. [Went, 1957] used a greenhouse with a cooling system consisting of air washers in which the water was chilled by refrigeration. The air was thus cooled to the desired wet bulb temperature, reheated to the desired dry bulb temperature and recycled through the greenhouse.

Permanent shading is often used in conjunction with evaporative cooling when there is sufficient sunlight for plant growth. Canham [1962] used water, containing a green dye, running in a film over the greenhouse roof. Cooling was effective but evaporation of water , which was mains tap water, left a calciferous deposit on the glass. This absorbed the green dye and formed an almost permanent form of shading.

Conclusions

Several methods are available for controlling greenhouse temperatures in summer. Garzoli [1971] compared 7 different cooling methods (natural ventilation, evaporative cooling with natural ventilation, forced ventilation, water sprays on greenhouse roof, shading, evaporative cooling with forced ventilation and refrigerated cooling with forced ventilation) under conditions of high solar radiation intensity and high ambient temperature. He concluded that greenhouses which are well-ventilated have lower demands for cooling. Shading can be used to reduce the solar heat input without seriously affecting the plants' light

requirements. The application of water to greenhouse crops is helpful so that evaporation from both plants and soil will use up much of the heat input. Evaporative cooling and refrigerated air conditioning can be used, providing they can be justified economically.

Humidifiers proved to be more effective than a horizontal pad in achieving a high evaporative efficiency. Powered humidifiers can produce more uniform temperatures along the greenhouse if properly spaced. It is necessary to maintain a humidity in the greenhouse below saturation in order to permit transpiration and produce optimum plant growth.

2.2.4 Greenhouse models

Research on greenhouse climate was pioneered by Wood [1909], while an analysis of the greenhouse energy balance was considered by Businger [1963] and more recently by Walker [1965], Takakura *et al.* [1969], Kimball [1974], Takakura [1974], and Horiguchi [1978] among others.

Early studies of the climate in conventional greenhouses concentrated on determining the thermal behaviour of greenhouses. More comprehensive models were subsequently developed based on energy and water mass balances for the crop-greenhouse system which consisted of the crop, air, soil and greenhouse cover. The balance equations were formulated in terms of the energy and mass fluxes relevant for each element which were defined in terms of the state variables of temperature and water vapour pressure. The modes of heat transfer included were thermal radiation, natural and forced convection, conduction and latent heat. The boundary conditions usually consisted of the outside air temperature, absolute humidity, solar radiation, long-wave sky radiation, wind speed and the soil

temperature at a specified depth beneath the greenhouse. Other inputs to the models were the physical characteristics of the crop and the greenhouse. The balance equations, with an appropriate set of boundary conditions, were solved numerically using computers. Models of this type have been developed by Garzoli and Blackwell [1981], Baille *et al.* [1985], Jolliet *et al.* [1985] and Short and Breuer [1985] and have been used primarily to determine the heat loss from greenhouses.

The exchange of energy and mass occurring in the greenhouse system are characterised by heat and mass transfer coefficients. Many of the convective heat fluxes are calculated from empirical correlation based on the Nusselt, Grashof, Prandtl and Reynolds numbers, which are found in the heat transfer literature [McAdams, 1954]. These relationships were frequently derived from data measured under idealised conditions and they are not necessarily directly applicable to the greenhouse. Bot [1983] has shown that the convective transfer of heat from the outer surface of a large multispan greenhouse roof occurs in the transition region between free and forced convection. The coefficient of convective heat transfer at the inner surface of the greenhouse roof has been shown by Kanthak [1970], Tantau and von Zabeltitz [1974] and Okada [1980] to be influenced by the type and position of the greenhouse heating system.

Numerous studies of energy balance of greenhouses have been conducted of which Seginer and Levav [1971] and Serodio [1977] provide detailed reviews. Early work [Takakura, 1967], [Morris and Winspear, 1971] and [Pozin, 1971] were constrained to use analytical techniques for solving heat balance equations; later work such as Selcuk [1970] and Serodio [1977] had the advantage of using computers to obtain numerical solutions.

Ventilation of greenhouses has been studied by Kozai and Sase [1978] and Kozai *et al.* [1980] using both computer and physical models; they deduced ventilation rates from an energy balance of the greenhouse.

Bot [1980] produced a computer model of the greenhouse climate dependent upon the outside weather conditions. The important physical processes were quantified and linked together but in the absence of a complete knowledge of the heat transfer processes in the greenhouse it was found that some of the parameters had to be estimated.

The simulation model [Chalabi *et al.*, 1991] used in this project was similar to that of Bot [1980] and Takakura [1974]; it simulates the dynamics of the energy balance of a greenhouse. Heat and water vapour exchanges occur between the 'nodes' of a greenhouse 'network': inside air, crop, inner roof, outer roof, ground, outside air and sky. This model was used in a number of greenhouse studies in Silsoe research Institute [Chalabi *et al.*, 1989, 1991], [Ching *et al.*, 1995] and also was used to describe the evaporative cooler in a greenhouse [Bailey, 1987, 1991].

Chapter 3 Greenhouse design

Introduction

The objectives of this chapter are: (i) to study the optical properties of a group of heat absorbing greenhouse glazing materials which exhibit selective transmittance of Photosynthetic Active Radiation (PAR), and (ii) to determine the sensitivity of the rate of freshwater produced to some design parameters of the greenhouse variables using a simulation model [Chalabi *et al.*, 1992]. This assessment was made using meteorological data recorded in Tenerife (Spain) for June and December.

3.1 Greenhouse description

The greenhouse cover consists of two layers, the inner forms a selective solar radiation absorber. The solar radiation absorbed evaporates seawater; the wind induced an air flow in the roof cavity and the air emerged saturated with water vapour. The water vapour transpired by the plants combines with the cooled and humidified ventilation air stream to generate a high relative humidity in the exhaust air. Pure water is condensed from the exhaust air in a heat exchanger, cooled by cold seawater (Fig. 3.1).

To control the flow of the air through the front evaporative pad and allow hot air to escape on still days, a relief vent of 30 cm is located between the lower roof and the top of the pad.

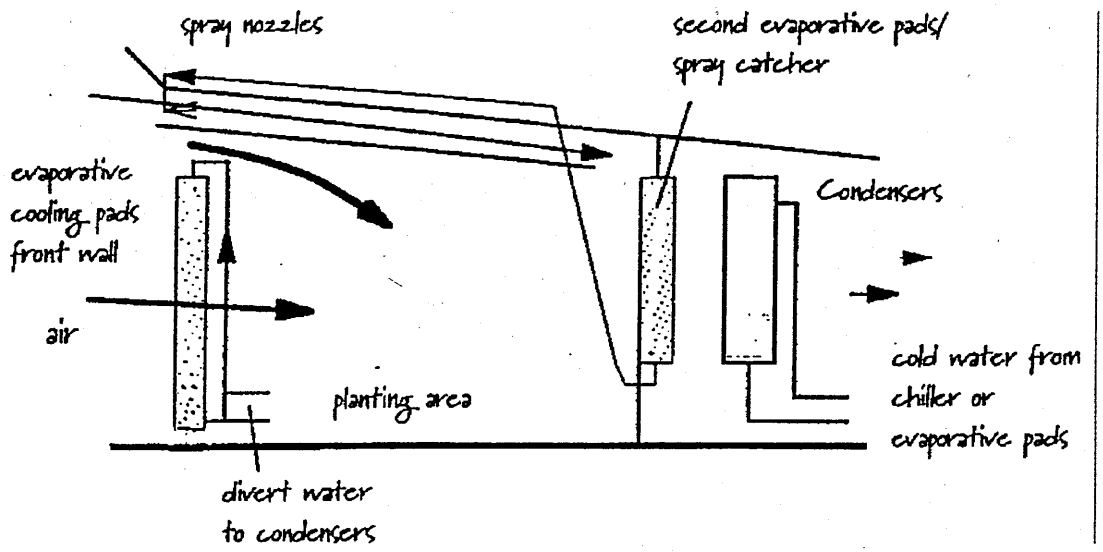

Fig. 3. 1 Air circulation of the Seawater greenhouse (Light works Ltd, 1994)

Seawater is extracted from a beach well and supplied to a header tank that is used to feed the greenhouse systems. The pipe to the greenhouse is 130 m long, and is buried in a trench.

It had been the original intention to use deep seawater as the cooling medium, but expense of the installation (pipe in deep sea) would have been prohibitive at this stage, so the expedient of the heat pump was adopted instead.

The simulation model [Chalabi *et al.*, 1991] consisted of energy and mass balances which enabled variations in the state variables of air, plant, greenhouse roof and soil temperatures, and absolute humidity to be predicted in response to changes in external weather conditions.

3.1.1 Roof cavity

One of the unconventional elements of the design was the double-layer roof which provided a space for a mist of seawater droplets to evaporate in the wind induced flow of air. The main design constraints on the roof structure was the requirement to maximise light transmission.

The rate of evaporation in the roof cavity is a function of parameters such as the minimum flow rate and initial temperature of the water, temperature and relative humidity of the air inside the cavity.

3.1.1.1 Experimental method

Energy conserving glazing materials for controlled environment agricultural applications are analysed for their optical properties.

A PAR sensor (Quantum sensor) with a sensitivity 1000 mV mol^{-1} m^{-2} s^{-1} was placed at an actionometric station at the University of Evora (Portugal). The altitude of the station is approximately 300 m above sea level, and it is shaded by any obstacles.

Three samples of 200 μm transparent materials (plastic film, corrugated GRP and flat GRP with shallow channels) with dimensions of 30 cm x 30 cm were used in the experiments which were made under two different sky conditions:

i) Clear sky and ii) Overcast sky.

For each of these conditions measurements were made at 10 h, 13 h, and 16 h local time, of the PAR transmission by measuring with and without each sample of the transparent material. The sample was placed horizontally 20 cm above the sensor. At each hour, 3 series of measurements of 60 s each were made. Some preliminary tests were made in order to check whether the sample should be closer to or further from the sensor, provided all the surface of the sensor was covered by a sample. Also, several angles (30-90 degrees) were tried in order to test the isotropy of the radiation transmitted through the material. The result for each hour was the average of the 3 values, for each sky condition and with and without the sample over the sensor.

The spectral transmission analyses of several cover materials as well as their transmissivity to PAR at different angles of incidence of radiation were measured and showed that the material used in the greenhouse roof diffusely transmitted the radiation; The average transmissivity to the PAR was about the

same (0.67) for both overcast and clear sky conditions and not very dependent on the angle of incidence.

The light transmission of three samples of roof material was measured in Evora University (Portugal) and Silsoe Research Institute laboratories (U.K.), and the results for PAR (400-700 nm) are given in Figs. 3.2, 3.3 and 3.4 and Table 3.1. Other measurements on a sample having the trade name Trilite GRP sheet see appendix D, which was used in the greenhouse roof, were carried out under the two sets of conditions (overcast and clear sky) but over a different period. In both cases measurements were taken at different times of the day. The aim of these experiments was to see whether the material had a transmission to PAR which was sensitive to the radiative environment, i.e., if the radiation was diffuse or specular, or if the transmissivity depended upon the angle of incidence of the beam.

In the overcast situation the fraction of diffuse (Rd) to global (Rg) solar radiation Rd / Rg changed from 0.85 (midday) to 0.92 (morning and late afternoon). In the clear sky situation the fraction Rd / Rg was 0.12 (midday) and 0.90 (morning and late afternoon). The average transmissivity of the sample to PAR was the same for both overcast and clear sky conditions and not very dependent on the angle of incidence. The average value of the transmissivity for PAR radiation was 0.67 and the change with angle of incidence was $\pm$ 5 %, i.e., the higher values corresponding to the lower angles of incidence (near midday) and vice versa, see Figs. 3.5, 3.6, 3.7 and 3.8.

The most suitable materials for roof cladding fell broadly into the category of profiled plastics. Glass was rejected at an early stage for reasons of excessive weight and difficulties of transport to the greenhouse site. After looking at the

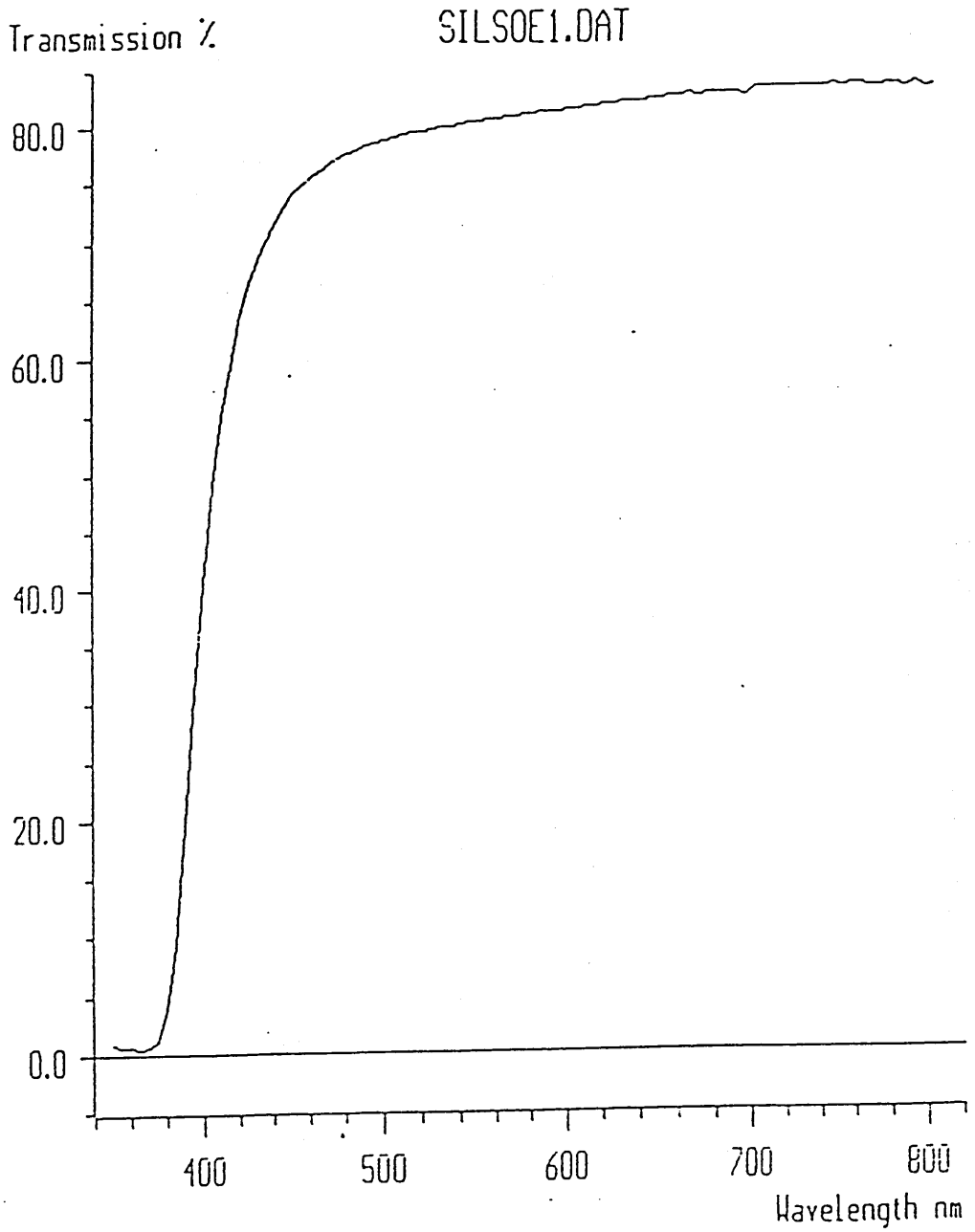

Fig. 3. 2 Light transmission of a thick plastic film

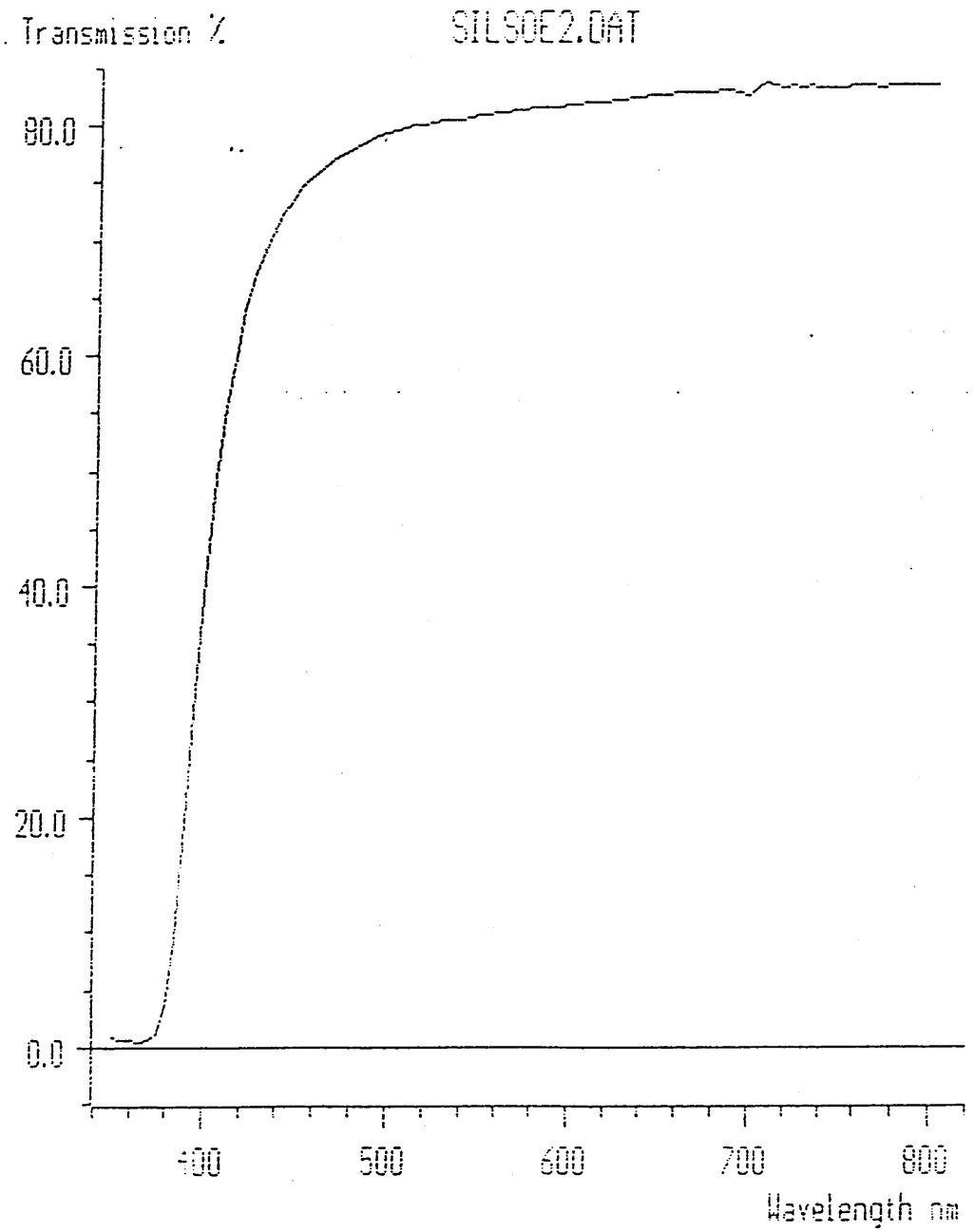

Fig. 3. 3 Light transmission of a flat GRP sheet with shallow channels

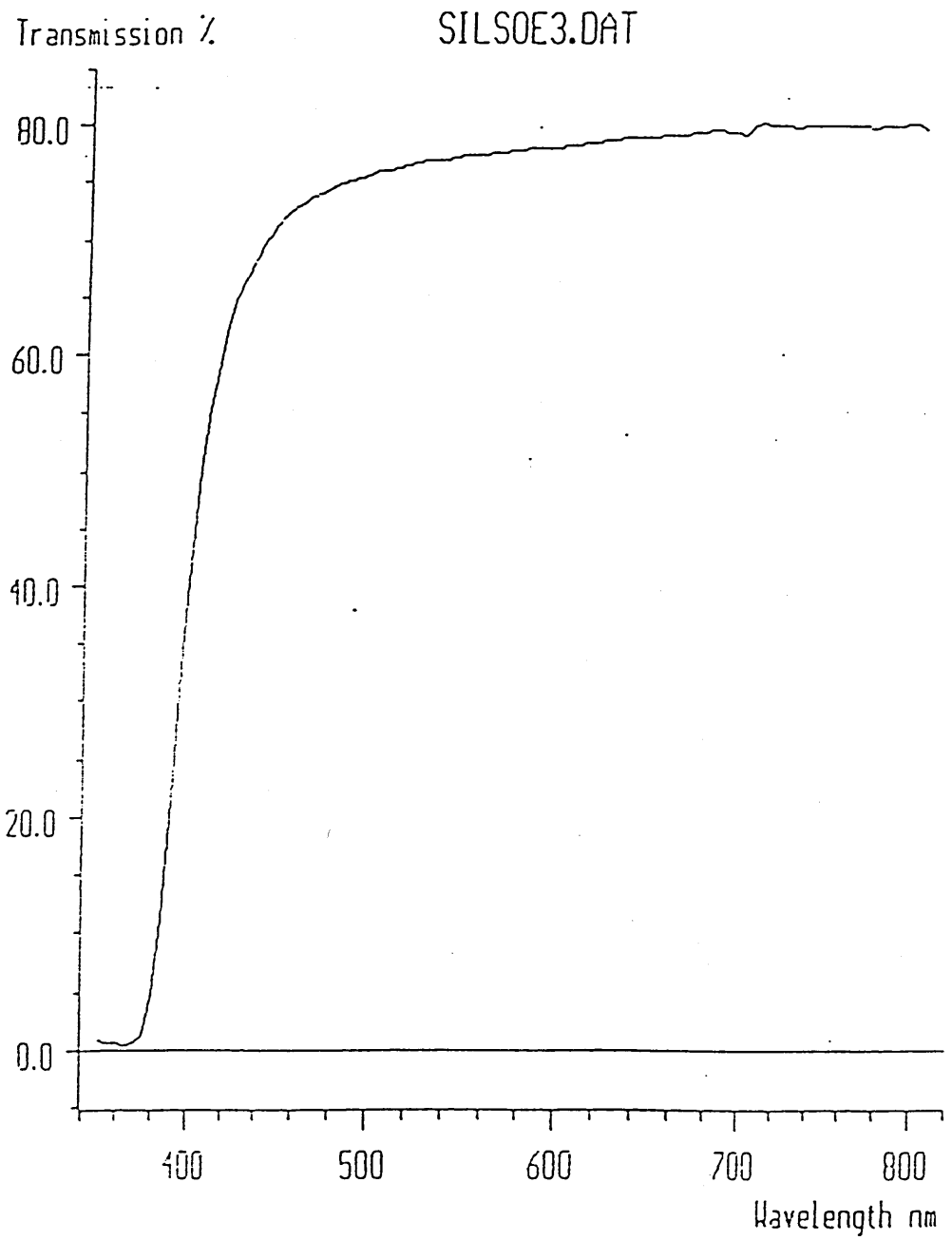

Fig. 3. 4 Light transmission of a corrugated GRP sheet

	Corrugated GRP		Thin film		Flat GRP with shallow channels	
	with cover	without	with cover	without	with cover	without
	1.301	1.608	1.265	1.635	1.131	1.598
	1.297	1.621	1.279	1.632	1.131	1.597
	1.287	1.625	1.259	1.625	1.084	1.579
	1.291	1.619	1.269	1.679	1.173	1.597
	1.279	1.621	1.261	1.667	1.173	1.585
Total	6.455	8.094	6.333	8.238	5.692	7.956
Average	1.295	1.618	1.267	1.648	1.138	1.591
PAR	0.797		0.769		0.715	

Table 3. 1 Measurements of the transmission to PAR of cover samples in Evora (Portugal)

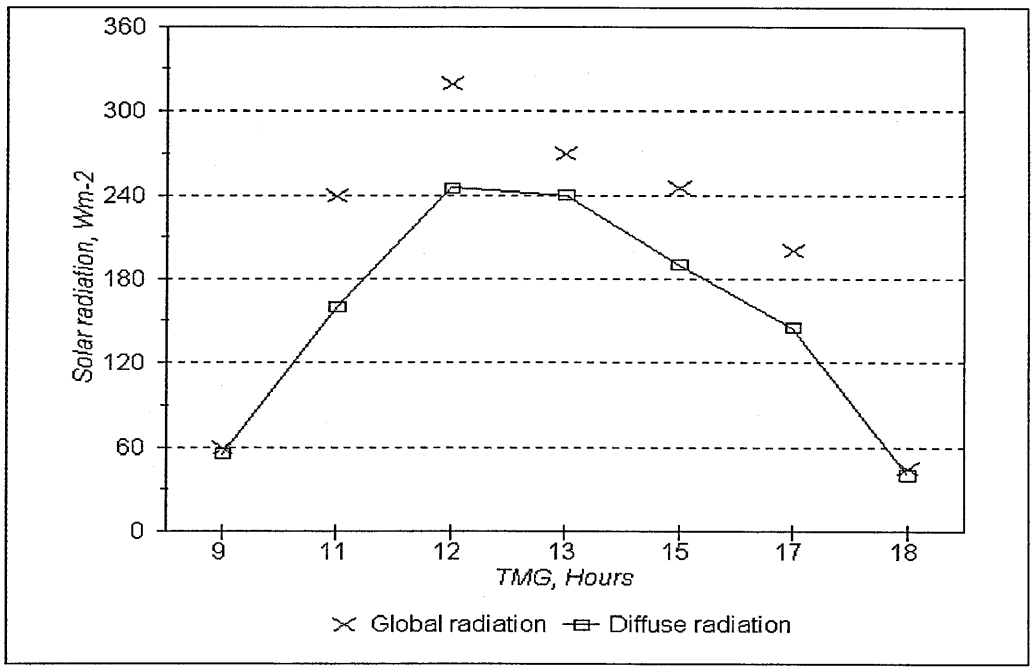

Fig. 3. 5 Solar radiation in overcast sky

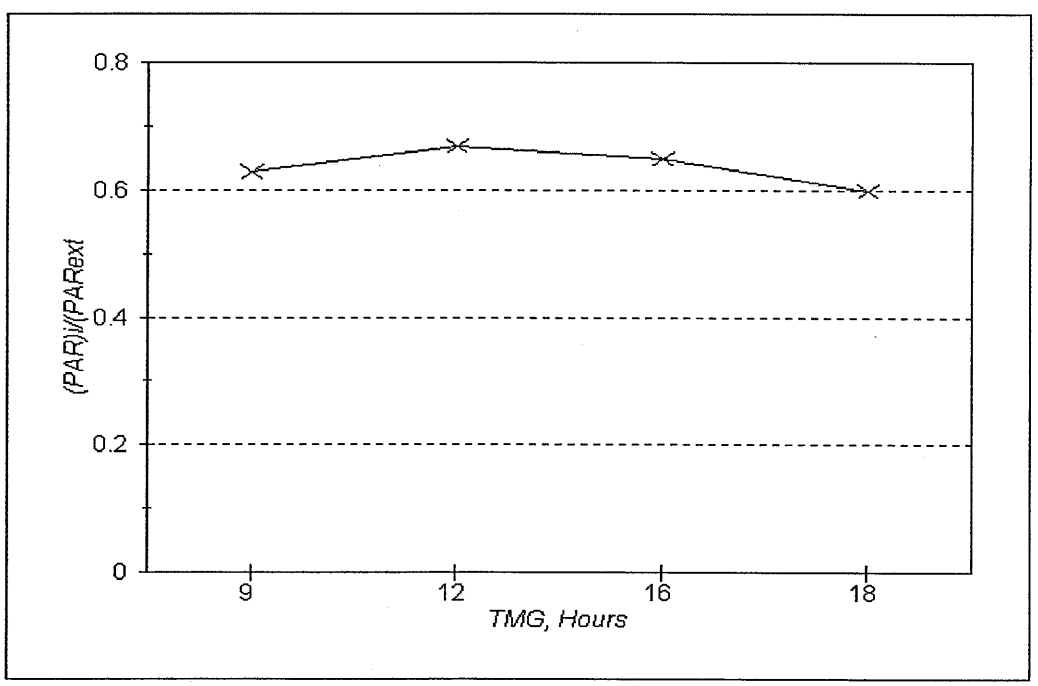

Fig. 3. 6 Transmitivity to PAR variations in overcast sky

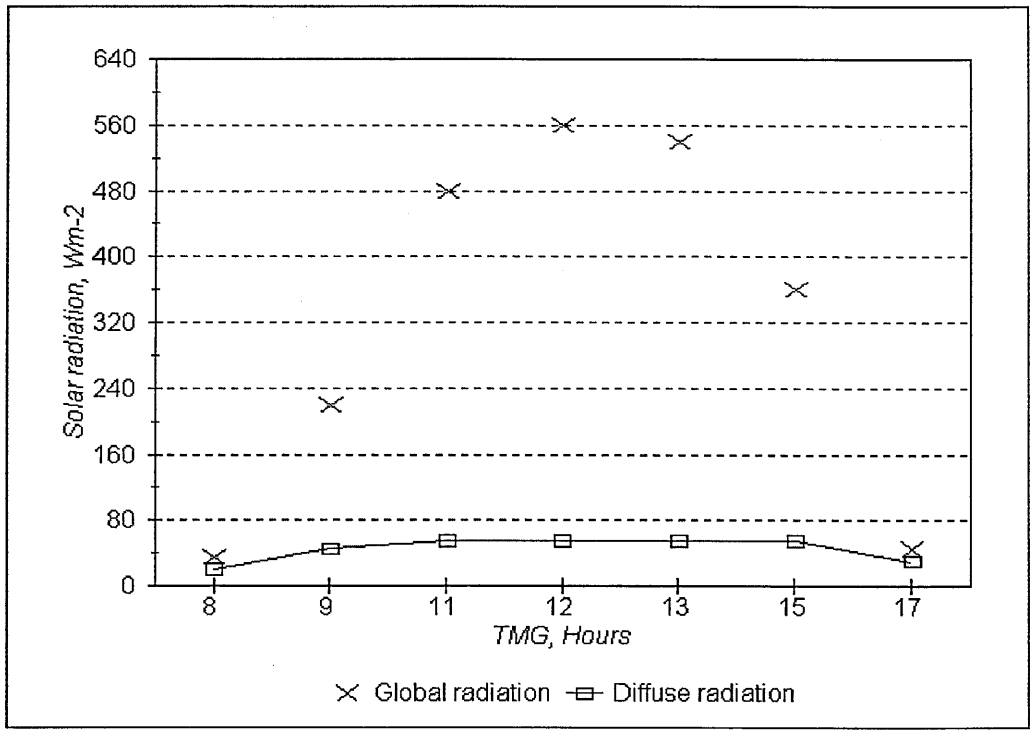

Fig. 3. 7 Solar radiation in clear sky

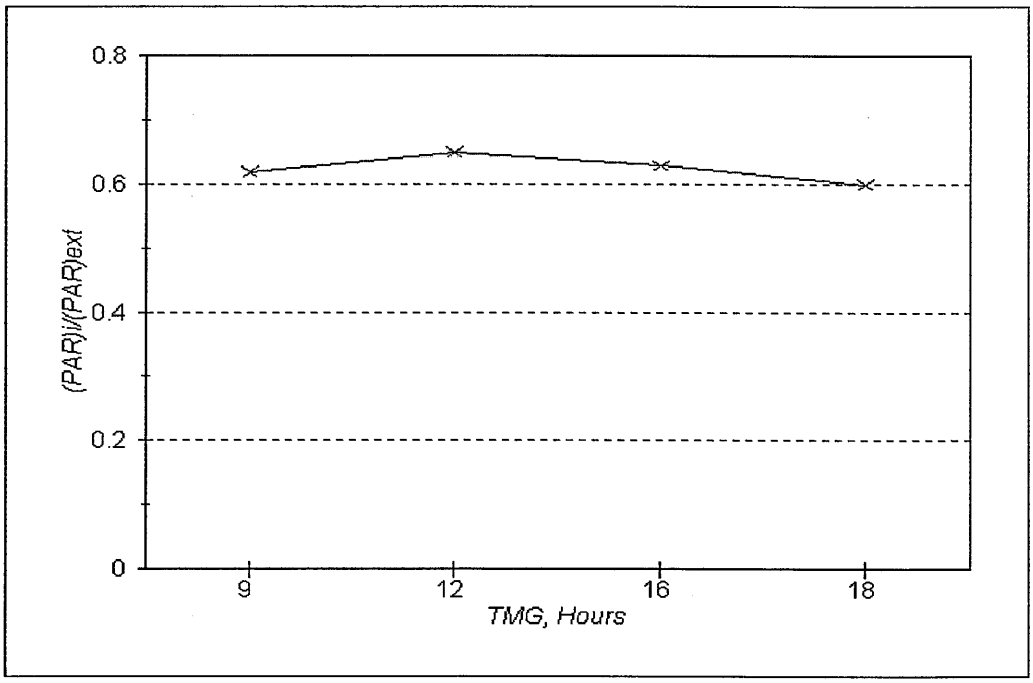

Fig. 3. 8 Transmitivity to PAR in clear sky

possibilities of clear PVC profiled sheet, extruded polycarbonate sheeting and profile GRP, the translucent GRP was selected because it was the cheaper.

3.2 Sensitivity analysis

A sensitivity analysis was carried out on the influence of the following variables on the water production by the condenser :

i) efficiency of the selective solar radiation absorber

ii) cooling water flow rate through condenser

iii) the condenser cooling water temperature

iv) the efficiency of the outlet humidification pad

v) Cooling the condenser using deep seawater

- Effect of air flow through roof cavity
- Effect of air flow through both greenhouse and roof cavity

vi) Cooling the condenser using water at the air wet bulb temperature

- Effect of air flow through roof cavity
- Effect of air flow through both greenhouse and roof cavity

3.2.1 Results and discussion

The values of parameters not being varied were fixed at :

Condenser area	2.31 m^2 m^{-2} of greenhouse floor
Condenser heat transfer coefficient	240 W m^{-2} K^{-1} (manufacturer)
Cooling water flowrate	0.012 kg m^{-2} s^{-1}
Seawater temperature	10 °C

The greenhouse had a plan area of 432 m^2, a length of 12 m and an average height of 4 m; the height of the roof cavity was 0.55 m.

The rate of evaporation of water from the cooling pad depends on the wet bulb temperature of the air entering the cooling pad, the pad efficiency and the rate of air flow; it is independent of the type of greenhouse and the extent of any crop.

The theoretical maximum reduction in temperature equals the wet bulb depression of the air approaching the cooler, so that the air leaving the cooler can be saturated. This is undesirable in greenhouse because transpiration is suppressed at very high humidity. Consequently, the efficiency of the evaporative coolers was fixed at 80 % [Montero, 1981].

3.2.1.1 Effect of efficiency of the selective solar radiation absorber

This does have some influence on the water produced, but it is not a strong one. The reason is that water is provided both by evaporation of the seawater in the roof cavity and as transpiration from the plants. As the efficiency of the selective absorber is reduced less evaporation occurs from the roof but transpiration is increased (Fig. 3.9).

3.2.1.2 Effect of cooling water flow rate through condenser

The fin and tube. seawater-cooled condenser was modelled as a cross flow heat exchanger with the water flow mixed and the air flow unmixed. The performance was calculated using the concepts of heat exchanger effectiveness and exchanger

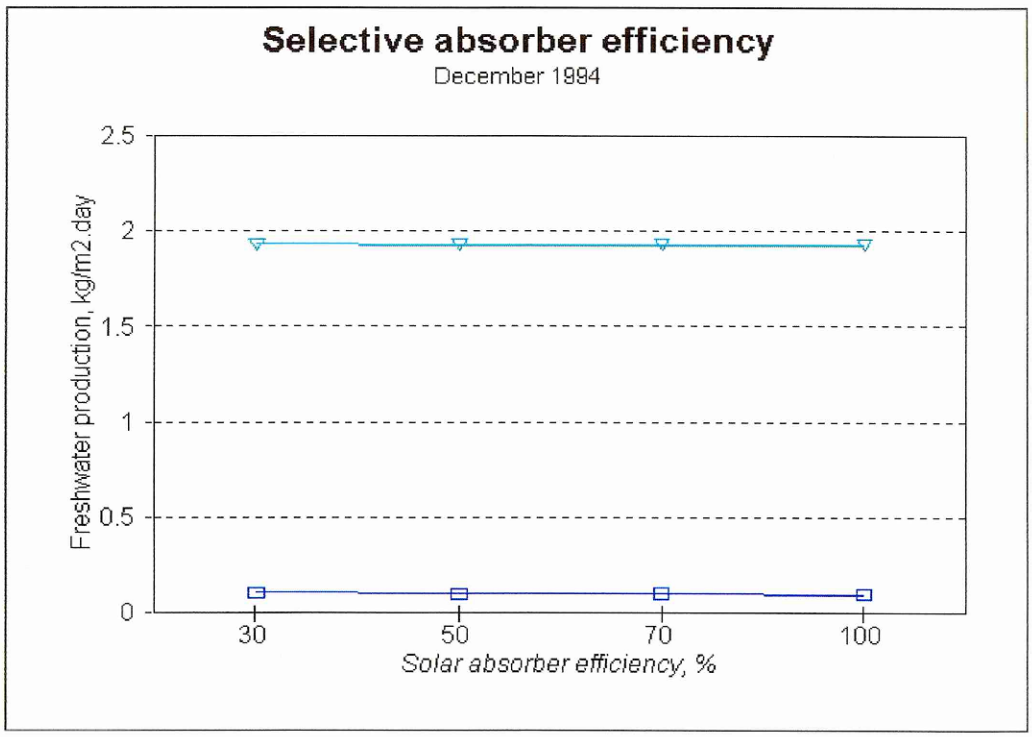

Fig. 3. 9 Effect of the selective solar absorber efficiency

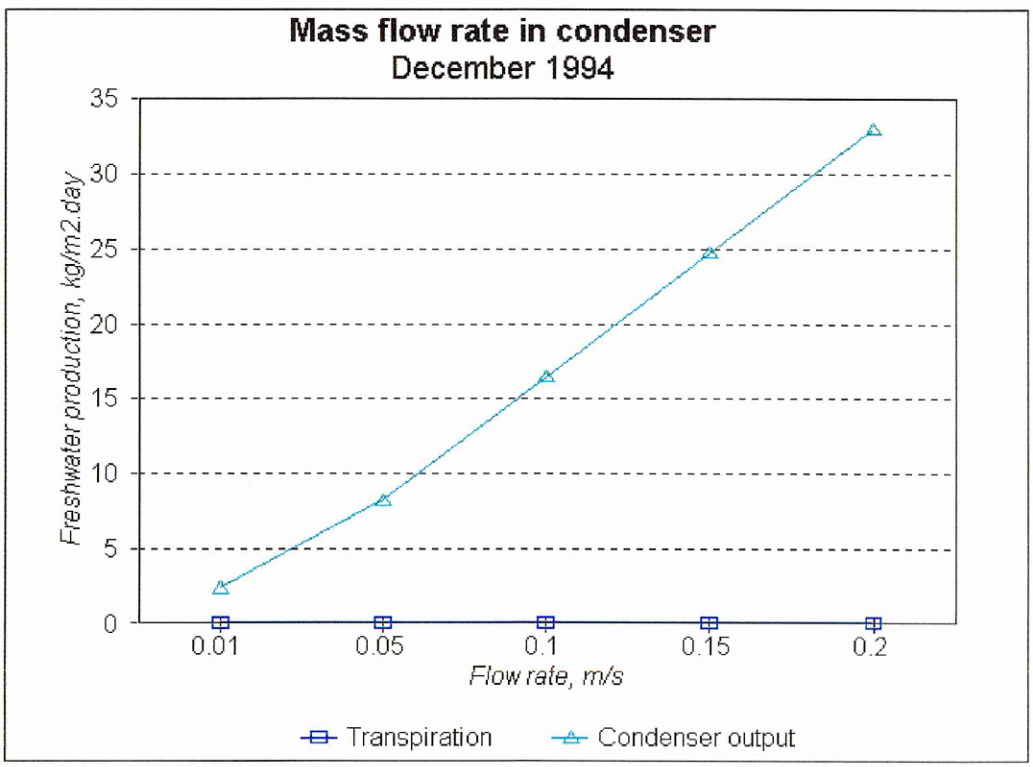

Fig. 3. 10 Effect of the condenser mass flow rate

heat transfer units. For a cross flow heat exchanger with one fluid mixed and one unmixed, the effectiveness is given [London, 1964] as:

$$\Sigma = 1 - exp\ (- P'\ C_{max} / C_{min}) \quad (1)$$

where

$$P' = 1 - exp\ (- NTU\ C_{min} / C_{max}) \quad (2)$$

and C_{max} and C_{min} are respectively the highest and lowest values of the products of the mass flow rate and specific heats of the air and water. The number of heat transfer units is:

$$NTU = A\ U / C_{min} \quad (3)$$

where A is the surface area of the condenser and U is the average heat transfer coefficient.

The water condensed was calculated from the change in moisture content and flow rate of the air passing through the condenser.

Figure 3.10 shows the influence of the condenser cooling water flow rate on fresh water production. The freshwater production increased with the increase of the mass flow rate until an upper limit. The graph does not show an upper limit but physically it mightbe one.

3.2.1.3 Effect of the condenser cooling temperature

The condenser cooling water temperature has a very strong influence on the amount of fresh water produced. The temperature of the seawater passing over the roof has little effect on the freshwater recovered from the roof. The

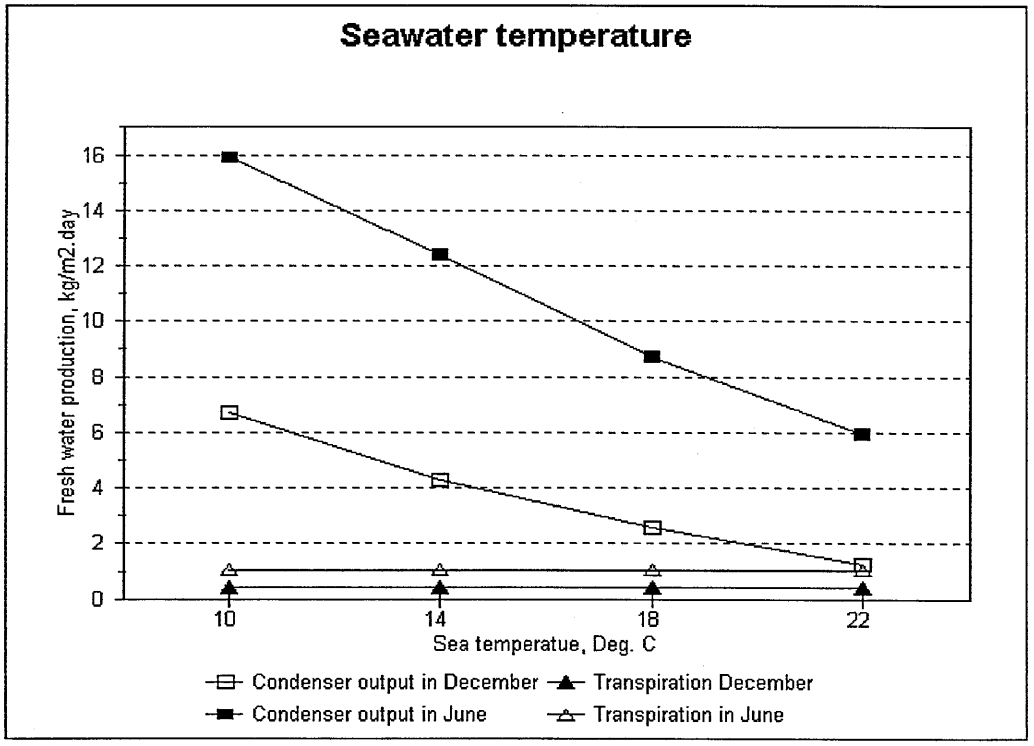

Fig. 3. 11 Effect of seawater temperature

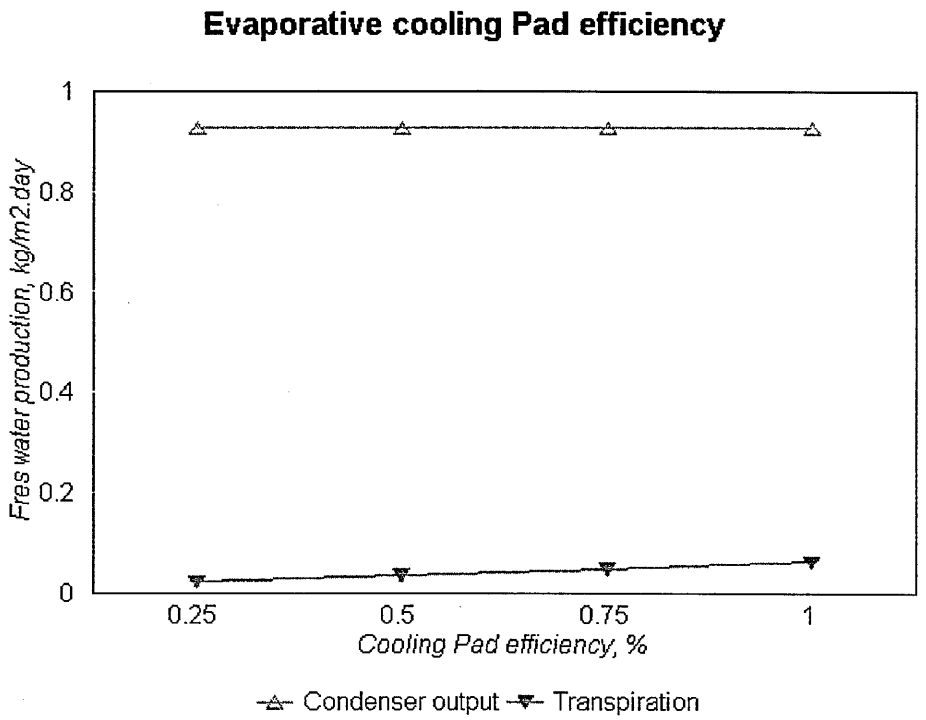

Fig. 3. 12 Effect of the evaporative cooling pad efficiency

condenser output decreased with the increase of cooling water temperature; at 22 °C the freshwater production was 6 kg m^{-2} day^{-1} in June (Fig. 3.11).

3.2.1.4 Effect of the efficiency of the outlet humidification pad

The efficiency of the second pad has little effect on the fresh water production (Fig. 3.12) because the cooling water temperature is low and the humidity was high before the air entered the rear pad.
For a condenser cooling water temperature of 10 °C the freshwater value was very low.

3.2.1.5 Cooling the condenser using deep seawater

- Effect of air flow through roof cavity

When using deep seawater to cool the condenser the fresh water production increased with increasing air speed (Fig. 3.13). With an air speed of 1.2 kg m^{-2} s^{-1} in the roof, the condenser output was 1.3 kg m^{-2} day^{-1} in June and 0.5 kg m^{-2} day^{-1} in December. Adding the second pad increased the freshwater production by 30% in June, and by 20 % in December.

- Effect of air flow through both greenhouse and roof

The fresh water production was much higher compared to the fresh water produced when the air was passing through the roof only (Fig. 3.14).

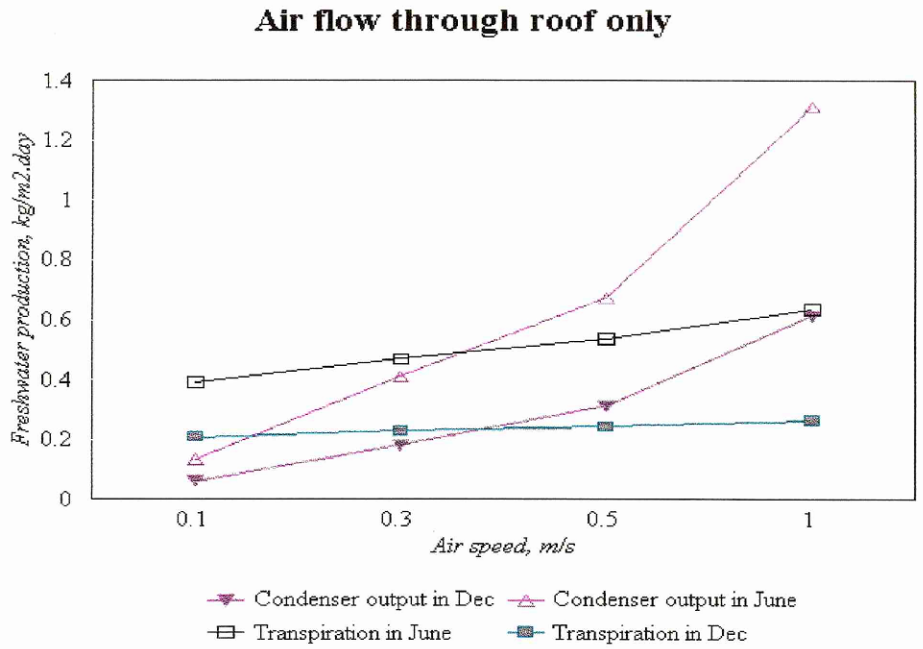

Fig. 3. 13 Effect of the air ventilation on the freshwater production for the months of December and June when using deep seawater to cool the condenser (1 pad)

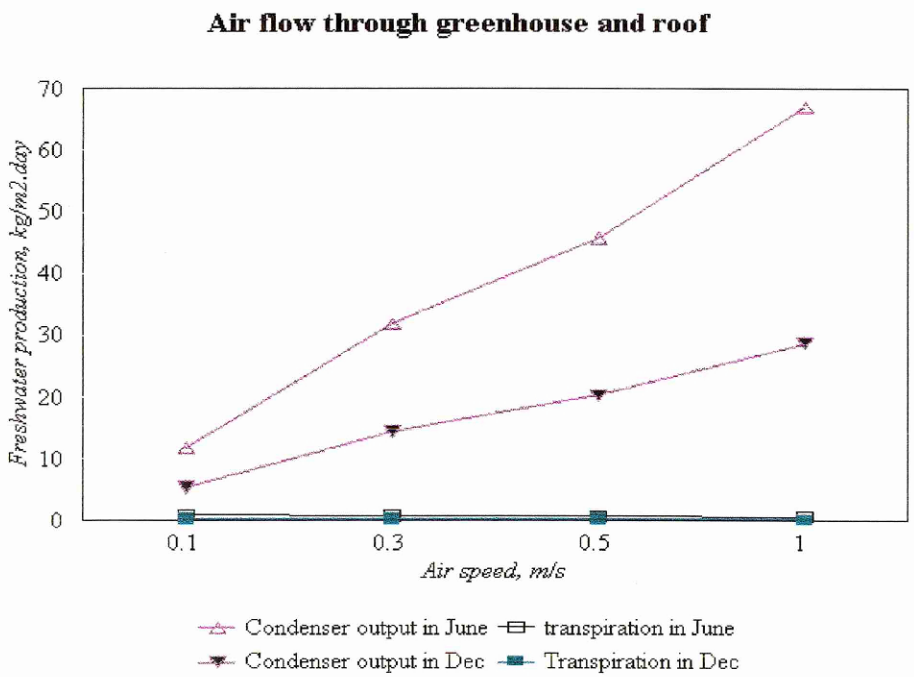

Fig. 3. 14 Effect of the air ventilation on the freshwater production for the months of December and June when using deep seawater to cool the condenser (2 pads)

3.2.1.6 Cooling the condenser using water at air wet bulb temperature

- Effect of air flow through roof cavity

When using water at the air wet bulb temperature - the maximum temperature reduction obtainable using evaporative cooling is equal to the wet bulb depression - to cool the condenser, the fresh water production increased when the air speed increased (Fig. 3.15). However, the water produced was less than the transpiration of the plants in the greenhouse. As there was no air flow through the greenhouse the transpired water condensed on the inner surface of the greenhouse roof. In principle this water could be collected. However, not ventilating the greenhouse is unrealistic as the temperature will become too high for satisfactory plant growth. When the second pad was used, the fresh water produced increased with increasing air speed.

- Effect of air flow through both greenhouse and roof cavity

The fresh water production increased when the air flow increased and gave 1 kg m^{-2} day^{-1} in June and 0.4 kg m^{2} day^{-1} in December, at an air speed of 1.2 kg m^{-2} s^{-1}; thus slowing down the air speed increases the freshwater production by raising the exit air temperature and humidity, but the higher temperature also increases transpiration. The fresh water production increased with increasing air speed and gave 8 kg m^{-2} day^{-1} in June and 3.3 kg m^{-2} day^{-1} in December, when the second pad was used (Fig. 3.16).

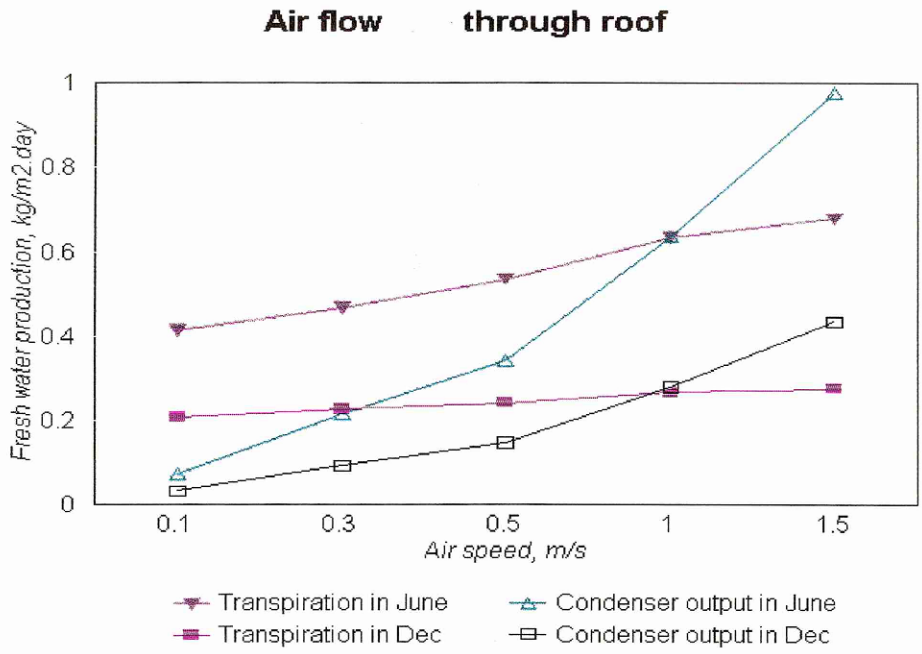

Fig. 3. 15 Effect of the air ventilation on the freshwater production for the months of December and June when using water at the air wet bulb temperature to cool the condenser

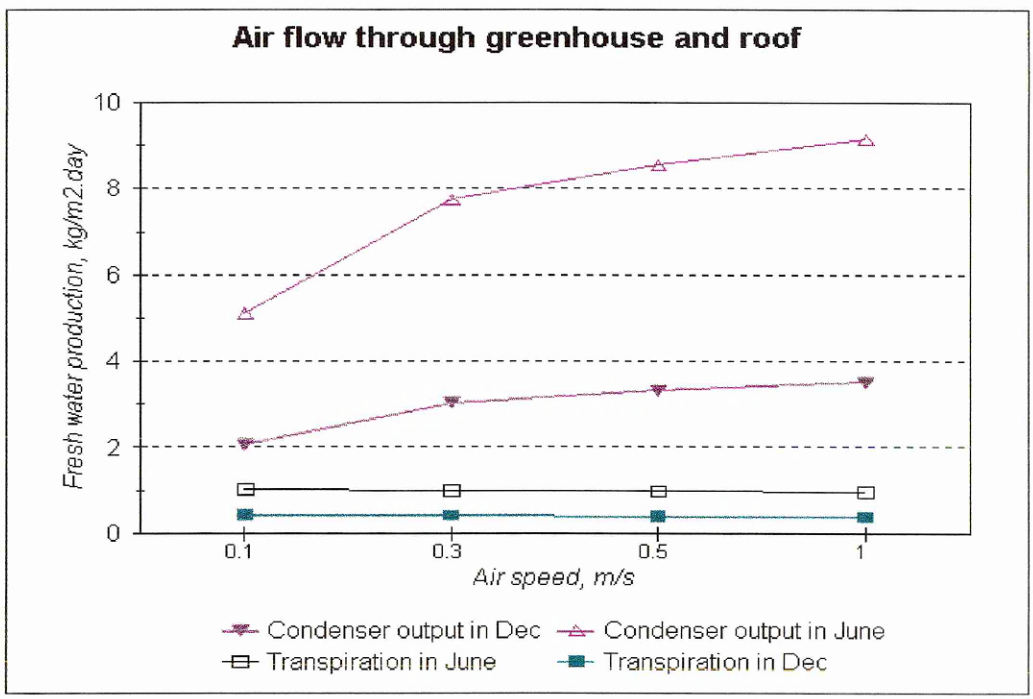

Fig. 3. 16 Effect of the air ventilation on the freshwater production for the months of December and June when using water at the air wet bulb temperature to cool the condenser

Conclusions

The spectral transmission analyses of several cover materials as well as the transmissivity to PAR radiation at different angles of incidence of the radiation was carried out and showed that the corrugated GRP material diffusily transmitted the radiation and will be used in the greenhouse roof; The average transmissivity to the PAR radiation was about the same (0.67) for both overcast and clear sky conditions and not very depending on the angle of incidence; the change with angle of incidence was ± 5 %.

The sensitivity analysis showed that the use of the outlet humidification pad increased the fresh water production compared to using only the inlet evaporative cooling pad; when using the second pad the condenser output increased 30 % in June and 20 % in December . The fresh water produced was higher when the air was passed through the greenhouse and roof compared to air passing through the roof only; the roof cavity should not be considered because of the small contribution to the water condensed (0.35 kg m^{-2} day^{-1} and 0.5 kg m^{-2} day^{-1} for the months of December and June).

The freshwater production increased with the increase of the mass flow rate until an upper limit.

The freshwater production was 6 kg m^{-2} day^{-1} with a condenser cooling water temperature of 22 °C. The use of deep seawater to cool the condenser should give more fresh water production than using water at the air wet bulb temperature, and using cooling water at the wet bulb temperature will give a lower condenser output than using surface seawater.

Chapter 4. Model

Introduction

The model of Chalabi *et al.*, 1991 was extended to include submodels to describe :

i) Evaporative cooling of ventilation air
ii) Selective absorption of solar radiation by the greenhouse roof
iii) Heating and humidification of air passing through the roof cavity
iv) Condensation of fresh water from the humid air leaving the greenhouse and the humidifiers in a seawater cooled heat exchanger.

4.1 Greenhouse model

The energy fluxes between the nodes of the model are thermal radiation, latent and sensible heat. The energy and moisture balance equations are defined per unit ground area specified at each node of the greenhouse : inside air (ia), crop (c), inner roof (ri). outer roof (ro), and ground (f). The ground node itself is sub-divided into seven layers. The heat flow is characterising the thermal conduction in the layers of the ground where the lowermost node (f7) acts a boundary node. The other boundary nodes are outside air (oa) and sky (sky) [Chalabi and Bailey, 1991].

The model is described by a set of coupled non-linear first order differential equations driven by processes specified at the boundary nodes : outside air temperature (Toa). sky temperature (Tsky), deep ground temperature (Tf7),

outside air moisture content (Woa), wind speed (wind) and solar radiation (Qsol). It is parameterized by a set of constants relating to the thermal. optical and geometrical properties of the seawater greenhouse (see appendix B) and Fig. 4.1.

The calculations of the radiative (Q^r), sensible ($Q^{c'}$) and latent heat fluxes ($Q^{l'}$) are based on equations similar to those specified in other greenhouse models. The thermal radiation flux is based on Stefan's law, the sensible heat flux is defined in terms of product of a transfer coefficient and a temperature difference whereas the latent heat flux heat is defined in terms of the product of a transfer coefficient and a vapour pressure difference.

4.1.1 Flow of air through the greenhouse

The aerodynamic studies and wind tunnel tests were made by Hellenic Technologies [1993] in order to analyse the optimum alternatives of greenhouse geometry regarding prevailing wind velocities.

The objective of the wind tunnel tests made by Grass *et al.* [1993] was to investigate the possibility of increasing the internal velocity, for fixed resistance, by modifying the intake and outlet geometry of the greenhouse using a simple air guide plate.

A simple theoretical model has been developed to provide a basis for generalising the findings from the Hellenic Technologies [1993] study. The model is based on an energy balance and provides an approximate

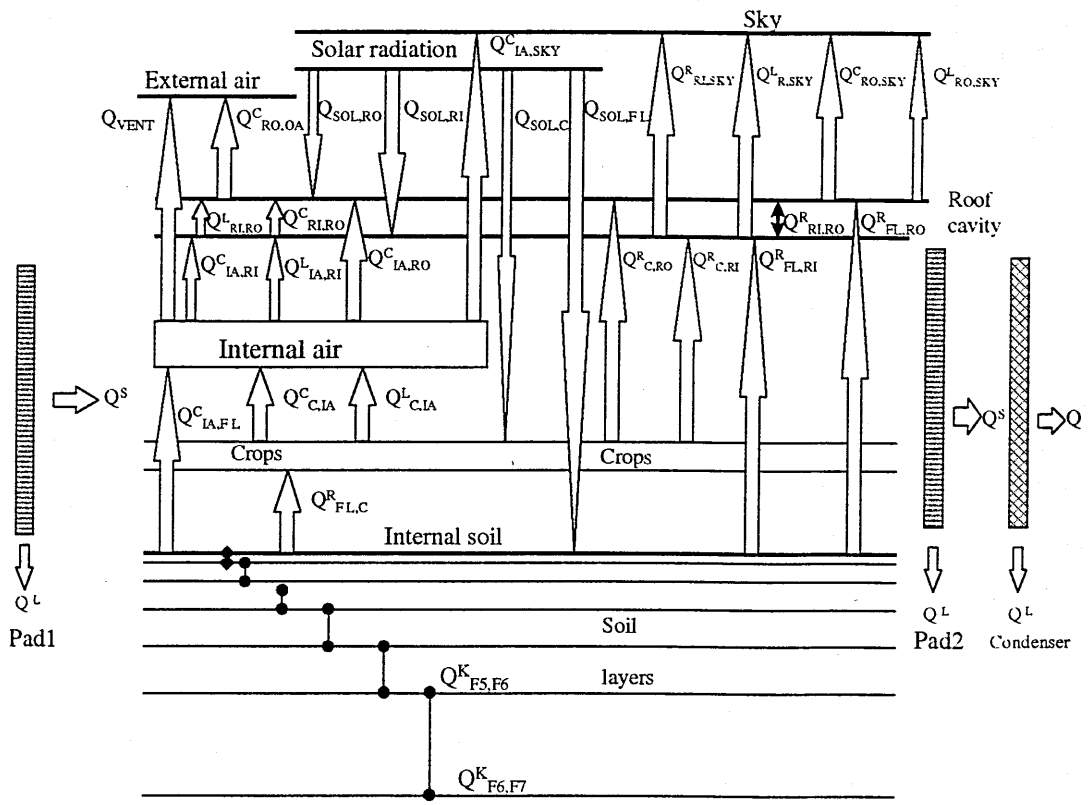

Fig. 4. 1 Energy fluxes included in the model

method for estimating the air velocity inside the greenhouse in relation to the approach wind velocity and internal flow resistance providing the flow resistance coefficients for the evaporative cooling pads.

Continuity equation :

$$U_0 = U_1 A_1 = U_2 A_2 \quad (1)$$

Energy equation

$$U_2 / U_1 = ((\alpha_a + \alpha_b)(A_2 / A_1)^2 + \alpha_c + 1 + (\alpha_a + \alpha_b)^{-1/2} = \beta' \quad (2)$$

where α_a *and* α_b are respectively the resistance coefficients for the upstream and downstream evaporative cooling pad forming a double layer. In the case of the Tenerife prototype there is only one layer thus the equation becomes:

$$U_2 / U_0 = (\alpha_a (A_2 / A_1)^2 + \alpha_c + 1 = \beta' \quad (3)$$

Values of α_a and α_c which are respectively the resistance coefficients for the Evaporative Cooling Pads (ECP) and the inside greenhouse shape were calculated by Grass *et al.* [1993] (α_a = 20.68 and α_c = 0.45) which led to the value of β' using equation (3). They used also the data of Hellenic technologies [1993] to derive the value of β' from the average of the measured percentage velocity reduction C ($C = (1-\beta')\ 100\%$) for 4 different resistance configurations tested in the model wind tunnel study:

Open suction greenhouse:	$\beta' = 0.83$
Double ECP at entrance only:	$\beta' = 0.71$
Double ECP at entrance and at exit:	$\beta' = 0.21$
Double ECP at entrance and single at exit:	$\beta' = 0.26$

The theoretical model predicts that the air velocity inside the greenhouse to be a fixed fraction of the approach wind velocity for a fixed configuration of internal flow resistance elements; this prediction is confirmed by the wind tunnel measurements reported by Hellenic Technologies [1993]. Grass *et al.* [1993] concluded that for small height vegetable plants, the additional friction to the air flow was negligible.

4.1.2 Convective heat transferConvective heat transfer

Thermal convection is the process in which heat transfer takes place between a solid surface and the fluid in contact with it. If the motion of the fluid is due to only buoyancy forces arising from density variations caused by differences in temperature, it is termed free or natural convection. If the motion is caused by externally imposed pressure differences, it is known as forced convection. In either case, the rate of heat transfer between the surface and the fluid is given by Newton' s law of cooling [McAdams, 1954]

$$Q = A\,h\,(T_S - T) \qquad \text{(W)} \qquad (4)$$

where A is the area of the surface (m^2)

h is the heat transfer coefficient $(W\ m^{-2}\ K^{-1})$

$T_S - T$ is the temperature difference between the surface and the bulk fluid (K)

This equation is deceptively simple; in practice the heat transfer coefficient can be a complicated function of the system geometry, the thermo-physical properties of the fluid and the nature of its motion. It is usually calculated from the Nusselt number (Nu) which represents the ratio of the heat actually transferred by convection to that would be transferred by conduction over the same distance if the fluid was stationary

$$Nu = h\, l' / k \tag{5}$$

where l' is a characteristic dimension of the system, h is the convective heat transfer coefficient and k is the thermal conductivity of the fluid.

Measurements of heat loss from flat surfaces in air can be described by the general relations

$$Nu = C_1\, Re^{\,n}\, Pr^{\,n} \tag{6}$$

$$Nu = C_2\, Gr^{\,m} Pr^{\,m} \tag{7}$$

The Reynolds number (Re) represents the ratio of the fluid dynamic to viscous drag forces, and determines whether the flow is laminar or turbulent.

$$Re = \rho\, v\, l' / \eta \tag{8}$$

where v , ρ , η are respectively the velocity, the density, and the dynamic viscosity of the fluid.

The Grashof number (Gr) represents the ratio of the buoyancy to viscous forces and determines whether the motion is laminar or turbulent.

$$Gr = g \beta l^3 \rho^2 (T_1 - T_2) / \eta^2 \qquad (9)$$

where g is the acceleration of gravity, β is the coefficient of cubical expansion, and $(T_1 - T_2)$ the temperature difference.

The Prandl number (Pr) represents the ratio of momentum diffusivity to thermal diffusivity; it is constant for air at the temperatures normally encountered in greenhouse and was taken as 0.71.

$$Pr = v \rho C_p / k \qquad (10)$$

where C_p is the specific heat of air.

Consequently, equations (6) and (7) can be written as

$$Nu = C'_1 Re^n \qquad (6a)$$

and

$$Nu = C'_2 Gr^m \qquad (7a)$$

The parameters C_1, C_2, C'_1, C'_2, m, and n change with the geometry and type of system. For forced convection, the exponent of Re is 0.5, for laminar boundary layer flow, while for a turbulent one, experimental results [Stanghellini, 1987] suggest it to be about 0.8. The exponent of Gr for natural

convection may be shown to be not larger than 1/3, and it is 1/4 for a laminar boundary layer flow.

4.1.2.1 Roof heat transfer

There are several expressions which are used to calculate the heat transfer coefficient at the outside of the greenhouse roof in terms of wind speed. Most of these expressions are empirically derived. The model uses the expression given by Bailey [1997]

$$HCRO = 8.0 + 3.87\ wind \tag{8}$$

The heat exchange due to free convection between the inside air and the inner surface of the roof depends on the Grashof number (Gr). Gr is function of geometry of the roof cover and is proportional to the temperature difference between the inside air and the inner surface of the roof. Bot [1983] has shown that the convective transfer of heat from the outer surface of a large multispan greenhouse roof occurs in the transition region between free and forced convection (Fig. 4.2)

$$Nu = 0.015\ Re^{0.8}\ Pr^{1/3} \tag{11}$$

$$Nu = 0.12\ Gr^{1/3}\ Pr^{1/3} \tag{12}$$

then. the equivalent Grashof number can be calculated as

$$Gr' = 0.002\ Re^{2.4} \tag{13}$$

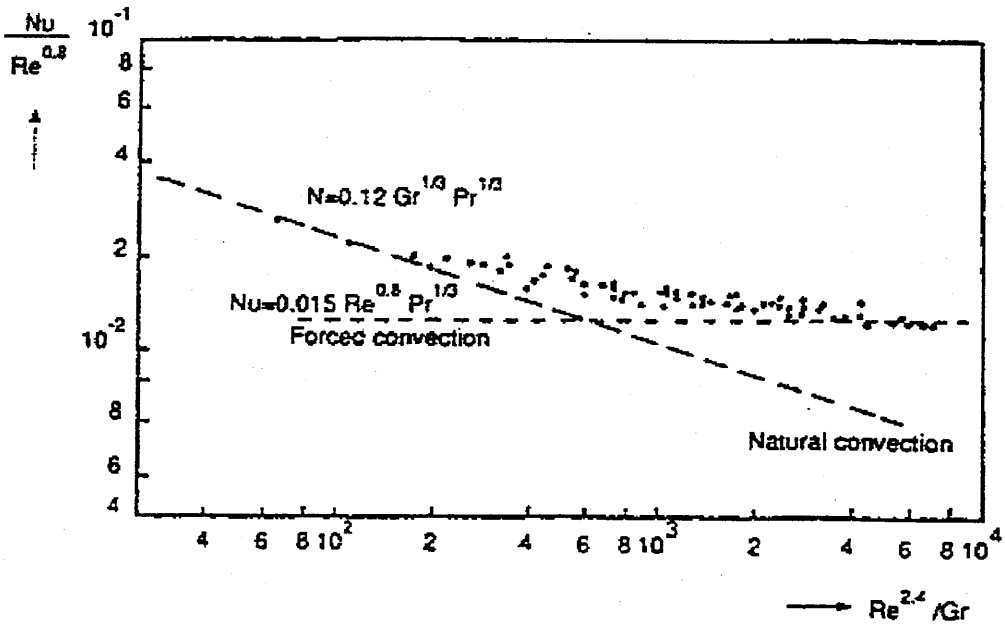

Fig. 4. 2 Convective heat transfer at the outside of a multispan glasshouse roof (Bot, 1983)

The strongest assumption was adopted, namely that Gr and Gr' have the same orientation of the flow, then:

$$Nu = 0.015\,(Gr + 0.02\,Re^{2.4})^{1/3} \tag{14}$$

The heat transfer coefficient for convection across the gap between the inner and the outer roof layers of the greenhouse is similar to that for natural convection between two flat parallel plates

$$Nu = C\,(Gr\ Pr)^{n} \tag{15}$$

4.1.2.2 Leaf heat transfer

For laminar flow. Parkhurst *et al.* [1968a] suggested the relationships for a warmer-than-air, horizontal, rectangular plate to be

$$Nu = 0.37\,Gr^{0.25} \tag{16}$$

or

$$Nu = 0.60\,Re^{0.5} \tag{17}$$

In the case of mixed convection the approach of Wang [1982] was taken in which Nu is taken as a function of Gr and Re is used to account for deviations. An equivalent Grashof number Gr', was obtained for forced convection by equating equations (16) and (17).

$$Gr' = 6.92\ Re^{2} \tag{18}$$

Borner [1965] proposed the resulting air movement should be obtained as the vector sum of the velocities of the free and forced flows. The air flow was considered vertical, and the plane of the leaf was also considered vertical. The direction of both the free and forced convective motions is then vertical and the mixed convection flux is given by [Stanghellini, 1987]:

$$Nu = 0.37\,(Gr + 6.92\ Re^{2})^{0.25} \tag{19}$$

4.1.3 Thermal radiation

Thermal radiation consists of electromagnetic radiation which is emitted by all bodies by virtue of their temperature. The thermal radiation exchanges between the nodes of a greenhouse are complex due to the nature of their geometric configurations. Rosa [1988] and Frangoudakis *et al.* [1988] presented detailed models of radiation exchanges within a greenhouse. These models are parameterised by theoretically derived shape radiation factors which are specific to the geometry in question.

The present model uses a simple equation [Gebhart, 1961] to calculate the heat transfer by radiation:

$$Q_r = h_r (T_1 - T_a) \tag{20}$$

where the radiative heat transfer coefficient h_r is defined as

$$h_r = \sigma F_{12} A\,(T_1^2 + T_2^2) \tag{20a}$$

where σ is Stefan's constant,

F_{12} is the fraction of the energy emitted by surface 1 which reaches surface 2 ($0 \leq F_{12} \leq 1$)

F is known as the shape , angle or configuration factor. For diffuse radiation F depends solely on the geometric relationship of the interacting bodies, and values for commonly encountered geometry were published by Hottel [1930] and Sparrow and Cess [1966].

Gases such as water vapour and carbon dioxide can absorb and emit thermal radiation. but their concentrations in air are so low that the effects are usually neglected for radiation exchange inside a greenhouse.

4.1.3.1 Sky temperature

The thermal temperature of the sky is influenced by air temperature, moisture content of the air and by the extent and type of cloud cover.

The emissivity of a clear sky is calculated using the equation proposed by Idso and Jackson [1969]:

$$\varepsilon = 0.261 \exp(-7.77\ 10^{-4}\ Ta^2) \qquad (21)$$

where Ta is the air temperature

The emissivity of a cloudy sky is given by Unsworth and Montieth [1975] ;

$$\varepsilon_S = (1 - 0.84\ cld) + 0.84\ cld \qquad (22)$$

where cld is the cloud cover (0 <= cld <= 1).

The effective sky temperature T_S is obtained from the formula [Bailey, 1993]

$$T_{sky}^4 = \varepsilon_s \, (T_a + 273.15)^4 \tag{23}$$

4.1.4 Conduction

When a temperature gradient exists in the ground, energy is transferred from the hotter to the colder by thermal conduction. The conduction heat transfer between two layers of the ground is given by Fourier's equation [McAdams, 1954]:

$$Q_k = \frac{k A (T_1 - T_2)}{l} \tag{24}$$

where k is the thermal conduction of the ground

l is the thickness of the layer

A is the cross sectional area through which the heat is conducted

$T_1 - T_2$ is the temperature difference

4.1.5 Latent heat

The transport of vapour towards a surface occurs by diffusion and convection, a process which depends on differences in the vapour concentration, which in

the case of water vapour are differences in the absolute humidity. It is possible to express the rate of mass transfer as

$$M' = m' A \ (Y_s - Y_\infty) \tag{25}$$

where m' is the mass transfer coefficient

Y is the absolute humidity

The equations which describe mass transfer are similar to those governing convection and as a consequence, under certain conditions [Grober and Erk, 1961], the mass transfer coefficient can be related to the convective heat transfer coefficient as

$$m' = h / \rho C_p \tag{26}$$

The transfer of latent to or from a surface when a vapour condenses or evaporates is given by:

$$Q_L = \frac{\lambda_0 \ h A \ (Y_s - Y_\infty)}{\rho \ C_p} \tag{27}$$

where λ_0 is the latent heat of vaporisation

4.1.6 Solar energy

The model assumes simply that the percentage of total solar energy absorbed by the internal nodes of a greenhouse is independent of the angle of incidence

and hence is constant during the day [Chalabi and Bailey, 1991]. The solar radiation absorbed by the outer and inner surfaces of the roof, and by the ground uppermost layer, are given respectively by:

$$Q_{SOL.RO} = a_{RO} Q_{SOL} \quad (28)$$

$$Q_{SOL.RI} = a_{RI} Q_{SOL} \quad (29)$$

$$Q_{SOL.FI} = a_{FI} Q_{SOL} \quad (30)$$

where a_i is the absorbtivity of node i.

The solar radiation absorbed by the crops is:

$$Q_{SOL} = a_c (1-exp(K_l L)(1+1 - a_{Fi})exp(-K_s L) \quad (31)$$

where K_l and K_s are the long and short wave radiation extinction coefficients of the crop, respectively.

The absorbtivity of solar radiation by each of the inside nodes are given in Appendix B.

4.2 Evaporative cooler

When warm dry air passes over an extended wet surface, water evaporates and the energy needed to evaporate the water is removed from the air which is cooled as a consequence. Thus the air leaving an evaporative cooler has a lower temperature and a higher moisture content than the air entering [Bailey, 1987].

The overall performance of the evaporative cooling system was evaluated by measuring its cooling effectiveness which depended upon the air temperatures :

$$\ddot{o} = \frac{Taia - Taoa}{Taia - Taw} \qquad (32)$$

where *Ta* is the air temperature, *ia* inside, *oa* outside and *w* the wet bulb temperature of the outside air. Similarly, the evaporative effectiveness of the cooling pad can be expressed as:

$$\ddot{o} = \frac{Yia - Yoa}{Yia - Ys'} \qquad (32a)$$

where Yoa, Yia are the absolute humidity of the external air and the air leaving the pad, and Ys' is the saturated absolute humidity at the web bulb temperature of the outside air.

Equations 32 and 32a strictly apply only in steady-state conditions when the temperature of the supply water for evaporative cooling is the same as the wet bulb temperature of the ambient air.

When used in greenhouseS evaporative cooling systems are generally designed to operate with an efficiency of 80 % [Montero, 1981]. The air leaving the cooler is then not saturated which permits plant transpiration to occur.

4.2.1 Evaporative cooling potential

The maximum temperature reduction obtainable using evaporative cooling is equal to the wet bulb depression. This was calculated as follows:
The vapour pressure, e, of air at temperature Ta is given by:

$$e = e_{S(Ta_w)} - \gamma(Ta - Ta_W) \qquad (33)$$

where e_S is the saturated vapour pressure

Ta_W is the wet bulb temperature

γ is the psychometric constant

The gradient of the saturation vapour pressure curve is

$$\frac{\delta e_{S(Ta)}}{\delta T} = \frac{e_{S(Ta)} - e_{S(Ta_w)}}{Ta - Ta_W} = \Delta \qquad (34)$$

where Δ is evaluated at the mean temperature $(Ta + Ta_W)/2$. Equations (33) and (34) can be rearranged to give the wet bulb depression.

$$Ta - Ta_W = \frac{e_{S(Ta)} - e}{\Delta + \gamma} \qquad (35)$$

The following relationships were used in evaluating this equation :

$$e_s(Ta) = Exp[70.4372-8.21n(Ta+273.15)+0.005711(Ta+273.15)-7235.4/(Ta+273.15)]$$

$$\Delta = e_s(Ta)[0.005711+(7235.4/(Ta+273.15)^2)-(8.2/(Ta+273.15))] \quad kPa\ K^{-1}$$

$$\gamma = 0.0646 + 0.000064Ta \quad kPa\ K^{-1}$$

Vapour pressure values were obtained from the moisture content values Y

$$e = \frac{Y.P}{0.622 - Y} \quad kPa$$

where P is atmospheric pressure, kPa.

In greenhouse applications, it is customary to operate evaporative cooling at 80% of the maximum efficiency. This ensures that the air entering the greenhouse is not saturated, so that plant transpiration can occur. The reductions in temperature obtainable with cooling efficiencies of 100 and 80% are given in Fig. 4.3 and the actual temperatures before and after cooling are given in Fig. 4.4. The values for 13.00 in September and October 1987 seems odd.

4.3 Condenser

The process of energy transfer that occurs in a metal heat exchanger between two fluids is extremely complicated. It involves convective heat transfer from the hot fluid to the wall, conductive transfer through the wall, and further

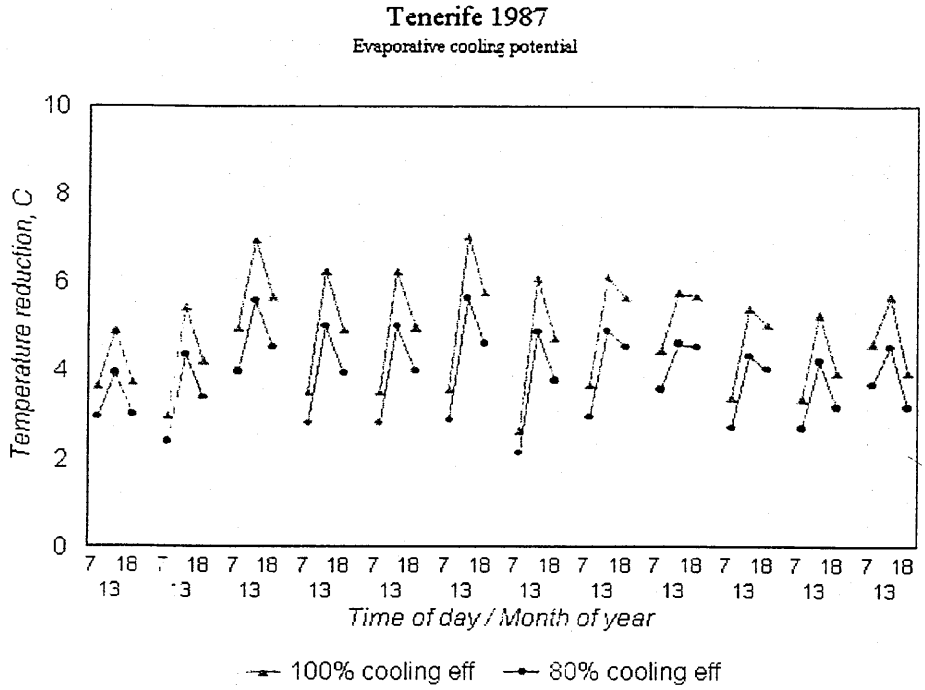

Fig. 4. 3 Reduction in air temperature obtainable with evaporative cooling

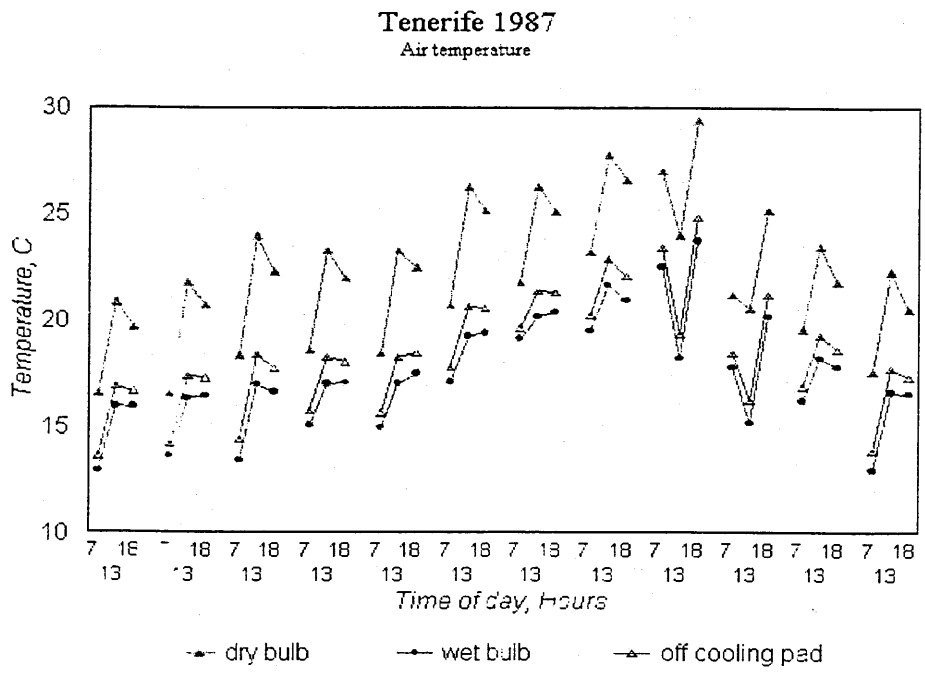

Fig. 4. 4 Air temperature with evaporative cooling

convective heat transfer from the wall to the cold fluid. The heat exchanger effectiveness is defined simply as [London, 1964]:

$$\Sigma = \frac{\text{actual heat transfer}}{\text{maximum possible heat transfer}}$$

The actual heat transferred is the energy lost by the hot fluid or the energy gained by the cold fluid. To a first approximation, neglecting all extraneous energy losses, these are equal, so that :

$$q = m''_h c_h (T_{hi} - T_{ho}) = m''_h c_h (T_{clo} - T_{cli}) \qquad (36)$$

where q is the rate of heat transfer

m'' is the rate of fluid flow

c is the specific heat of fluid

T is the temperature

The subscripts h and cl refer to the hot and cold fluids, respectively, and the subscripts o and i to fluid inlet and outlet.

The product $m''c$ of the fluid mass flow rate and the specific heat is called the capacity rate. It is possible for the hot and cold fluids to have the same capacity rate. However, it is more likely that the capacity rates will not be equal and so a minimum capacity rate C_{min} and maximum capacity C_{max} can be identified.

The maximum possible heat transfer is then :

$$q_{max} = C_{min}\,(T_{hi}-T_{cli}) \tag{37}$$

and therefore the effectiveness is :

$$\Sigma = \frac{m''_h C_h (T_{hi}-T_{ho})}{C_{min}\,(T_{hi}-T_{ci})} = \frac{m''_{cl} C_{cl} (T_{clo}-T_{cli})}{C_{min}\,(T_{hi}-T_{ci})} \tag{38}$$

where C_{min} is the smaller of C_h and C_c .

The combination UA/C_{min} is called NTU (Number of transfer units) where U is the overall heat-transfer coefficient, and A the appropriate area for heat transfer. The effectiveness-NTU relation for a counter-flow heat exchanger is described as [London, 1964]:

$$\Sigma = 1-exp((exp(-NTU*C_{min}/C_{max})-1)*C_{max}/C_{min}) \tag{39}$$

where the capacity rate ratio C_{min}/C_{max} is simply the ratio of mass flow times specific heat capacity for the two streams.

4.4 Thermal and mass balance equations

The energy balance equations were expressed in the form:

$$dT/dt' = Q/m''c \tag{40}$$

where T is the temperature

t' is the time

Q is the net energy transfer into the element

m is the mass of the element

c is the specific heat of the element

4.4.1 Thermal balance equations

The heat balance equations are specified at each of the internal nodes. Each of these nodes has a thermal capacity θ associated with it which is given by the product of the node's density, heat capacity and 'length' dimension. The energy fluxes which contribute to these energy balances are shown in Fig. 4.1. The heat balance differential equations are:

Roof outer surface

$$d/dt\ T_{ro} = (Q^{c'}_{ro,ri}+Q^{r}_{ro,ri}+ Q^{l'}_{ro,ri}+Q^{r}_{sol,ro}+Q^{r}_{ro,oa}+ Q^{c'}_{ro,sky}+ Q^{l'}_{ro,sky}+ Q^{c'}_{cri,ro}+ Q^{l'}_{cri,ro})/\theta_{ro} \quad (41)$$

Roof inner surface

$$d/dt\ T_{ri} = (Q^{c'}_{ia,ri}-Q^{l'}_{ia,ri}+ Q^{r}_{sol,ri}+ Q^{r}_{c,ri}+Q^{r}_{fl,ri}+Q^{c'}_{ro,ri}+ Q^{r}_{ro,ri}+ Q^{l'}_{ro,ri}+ Q^{c'}_{ri,sky}+ Q^{l'}_{ri,sky} + Q^{c'}_{cri,ro}- Q^{l'}_{cri,ro})/\theta_{ri} \quad (42)$$

Greenhouse air

$$d/dt\ T_{ia} = (Q^{c'}_{c,ia}+ Q^{l'}_{c,ia}+ Q^{c'}_{fl,ia}+ Q^{c'}_{ia,ri}A_r/A_f+ Q^{l'}_{ia,ri}+ Q^{c'}_{ia,ro} + Q_{inf} + Q_{vent} + Q^{c'}_{ia,sky} + Q^{c'}_{cri,ro} + Q^{l'}_{cri,ro})/\theta_{ia} \quad (43)$$

Crop

$$d/dt' \, T_c = (Q^{l'}_{c.ia} + Q^{c'}_{c.ia} + Q^{r}_{f1,c} + Q^{r}_{c,ri} A_r/A_c + Q^{r}_{c,ro} A_r/A_c + Q^{r}_{sol,c}) / \theta_c \quad (44)$$

Surface layer of floor

$$d/dt' \, T_{F1} = (Q^{c'}_{f1,ia} + Q^{k}_{f1,f2} + Q^{r}_{f1,c} + Q^{r}_{f1,ri} A_r/A_f + Q^{r}_{f1,ro} + Q^{r}_{sol,f1}) / \theta_{f1} \quad (45)$$

Surface layers of floor

$$d/dt' \, T_{f,i} = (Q^{c'}_{f(j-1)fj} - Q^{c'}_{fj\,f(j+1)}) / \theta_{fj} \; ; \quad j = 2,...,6 \quad (46)$$

4.4.2 Moisture Balance Equation

The moisture balance differential equation is specified at the inside air node :

$$d/dt' \, Y_{ia} = (M^{\cdot}_{inf} + M^{\cdot l'}_{c,ia} - M^{\cdot l'}_{ia.ri}) / (\rho(T_{ia}) S_{ia}) \quad (47)$$

where the first term is the moisture added by infiltration,

$$M^{\cdot}_{inf} = V_{al} \, \rho(T_{ia}) (Y_{oa} - Y_{ia}) \quad (48)$$

where V_{al} *is the air leakage rate*

the second term is that added by crop transpiration,

$$M'^{l'}_{c,ia} = Q^{l'}_{c,ia} / \lambda_0 (T_c) \quad (49)$$

and the last term is the moisture loss by condensation on the inner roof :

$$M'^{l'}_{ia,ri} = Q^{l'}_{ia,ri} (A_r/A_f \lambda(T_{ri})) \quad (50)$$

The moisture added by pad1 is expressed as

$$M'^{l'}_{p} = m'\eta (Ys - Yaep) \quad (51)$$

where *Ys and Yaep* are the moisture contents of the air at saturation and the air entering pad1and m' the mass flow per unit floor area of the greenhouse and η the pad1 efficiency.

4.4.3 Solution of thermal and mass balance equations

The simulation model then integrates the above equations over discrete time intervals to provide a new value of T_1.

$$T_1 = T_0 + \int_{t}^{t1} (Q/m''c)\, dt \quad (52)$$

The time step of the integration T_1 is chosen to be shorter (20 s) than the time constant simulated by equation (40). There were no effect on the freshwater production when the time step was varied from 20 s to 120 s.
The differential equations were solved using the ACSL (Advanced Computer Simulation Language).

Chapter 5 Materials and methods

5.1 Greenhouse

5.1.1 Location

The experimental greenhouse, which formed half of the total structure had a plan area of 216 m^2, a length of 12 m and a maximum height of 6 m (average height of 4 m), the height of the roof cavity was 0.55 m.

The site selected for the greenhouse was Plataforma Eolica de Grenadilla, situated in Tenerife, Canary Island, Spain. It is located on the windward coast with a predominantly rocky shoreline.

The greenhouse was situated approximately 60 m from the shoreline at an elevation of 8 m above the mean high water line (Fig. 5.1).

5.1.2 Physical description

5.1.2.1 Greenhouse

The description of the greenhouse is mentioned in chapter 3, section 3.1.

5.1.2.2 Roof cavity

The design of the roof was based upon a study of Crool [1994]. A more conventional roofing method was arrived at, where the cladding is assumed to play no part in the structural integrity of the roof. The support of the

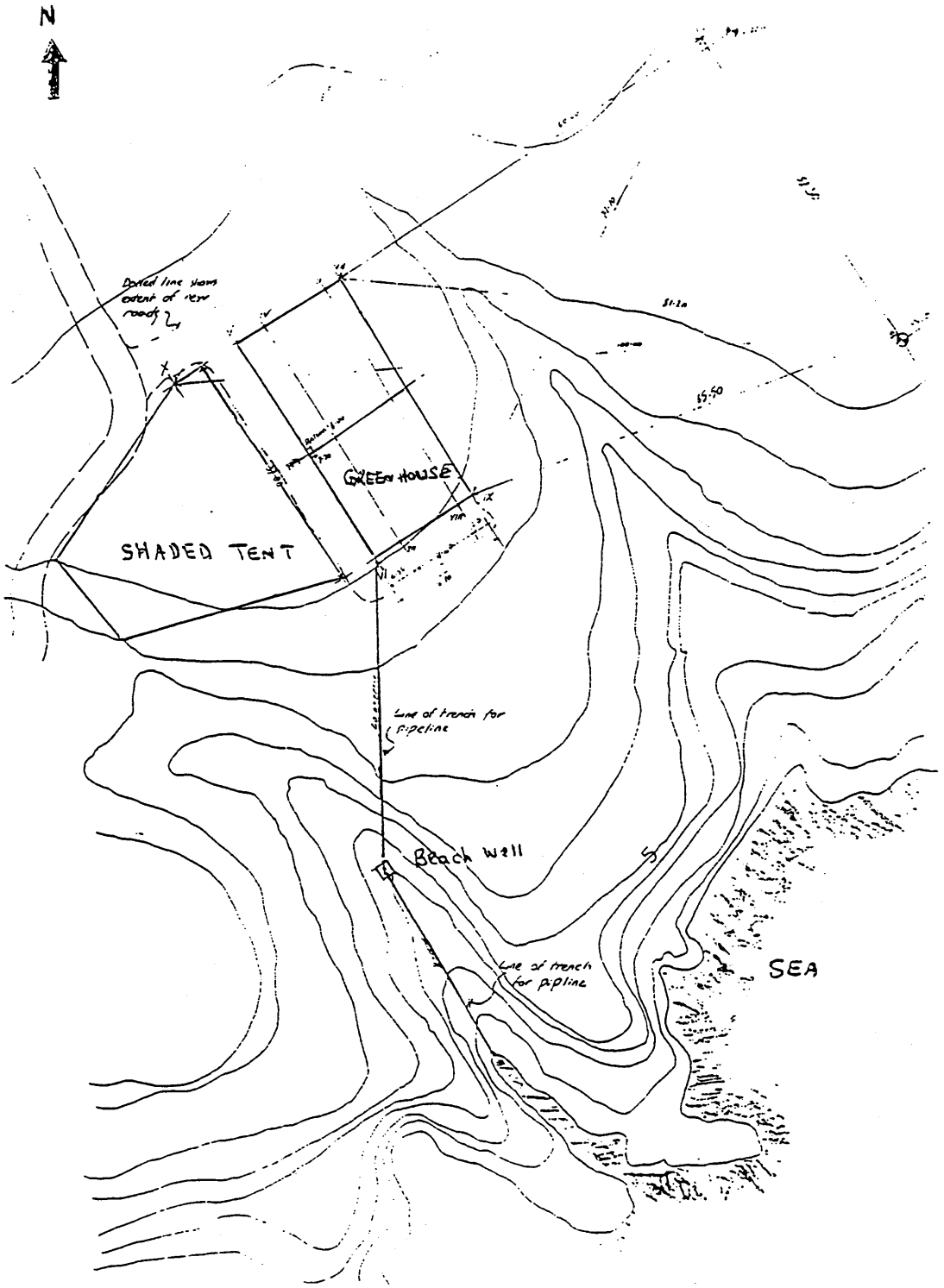

Fig. 5. 1 Greenhouse location (light works Ltd, 1995)

cladding load, and the transmission of wind and static loads was dealt with by conventional monopitch steel framework using proprietary lattice rafters.
The top skin was fixed to the underside of the upper purlins; the sheets were notched around the purlin bracket and sealed to create a free cavity. The lower skin, which was subject to a constant flow of seawater, was laid on the upper side of the lower purlin. In this way a roof void was formed with the transverse purlins on the outside and the lattice rafters between the two skins. This achieved an average gap of 550 mm between the two layers of the roof cladding into which a fine mist of seawater was sprayed. The upper skin formed a continuous plane to the rear of the building, protecting the condenser units, while the lower skin terminated at a gutter which transferred warm seawater running along the roof into a secondary evaporative pad (Fig. 5.2)

5.1.2.3 Control flap and control vents

To control the flow of air through the roof cavity and body of the greenhouse a number of trim-tabs and control vents were designed into the front wall. An air control fin, 600 mm deep winged at the top edge of the roof cavity and capable of adjustment between about 30° from the vertical, to give a minimum amount of ventilation, to horizontal (fully open). This could be used to effectively close off the entrance to the roof space.
To control the flow of the air through the primary CELdek™ evaporation pad and to allow hot air to escape on still days, a relief vent was located between the lower roof skin and the top of the CELdek™ panels (Fig. 5.2). Like the

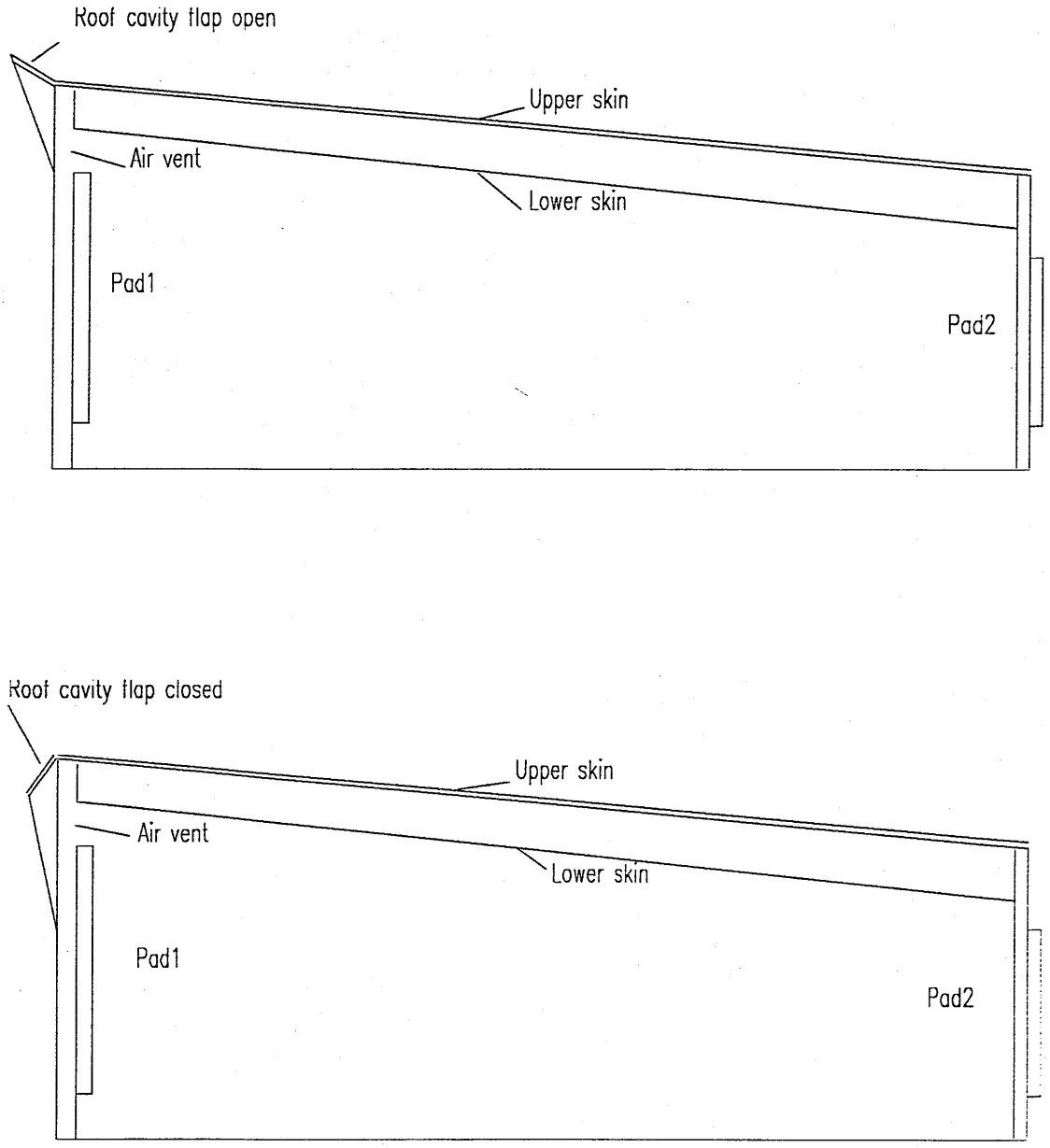

Fig. 5.2 Control flap (open and closed position) and control vents

air control flaps, these vents were operated (manually or automatically) by a rack and pinion, shaft driven, actuating system.

5.1.2.4 Spray nozzles in roof cavity

The nozzles were spaced 200 mm apart, and produced water jets, 2 mm in diameter, along the entrance to the roof cavity. The water ran down the roof and collected in a gutter that channeled it to the top of the second evaporative pad directly before the heat exchangers. It drained into a tank which fed a multistage centrifugal pump which recirculated the water.

5.1.2.5 Evaporative cooling pads

Seawater was recirculated over the front pad through which the wind blew into the greenhouse providing humidification and cooling. The water dripping off the pad flowed through a gutter and collected in a drain tank. A submersible pump in this tank pumped water back to the top of the pad. A loop was provided to divert the water to the heat exchangers at the back of the greenhouse, where the ventilation air left the greenhouse (Fig. 5.3).

5.1.2.6 Heat pump

A heat pump of nominal capacity 100 kW was used to simulate the cold seawater to cool one of the two condensers.

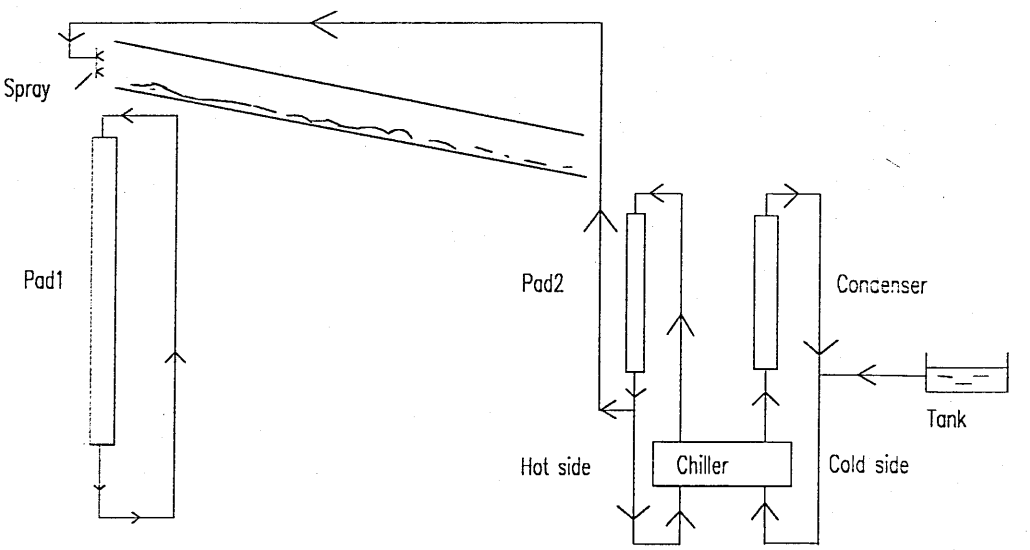

Fig. 5.3 Seawater circuit

An insulated tank was positioned just below the level of the main header tank. A centrifugal pump fed the water from the tank to the heat pump. The water then passed through the heat exchanger and returned to the tank.

The heat rejected by the heat pump was dissipated by the rear evaporative cooling pad. Outlets from the bottom of this pad led to the suction side of a circulating pump feeding the heat pump. Hot water leaving the heat pump was fed into a perforated pipe running along gutters at the top of the evaporative pad (Fig. 5.3).

5.1.2.7 Condenser

The seawater-cooled condenser was one of the most critical elements in the greenhouse. A fin and tube assembly fabricated from cupri-nickel and titanium had external dimensions of 2 m x 4 m, an internal surface area of 312 m^2 and a fin spacing of 3 mm.

5.1.3 Horticulture

The inside of the greenhouse was divided into ten beds, each being 1.2 m wide and 9.7 m long. Paths 40 cm wide were formed between each bed to allow access to all plants (Fig. 5.4).

The greenhouse planting area was covered with a 30 cm deep layer of clay loam soil. Sphagnum moss pit and goat manure were incorporated as the soil was rotavated. Black plastic woven mulch was used to cover the planting area.

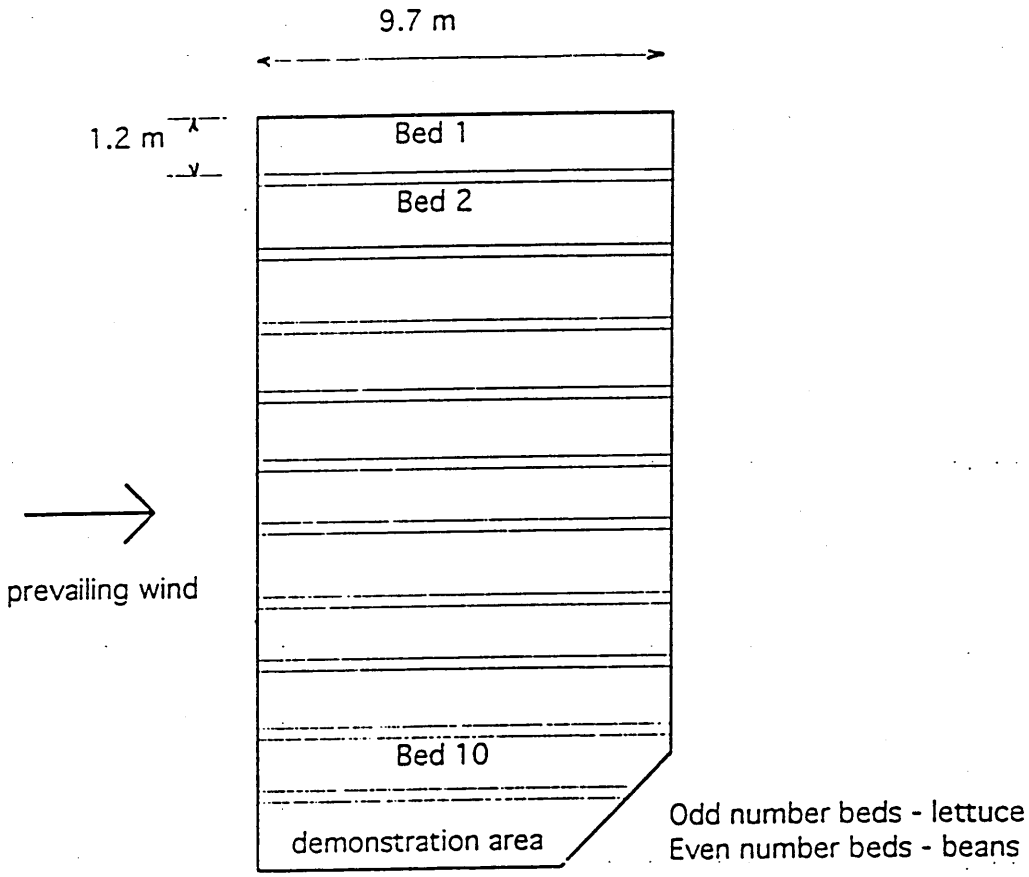

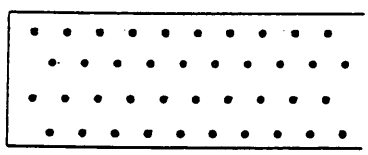

lettuces: 4 rows spaced 30 cm and 30 cm between plants

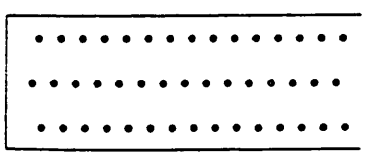

beans: 3 rows spaced 40 cm, stations spaced 20 cm, 2 seeds per station

Fig. 5.4 Planting area (Light works Ltd, 1994)

To make the most efficient use of the product water, drippers were used for each plant; each bed had an individually controlled irrigation (1 liter per hour) line running along its length with self regulating drippers. The planting scheme [Light works Ltd, 1994] consisted of 50 % French beans and 50 % lettuces.

5.2 Measurement system

5.2.1 Variables

During all the experimental runs, the following climatic parameters (Table 5.1) were continuously monitored with a data logger (Delta-T):
Outside climate: Dry and wet bulb temperatures, solar radiation, wind speed, and wind direction.
Inside climate: Dry and wet bulb temperatures inside the greenhouse and roof cavity, soil, crop, and roof fiber-glass temperatures.
Others sensors were used during some experiments to measure fresh and salt water temperatures. net radiation above the canopy, and flow rates of fresh and seawater.

5.2.2 Sensors

5.2.2.1 Temperature

All temperatures were measured using thermistor sensors. General purpose thermistors with a resistance of 2 KΩ at 25° C and an accuracy stated by the manufacturer to be ± 0.1° C over the range 0 to 70° C, were used to measure

Parameters	Sensors
Meteorological station	
Solar radiation	Dome solarimeter
Total radiation	Net radiometer
Air temperature	Ventilated psychrometer
Air humidity	Ventilated psychrometer
Wind speed	High resolution anemometer
Wind direction	Wind vane
Seawater greenhouse	
Air temperature leaving pad1	Ventilated psychrometer
Air temperature entering and leaving pad2	Ventilated psychrometer
Air temperature inside greenhouse at 1.6 m	Thermistor
Crop temperature	Thermistor
Soil temperature at 0 m and -1 m	Thermistor
Air humidity leaving pad1	Ventilated psychrometer
Air humidity entering and leaving pad2	Ventilated psychrometer
Air humidity inside greenhouse at 1.6 m	Ventilated psychrometer
Ventilation air velocity inside greenhouse	High resolution anemometer
Roof cavity	
Air temperature inside roof cavity	Ventilated psychrometer
Inner roof temperature	Thermistor
Outer roof temperature	Thermistor
Air humidity inside roof cavity	Ventilated psychrometer
Ventilation air velocity inside roof	High resolution anemometer

Table 5. 1 Variables measured during the experiments and sensors

soil temperatures (Fig. 5.5): ground (sensors covered with a layer of 2 cm of soil) and 1m deep (the sensor was in a hole 1m deep filled with soil), inner and outer roof layers (to avoid heating the sensors were covered with a white compound and attached to both roof surfaces), and inside air temperatures (sensors were positioned after the pad at a height of 1.6 m and in the middle of the greenhouse at heights of 1.6 and 3.2 m). Another version of these sensors which had a sheath-to-cable seal and corrosion-resistant cable to improve operational life, was used to measure the temperature of the fresh water produced. Similar sensors were used to measure temperatures of the seawater leaving the front evaporative cooling, entering and leaving the rear evaporative pad and leaving the roof cavity. The leaf temperatures were measured by a high precision thermistor, which was attached to the leaves (Fig. 5.5), with an accuracy of $\pm 0.1°$ C over the range 0-70 °C.

5.2.2.2 Humidity

The wet and dry bulb temperatures of the outside air, the air after the front and rear evaporative cooling pads, and in the roof cavity were measured by ventilated psychrometers. A 12V DC fan provided ventilation to achieve the wet bulb temperature. The relative humidity (RH), and vapour pressure were subsequently calculated from the logged wet and dry bulb temperatures by the use of an appropriate formulae [British Standard, 1965].

The length of the cables used were 15 m. 20 m, 35 m, 40 m and 50 m; the resistance of each cable core is 8.8 Ω per 100 m.

Close matching of the temperature sensors is particularly important if readings of the relative humidity (RH) are to be derived from the wet and dry

Fig. 5.5 Crop and soil temperature thermistors

temperatures, since RH is determined from the temperature difference between the sensors.

5.2.2.3 Solar radiation

Solar radiation was measured by a Delta-T Dome Solarimeter. The sensor was a high quality, blackened thermopile protected with a transparent glass covering dome. The sensor has a flat spectral response over the range 0.3 to 3.0 μm, this being the full solar spectrum.

Heating of the sensor by incoming solar radiation produced a signal in the microvolt range. Each sensor was supplied with its own calibration factor to convert the output voltage into units of W m^{-2} (Table 5.2).

5.2.2.4 Net Radiation

The net flux of radiant energy experienced by a surface was measured by a net radiometer (pyradiometer). Net radiation is the balance of the downward and upward fluxes of the combined short-wave and long-wave radiation. The spectrum of radiant energy involved includes short wavelengths of solar origin (0.3 - 3 μm) and longer wavelengths of terrestrial and atmospheric origin (3 - 100 μm). The net radiometer has a typical sensitivity of 10 mV $kW^{-1}m^{-2}$. The output voltage is directly proportional to net irradiance. and will be positive during the day, rising to a maximum of about 700 W m^{-2}. and range from zero to small negative values (< -100 W m^{-2}) at night.

Sensors	Calibration factors
Dome solarimeter	19.13 x 10^{-3} mV kW^{-1} m^{-2}
Net radiometer	9.86 mV k W^{-1} m^{-2}
Ventilated psychrometer	2 KΩ at 25 °C
Wind vane	2.712 Ω / degree
Anemometer	10 kHz per ms^{-1} Pulse rate

Table 5. 2 Sensors calibration factors

5.2.2.5 Wind speed

Three anemometers were used during the course of the experiments. These were capable of measuring wind speeds of over 75 m s^{-1} with a threshold of 0.15 m s^{-1}. The calibration factor varied by less than ± 1% over the range 10-55 m s^{-1}.

5.2.2.6 Wind direction

A wind vane was used to measure the wind direction. It incorporated a micro-torque wire-wound 1 kΩ potentiometer with a filled gap to provide smooth operation and a long life.

The maximum wind speed was 75 m s^{-1} with a threshold of 0.6 m s^{-1} (the fin commenced movement when aligned at 45 degrees to the air flow).

The accuracy obtainable in steady winds over 5 m s^{-1} was ± 2 degrees.

5.2.2.7 External conditions

A set of meteorological instruments, mounted near the greenhouse, included a psychrometer, net radiometer, solarimeter, anemometer and wind vane (Fig. 5.6).

5.2.2.8 Data recording

A Delta-T logger was used to record experimental data. It accepted analogue and digital inputs. and had 4 resident channels (2 digital inputs, 2 relay outputs) and the memory held over 16000 timed readings.

The logger accepted voltage, current, resistance, logic state, pulse train and contact closure inputs. in almost any type of measuring configuration. A sensor library of pre-stored and user-defined conversions factors turned measured quantities into engineering values.

The Delta-T logger was programmed with software running on a PC computer. Each channel was configured for an individual sensor type, the measurement range, and data conversion characteristic.

Programming the logger, and the subsequent collection of data, was carried out via the built-in RS232 serial port. This allowed direct connection to a computer and to printers .

The analogue input card had a capacity of 30 channels for single-ended voltage measurement, or 2-wire resistance measurements, or 15 channels for differential voltage or 3-wire resistance measurements.

The digital input card provided 15 pulse or event counting channels, with 16-bit capacity (total counts 65472). A total of 62 counter channels were provided, if the two resident digital inputs were also used as counters.

Logging was started from the Delta-T's front panel keypad.

The two resident output relay channels were used in two ways:

i) To provide warnings of malfunctions: signal sensor faults, battery failure or memory full

ii) For warming-up: for energy conservation to power-up a sensor prior to taking a reading

Current readings from all active channels could be displayed on the computer screen by using the channel report facility. This also listed any malfunctions detected during logging. Data in files already collected could also be scrolled through on the screen.

Fig. 5. 6 Weather stations in December 1994 and June 1995

5.3 Experiments

5.3.1 December

The first series of experiments were carried out in Tenerife from 20-23 December 1994 . Sensors to measure the required environmental variables were installed in the greenhouse and the roof cavity, and the outside variables were measured with sensors in a meteorological station placed 3m (there were not enough cables to place it in the best position) on the right side of the greenhouse (seaside) (Fig. 5.2). The readings of all the sensors were recorded every 5 minutes using the data logging system. Three experiments were carried out:

i) Closed greenhouse (no air flow in roof, no ventilation air flow)
ii) Greenhouse with ventilation open (air gap)
iii) Greenhouse with ventilation open and roof cavity open

During all experiments, manual spot measurements were made of the seawater temperature entering and leaving the two evaporative cooling pads and the roof cavity. the fresh water temperature, and the seawater flow rate entering both evaporative cooling pads and the roof cavity.
As the 15 analogue channels of the logger were not sufficient to measure all the variables needed, manual spot measurements were made of the variables not connected to the logger (Table 5.3).
Sensors were positioned in the middle of the greenhouse (Fig. 5.3), at a height of 1.6 m above the soil in one row of green beans which was 45 cm high.

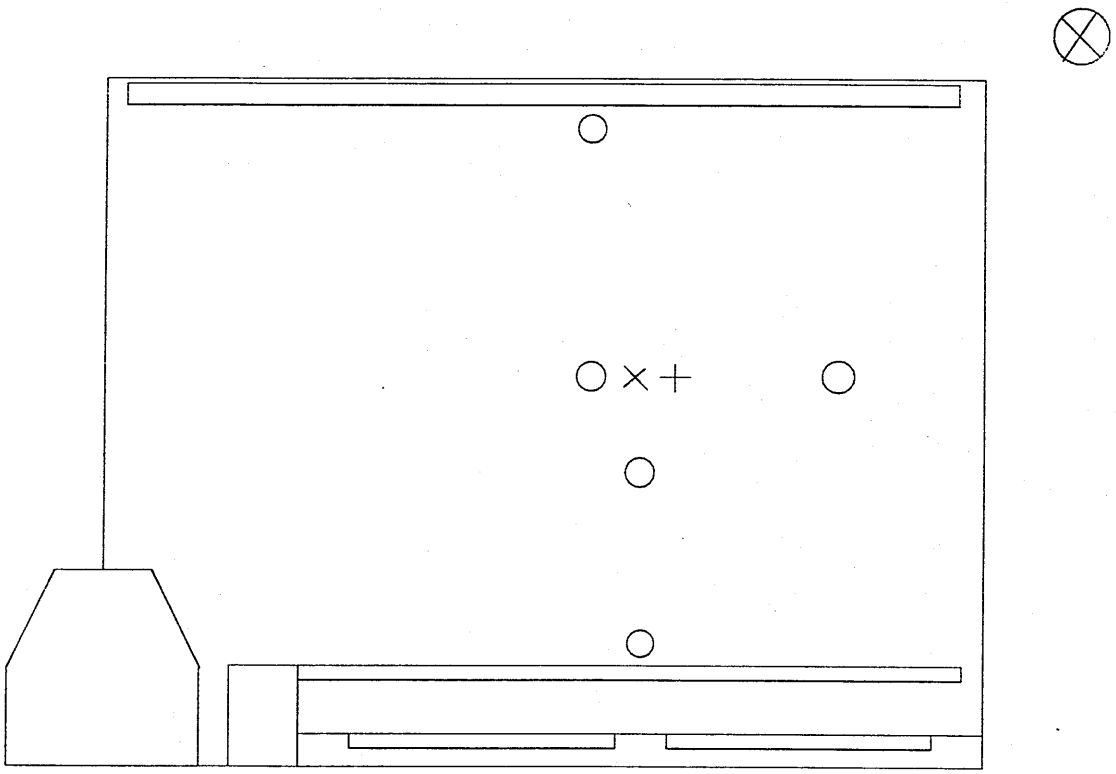

Thermistors

Psychrometers

Anemometers

Weather station

Fig. 5. 3 Sensors position in December 1994

A first measurement test was made for 2 hours to check the consistency of the measured variable values, the sensors were recorded every 10s. An air temperature profile inside the greenhouse was measured during the first experiment. During the third experiment, the anemometer measuring the ventilation air velocity entering the air gap was used to measure the ventilation air velocity inside the greenhouse. An air velocity profile in the middle of the greenhouse was measured also during the third experiment. A check of the air temperature inside the greenhouse was made by positioning a thermistor sensor near the psychrometer at the same height. The crop temperature measurements were first made 2m and 6m along a 10m row of lettuces and then in the middle of the row (5m).

5.3.2 June

The second series of experiments was carried out in Tenerife from 2-15 June 1995. Sensors to measure the required environmental variables were installed in the greenhouse and in the roof cavity, and the outside variables were measured with sensors in a meteorological station placed 30 m in front of the greenhouse. Figure 5.4 shows the position of the sensors. There were 30 analogue channels (another analogue input card of 15 channels was added) and 15 digital channels for measurement. The readings of all the sensors were recorded every 5 minutes using the Delta-T logger. Two experiments were carried out:

i) Closed Greenhouse

ii) Air flow through both greenhouse and roof cavity

20/12/94

Seawater flow rate pad1 = 5.4 m^3/h
Seawater flow rate pad2 = 11.6 m^3/h

Time	Taep2 °C	Waep2 %	Talp2 °C	Walp2 %	Talc °C	Walc %
15.00	19.9	81.8	19.0	87.3	19.8	83.4
15.20	19.6	81.4	18.4	89.5	19.9	83.5
15.35	19.0	78.7	18.8	84.5	18.7	84.5
16.00	18.5	80.5	18.1	83.6	18.1	85.3
16.35	18.6	80.6	18.0	83.5	17.8	86.8

Water temperature in °C							
Time	Pad1		Pad2		Condenser		Fresh water
	in	out	in	out	in	out	
12.30	17.5	17.3	22.5	16.2	8.9	14.1	19
14.50		17.8	23.5	17.1	8.9	14.1	19.4
15.40		17.4	22.9	17.4	9.0	14.1	16.1
16.55		16.5	21.7	16.3	8.9	14.1	14.8

21/12/94

Seawater flow rate in roof = 2.5 m^3/h

Time	Talp1 °C	Walp1 %	Tia °C	Wia %	Taep2 °C	Waep2 %	Talc °C	Walc %
15.00	19.1	74.5	19.8	71.3	19.2	72.2	19.7	71.7
15.30	20.2	75.8	20.1	75.3	19.6	76.4	21.2	74.2

Water temperature in °C									
Time	Pad1		Pad2		Roof		Condenser 1		Fresh water
	in	out	in	out	in	out	in	out	
11.00	17.3	16.9	18.4	16.3			8.9	13.4	15.4
15.00	17.1	17.0	21.8	15.8	16.8	17.8	8.7	15.4	15.4
16.00	17.6	17.6	20.6	15.9	16.5		8.6	13.7	15.6

Table 5. 3 Manual spot measurements

There were 2 days of experiments for the closed greenhouse only and 3 days for the ventilated greenhouse and roof cavity.

Sensors were positioned in one row of green beans (height 30 cm) in the middle of the greenhouse. A first measurement test was made during 24 hours to check the consistency of the measured variable values. After series of measurements of the ventilation air speed leaving the rear pad the anemometer was moved to measure the air speed inside the greenhouse and the speed after the condenser. A wind speed profile in front of the rear pad was measured during the third experiment. The crop temperature measurements were made in the middle (5 m) of a row of lettuces.

The predominant direction of the wind approaching the greenhouse was measured and was in general NNE (55 degrees) while the front pad was orientated towards NE (45 degrees).

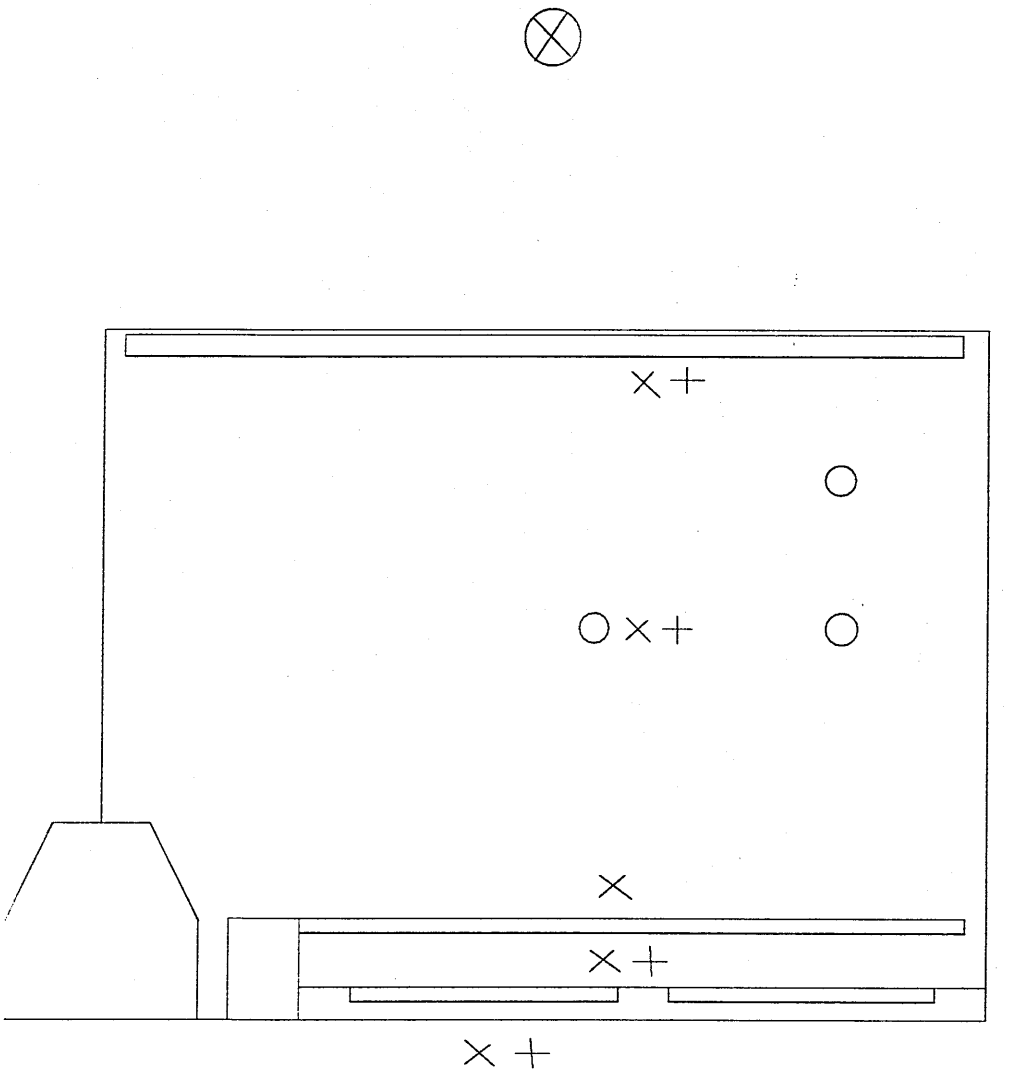

Thermistors

Psychrometers

Anemometers

Weather station

Fig. 5. 4 Sensors position in June 1995

Chapter 6 Evaporative cooler rear pad

Introduction

The purpose of this chapter is to develop a model which describes the heat and mass transfer characteristics of a CELdek™ pad used as an evaporative heat exchanger and as a condenser. Experimental data were recorded in a prototype greenhouse in Tenerife where CELdek™ was used as an evaporative heat exchanger to dissipate energy from a water chiller. The performance of a prototype condenser with cooling tubes inserted in the the CELdek™ matrix and over which the condensed water was recirculated was measured in the laboratory. Heat and mass transfer coefficients were obtained for a fixed rate of water flow over the CELdek™ pad when used as an evaporative heat exchanger. Heat and mass transfer coefficients, based respectively on the tube fluid to water film and the water film to air. were obtained for the condenser.

6.1 Theory

6.1.1 CELdek™ evaporator

The heat rejected by the heat pump was dissipated by the evaporative cooling pad. Outlet from the bottom of this pad lead to the suction side of a circulating pump feeding the heat pump. Hot water leaving the heat pump was fed into a perforated pipe running along gutters at the top of the evaporative pad (Fig. 6.1).

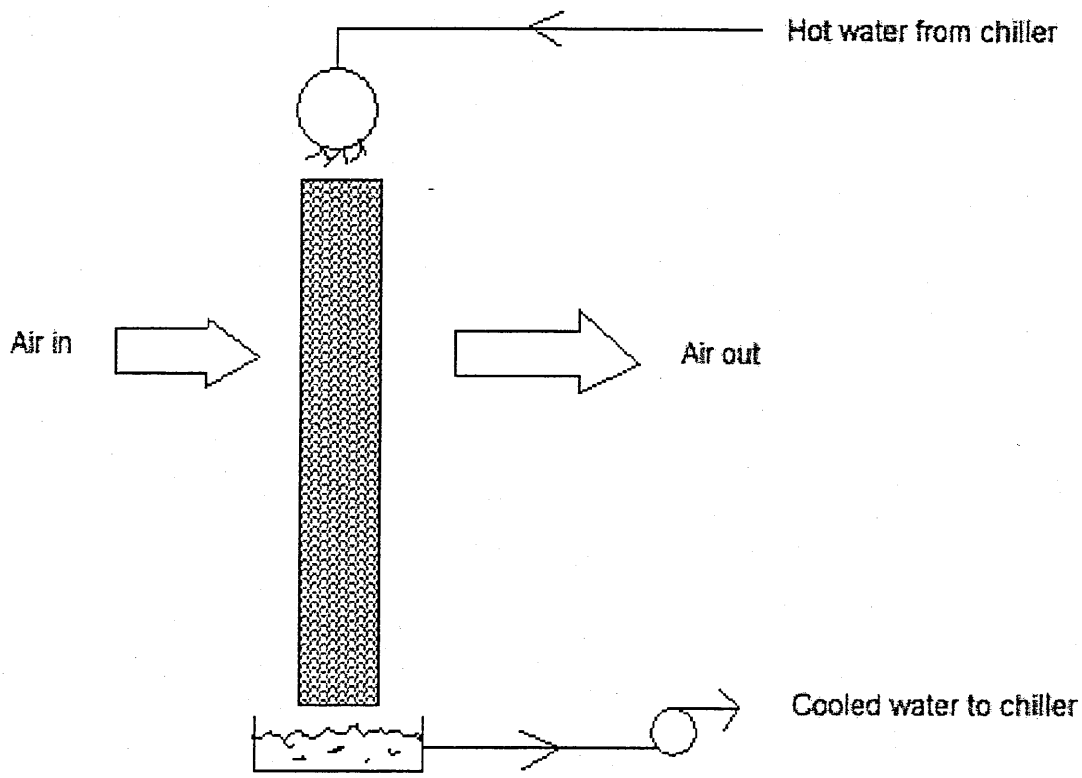

Fig. 6. 1 Evaporator CELdek™

The rear pad was considered as a cooling tower-heat exchanger; the packing was cellulose. The heat given to the air stream was at the expense of the sensible heat of the water.

Heat and mass transfer coefficients for the CELdek™ evaporator was determined using experimental data for Tenerife.

The basic equations for combined mass and heat transfer phenomena have been given by Merkel [1925] and McAdams [1954]. The equations for the air-water system involve a mass transfer coefficient, k_y, together with the enthalpy as driving force.

In the evaporator, mass and energy balances for an infinitesimal volume of thickness dz and cross sectional area A (Fig. 6.2) give [McAdams *et al.*, 1954]

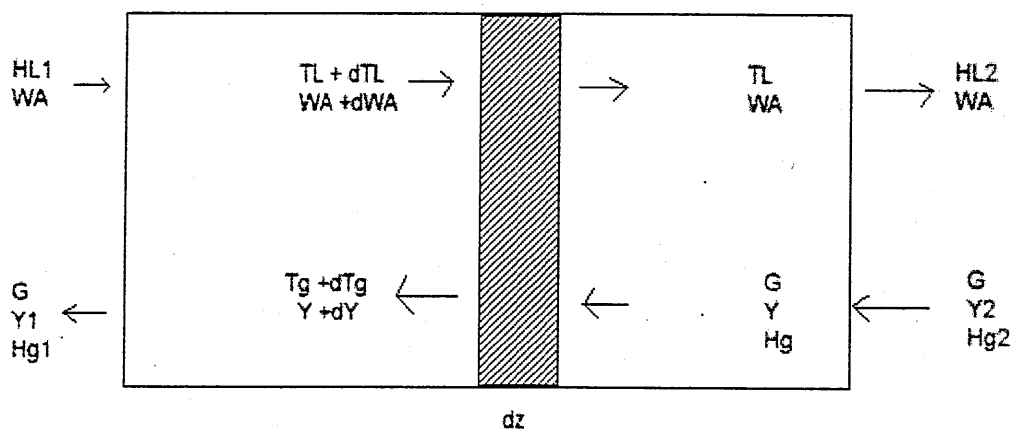

Fig. 6. 2 Evaporation mathematical model

$$G\,dH_g = W_A\,c_g\,dT_g \qquad (1)$$

where

$$H_g = c_s T_g + \lambda_0 Y \qquad (2)$$

The heat and mass balance at the water-air interface in the same infinitesimal volume of height dz give

(i) Heat transfer from bulk water to interface

$$dq_w = W_A c_g \, dT = h_l \, a_h A \, (T_L - T_i) \, dz \qquad (3)$$

where T_L and T_i are the water temperatures at the bulk and interface respectively.

(ii) Heat transfer from interface to air (sensible q_s and latent q_l):

$$dq_s = G' \, c_g \, dT_g = h_g \, a_h (T_i - T_g) \, dz \qquad (4)$$

$$dq_l = G' \, dY = \lambda_0 \, k_y \, a_m (Y_i - Y) \, dz \qquad (5)$$

The addition of equations (4) and (5) gives the total heat expressed by equation (6) as well as the total heat given by air:

$$dq_w = dq_s + dq_l = G' \, dH_g$$
$$G' dH_g = k_y \, a_m (H_i - H_g) \, dz \qquad (6)$$

The contact areas per unit volume of the CELdek™ the heat and mass transfer, a_h and a_m respectively are assumed equal ($a_h = a_m = a$) along the pad.

During adiabatic humidification of air, i.e. when water temperature is equal to the air wet bulb temperature and the air stream enthalpy is almost constant, the following relations hold across the CELdek™ [Younis *et al.*, 1993]

$$c_g\,(T_{g2} - T_{g1}) = \lambda_0 (Y_2 - Y_1) \tag{7}$$

$$-G'\,c_g\,dT_g = h_g\,a\,(T_L - T_g)\,dz \tag{8}$$

where T_L substitutes T_i

Integrating the last equation between the inlet and outlet conditions gives

$$Ln\left(\frac{T_{g1} - T_L}{T_{g2} - T_L}\right) = \left(\frac{h_g\,a}{G'\,c_g}\right) Z \tag{9}$$

Hence

$$h_g\,a = \frac{G'\,c_g}{Z}\,Ln\left(\frac{T_{g1} - T_L}{T_{g2} - T_L}\right) \tag{9a}$$

A similar expression for mass transfer can be obtained by the use of equation 5,

$$Ln\left(\frac{Y_L - Y_{g1}}{Y_L - Y_{g2}}\right) = \left(\frac{kya}{G'}\right) Z \tag{10}$$

Hence

$$kya = \frac{G'}{Z} Ln \frac{(Y_L - Y_{g1})}{(Y_L - T_{g2})} \qquad (10a)$$

6.1.2 CELdek™ prototype condenser

The condenser was made from CELdek™ and had been modified by Light Works Ltd [1994] by the insertion of water tubes through which the simulated cold seawater flowed. Pure water was pumped to the top of the pad from a sump to increase the effective heat/mass exchange area. Vapour from the humid air was condensed by this water as it descended over the wet surface of the pad (fig. 6.3).

The heat transfer from the water inside the tube to the spray water interface is dealt with using an over-all coefficient of heat transfer U as suggested by Colburn [1933] and Hougen [1934]

$$\frac{1}{U} = \frac{Do}{D_i h_i} + \frac{Do\,L}{D_m k} + \frac{1}{h_{LEC}} \qquad (1)$$

The rate of heat transfer to the interface would be given by

$$dQ_T = U(T - t_i) \qquad (2)$$

The transfer of enthalpy from the air-water interface to the air-stream is treated as a problem in the simultaneous transfer of heat and mass using a mass

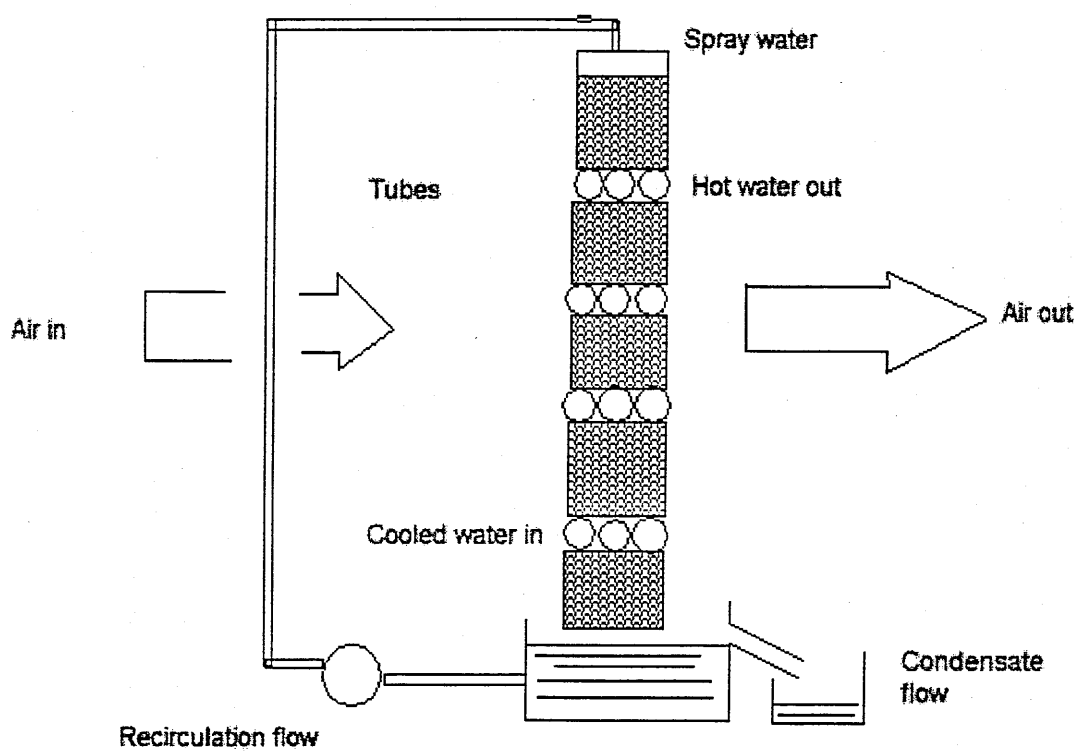

Fig. 6. 3 Experimental celdek™ condenser

transfer coefficient, k_y, with an enthalpy potential difference after Merkel [1925] and Hirsch [1927]

$$dQ_T = G'dH = k_y(H - H_i)dA \qquad (3)$$

The film coefficient for the transfer of heat from the outer surface of the tube to the spray water is included in U (equation 1), that for the transfer from the spray water to the air-water interface is included in K:

$$\frac{1}{K} = \frac{1}{k_y} + \frac{m}{h_L} \qquad (4)$$

[Parker *et al.*, 1960] proposed the new idea of dividing the exchanger at the bulk spray water temperature, rather than at the interface temperature as has been the practice before. Consider an element of an evaporative cooler, Fig. 6.4. One can write:

The heat gained by the tube fluid

$$W_A c\, dT = U A\, dz\, (T - t) \qquad (5)$$

Can be rewritten

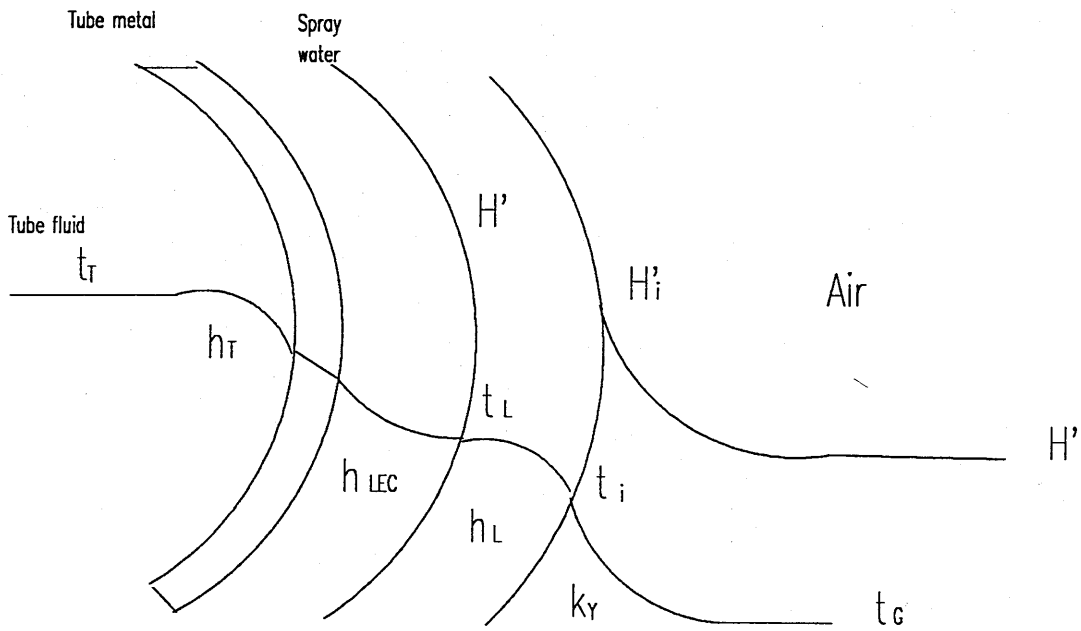

Fig. 6. 4 Temperature and enthalpy gradient (Parker and Treybal, 1960)

$$\frac{dT}{dz} = \frac{UA}{W_A c}(T - t) \qquad (5a)$$

The net heat gain of the spray water,

$$wcdt = K A\, dz\, (H^* - H) - U A\, dz\, (T - t) \qquad (6)$$

where m is the proportionality constant appropriate to the range of spray water temperature, t, involved.

Subtracting Equation (6a) from Equation (5a) results in Equation (9). Multiplying Equation (6a) by m and subtracting Equation (7a) from the result yields Equation (10):

$$\frac{dy}{dz} = a_1 y + b_1 x \qquad (9)$$

$$\frac{dx}{dz} = a_2 y + b_2 x \qquad (10)$$

where

$$y = (t - T) \quad and \quad x = (H^* - H)$$

$$a_1 = -\frac{UA}{wc} - \frac{UA}{W_A} \qquad b_2 = \frac{KA}{wc}$$

$$a_2 = m\frac{UA}{wc} \qquad b_2 = m\frac{KA}{wc} - \frac{KA}{W_A}$$

Equation (9) and (10) are a system of simultaneous differential equations whose solution is

$$y = M_1 e^{r_1 z} + M_2 e^{r_2 z} \qquad (11)$$

$$z = N_1 e^{r_1 z} + N_2 e^{r_2 z} \qquad (12)$$

Can be rewritten

$$\frac{dt}{dz} = \frac{KA}{wc}(H^* - H) - \frac{UA}{wc}(T - t) \qquad (6a)$$

The heat gained by the air,

$$W_A\, dH = K A\, dz\, (H^* - H) \qquad (7)$$

can be rewritten

$$\frac{dH}{dz} = \frac{K A}{W_A}(H^* - H) \qquad (7a)$$

Since the spray water is recirculated, its inlet temperature is equal to its outlet temperature for steady state operation.

Hence

$$\frac{dH}{dz} = m\frac{dt}{dz} \qquad (8)$$

where r_1 and r_2 are roots of the quadratic equation

$$r^2 + (a_1 + b_1)r + (a_1 b_2 + a_2 b_1) = 0 \qquad (13)$$

constancy of U and K is implied. The M_i are related to the N_i by

$$N_1 = -M_i(r_i + a_1)/b_1, \; i = 1, 2$$

or

$$N_1 = -M_i a_2/(r_i + b_2) \qquad (14)$$

In short, only two of the four constants, M_i, N_1 may be chosen independently. Integrating Equations (11) and (10) from z = 0 to z = 1, that is from air inlet to outlet, yields

$$(T-t)_m = \frac{M_1(e^{r_1}-1)}{r_1} + \frac{M_2(e^{r_2}-1)}{r_2} \qquad (15)$$

$$(H^*-H)_m = \frac{N_1(e^{r_1}-1)}{r_1} + \frac{N_2(e^{r_2}-1)}{r_2} \qquad (16)$$

The pair of Equations (15) and (16) together with the relationship

$$UA\,(T-t)_m = KA\,(H^*-H)_m = WC\,(T_2-T_1) = W_A\,C\,(H_2-H_1) \qquad (17)$$

permit the design of an evaporative cooler heat exchanger, provided the transfer coefficient, U and K, can be evaluated as functions of the process conditions.

The film coefficient for heat transfer between the outer tube surface and bulk spray water in a falling film is represented by [Treybal, 1981]

$$h_{LF} = (982+15.58t_L) (\Gamma \backslash d_0) \qquad W/m^2 K \qquad (18)$$

Owing to recirculation the spray water attained a constant temperature. Since there was no temperature or concentration gradient in the water, the water offered no resistance to the transfer of heat or mass. Thus the only film coefficient involved was that of the air film. The constant temperature attained by the spray water is the adiabatic saturation temperature. The film coefficient was based on the arbitrary assumption that the transfer area is the outside surface of the tubes wetted by the spray water; it is represented by [Treybal, 1981]

$$k_y = 0.0043 [G'_{min} (1 + Y')]^{0.905} \qquad W/m^2 s \Delta Y' \qquad (19)$$

The water heat transfer coefficient of an evaporative cooler is constant then

$$h'_L = 11\ 360 \qquad W/m^2 K \qquad (20)$$

Parker et al. [1960] proposed the following iterative procedure

1. compute h_{LF} from equation 18 and estimate $h_{Lec} = F h_{LF}$ *with* $F = 0.8$
2. take $h'_L = 11360$

3. compute U and K as first estimates
4. with these obtain first estimates of r_1 and r_2 through equation 13
5. with r_1 and r_2 compute $(T-t)_m$ and $(H^*-H)_m$ using equations 15 and 16
6. compute second approximation to U and K by

$$U = Q/A\,(T-t)_m$$

and

$$K = Q/A\,(H^*-H)_m$$

7. repeat steps (4)-(6) until U and K become constant. These are the values which account for the performance

6.2 Experiments

6.2.1 Experiments in Tenerife

The pad, with a surface area of 2 m x 12 m and a thickness of 20 cm, was considered as a cooling tower-heat exchanger; the packing was cellulose.

Heat and mass transfer coefficients for the CELdek™ evaporator were determined using experimental data, recorded in the prototype greenhouse in December 1994 and June 1995.

Thermistors were used to measure the temperatures of the seawater entering and leaving the evaporation pad. The air speed inside the greenhouse was measured by an anemometer. The wet and dry bulb temperatures of the air entering and leaving the evaporative cooling pad were measured by ventilated psychrometers.

6.2.1.1 Results and discussions

The CELdek™ evaporator performance is affected by the material and configuration of the packing, and also by water and air loading and the ambient weather conditions. Low water loading results in poor water distribution, whereas high water loading causes flooding, producing excessive air pressure loss. The main function of the heat exchanger is to increase the contact area between the air and water and to maximise the residence time of the water in the CELdek™. It is expected that the packing material will influence the wetting characteristic and hence the contact area between the air and water. The packing characteristics can be expressed by the expression [Tezuka, 1972]:

$$Hg.a = a_1 (G')^{b}_1$$

where the coefficients a_1 and b_1 depend mainly on the material and its configuration.

The measurements were made with a water mass flow rate of w = 0.3 kg m^{-2} s^{-1} and air mass flow rate of concerning the range 0.2 to 0.9 kg m^{-2} s^{-1}. Figs. 6.5 and 6.6 show the effect of air mass flow rate on the air heat and mass transfer coefficients (hg a) and (ky a) respectively for the CELdek™ packing material. The results indicated that an increase in the air mass flow rate increases both the air heat and mass transfer coefficients.

A transformation of the data which enhances the fit and predictability of the heat and mass transfer coefficients is as follow:

$$(Hg.a) = 0.53(G')^{1.79}$$

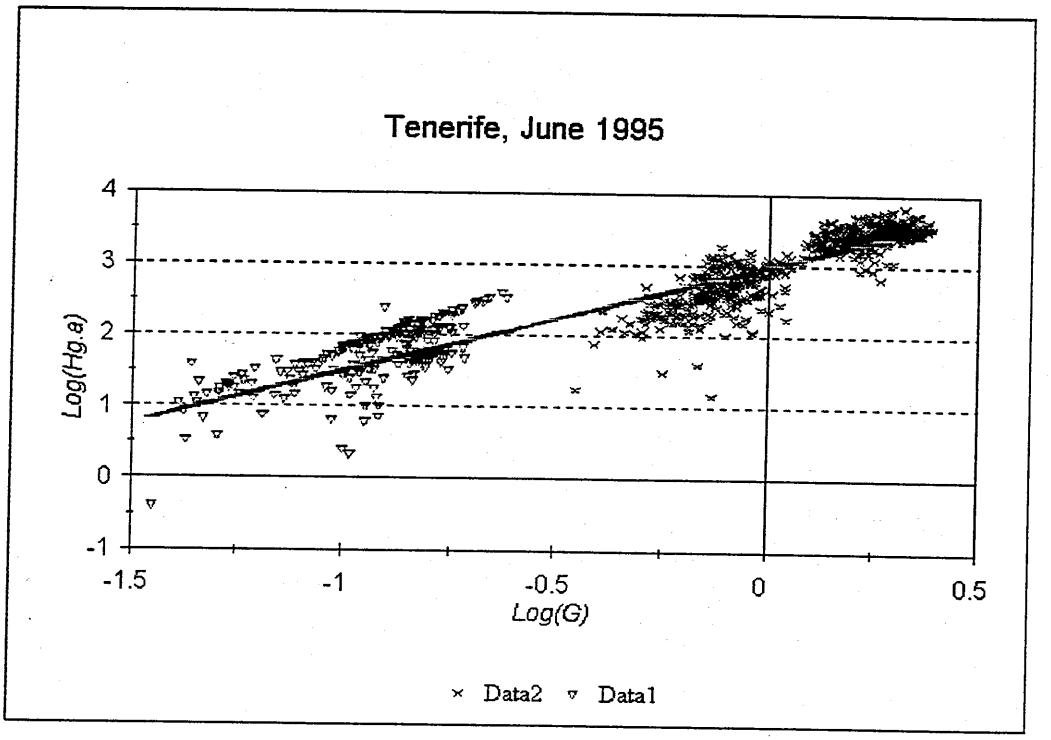

Fig. 6. 5 Effect of air mass velocity on the heat transfer coefficient

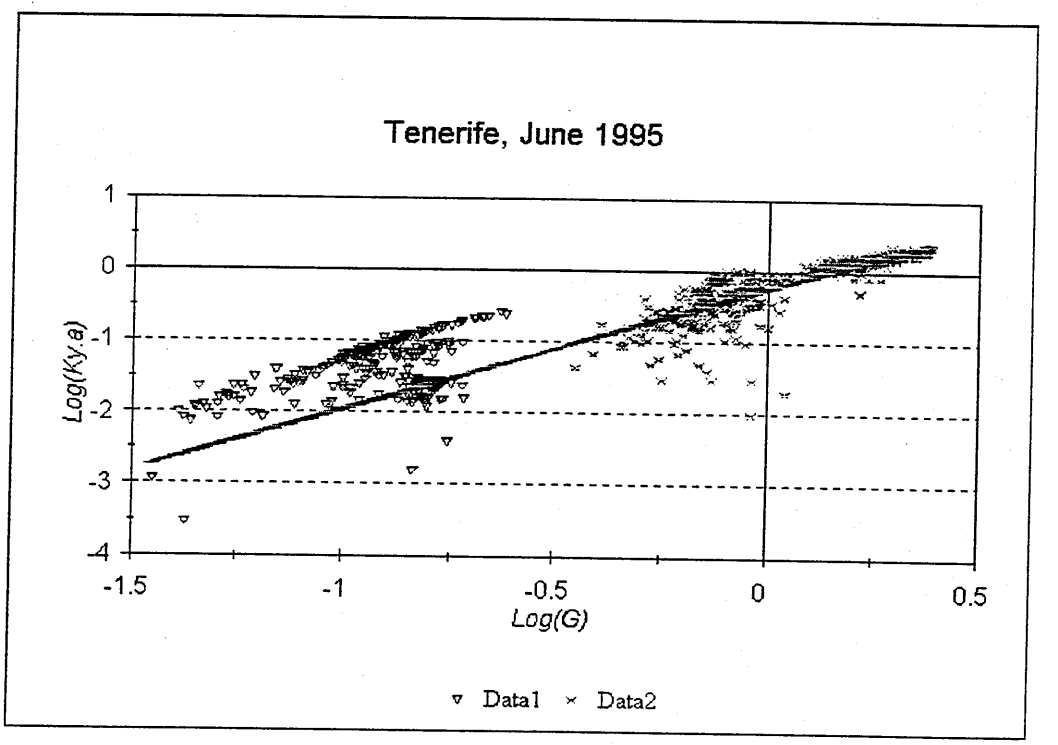

Fig. 6. 6 Effect of air mass velocity on the mass transfer coefficient

and

$$(Ky.a) = 0.64(G')^{1.71}$$

6.2.2 CELdek™ condenser experiments

The prototype CELdek™ condenser, tested in the laboratory was made from CELdek™ 7090 and was 0.34 m high, 0.38 m wide with a face area of 0.13 m^2 and a thickness of 0.1 m. Eleven lengths of copper tube, 5 mm outside diameter and 2 mm wall thickness , were inserted at 40 mm centres to convey the cooling water.

Water was recirculated over the condenser from the sump, at a flow rate of 3.4 l min^{-1}. The temperatures of the recirculated water in the condenser were measured as it entered and left the condenser. Condensation increased the water in the sump and was collected through an overflow into a measuring cylinder. Measurements were performed over 10 min periods. Air was passed through two layers of CELdek™, supplied with water and emerged virtually saturated. A centrifugal fan created the air flow through the humidifier and condenser. Air speed was measured using a hand-held anemometer at the inlet of the condenser, and inside the rig. Temperatures of air at the inlet, inside and the outlet were measured manually using thermistors. Relatively cold water was recirculated inside the tubes at a flow rate of 1.5 l min^{-1} from the sump which contained a cooling coil to maintain a constant water temperature.

6.2.2.1 Results and discussions

The performance of the CELdek™ condenser is described in terms of two transfer coefficients, U and K mentioned in equations (1) and (4), where U is the heat transfer coefficient accounting for the transfer of heat from the tube fluid to the spray water, and K is the mass transfer coefficient accounting for enthalpy transfer from the spray water to the air stream.

Values of U and K were determined from the CELdek™ condenser test data by an iterative process, mentioned in 6.1.2, using initial estimates of U and K as starting values. Table 6.1 shows that the overall mass transfer coefficient K is equal to the mass transfer coefficient ky, which means that the enthalpy transfer resistance of the water is negligible compared to that of the air.

Data	K	ky	U
1	0.0227	0.0227	4048.2
2	0.0206	0.0206	7190.3

Table 6. 1 Values for U and K

Chapter 7 Measurements and validation of simulation model

Introduction

Experimental data recorded during the months of December 1994 and June 1995 on the seawater greenhouse were analysed and used to validate the simulation model.

7.1 Measurements

During the experiments both in December 1994 and June 1995, a number of microclimate measurements were recorded. The outputs from the various internal and external sensors were recorded on a data logger at 5 minutes intervals as described in chapter 5.

7.1.1 Solar radiation

Figs. 7.1 and 7.2 show the measured values of external solar radiation, external net radiation and solar radiation inside the greenhouse during 3 day periods in December and June. The maximum values were 830 W/m^2, 550 W/m^2 in December and 1300 W/m^2, 600 W/m^2 and in 350 W/m^2 respectively in June; the solar radiation inside the greenhouse was not measured in December due to the lack of sensors.

The average value of the light transmissivity diurnal variations of the greenhouse in June, i.e. the ratio of the internal to the external solar irradiances, was 0.14, as

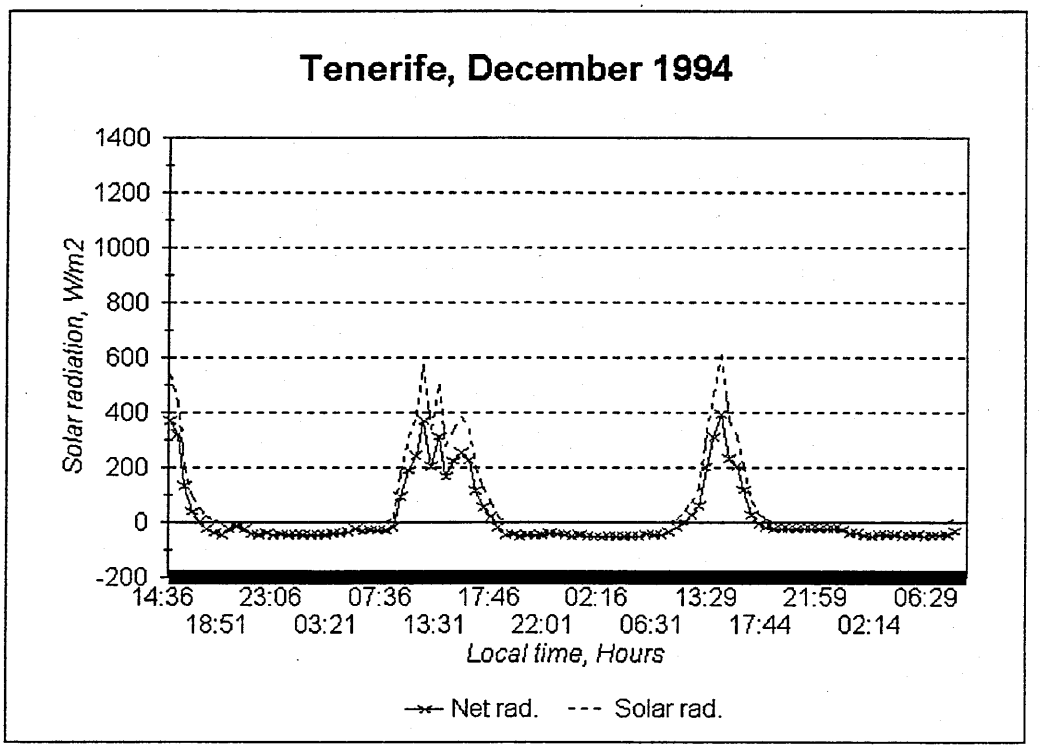

Fig. 7. 1 Radiation variations in December

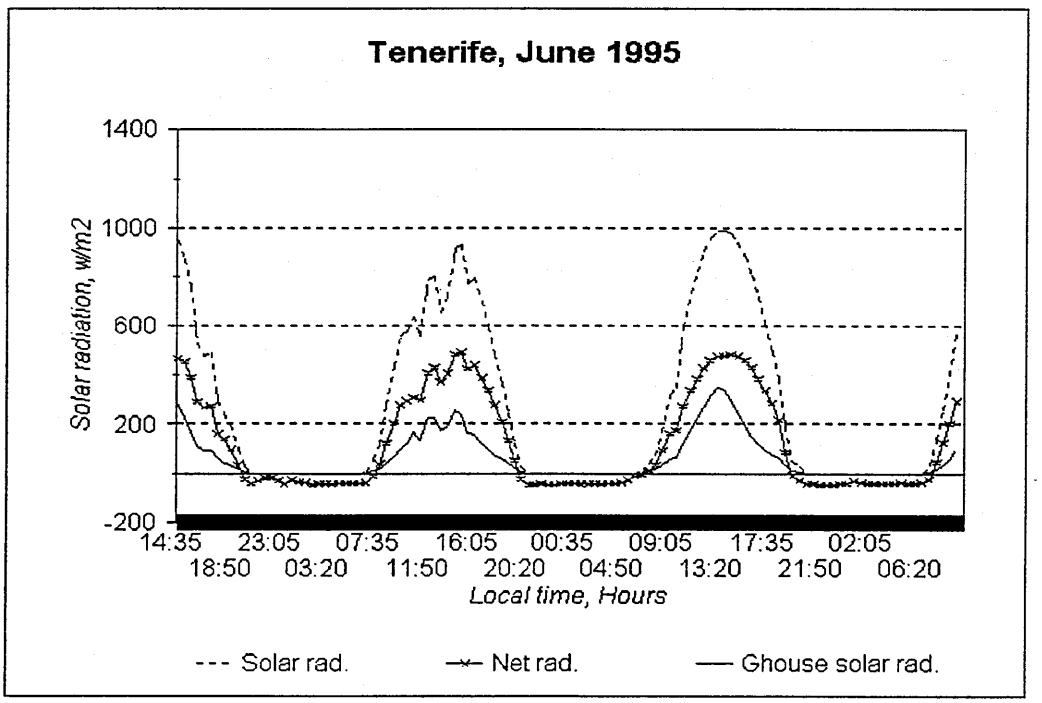

Fig. 7. 2 Radiation variations in June

shown in Fig. 7.3. The maximum value occurred during the day and was 0.5 and the minimum value occurred during the night and was 0.05.

7.1.2 Wind

In normal greenhouses the movement of warm air out of a greenhouse with an influx of cold air depends on the wind speed and direction, and on the temperature inside and outside the greenhouse. Mass transport of water vapour occurs with this movement of air.

The wind speed in June was generally higher during the day than at night, and had a mean daytime direction of 55 degrees (NNE) (Fig. 7.4). The fluctuations in wind speed, and the air speeds after pad1 and pad2 are shown in Fig. 7.5. The wind speed varied from 1 to 4 m s^{-1} while the air speeds after pad1 and pad2 varied from 0 to 0.3 m s^{-1} and from 0 to 0.6 m s^{-1} respectively.

The fluctuations of the wind speed, and the greenhouse and roof cavity air speeds are shown in Fig. 7.6 and 7.7. The wind speed varied from 2 to 12 m s^{-1} in December and from 1 to 6.8 m s^{-1} in June, while the greenhouse and roof cavity air speeds varied from 0 to 1 m s^{-1} and 0 to 4 m s^{-1} in December and from 0 to 0.4 m s^{-1} and 0 to 2.4 m s^{-1} in June. The spatial distribution of air flow inside a greenhouse was not studied, the general magnitude of air speeds in greenhouses reported in the literature varied widely. Aldrich *et al.* [1983] proposed that in general the air speed across leaf surfaces should be at least of 0.1 to 0.25 m s^{-1} to facilitate CO_2 uptake; He concluded that an air speed of 0.5 to 0.7 m s^{-1} was considered optimum for plant growth under controlled conditions.

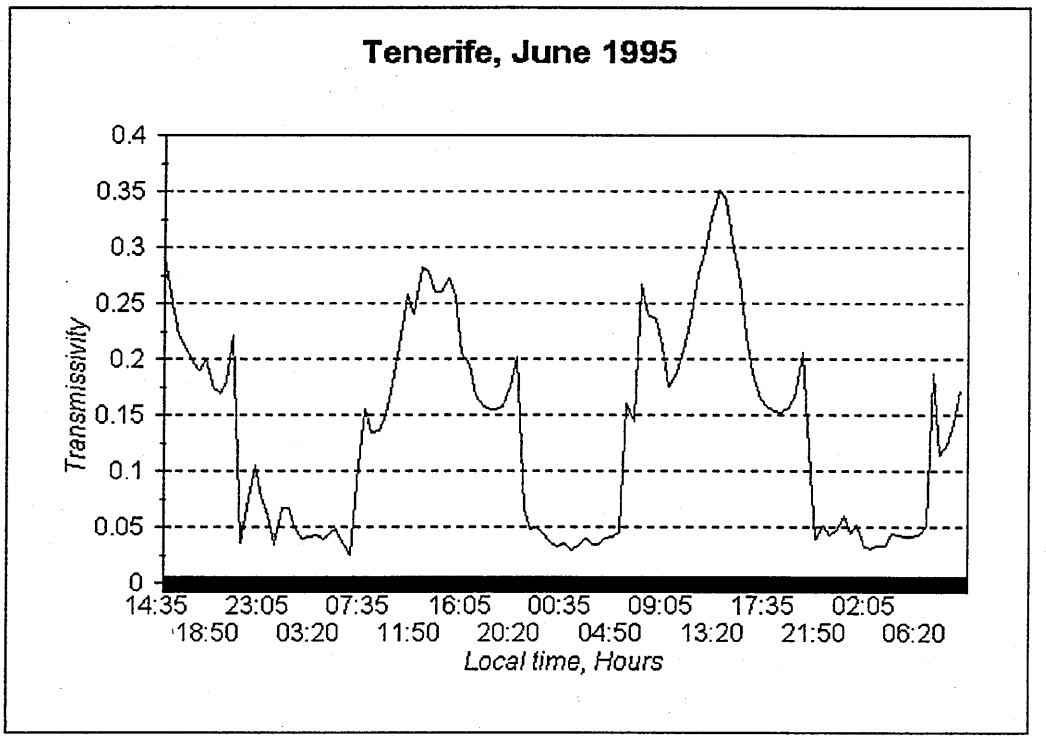

Fig. 7. 3 Light transmission variations

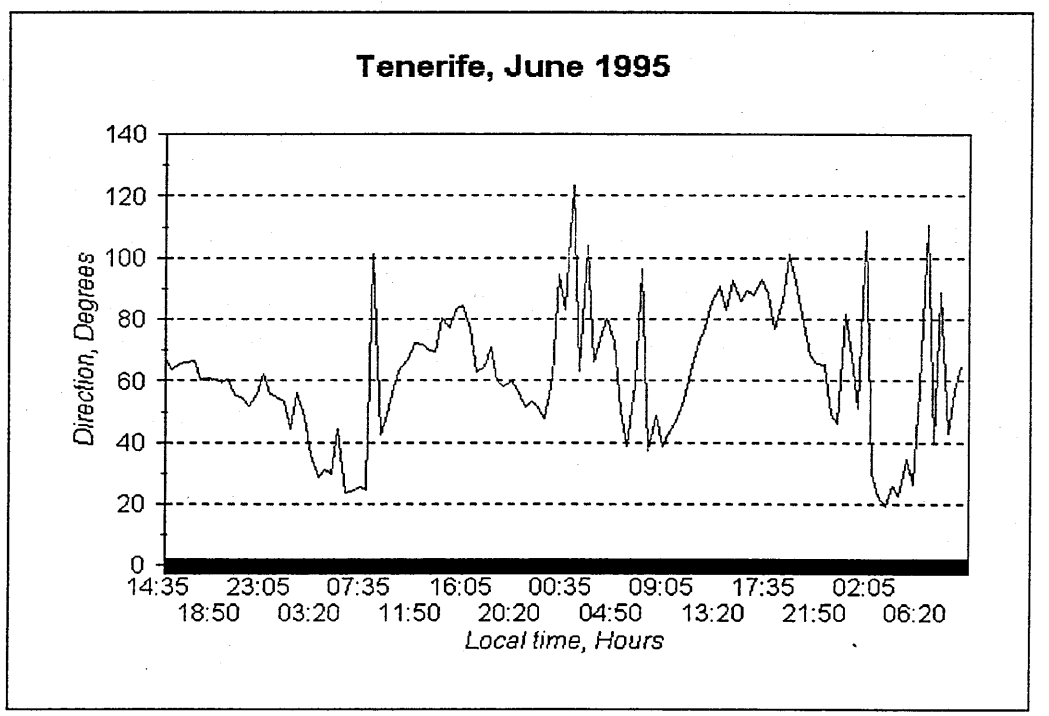

Fig. 7. 4 Wind direction variations

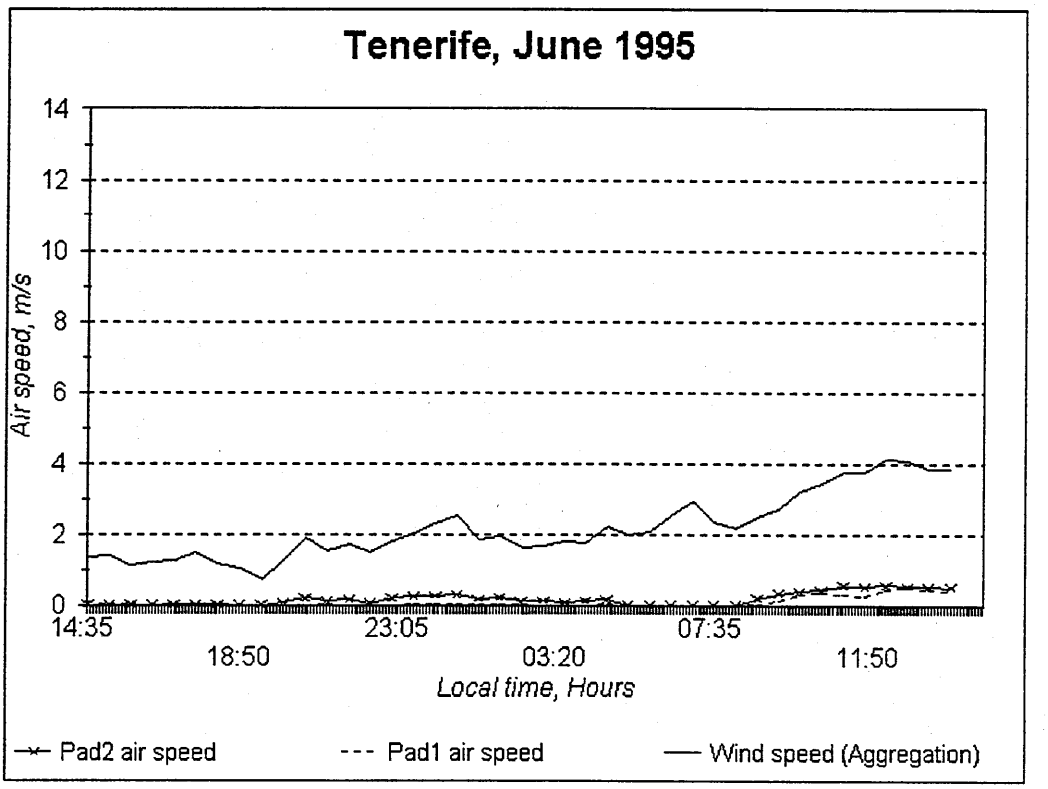

Fig. 7. 5 Fluctuations of the wind speed and air speed after pad1 and pad2

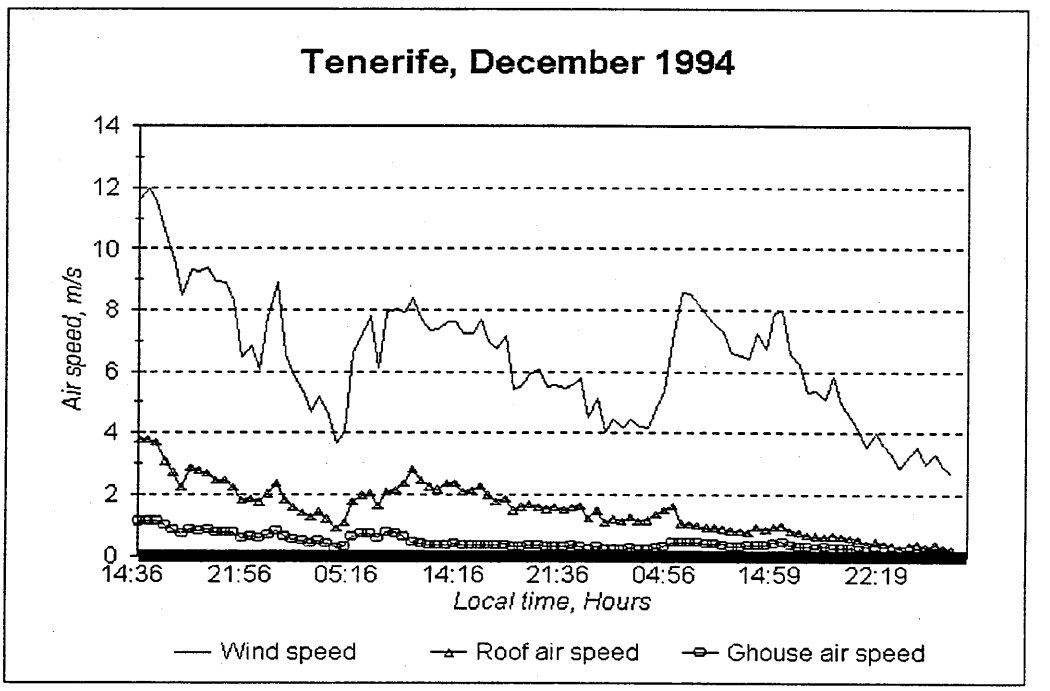

Fig. 7. 6 Fluctuations of the wind speed and air speed in the roof cavity and greenhouse

The studies of Hellenic Technologies [1993] and University College London [Grass *et al.*, 1994] were used to predict the air speeds in the roof cavity and in the greenhouse when they were not measured (see Chapter 4); Fig. 7.8 shows the variations of the coefficient β which is the ratio of the air speed in the greenhouse, or the roof cavity, to the wind speed; the mean value was 0.05 for the greenhouse and 0.27 for the roof.

7.1.3 Evaporative cooling pad

The mean values of the evaporative cooling efficiency of the front pad calculated using the measured air temperatures was found to be 42 % in December and 60 % in June (Figs. 7.9 and 7.10).

The maximum outside air temperatures during the experiments in December and June were 22 °C and 24 °C respectively. In the prototype greenhouse the rear pad was not used for humidifying the air but as a heat exchanger to dissipate heat from the chiller. Figures 7.11 and 7.12 show the fluctuation of the air temperatures entering and leaving the two evaporative cooling pads over one day. The mean reductions in air temperature were 2 °C for the front pad and 1 °C for the rear pad.

Figures 7.13 and 7.14 show the June fluctuation of the air temperatures entering and leaving evaporative cooling pad1 and pad2; over 3 days the average reduction

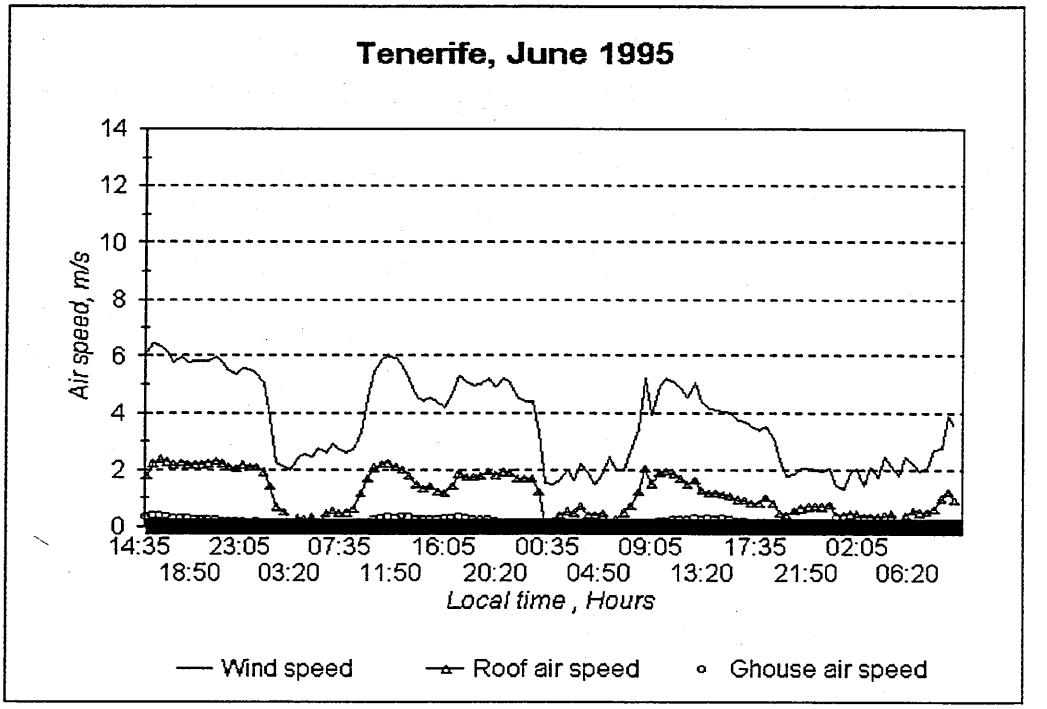

Fig. 7.7 Fluctuations of the wind speed and air speed in the roof cavity and greenhouse

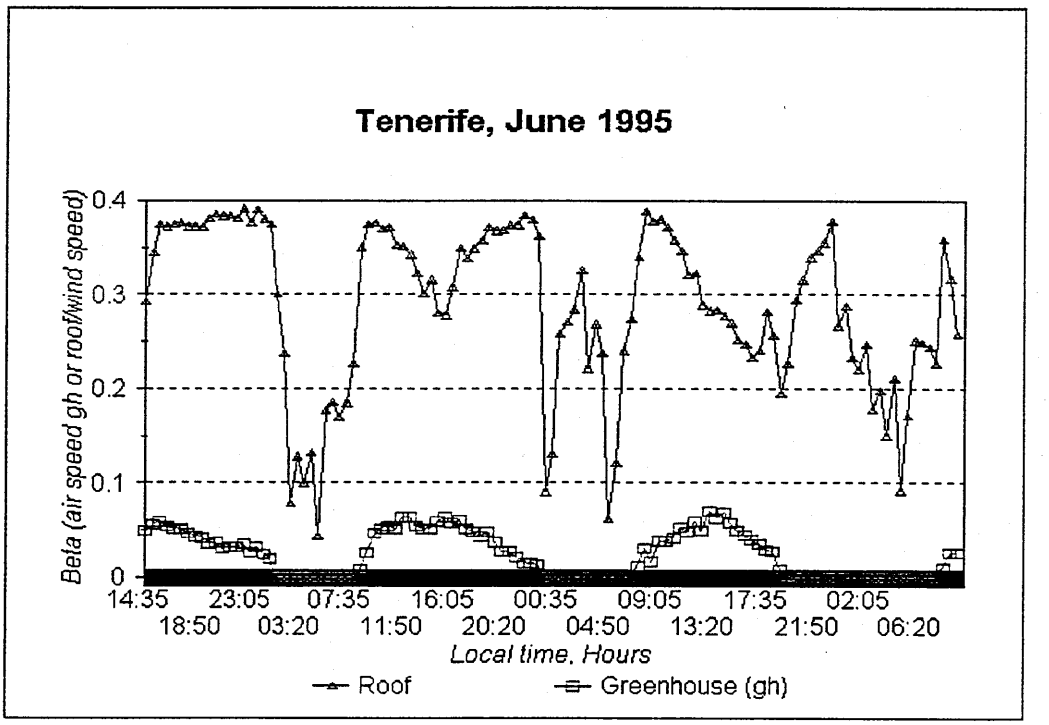

Fig. 7.8 Variations of the rating of the air speed in the greenhouse, or the roof cavity to the wind speed

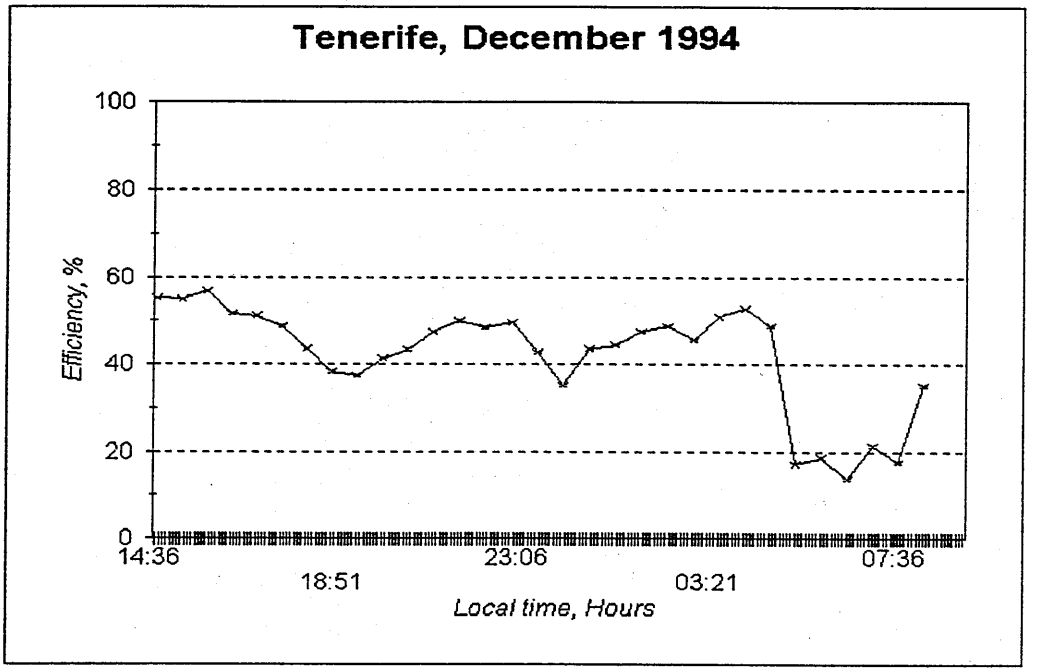

Fig. 7.9 Fluctuations of evaporative cooling pad efficiency in December

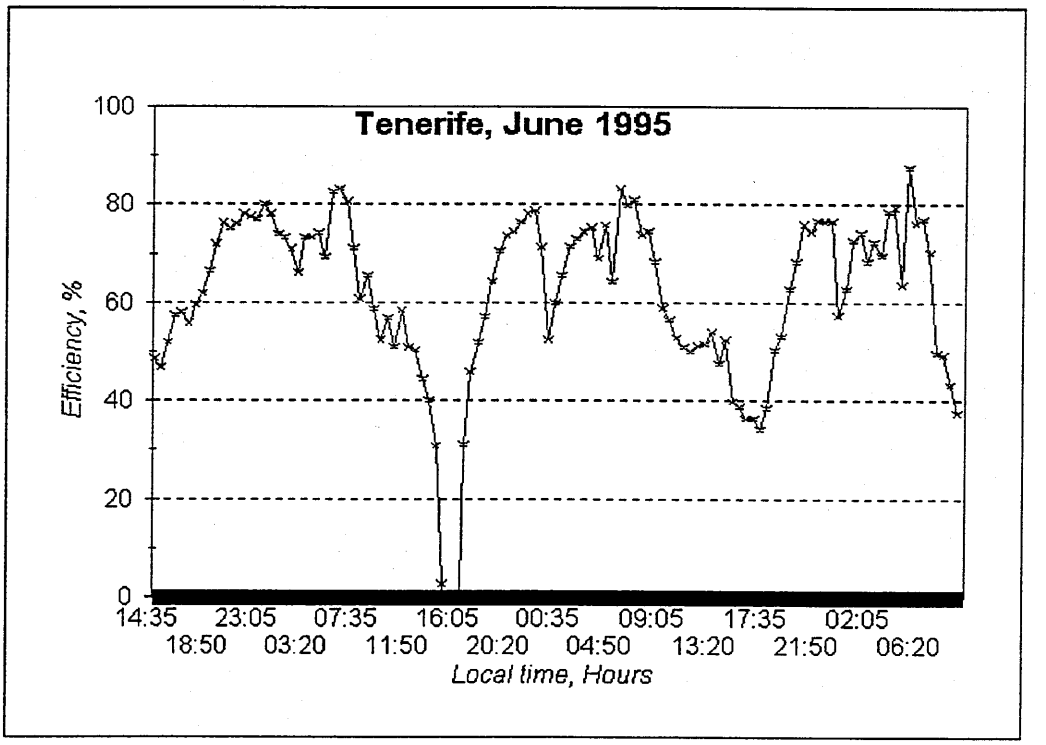

Fig. 7.10 Fluctuations of evaporative cooling pad efficiency in June

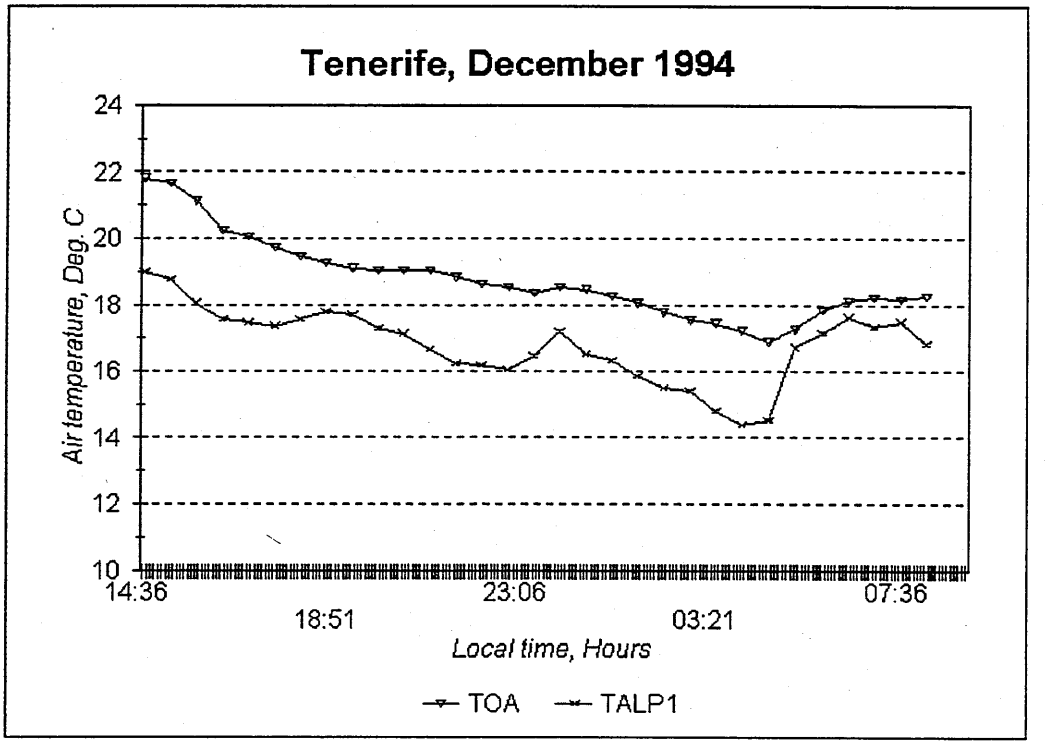

Fig. 7.11 Variations of the air temperature entering and leaving pad1

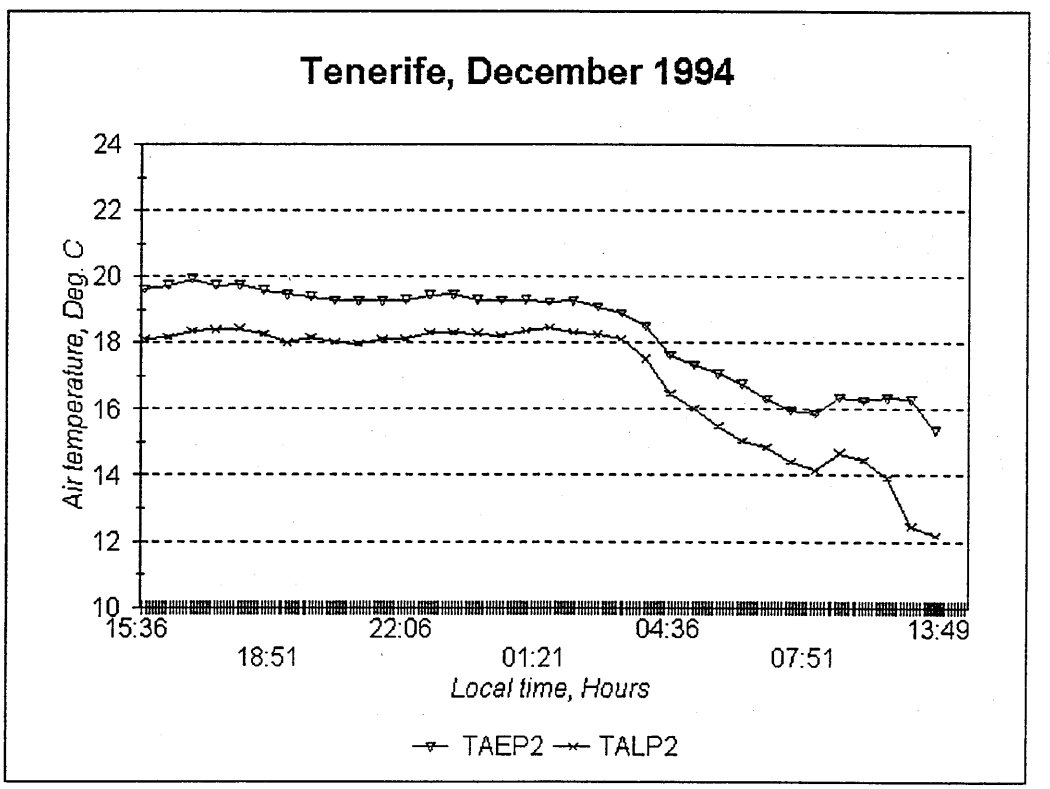

Fig. 7.12 Variations of the air temperature entering and leaving pad2

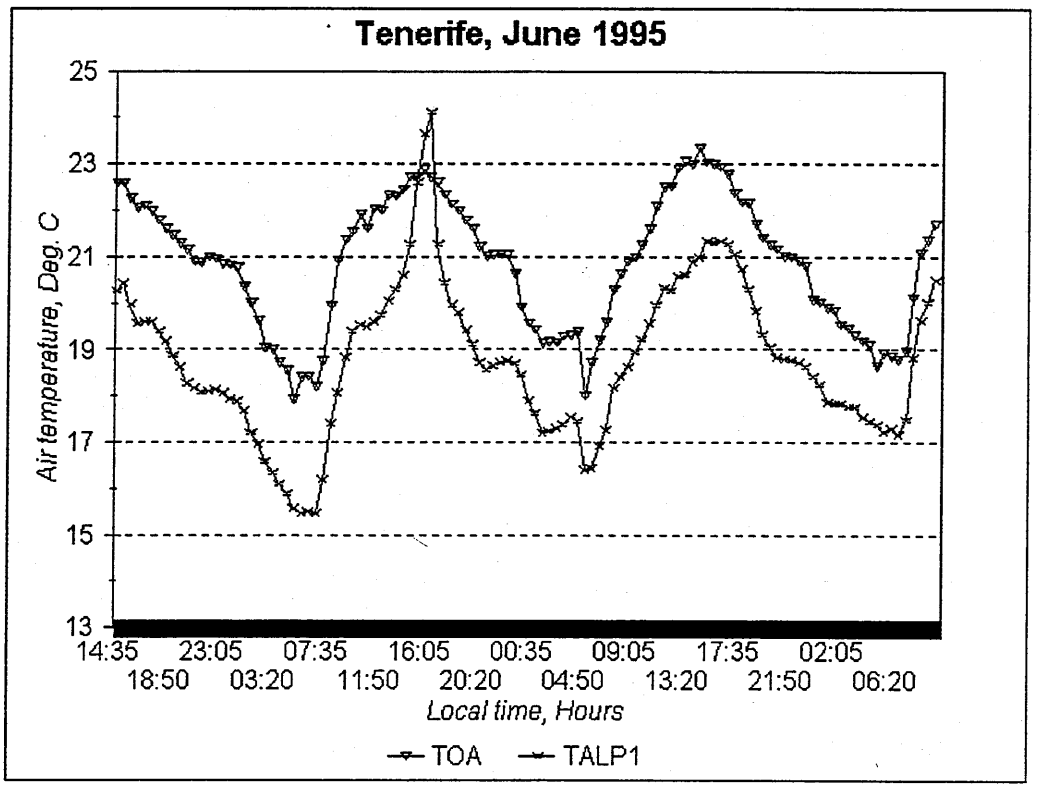

Fig. 7.13 Variations of the air temperature entering and leaving pad1

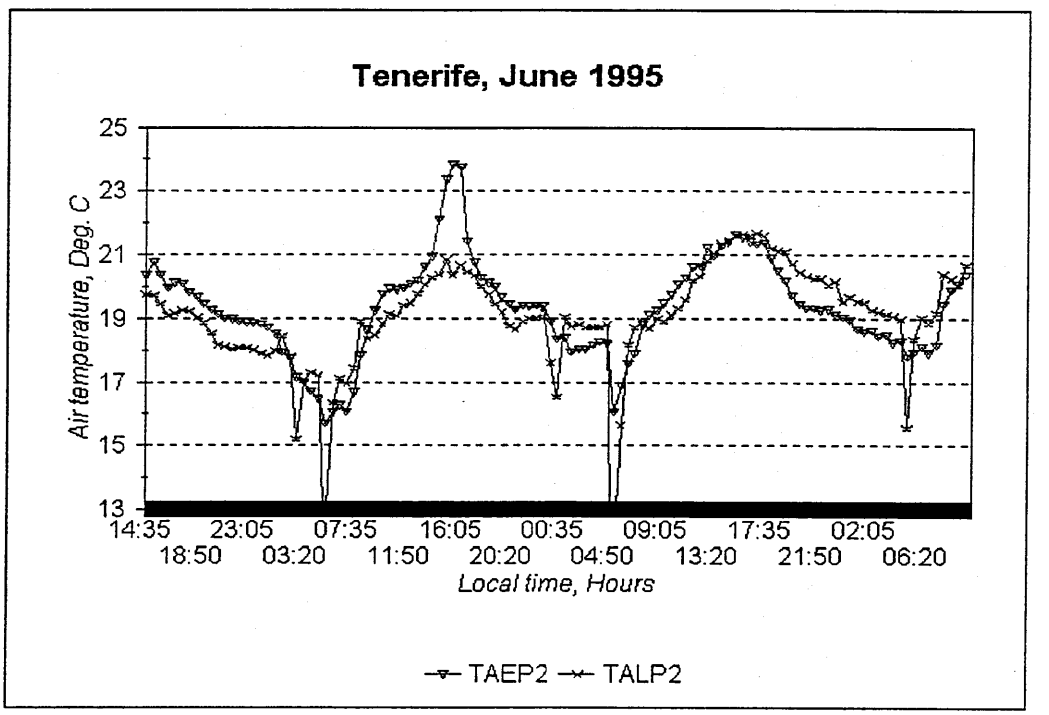

Fig. 7.14 Variations of the air temperature entering and leaving pad2

in air temperature was 2 °C. The overlap of the curves showed that there was no cooling from 12:35 to 21:00 in pad1, but significant cooling in pad2; this was due to a change of wind direction.

The temperature of the air leaving pad1 was the lowest, which was achieved by the evaporative cooling pad and was independent of the greenhouse and its contents. The mean values of the relative humidity of the air leaving pad2 varied from 86 % (no water circulating and the roof cavity was closed) to 93 % (roof open and water circulating in the roof cavity) (Fig. 7.15).

The temperature difference of the seawater entering and leaving pad2 was 5 °C during the day and 2.5 °C during the night as shown in Fig. 7.16; this pad cooled the seawater entering the condenser.

Spot readings made during one day, of vertical profiles of air speed after pad1 and pad2 are shown in Fig. 7.17; There were small increases of air speed with height. The air speed leaving pad2 was higher than pad1 due to the smaller face area of pad2, see Fig. 7.5.

7.1.4 Roof cavity

The roof cavity interacts with the exterior by reflecting some of the short-wave irradiance and by emitting long-wave radiant energy. Also, sensible heat is exchanging between the roof and the exterior, according to the temperature difference and the heat exchange coefficient. The seawater provides partial shading of the greenhouse; the heat absorbed by the seawater is rejected via pad2 located in the exhaust air stream from the greenhouse.

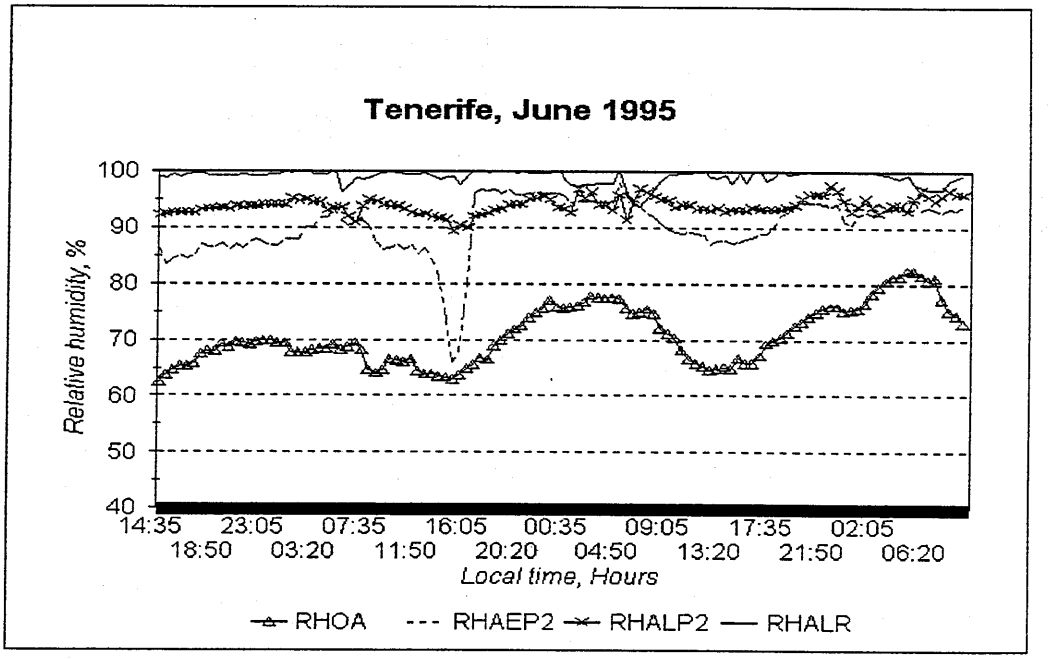

Fig. 7.15 Variations of the relative humidity of the air outside the greenhouse, the air entering and leaving roof and pad2

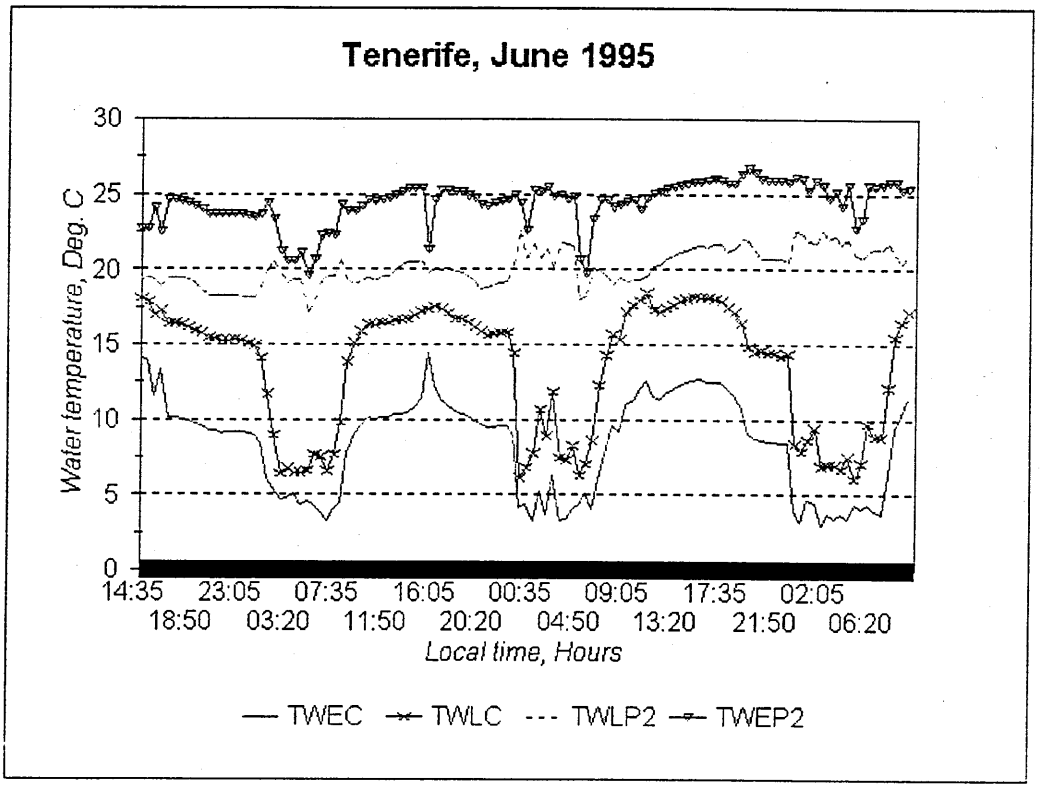

Fig. 7.16 Variations of the water temperature entering and leaving pad2

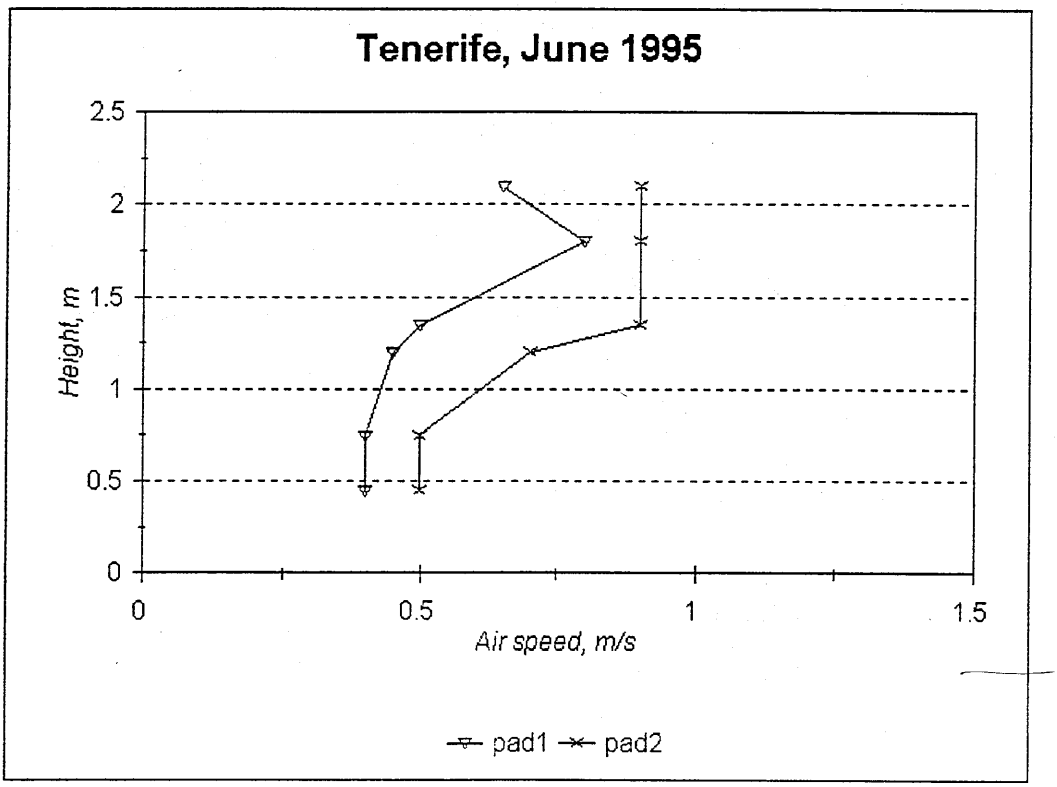

Fig. 7.17 Variations of air speed with distance from ground (height)

The variations of the air temperature entering and leaving the roof cavity in December and June is shown in Figs. 7.18 and 7.19. The air temperature inside the roof cavity was lower than the outside temperature in December due to the high wind speed (4 m s^{-1}) which cooled the roof cavity through the wide openings at both ends, and it was higher in June; the maximum temperatures were 21 °C and 26 °C, respectively.

The water temperature leaving the roof increased by as much as 4 °C during the day as shown in Fig. 7.20.

The mean values of the relative humidity of the air leaving the roof cavity varied from 59 % (no water circulating and roof cavity closed) to 92 % in December (roof open and water circulating in the roof cavity) and was 98 % in June (Fig. 7.15). The water circulation in the roof cavity increased the relative humidity by 33 percentage points.

7.1.5 Greenhouse

The vegetation is the most important source of water vapor inside the greenhouse and thus strongly affects condensation and transpiration fluxes. The maximum and minimum inside air temperatures were 22 °C and 16 °C in December, and 26 °C and 16 °C in June.

It was possible to notice a very small difference (mean difference of 0.15 °C) in crop temperature (Tc) between the position of the sensors at 2m and 6m along the row (Fig. 7.21). There were no big differences between the inside air temperature (Tia) measured at the heights of 1.6 m and 3.2 m, the average difference was 0.13 °C (Fig. 7.22); this supports the assumption of a perfectly homogenous air temperature.

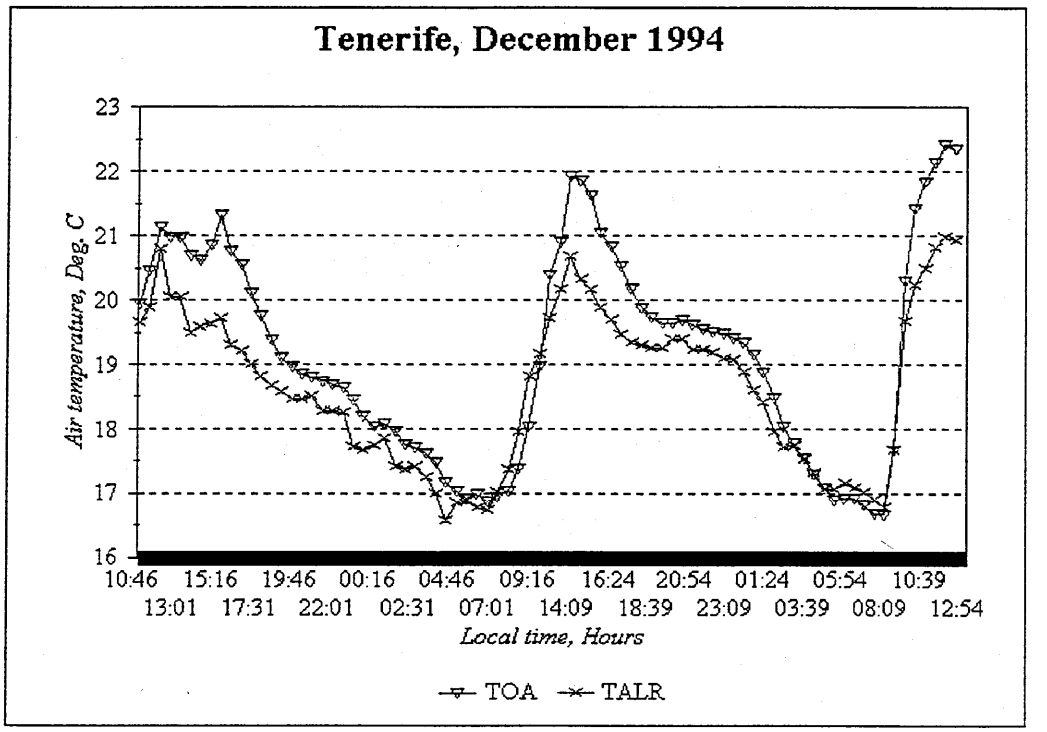

Fig. 7.18 Variations of the air temperature entering and leaving the roof cavity

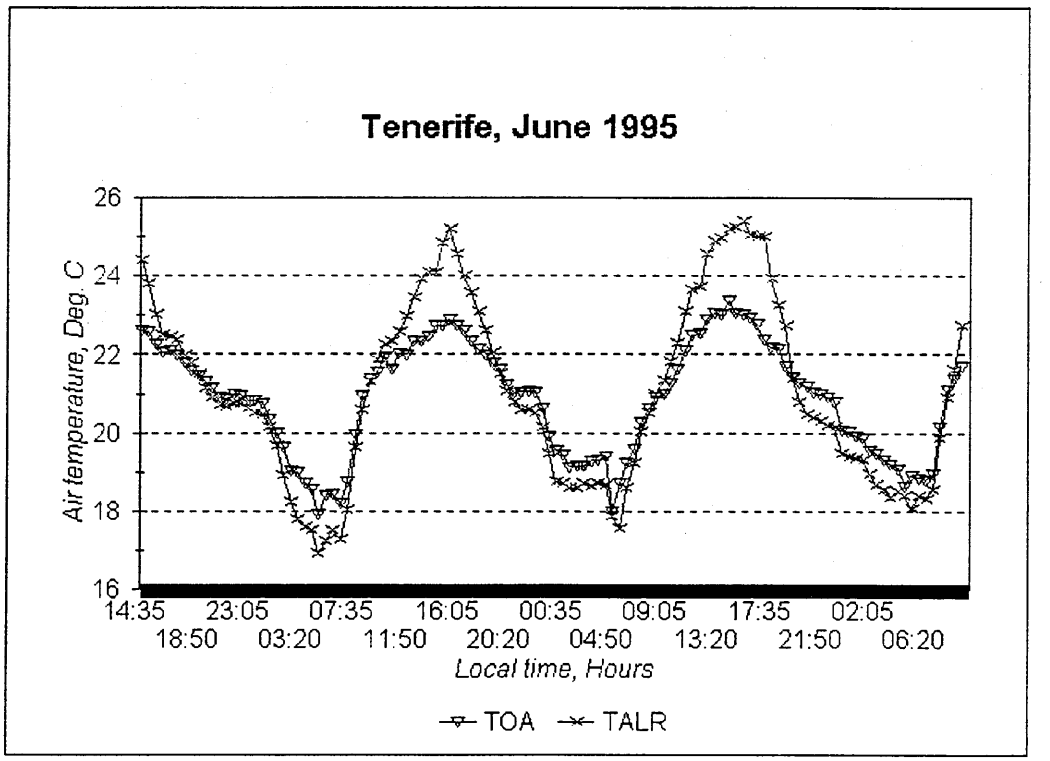

Fig. 7.19 Variations of the water temperature entering and leaving the roof cavity

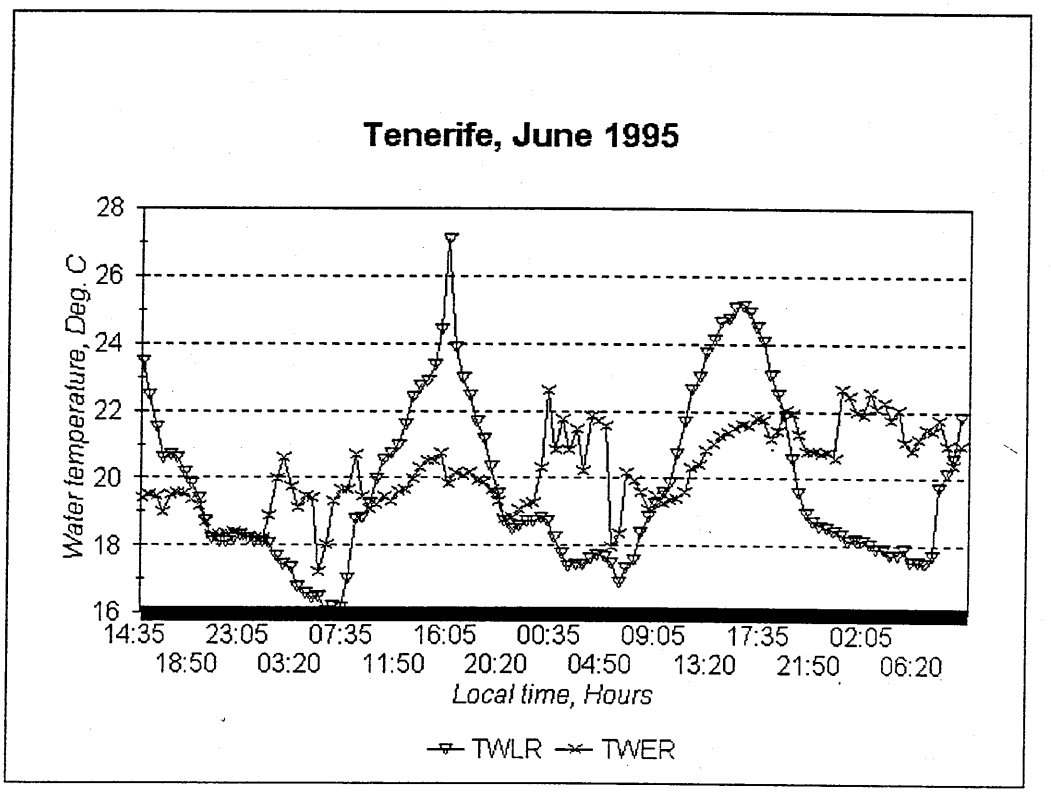

Fig. 7.20 Variations of the water temperature entering and leaving the roof cavity

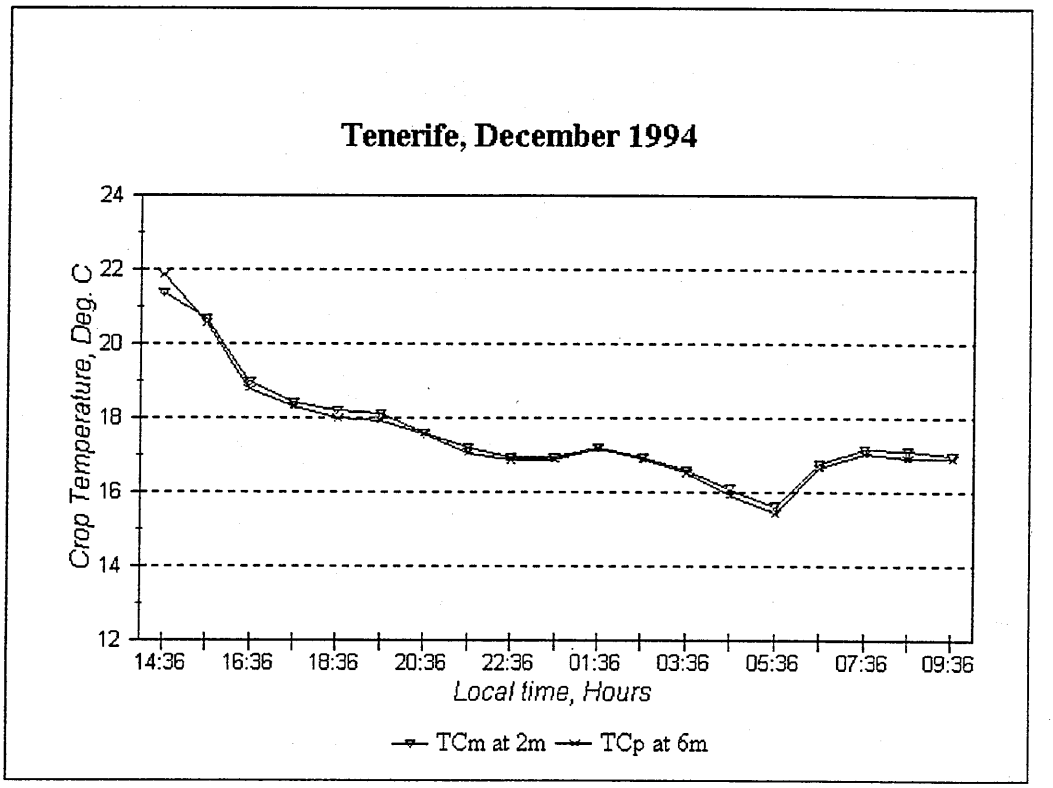

Fig. 7.21 Measured crop temperature at different distance from inlet pad

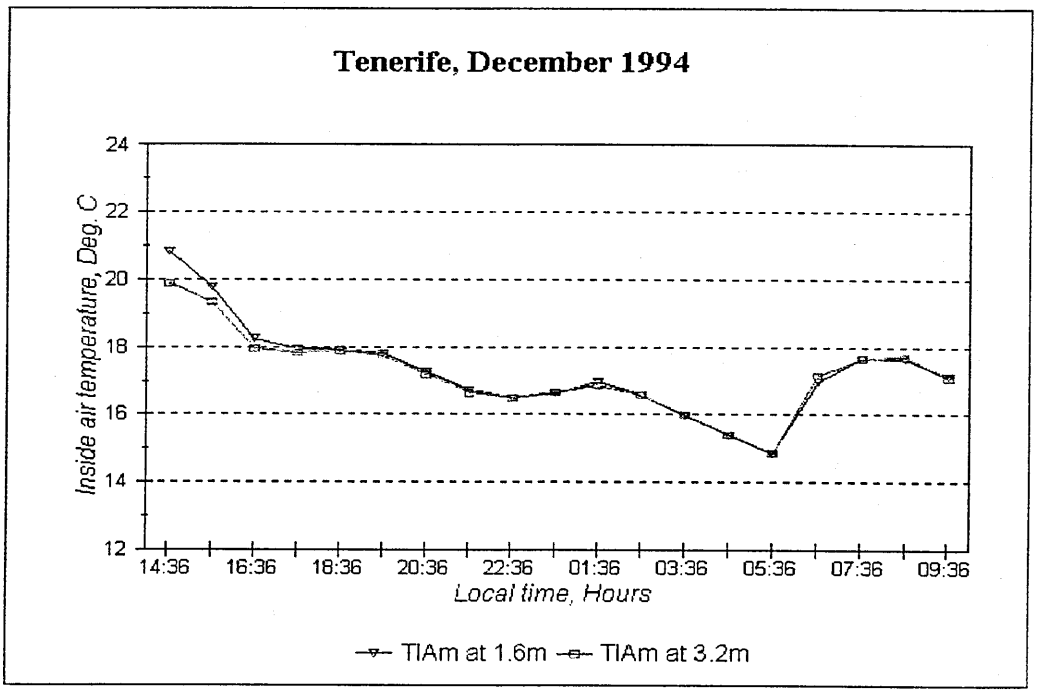

Fig. 7.22 Measured inside air temperature at different heights

Measurements of the inside air temperature with a thermistor covered with an aluminium foil and with a psychrometer were compared (Fig. 7. 23), the average temperature difference was 0.55 °C and the root mean square (*r.m.s*) was 0.82 °C. The relative difference between the two instruments was higher during the day than the night due to the lack of ventilation;

The crop temperature was always lower than the adjacent air temperature. The exceptions were probably due to a more intense evaporative cooling effect on the air.

7.2 Model validation

The simulation model predicted the heat exchange by conduction, thermal radiation, natural and forced convection, between twelve 'nodes' in the greenhouse as described in Chapter 4. The model predicted how the temperature of the nodes varied in response to changes in external air temperature, solar irradiance, wind speed, cloud cover and deep soil temperature.

The validation of the simulation model by comparison its predictions with the experimental data is the primary emphasis of this section.

Several parameters were considered in assessing the model; these were the air (inside the greenhouse, leaving pad1, pad2 and the roof cavity) and crop temperatures, humidity of the air (inside greenhouse, after pad2, after condenser and in roof cavity), water condensed in the condenser. The most important parameters for validation were the humidity and the water produced by the condenser as these indicated the suitability of the greenhouse for freshwater production.

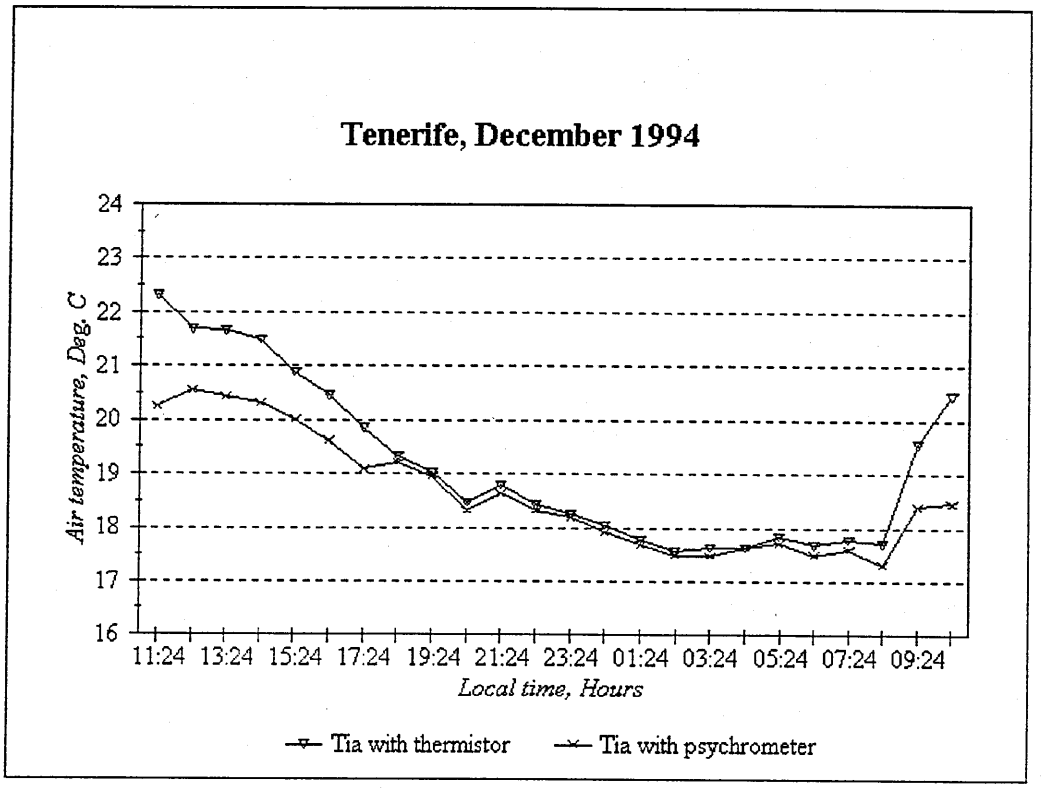

Fig. 7.23 Comparison of the measurements of the inside air temperature with a thermistor and a psychrometer

Validations were made by comparing the model predictions and measurements. Results are presented to illustrate the validation of the model.

7.2.1 Roof cavity

Predicted and measured air temperatures leaving the roof cavity are shown in Figures 7.24 and 7.25. Good agreement was revealed through the 2 experiments (roof cavity open and closed, and water circulating and not circulating in the roof cavity). The mean difference was -1.08 °C and the *r.m.s.* was 1.44 °C for the month of December and -2.10 °C and 2.15 °C respectively for June.

The diurnal courses of predicted and measured inside and outside roof cover temperatures are shown in Figs. 7. 26 and 7.27; the *r.m.s.* for the months of December and June were 2.75 °C and 0.82 °C, while the average difference was -1.49 °C and -0.33 °C respectively.

7.2.2 Evaporative cooling pad

The efficiencies obtained from the measured data for both evaporative cooling pads were used as inputs to the model. Figures 7.28, 7.29 and 7.30, 7.31 show the comparison of predicted and measured air temperatures leaving pad1 and pad2. Good agreement was revealed, the mean difference was 0.29 °C, 0.47 °C for the month of December and -0.05 °C and 0.32 °C respectively for June; the *r.m.s* was 0.39 °C and 0.57 °C for the pad1 in December and 0.83 °C and 0.92 °C for pad2 in June. This shows that the model predicted the air temperatures leaving pad1 and pad2 well for the months of December and June.

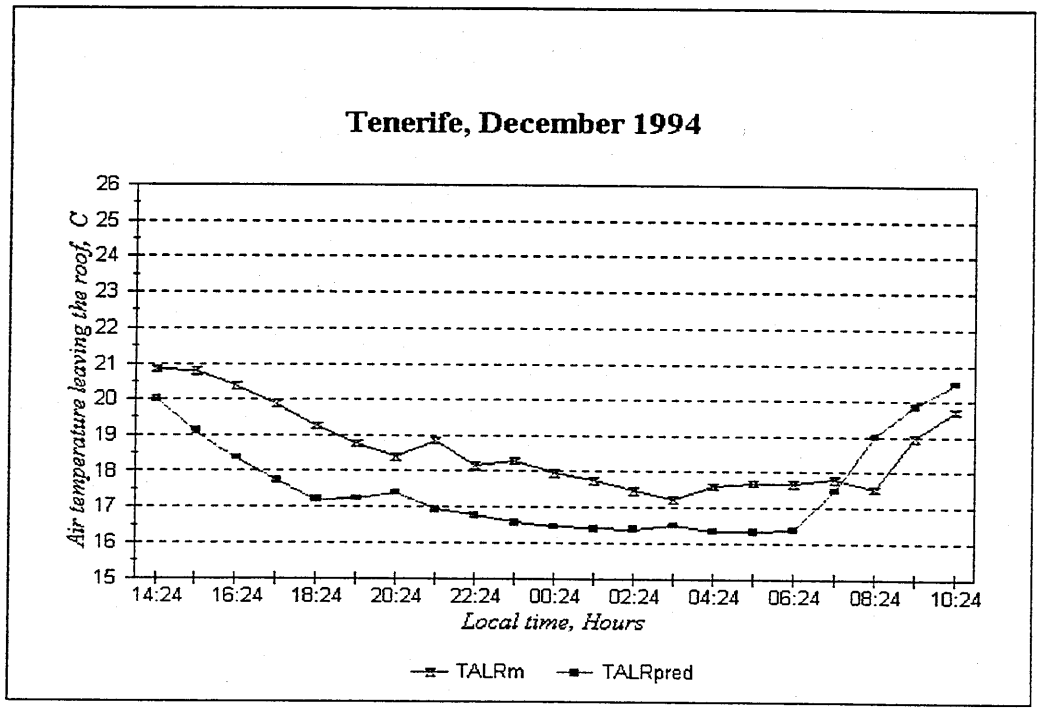

Fig. 7.24 Predicted and measured air temperature leaving the roof cavity

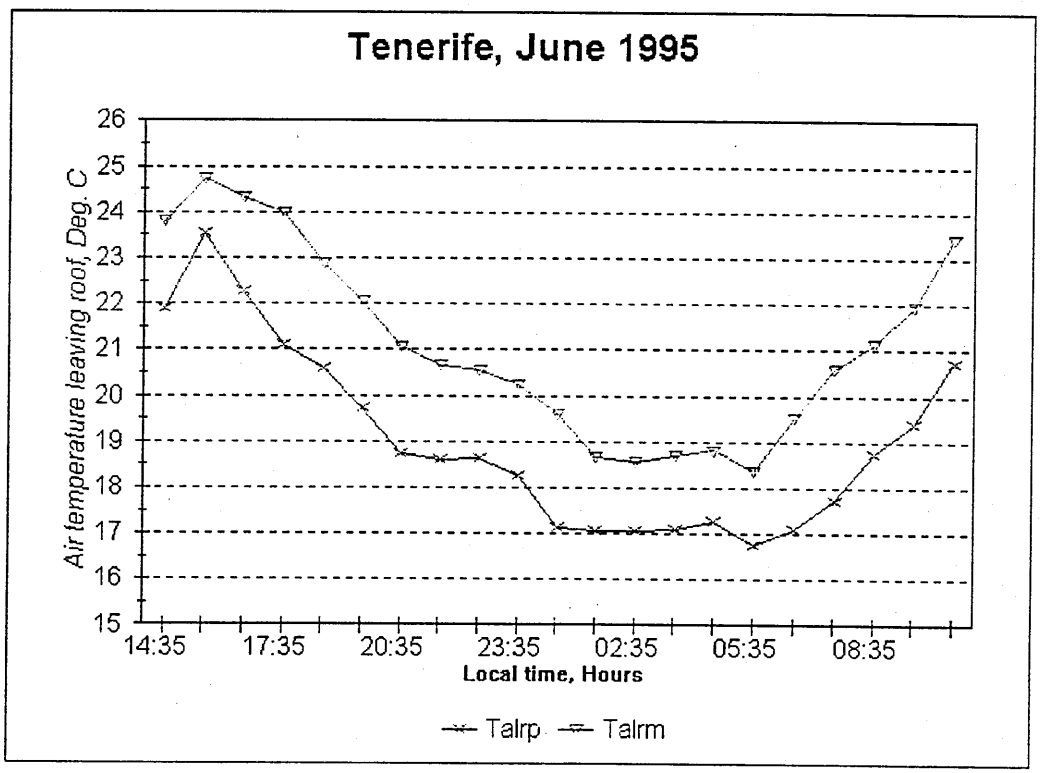

Fig. 7.25 Predicted and measured air temperature leaving the roof cavity

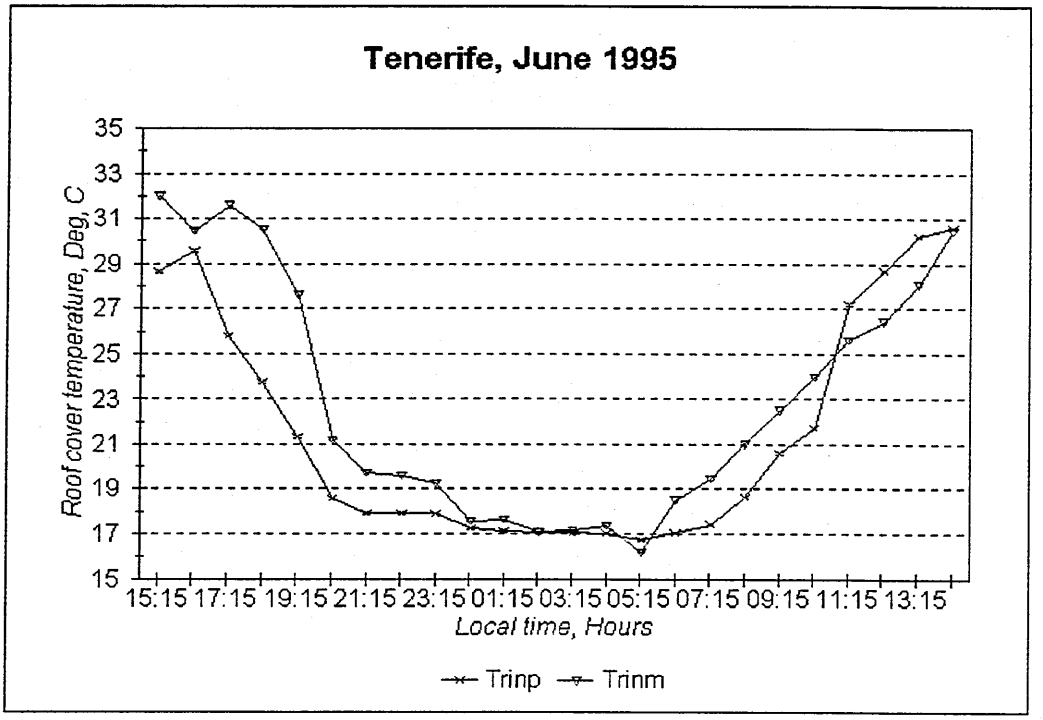

Fig. 7.26 Predicted and measured inside cover temperature

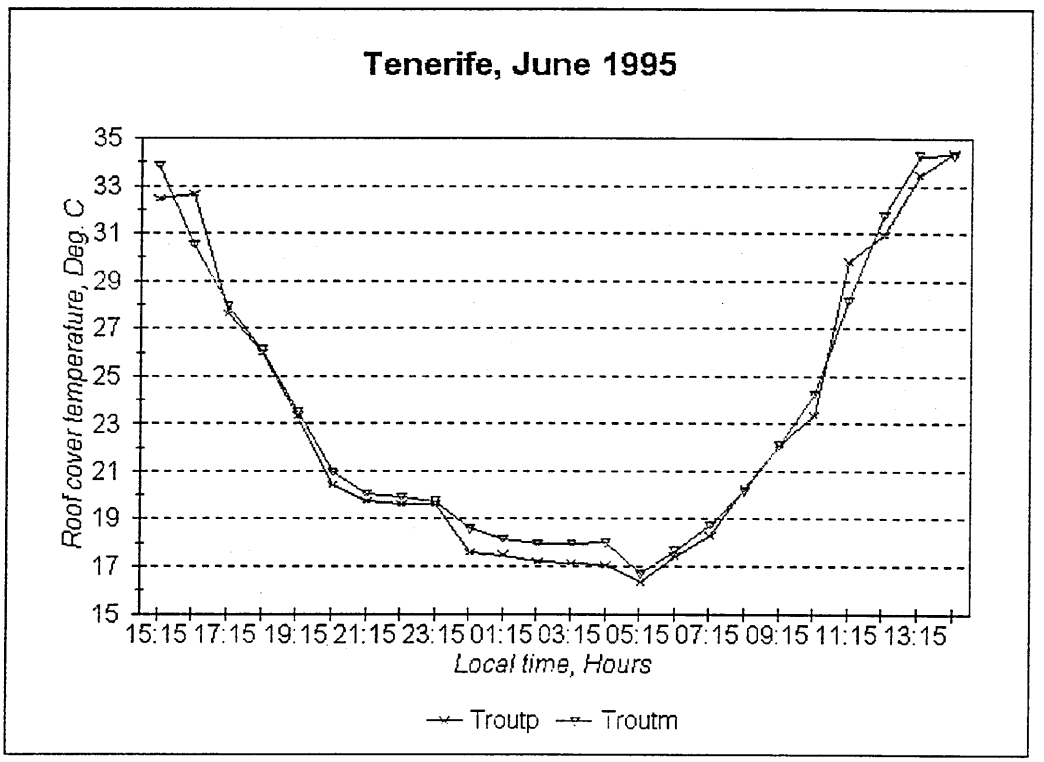

Fig. 7.27 Predicted and measured outside cover temperature

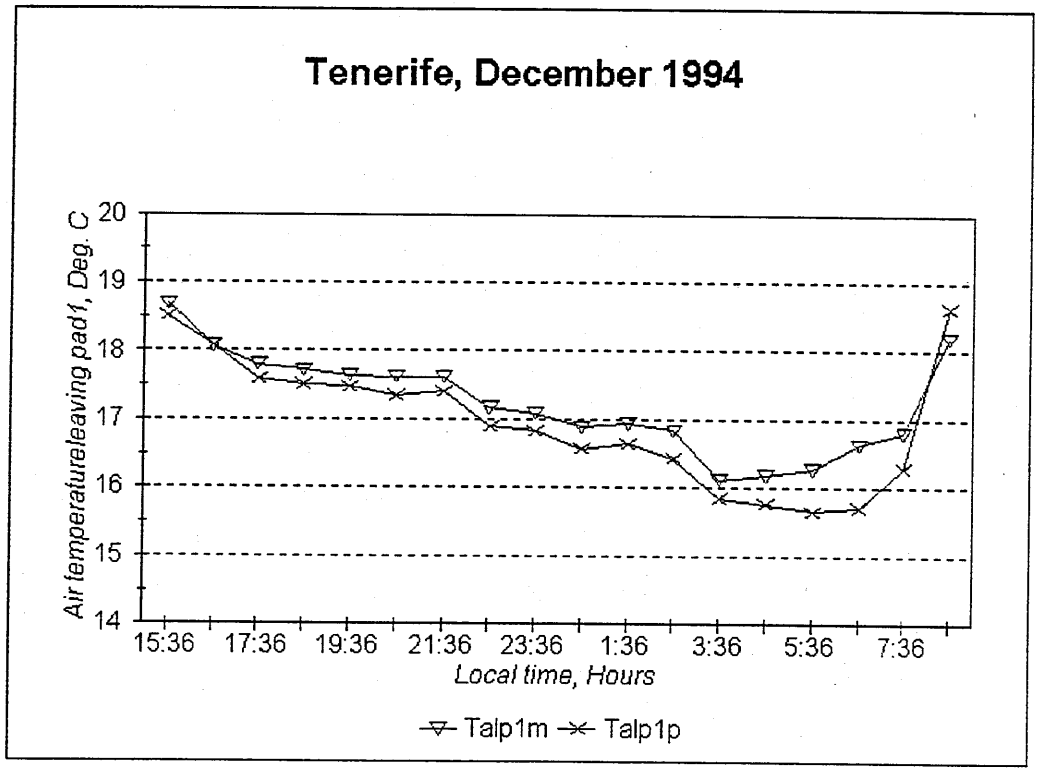

Fig. 7.28 Predicted and measured air temperature leaving pad1

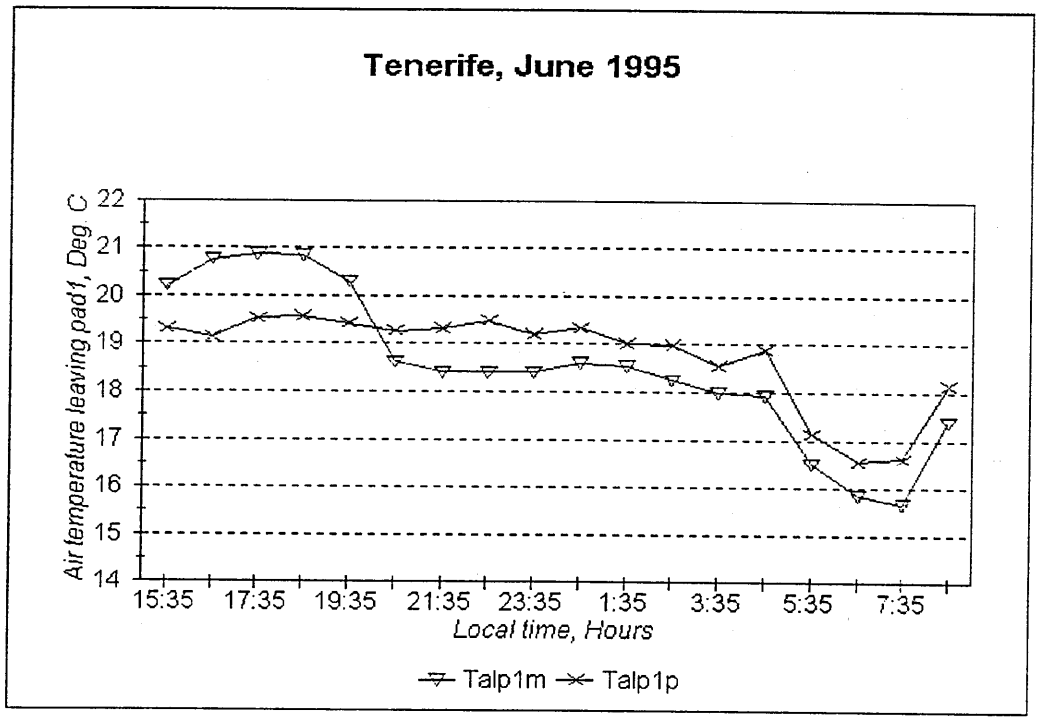

Fig. 7.29 Predicted and measured air temperature leaving pad1

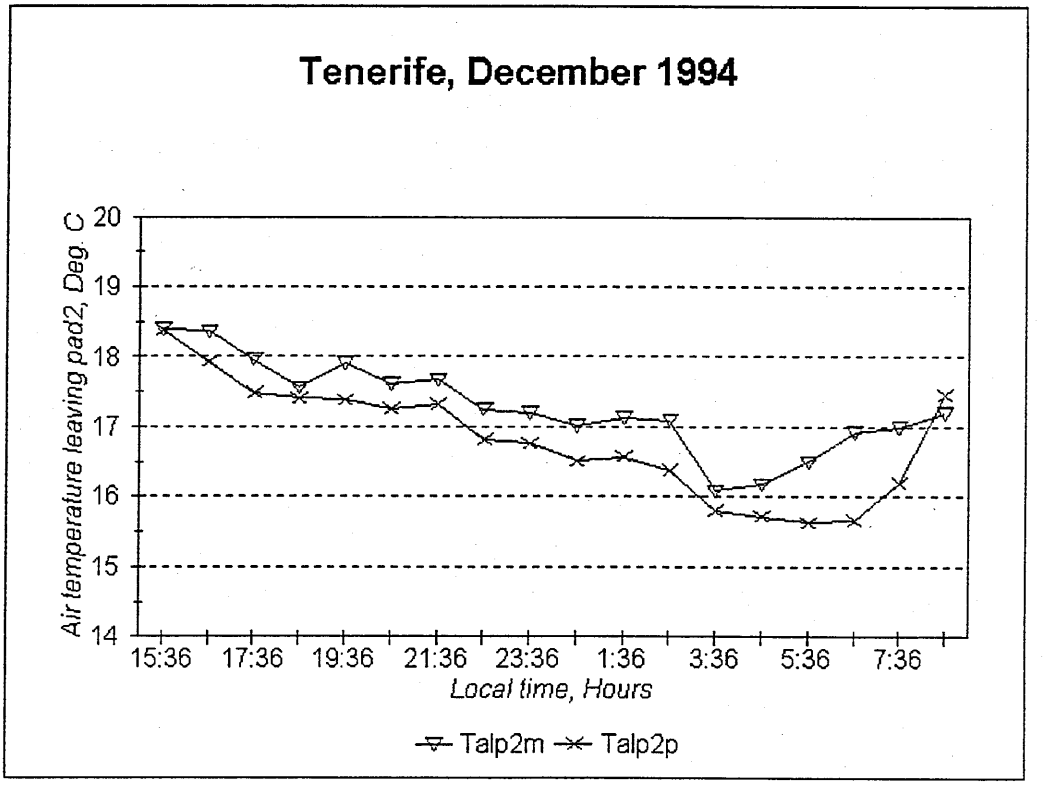

Fig. 7.30 Predicted and measured air temperature leaving pad2

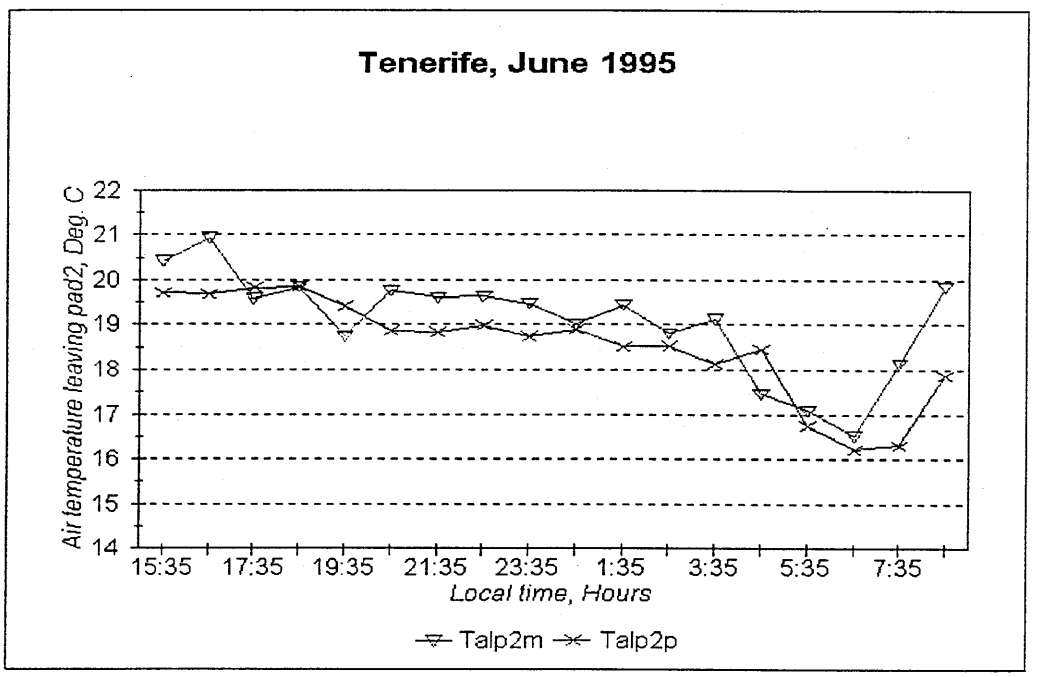

Fig. 7.31 Predicted and measured air temperature leaving pad2

7.2.3 Greenhouse

7.2.3.1 Inside air and crop temperatures

Measurements of inside air and crop temperatures were shown to support well the model predictions. Shown in Figs. 7.32 and 7.33 are comparisons between measured and predicted inside air and crop temperatures. At night the simulated air temperatures differed from the experimental ones by less than 1 °C. During the day the calculated air temperatures were lower than the experimental ones by up to 3 °C.

The predictions of the inside air temperature were shown to be very close; the *r.m.s.* was 0.57 °C in December and 0.93 °C in June, and the mean difference of the measured and predicted inside air temperature was -0.43 °C and -0.14 °C respectively. Though not perfectly matching the experimental data, the measurements of the crop temperature were shown to be larger than the predictions. The *r.m.s* was 1.68 °C in December and 3.87 °C in June and the mean difference was -1.62 °C and -3.02 °C respectively. Some of the differences can be explained by the model not accounting for changes in ventilation due to variations in wind direction.

7.2.3.2 Humidity

Predictions of the relative humidity of the inside air, air leaving pad2 and condenser are shown in Figs. 7.34, 7.35 and 7.36. Though the predicted relative humidity of the inside air during daytime was as low as 84 %, that during the night was

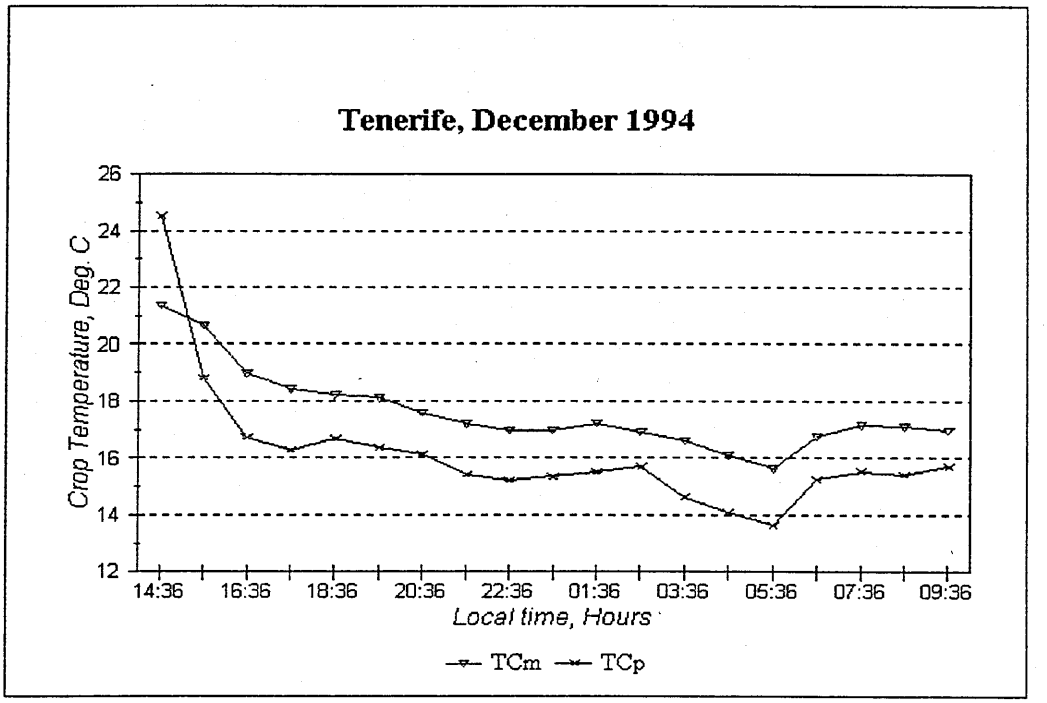

Fig. 7.32 Predicted and measured crop temperature

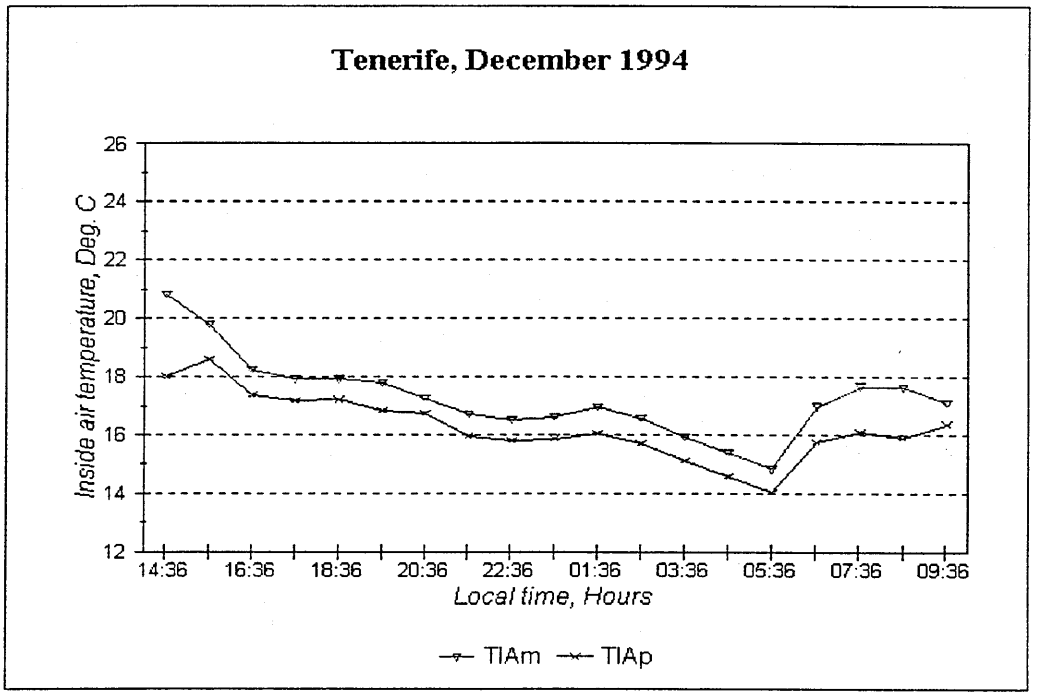

Fig. 7.33 Predicted and measured inside air temperature

predicted higher at 92 % , the measured relative humidity was 93 % during the day and 97 % during the night. This showed that condensation mainly occurs in the inner roof in the evening and during the night when no solar radiation is available. The external air humidity was higher in Winter than in Summer; the average relative humidity was 87 % in December and 67 % in June, this effect is due to the lower cover temperature in Winter.

Compared to the temperatures of the air inside the greenhouse, and entering and leaving pad1 and pad2, the model was shown to be less accurate in predicting the humidity level.

Comparisons between predicted and measured relative humidity of the inside air, the air leaving pad2 and condenser, showed that the mean difference were -8.20 %, -13.01 and 4.65 and the *r.m.s* were 0.08 %, 0.13 % and 0.07 % respectively.

7.2.4 Condenser

Some measurements of the fresh water production were made manually during December experiments. Two measurements were made on 21 / 12 / 94 and on 22 / 12 / 94 giving 0.5 l min^{-1} and 0.45 l min^{-1} respectively; the predicted values were 1.2 l min^{-1} and 1.0 l min^{-1}.

The freshwater produced in December was 0.9 l min^{-1}. The variations in freshwater production in June are shown in Fig 7.37, the average water produced was 0.8 l min^{-1}. The conductivity of the freshwater produced was between 10 and 230 mS cm^{-1} and the total dissolved salt was between 10 and 100 ppm; the maximum figure for continual human consumption is about 500 ppm. This is much purer than local well water (conductivity from 1200 to 1600 mS cm^{-1}). The watering requirements were 0.3 l per day for the lettuces and 0.15 to 0.3 l per day

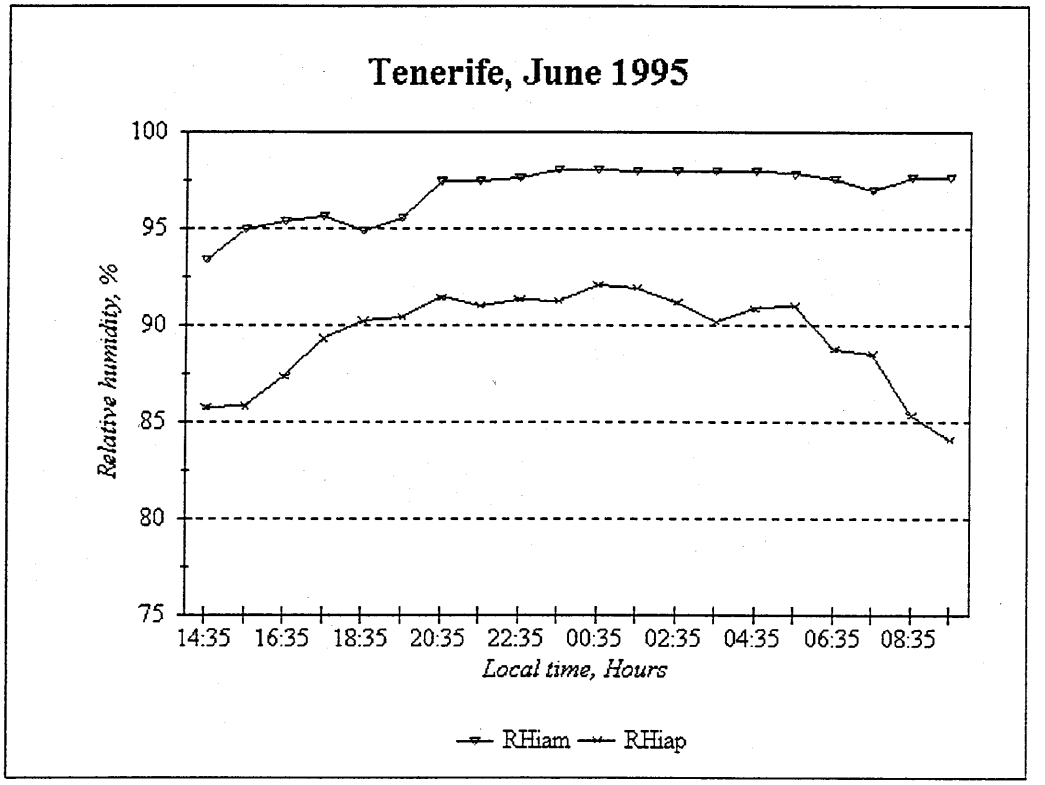

Fig. 7.34 Predicted and measured inside air relative humidity

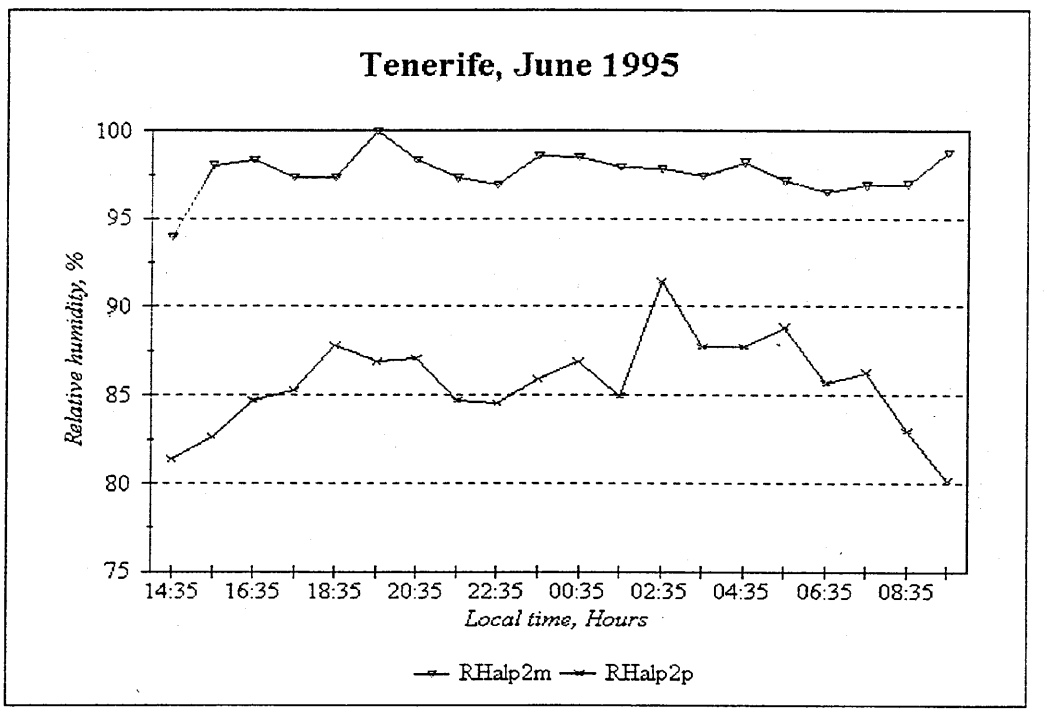

Fig. 7.35 Predicted and measured relative humidity of the air leaving pad2

for the French bean plants thus, the freshwater produced was of good quality for plant irrigation and the quantity was sufficient for the crops and nursery plantings.

Conclusions

The ambient temperatures inside the greenhouse were reduced from 2 to 4 °C compared with outdoor temperatures and the relative humidity was generally maintained at 85 %. This contributed to create an ideal environment for plant growth of a wide range of species and is of particular value in very dry and hot areas of the world where certain crops are only produced at a very high cost, if produced at all. The model predicted well the air temperature leaving pad1 and pad2

The crop temperature was always lower than the adjacent air temperature. The exceptions were probably due to more intense evaporative cooling effect on the air. The measurements of the crop temperature were shown to be larger than the predictions while the predictions of the inside air temperature were shown to be very close.

The simulation model was shown to be good for validating the heat transfer and less accurate in predicting the mass transfer; it only gave the trend of the freshwater production. The water output was adequate (0.8 l min^{-1}) for the greenhouse agriculture and drinking water.

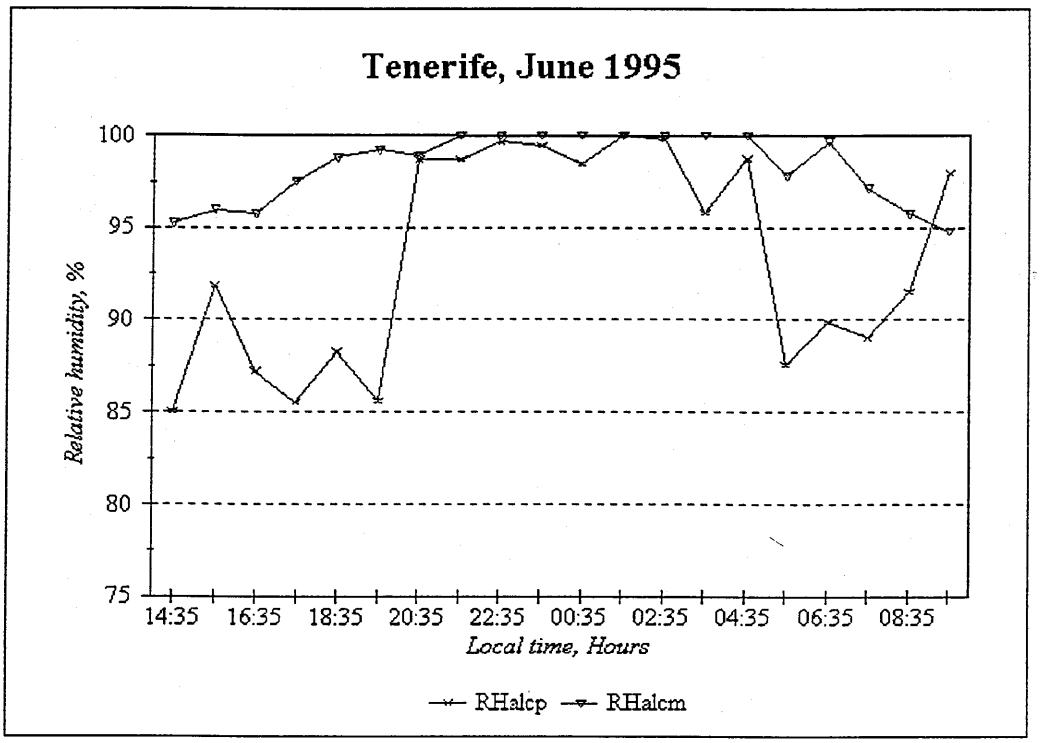

Fig. 7.36 Predicted and measured relative humidity of the air leaving the condenser

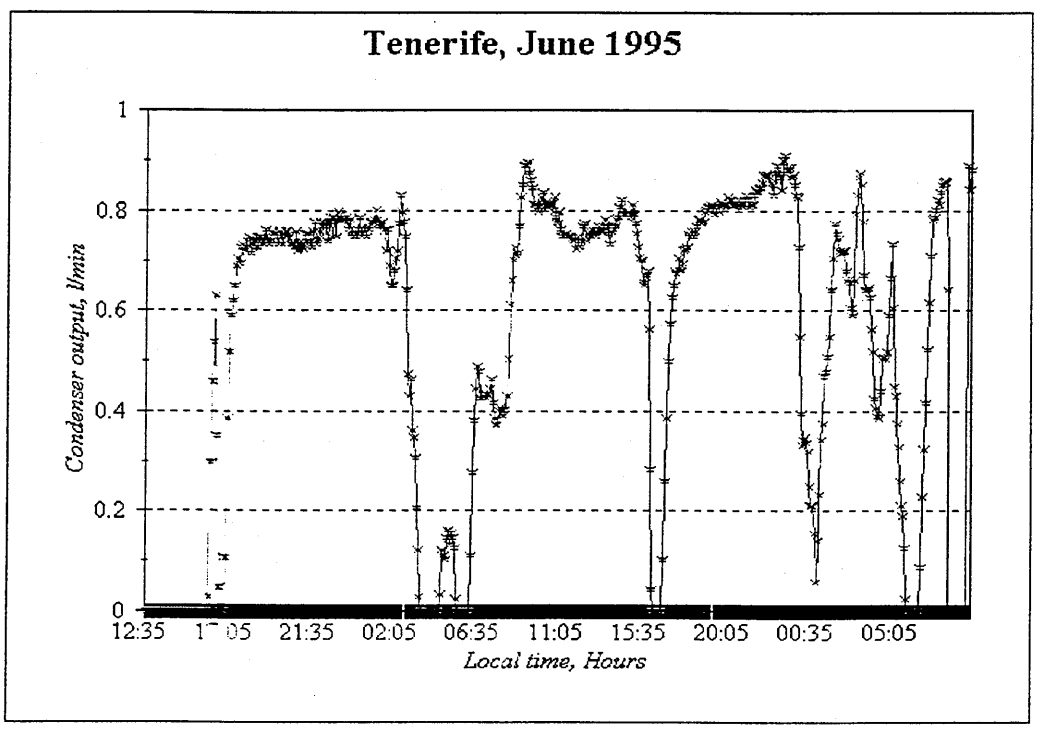

Fig. 7.37 Variations of the freshwater production

Chapter 8 Seawater greenhouse performance

8.1 Introduction

This chapter presents an analysis of the contributions of the components of the seawater greenhouse to the total water production, and how the latter is affected by solar radiation, wind speed, temperature and humidity of the ambient air and temperature of the water used to cool the condenser.

The effect of these parameters on the seawater greenhouse and component performance was predicted based upon experimental results and simulations.

8.2 Performance of each system of the greenhouse

The contribution of each element of the system in adding vapour to the air passing through the greenhouse and the roof cavity was assessed by simulations using meteorological data recorded during the months of December 1994 and June 1995 in Tenerife.

8.2.1 Evaporative cooling pad

The maximum rates of water evaporation from the cooling pad in Tenerife for the months of December and June were 2.2 kg day $^{-1}$ and 1.85 kg day $^{-1}$ per square meter of greenhouse floor respectively, as shown in Figs. 8.1 and 8.2. The evaporation from pad1 and pad2 represented 58 % and 32 % of the total evaporation rate in December and 25 % and 55 % in June respectively.

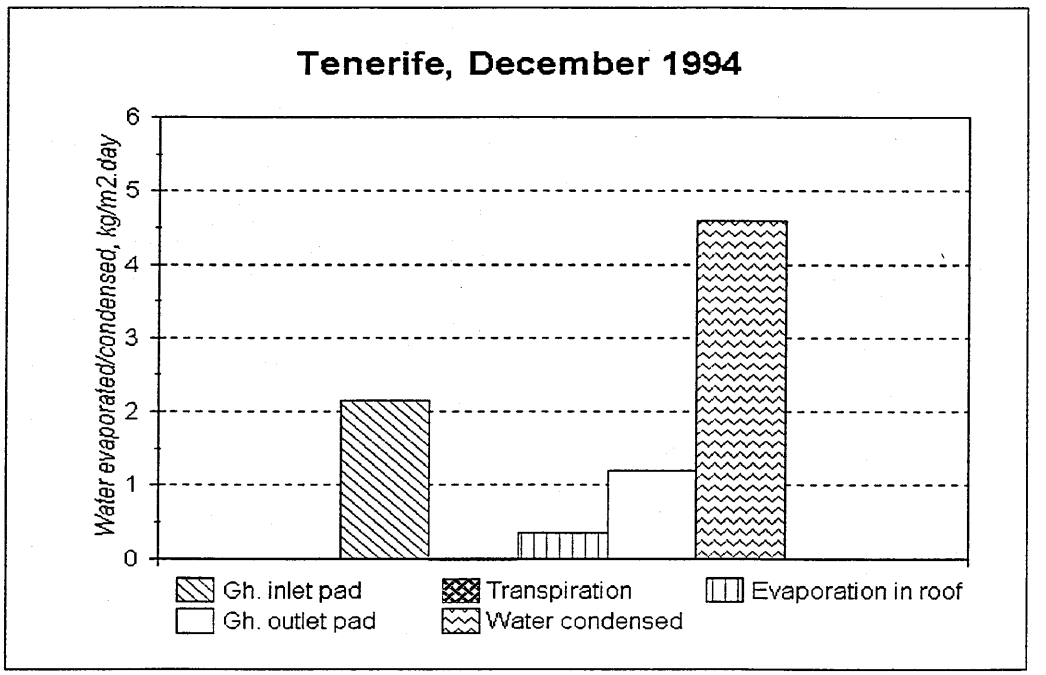

Fig. 8. 1 Contribution of system components to vapour production and water output of the condenser for the month of December

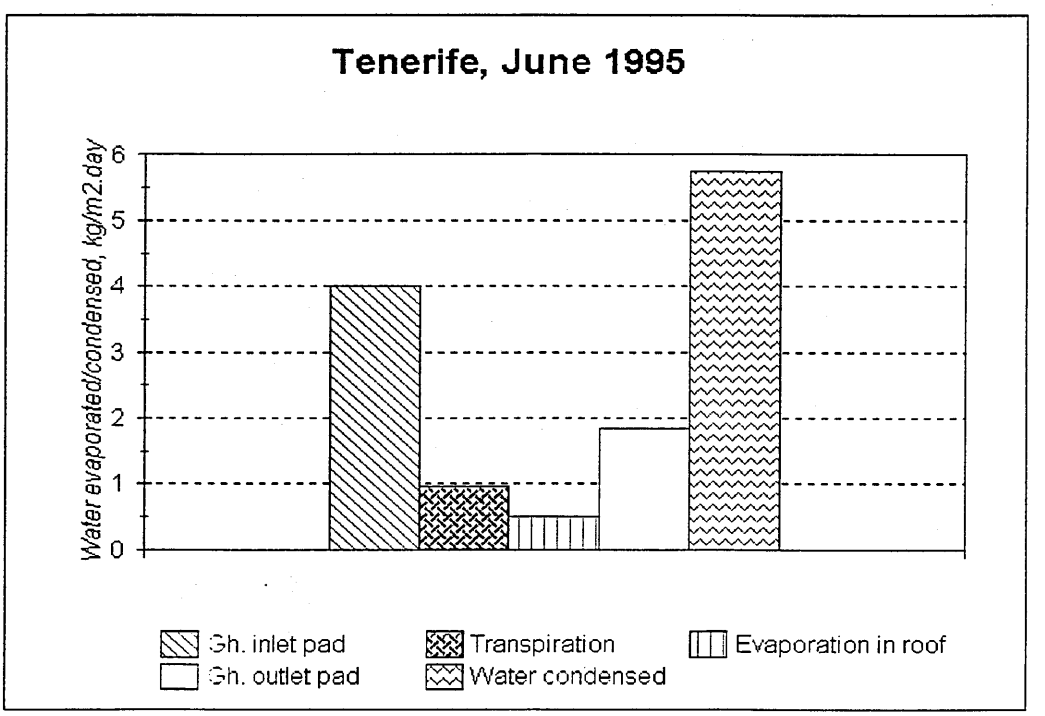

Fig. 8. 2 Contribution of system components to vapour production and water output of the condenser for the month of June

8.2.2 Greenhouse

Figures 8.1 and 8.2 show the prediction of transpiration rate of the plant; as expected, most of the water was transpired during day time in proportion to solar radiation. The daily water evaporation , transpiration and condensation was 2.2 kg m^{-2}, 0.2 kg m^{-2} and 4.6 kg m^{-2} respectively for the month of December and 1.85 kg m^{-2}, 0.96 kg m^{-2} and 5.7 kg m^{-2} respectively for the month of June. The transpiration represented 5 % and 13 % of the total evaporation rate for the months of December and June respectively.

In December, the lower condensation than during June was to be expected, since transpiration by small plants during December does not supply much water to the greenhouse system; the transpiration rate is lower due to the higher relative humidity.

8.2.3 Roof cavity

The rate of water evaporation from the roof cavity was 0.35 kg m^{-2} and 0.5 kg m^{-2} per day for the months of December and June respectively (Figs 8.1 and 8.2). The evaporation in the roof cavity represented 9.5 % and 7 % of the total evaporation for the months of December and June respectively. The contribution of the roof cavity in adding water vapour to the system was less than 10 %.

The water on the roof did not absorb a significant amount of solar radiation. This occurred because the heat removed by the water leaving the roof increased, thus the average roof temperature is lower and the saturated vapour pressure of the air leaving the cavity is reduced.

8.3 Greenhouse performance in Tenerife and Cape Verde

The model was used to predict the rate of water evaporated/condensed per m^2 of floor area for a seawater greenhouse in the Canaries and in the Cape Verde Islands. Meteorological data recorded at the Aeropuerto Reina Sofia in Tenerife and at Mindelo (S. Vicente) in Cape Verde were used to generate a consistent set of hourly average values of solar radiation, ambient temperature, cloud cover and air moisture content.

The roof cavity was not considered because of the small contribution to the water condensed as mentioned in the section 8.2.3.

The rate of freshwater production was simulated using with three different seawater temperatures: surface, and at depths of 100 m and 650 m for the island of Tenerife (Table 8.1).

8.3.1 Effect of solar radiation

The effect of the increase in solar radiation on water evaporation rate in Tenerife and Cape Verde is shown in Figs. 8.3, 8.4, 8.5 and 8.6; water evaporation rate increased as the solar radiation increased because the increase of solar radiation produced additional cooling load on the evaporative cooling system. Increasing solar radiation from 550 to 880 W m^{-2} increased water evaporation rate by 30 % in June and from 460 to 760 W m^{-2} increased water evaporation rate by 54 % in December. At night, transpiration was shown to be an almost constant rate of 0.003 kg m^{-2}. Soon after sunrise, transpiration increased with solar radiation but at a slower rate than the evaporation of pad1 and pad2. When solar radiation suddenly decreased, the transpiration rate seemed to respond instantaneously.

	Tenerife			Cape Verde		
	Tsurf	T-100m	T-650m	Tsurf	T-100m	T-650m
Jan	19	18.5	10	22.5	17.8	10
Feb	18	17.5	10	21.5	16.8	10
Mar	18	17.5	10	21	16.3	10
Apr	18	17.5	10	21.5	16.8	10
May	19	18.5	10	22.5	17.8	10
Jun	20	19.5	10	23.5	18.8	10
Jul	21	20.5	10	24	19.8	10
Aug	21.5	21	10	25	20.3	10
Sep	21.5	21	10	25	21.3	10
Oct	21.5	21	10	25.5	21.3	10
Nov	21	20.5	10	25	21.8	10
Dec	20	19.5	10	24	21.3	10

Table 8. 1 Monthly seawater temperature variations at different depths

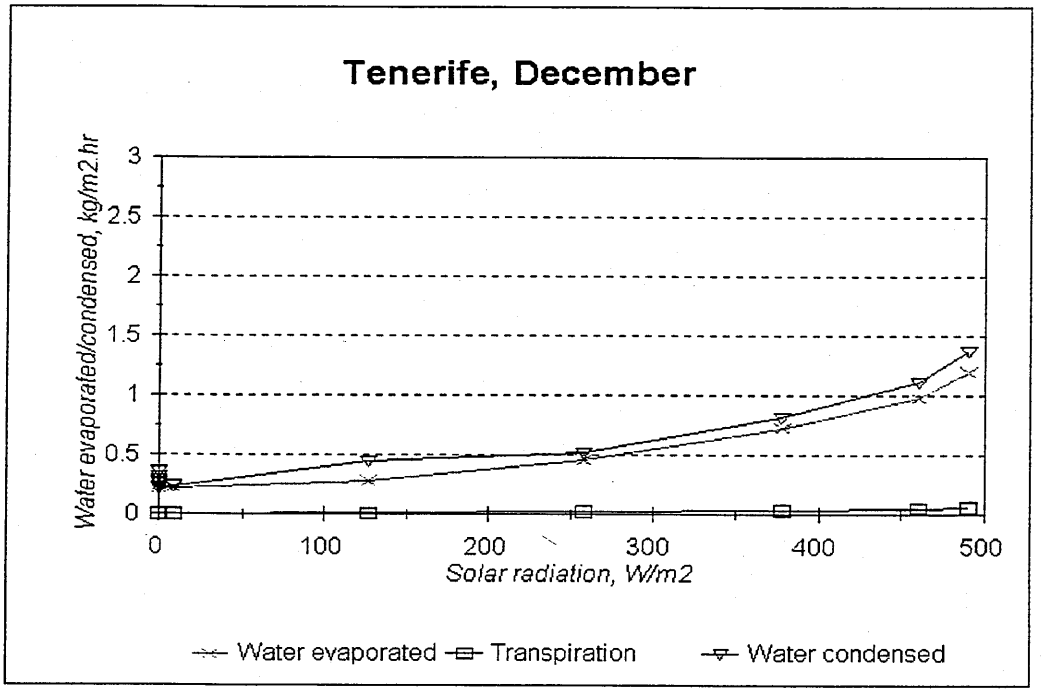

Fig. 8. 3 Influence of solar radiation on water evaporated, condensed and crop transpiration in December

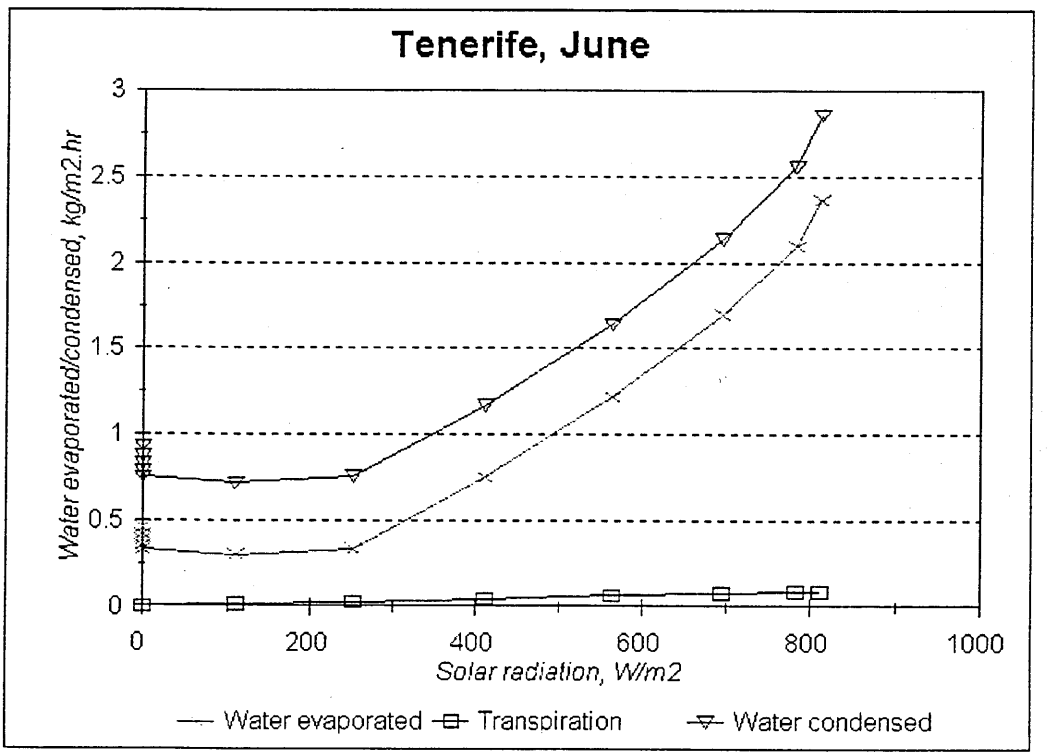

Fig. 8. 4 Influence of solar radiation on water evaporated, condensed and crop transpiration in June

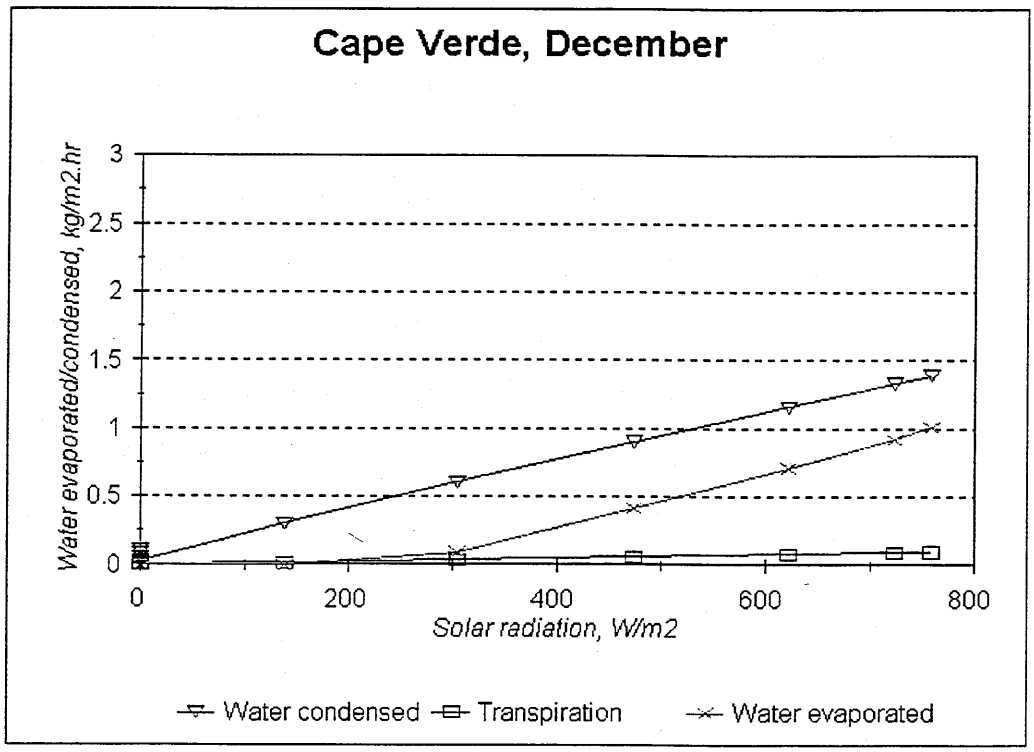

Fig. 8. 5 Influence of solar radiation on water evaporated, condensed and crop transpiration in December

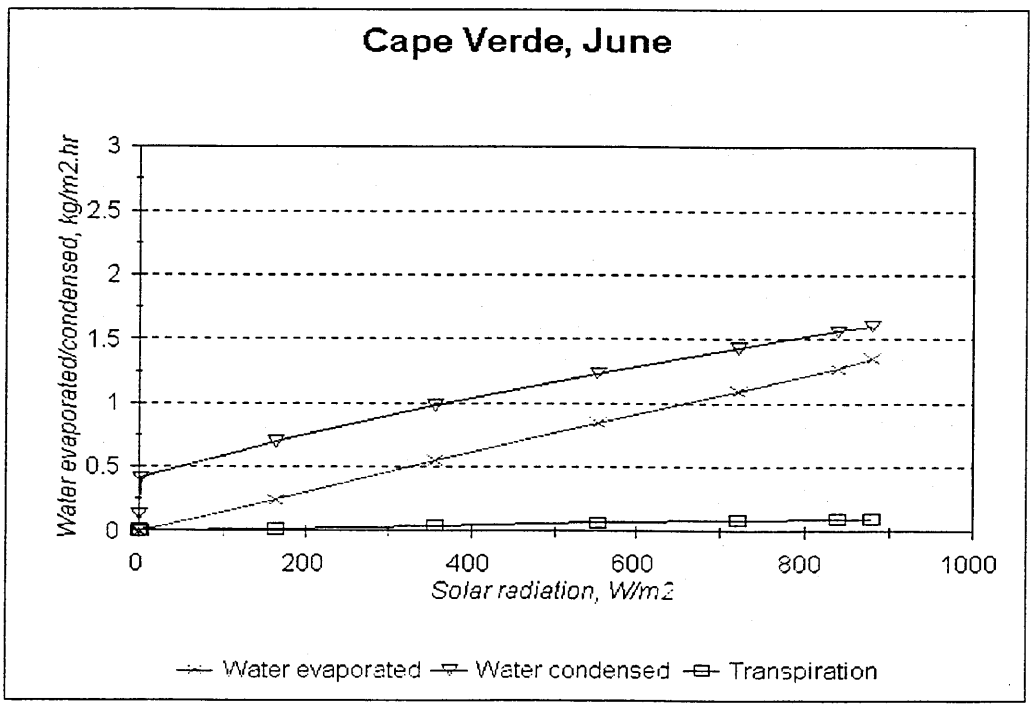

Fig. 8. 6 Influence of solar radiation on water evaporated, condensed and crop transpiration in June

8.3.2 Effect of outside air temperature

Figures 8.7, 8.8 show the effect of the variation in outside air temperature on water evaporation, water condensation and transpiration rates for Tenerife and Cape Verde. While the increase in evaporation and condensation rates was non linear, the transpiration rate was linear and constant. An increase of outside air temperature from 18 to 32 °C, in Tenerife and Cape verde, at evaporative cooling pad efficiency of 80 %, increased the evaporation and condensation rates by 83 % and 82 % during December (in Tenerife), and 90 % and 73 % during June, respectively. As shown in Figures 8.9 and 8.10, in Cape Verde, increasing the outside air temperature increased the evaporation rate from 0 to 1.2 kg m^{-2} per hour in December and 0 to 1.6 kg m^{-2} per hour in June, and increased the condensation rate from 0.4 to 1.8 kg m^{-2} per hour in December and from 0.6 to 2.5 kg m^{-2} per hour in June.

8.3.3 Effect of wind speed

The effect of wind speed on evaporation rate and condensation rate was not a very strong one because the ventilation air changes in volumetric flow and in water vapour content; the only parameter remaining constant, is the mass flow rate of the dry air. As shown in Figures 8.11 and 8.12, water condensation increased 25 % (in Tenerife) and 36 % (in Cape Verde) as the wind speed increased while the evaporation and transpiration rates were constant.

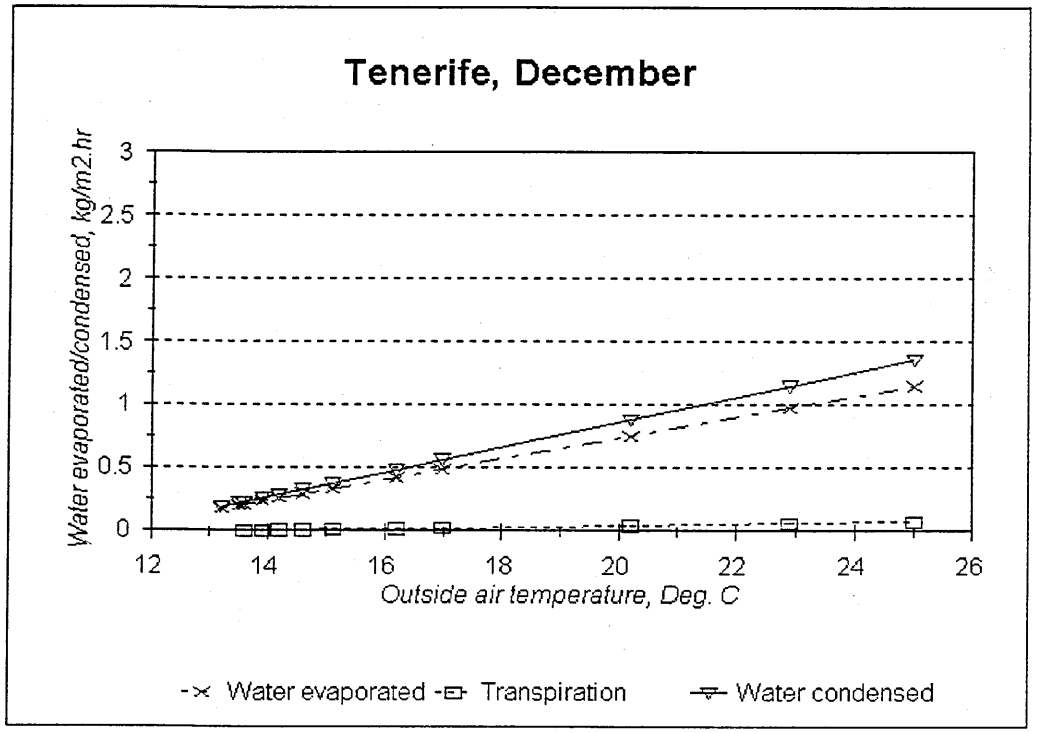

Fig. 8.7 Effect of the outside air temperature on the condenser output

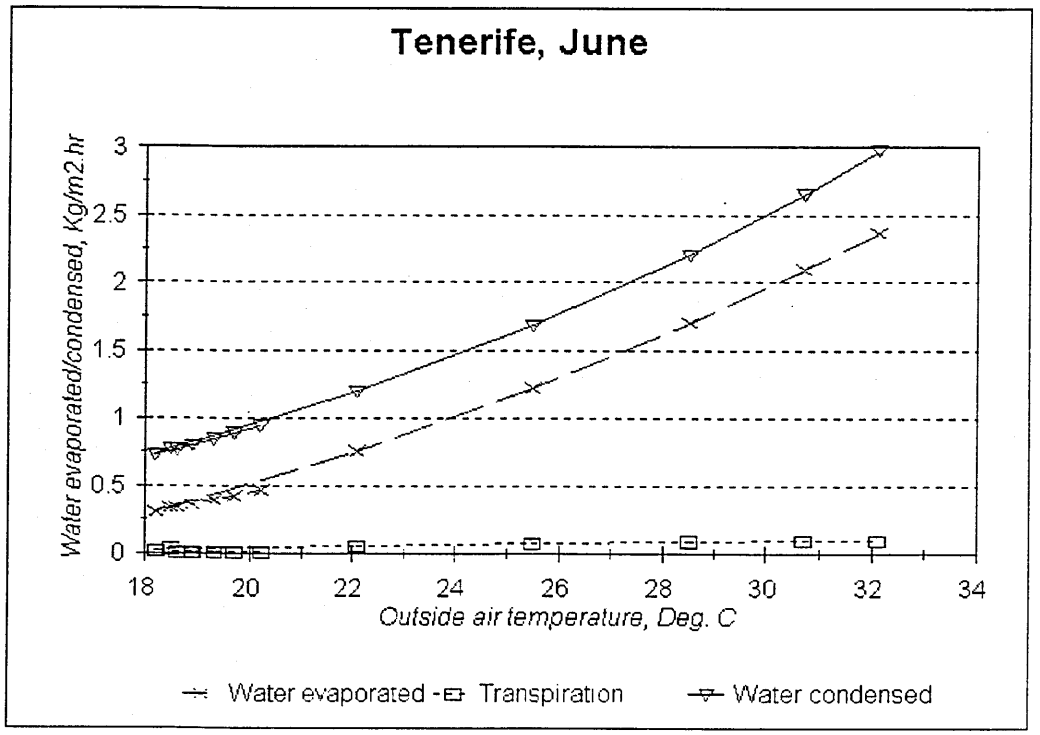

Fig. 8.8 Effect of the outside air temperature on evaporation, transpiration and condensation rates

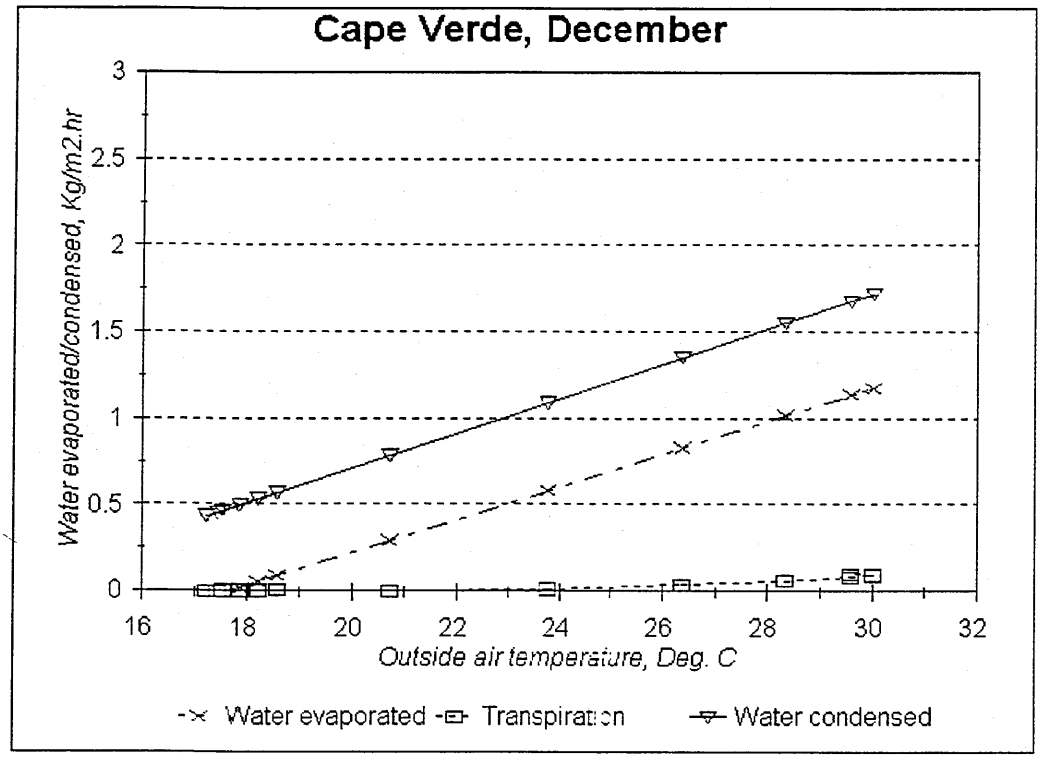

Fig. 8.9 Effect of the outside air temperature on the condenser output

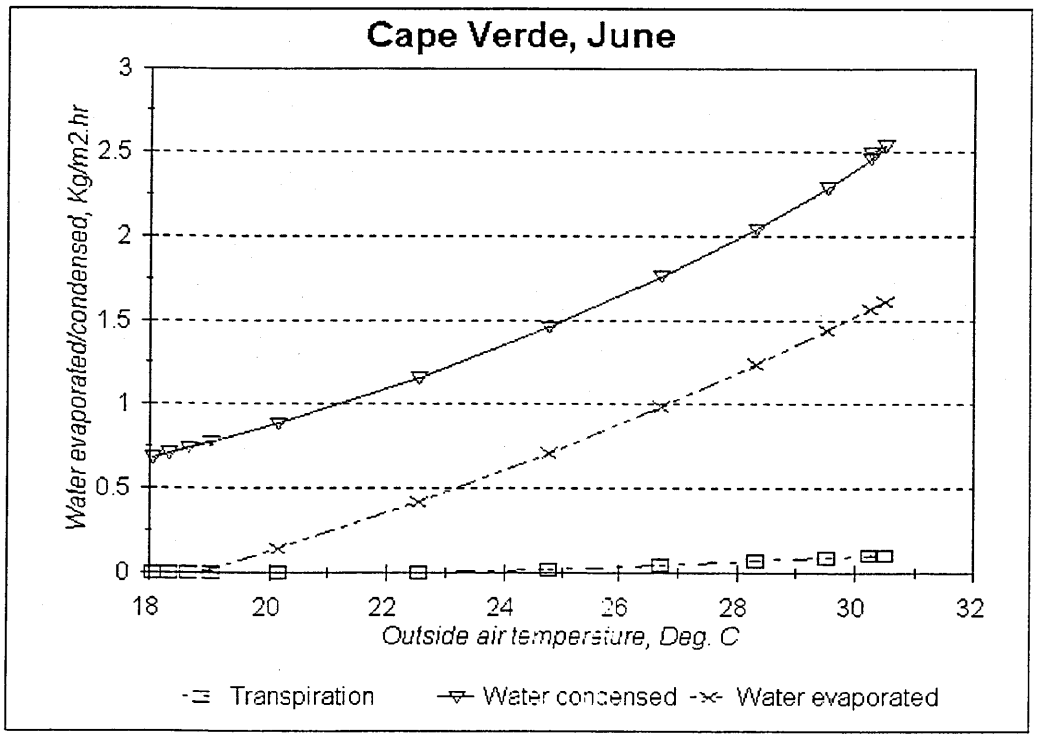

Fig. 8.10 Effect of the outside air temperature on the condenser output

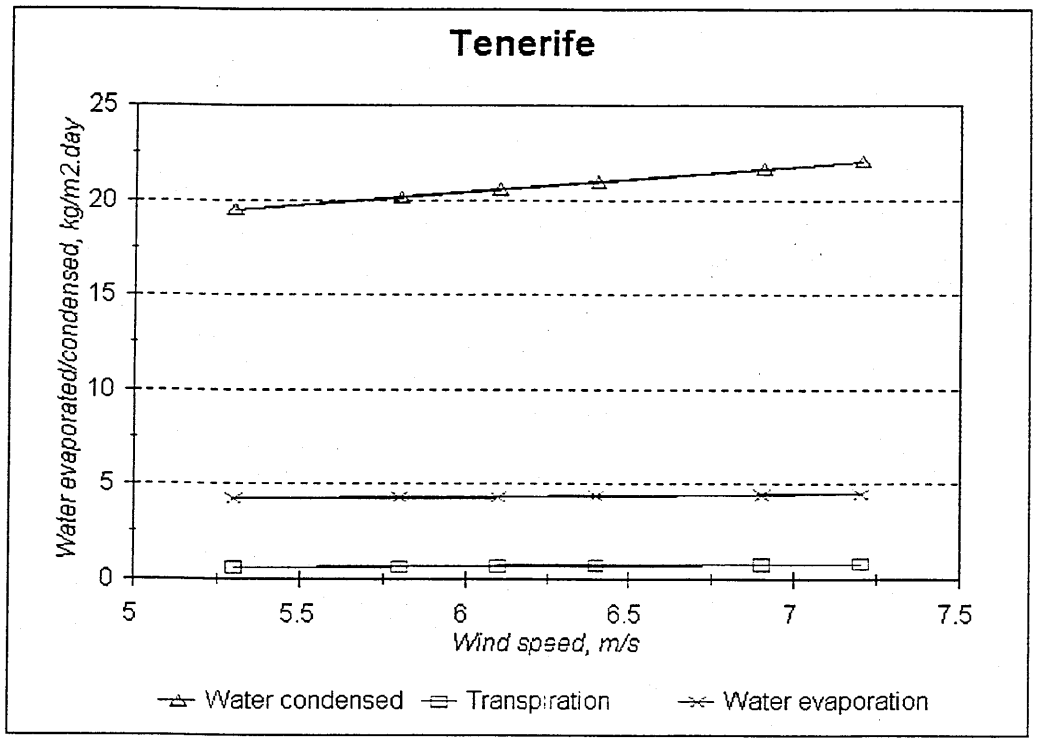

Fig. 8.11 Effect of the wind speed on water evaporation, water condensation and transpiration

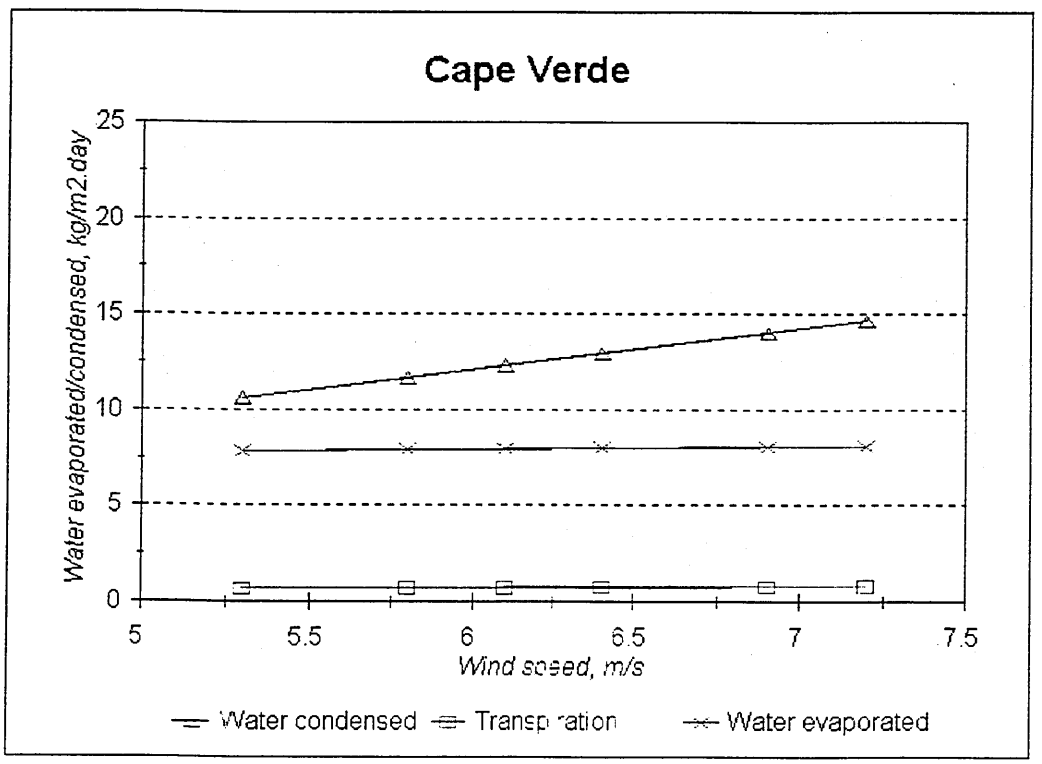

Fig. 8.12 Effect of the wind speed on water evaporation, water condensation and transpiration

8.3.4 Effect of seawater temperature

Figure 8.13 shows for Tenerife that the condenser output was 104, 193, 350 kg m^{-2} per year when using temperature at surface (average temperature 19.9 °C), and at depths of 100 m (19.4 °C) and 650 m (10 °C). The freshwater production maxima 43, 31 and 21 kg m^{-2} using seawater from 650 m, 100 m and the surface, respectively, occurred during the month of September and the freshwater production minima 17.5, 5.7 and 1.5 kg m^{-2} occurred in December (Fig. 8.14). Figures. 8.15 and 8.16 show for Cape Verde that the freshwater production was 96, 181 and 327 kg m^{-2} per year when using temperatures at surface, and at depths of 100 m and 650 m. The freshwater production increased 3.4 and 1.8 times when using seawater from 650 m and 100 m compared to the surface seawater temperature. The performance of the condenser was found to depend strongly on the cooling water temperature.

8.4 Economics of seawater greenhouse

The use of desalination is an alternative to the long distance transport of freshwater, and decisions determining its appropriateness should be made on the basis of economics. The subject of water economics is complex, since natural water supplies for cities and agriculture are frequently confused with water used for hydroelectric power production. There are many difficulties in assigning costs because of the confusion between cost and price, particularly when municipal ownership is involved.

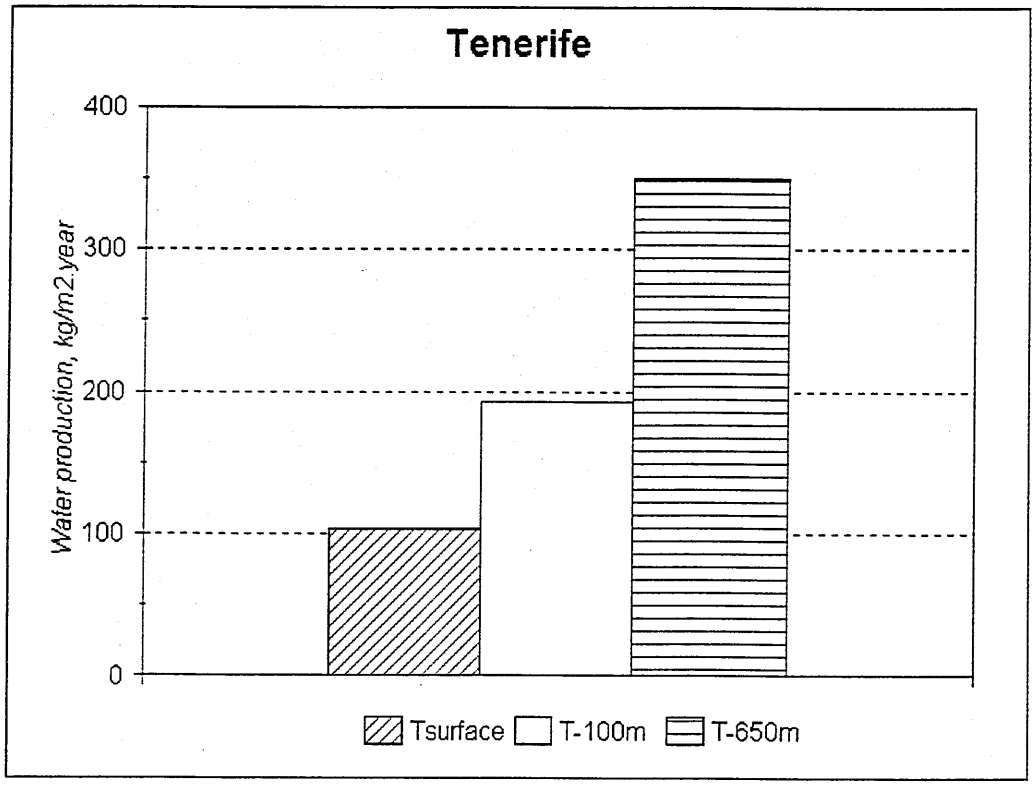

Fig. 8.13 Annual freshwater production using seawater temperature at different depths

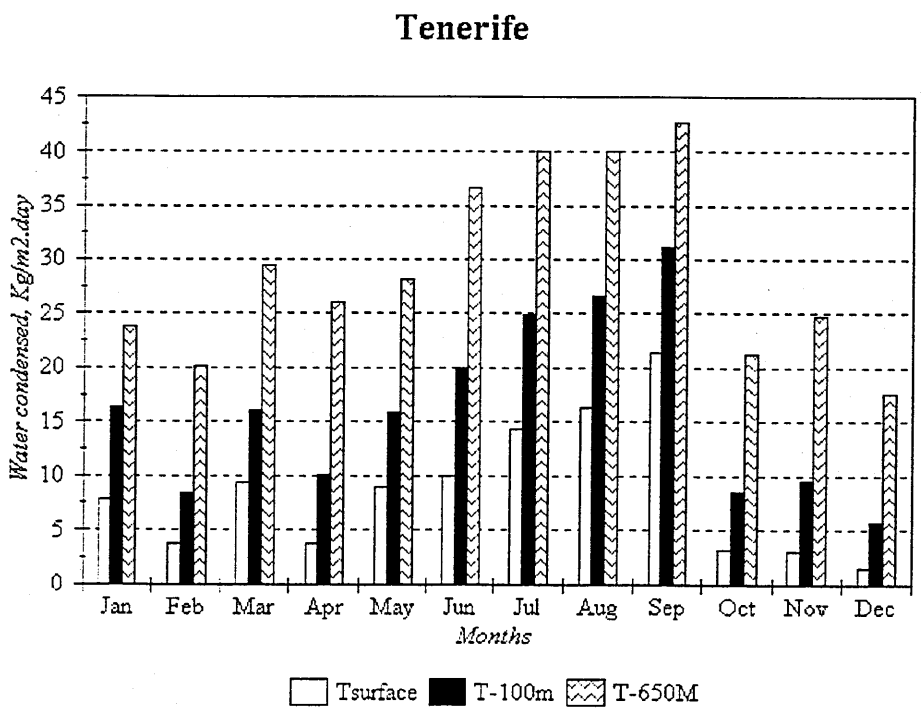

Fig. 8.14 Monthly water production using seawater temperature at different depths

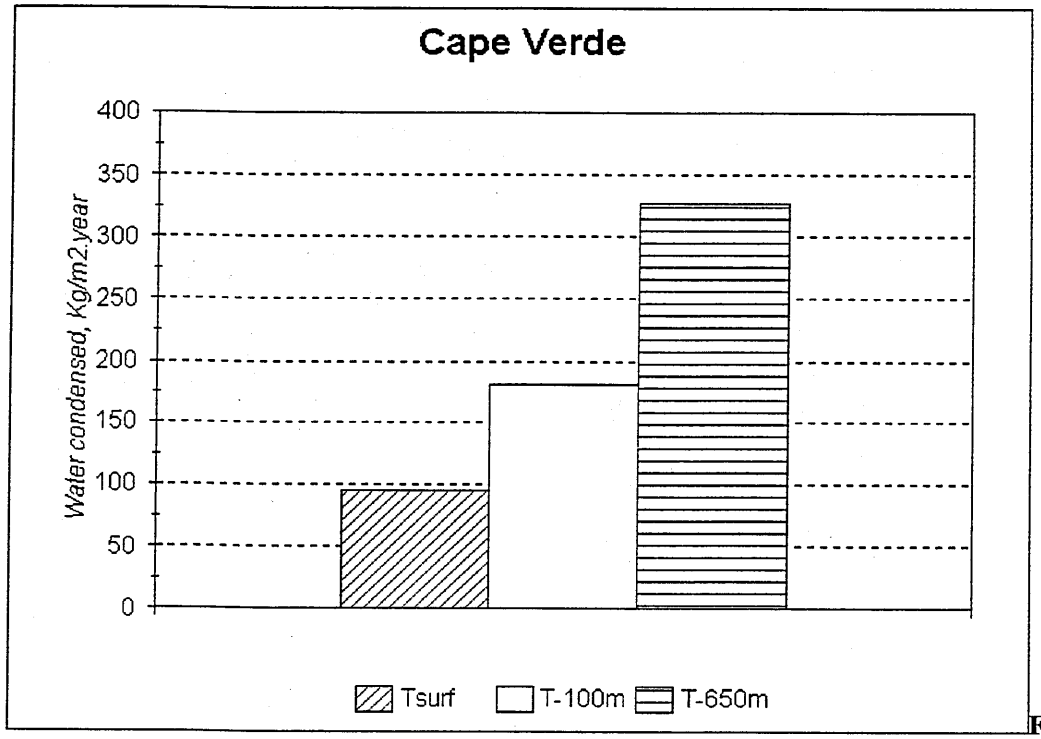

Fig. 8.15 Annual freshwater production using seawater temperature at different depths

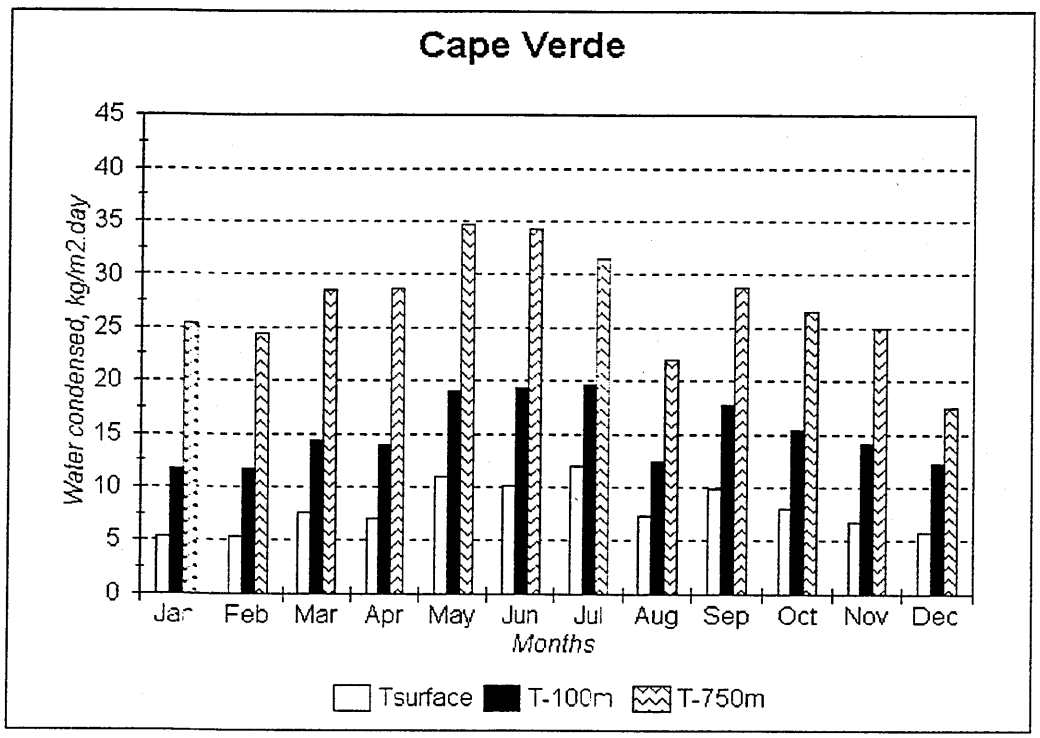

Fig. 8.16 Monthly water production using seawater temperature at different depths

Very often with municipal ownership, the price at which water is sold represents only a fraction of the capital investment, the resulting price may be much less than it would be if based on the amortization of the entire investment. It is important, therefore, in considerating the preparation of economic comparisons between desalination plants and the seawater greenhouse, to consider comparable total costs in the different cases if the comparison is to be valid.

8.4.1 Desalination plants

Four major cost elements in the production of desalted water are the cost due to capital amortization of the desalination plant equipment, cost of operation (including the cost of heat energy used for water production and the cost electrical energy required for operating pumps and auxiliary machines), and maintenance costs.

Gomkale [1968] made a detailed economic study of the comparative merits of a number of systems for supplying freshwater in the desert regions of India. His studies are summarised in Fig. 8.17 which shows the water cost comparison for different techniques of desalination.

Commercial desalination plants with capacities 45 m^3 d^{-1} supply freshwater at approximately £ 1.6 m^{-3} [Malik, 1982]; plants with higher capacities (227 m^3 d^{-1}) may reduce the cost to less than £ 1.4 m^{-3}.

8.4.2 Solar distillation

Solar radiation is the most important parameter affecting still productivity. It is the driving force in the distillation process. The fraction of solar radiation available for the process is a function of the still design.

Lof, G.O.G [1980] updated some previous comparative economic analyses of desalination methods (Lof, 1962, Bloemer *et al.*, 1965a, b), by multiplying them by a factor to correct for inflation. This factor was based upon the ratios of the building-material- labour index and plant cost index for mid-1962 to 1976.

The results of Lof's [1980] analysis showed that the cost of water produced by a solar still is approximately £ 0.80 m^{-3}. Large scale plants (> 3800 m^3 d^{-1}) using conventional energy sources can produce water at half the cost of a solar still; while small plants (< 38 m^3 d^{-1}) using conventional energy sources produce water at costs approaching or exceeding £ 0.80 m^{-3}.

These analyses are only as good as the data and assumptions (e.g., operation and maintenance, material and labour costs, wage rates, depreciation rates, interest rates and fuel cost escalation rates) they were based upon.

8.4.3 Seawater greenhouse

The Seawater Greenhouse represents a new approach to providing fresh water for growing crops. The prototype greenhouse was too small, and because of the need to use a chiller (with a high consumption of electricity) to simulate the cold seawater, cannot be used as the basis for an economic analysis. However, the

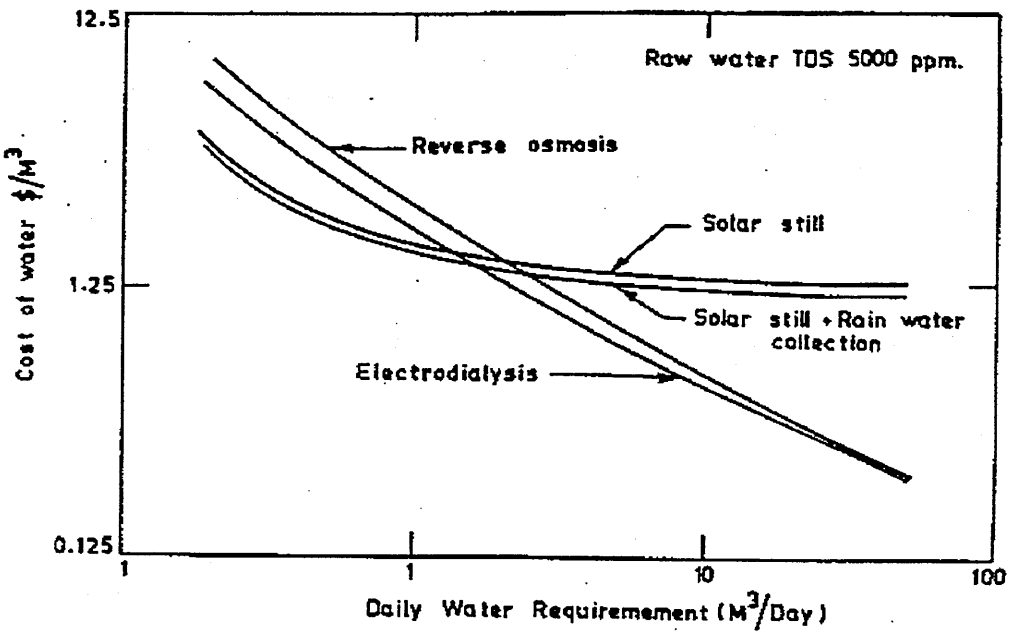

Fig. 8. 17 Water cost comparison for different techniques of desalination (After Gomkale, 1968)

Seawater Greenhouse was useful in providing the data needed for the design, modeling and performance analysis of different components of the system.

An economic assessment based on the seawater greenhouse model, was however carried out by ODA [1996] for a reference scheme in Oman (large scale) and a low cost solution for Gaza (Palestine). These are discussed below.

8.4.3.1 Tenerife prototype

As mentioned above, the Tenerife prototype was too small to benefit from the economies and effects of scale that would be found in a larger, commercial greenhouse.

8.4.3.2 Oman and Gaza schemes

The reference scheme located on the coast of Oman ODA [1996] was a 1 ha greenhouse (20 x 500 m^2) with 16 ha of shade tent for crop production; the seawater was drawn from a depth of 1 km. A pipeline of 0.7 m of diameter and 4 km of length was used to achieve the required flow of cool seawater (0.5 m^3 /s). This scheme indicated that it would produce freshwater at an average of 50 l day^{-1} m^{-2} of greenhouse.

The capital costs of the major components (greenhouse structure, pipeline, heat exchangers, condensers) were estimated by obtaining quotations from suppliers. The main costs are given in Table 8.2. The operating and maintenance costs (Table 8.3) assumed that labour costs need to include skilled staff to operate the equipment and oversee the intensive horticulture; maintenance costs of the shade

tent and the greenhouse was taken as 5% of the capital costs for the annual replacement of parts, and operating costs for the mechanical and electrical plant were estimated to be 2% of the capital costs. Power cost was assumed to be 10 p per kWh.

The economics of the scheme in Oman showed a moderate profit (a rate of return of 5.3% per year).

A sensitivity study of the scheme in Oman was carried out to assess the effect of the main parameters on the calculated rate of return. Fig. 8.18 shows that the income from the crops produced in the greenhouse and in the shade tent are the main factors. The rate of freshwater production and labour costs had only a small influence on the rate of return.

An alternative concept for a low cost solution (Gaza) ODA [1996] was studied with a longer greenhouse (100 m front to back), with seawater drawn from a depth of 100 m. The simulation of the amount of excess water produced per hectare was lower than in the Oman Scheme and so a smaller shade tent was adopted. The same approach as for the Oman scheme was used to show that the rate of return increased from 6% to 23%. This is due mainly to the large reduction in costs associated with the deep sea pipe. The smaller capital cost associated with this new configuration and the higher rates of return would make this the favoured option for all locations [ODA, 1996]. However this would require confirmation of the predicted performance by a pilot project.

Item	Annual cost
Electricity costs	£1,790
Greenhouse costs	
Maintenance	£31,460
Manure, sprays, etc.	£13,125
Labour	£26,087
Shade tent costs	
Maintenance	£40,833
Manure, sprays, etc.	£3,728
Labour	£27,163
Mechanical & electricity costs	£28,584
TOTAL	£172,771

Table 8. 2 Annual operating and maintenance costs for Oman (ODA, 1996)

Items	Costs	Background data
Greenhouse		
Area of Greenhouse		20 m x 500 m
Cost of structure	£200,000	£20 per m^2
Front evaporator	£12,500	£250
Back evaporator	£12,500	£250 per m^3
Condenser	£250,000	£20 per m^2
Fans	£54,200	£542 per 5 m
Piping	£100,000	£200 per m width
Installation	£42,920	£10% of equipment costs
Shade tent		
Area of tent		326.7 m x 500 m
Cost of tent	£816,667	£5 per m^2
Pipeline		
Size of pipe		710 mm x 4 km
Cost	£ 1,000,000	

Table 8. 3 Summary of main capital costs for Oman (ODA, 1996)

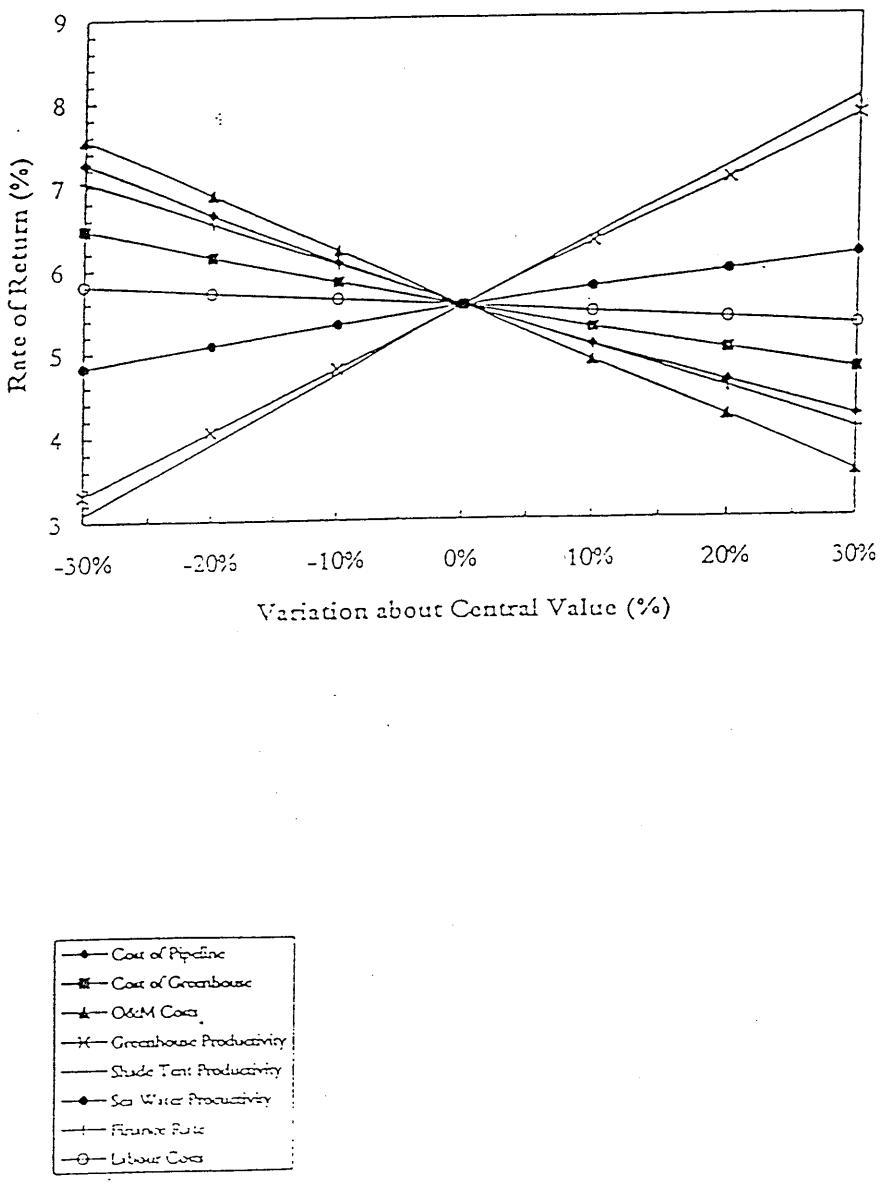

Fig. 8.18 Sensitivity study of the seawater greenhouse reference scheme (ODA, 1996)

8.4.3.3 Investment analysis

Malik [1982] defined the cost of water for a solar distillation as:

$$Cw = \frac{10\,I'(IA_m + MR_m + TI_m) + 1000\,(O'C' + S')}{A'(Y_D + Y_R)}$$

where

Cw = cost of water (pounds per m^3)
I' = total capital investment (pounds)
Ia_m = annual interest and amortisation rate (percentage of investment)
Mr_m = annual maintenance and repair labour and materials (percentage of investment)
Ti_m = annual taxes and insurance charges (percentage of investment)
O' = annual operating labour (man hours)
C' = operating labour wage (pounds per man hours)
Y_D = annual unit yield of distilled water (liter per m^2)
Y_R = annual unit yield of collected water (liter per m^2)
A' = area of distiller on which yields are based
S' = total cost (fixed and operating) of salt-water supply

The capital costs of the greenhouse and the other major items (structure, pipeline, heat exchangers and condensers) were estimated by obtaining quotations from suppliers.

The results of the analysis are summarised in Table 8.4. It is seen that for small area (small water output), in Tenerife, the water production cost for the prototype greenhouse was very high (£ 659 m^{-3} using the deep seawater and £ 384 m^{-3} using surface seawater); significant reduction in the cost of the water output may be achieved in Gaza (£ 40 m^{-3} and £ 2.2 m^{-3}) and in Oman (£ 5.7 m^{-3} and 0.2 m^{-3}). This show that larger area with higher water output is the most cost effective system. The most important variable is the value of the crops produced.

However, these cost projections are largely approximate on account of the numerous assumptions made regarding labour requirements, wage rates, and depreciation rates.

Conclusions

The simulations showed that the major sources of vapour were both evaporative pads (90 %) followed by the roof cavity (9.5 %) and plant transpiration (0.5 %) in December, while in June the two pads contributed 80 %, the plant transpiration 13 % and the roof cavity 7 % of the total water evaporated.

The condensation was much lower in December than in June since transpiration by small plants during December does not supply much water to the greenhouse system.

As shown in the sensitivity analysis, in Chapter 3, the contribution of the roof cavity in adding water vapour to the system was not very significant. The freshwater production increased by 7 % in Tenerife and by 12 % in Cape Verde when the wind speed increased from 5.5 m s^{-1} to 7.3 m s^{-1}. The performance of the condenser was found to depend strongly on the cooling water temperature.

The decision to utilise seawater greenhouses for the production of freshwater and crops, in general, should be based upon the economics of the system relative to the available alternatives. The economics of this design require an extensive area of cultivation behind the greenhouse and the production of high value products both inside and outside the greenhouse.

The Gaza and Oman schemes have not yet been tested at a demonstration scale and so the results should be treated with caution.

	Tenerife	Gaza	Oman
Area of greenhouse (m^2)	217	2000	10000
Annual yield of produced water (litre)	79200	4380000	21900000
Total capital investment (pounds)	1030000	1155000	1622000
Annual interest and amortization rate	0.12	0.12	0.12
Annual maintenance and repair labor and material	0.07	0.07	0.07
Annual taxes and insurance charges	0.16	0.16	0.16
Annual operating and labor wages (pounds)	3000	15500	55000
Total cost (fixed and operating) of seawater supply (pounds)	2000	20000	100000
Costs of water £ per litre	**0.3843**	**0.0022**	**0.0003**

Table 8.4 Costs of the water production for Tenerife, Gaza and Oman

Chapter 9 Conclusions and further works

General discussion

Remote areas in arid regions need freshwater badly while enjoying (or suffering) high intensity of solar energy. Effective utilisation of this solar energy in producing freshwater from the sea has been the aim of many research and engineering works in the field of solar desalination.

Radiation is the major mode of energy exchange between plants and their environment; solar radiation provides the main energy input to plants, with much of this energy being converted to heat, driving thermal radiation exchanges and processes such as transpiration. Means must be found to supply fresh water for drinking and agriculture in desert areas, which would enable development of self-sufficient communities in dry and arid areas. One of the ways to achieve this goal is the seawater greenhouse project.

Ninety percent of the water used to irrigate greenhouse plants is converted to water vapour during transpiration. In summer when high solar radiation produces high rates of transpiration, and ventilation is used to limit greenhouses temperatures, most of the irrigation water is removed as vapour by the ventilation air. The evaporative cooling process created a cool and humid environment particularly suitable for the crops (lettuces and French beans) which are at the same time important and expensive to produce in the Canary Islands.

A literature review was carried out on the different desalination methods. This review was supplemented by the function of the greenhouse, its roof cavity

with the selective absorber and the different cooling methods. All this work and the different greenhouse models are described in Chapter 2.

Thermodynamic submodels describing the thermal and mass balances of the direct contact condenser, the front and rear evaporative cooling pads and the roof cavity were developed and incorporated into the Silsoe Greenhouse Environmental Model discussed in Chapter 4. This simulation model was used to determine design parameters of the seawater greenhouse. These show how the performance in terms of fresh water production depends on some design parameters. A sensitivity analysis was carried out (Chapter 3) and showed the strong influence of the seawater temperature on fresh water production; the use of a second evaporative cooling (rear pad) gave more fresh water.

An optical properties study showed that the corrugated GRP material diffusely transmitted the radiation. After looking at the possibilities of clear PVC profiled sheet, extruded polycarbonate sheeting and profiled GRP, the translucent GRP was selected because it was the cheaper (Chapter 3).

A network of climate instruments was assembled, tested, installed and used to measure the microclimate of the seawater greenhouse and the outside climate (Chapter 5) in Tenerife during December 1994 and June 1995.

Measurements of the inside climate included dry and wet bulb temperatures inside the greenhouse and roof cavity, and soil, crop and roof temperatures. Dry and wet bulb temperatures, solar radiation. wind speed and wind direction were also monitored. Others sensors were used during some experiments to measure fresh and salt water temperatures, net radiation above the canopy, and

flow rates of fresh and seawater. The data obtained were used for calibration and validation of the model in this study.

Data of the CELdek™ evaporator were recorded in Tenerife to determine relationships of the heat and mass transfer coefficients which were used to validate the seawater greenhouse model. Chapter 6 demonstrated the mathematical model developed to estimate relationships between the volumetric overall heat transfer coefficient and overall mass transfer coefficient, based on the mass velocity of the air with a fixed mass velocity of water.
Experiments were performed on a prototype CELdek™ heat exchanger in the laboratory. Data were used to determine the film coefficient for the transfer from the spray water to the air-water interface and the overall coefficient of heat transfer based on the outside tube surface, from tube fluid to bulk water; the latter were used to design the CELdek™ condenser.

Chapter 7 provides the data recorded and analysed in Tenerife during the two experiments in December 1994 and June 1995. These measurements on air (inside the greenhouse, leaving pad1, leaving pad2 and the roof cavity) and crop temperatures, humidity of the air (inside greenhouse, after pad2, after condenser and in roof cavity) enabled the model to be validated. The agreement between the measured and predicted values verified that the model closely represented the thermal and mass balances of the direct contact heat exchanger and the roof cavity.

The final part of the project was to determine the performance of the different systems of the greenhouse. The simulations showed that the major sources of

vapour were both evaporative pads (90 %) followed by the roof cavity (9.5 %) and plant transpiration (0.5 %) in December, while in June the two pads contributed 80 %, the plant transpiration 13 % and the roof cavity 7 % of the total water evaporated.

The utilisation of the seawater greenhouse as a source of freshwater for agriculture is essentially determined by the economic viability. From the discussion made so far in Chapter 8, it is clear that the cost of production of freshwater from the seawater greenhouse is about £ 0.2 per m^3 for greenhouses of areas larger than 10 000 m^2. The cost would rise at lower areas because of labour wages at the manufacturing plant do not get reduced proportionately. Further analysis must be made for greenhouse with larger areas in terms of crops productions.

Conclusions

- The sensitivity analysis showed the strong influence of the seawater temperature on fresh water production; the use of a second evaporative cooling (rear pad) gave more fresh water. The freshwater production increased with the increase of the mass flow rate until an upper limit.

- The validity of the seawater greenhouse simulation model has been checked using measurements of selected input and output; the model has been revised as a result of the validation exercise. The simulation model was good for predicting the heat transfer but poor at predicting the mass transfer.

- The mathematical model of the thermal behaviour of the seawater greenhouse was general in that it could be used to represent the

performance of the seawater greenhouse in any location, given the relevant meteorological data.

- The data obtained in this study were systematic and accurate. They are extremely valuable for studies related to seawater greenhouse microclimate , greenhouse microclimate modeling and plants irrigation.

- The actual performance of individual systems have been determined using experimental data recorded on the prototype seawater greenhouse in Tenerife.

  The performance of the greenhouse and its components confirmed the results of the sensitivity analysis. It was shown that the roof cavity contribution in terms of water vapour was too small (10 %) to be economic.

  The freshwater production increased 3.4 and 1.8 times when using seawater at depths of 650 m and 100 m compared to the surface seawater temperature; these show the effect of the seawater temperature on the performance of the condenser.

- The economics of this design require an extensive area of cultivation behind the greenhouse and the production of high value products both inside and outside the greenhouse.

- The Gaza and Oman schemes have not yet been tested at a demonstration scale and so the results should be treated with caution.

Recommendation for further work

The primary goal of the seawater greenhouse modeling is to evaluate the various parameters which affect the freshwater production. The model developed in this study is capable of accurately predicting various microclimatic variables and the production of water necessary for the irrigation. The first suggestion for further studies is:

- The need to do experiments on the prototype CELdek™ heat exchanger and get more data by varying the following variables: air flow rate, water flow rate in tubes, and solar radiation.

- The design and test of the CELdek™ condenser using the method proposed in Chapter 6

- The test of the different schemes at a demonstration scale in order to get the real costs and the rate of return.

- The model, previously simulated using the Advanced Continuous Simulation Language (ACSL) could be rewritten using SIMULINK (see appendix C). SIMULINK which is an extension to the MATLAB numerical computational package, allows large dynamic models to be simulated using rather novel 'iconographic' programming techniques. The model is constructed using mouse-driven commands to connect a variety of linear and non-linear blocks contained within SIMULINK ' s iconographic libraries. The program then automatically formulates and solves the model

equations on the basis of the overall block diagram, utilising user-specified integration routines.

The advantage of the model in this form include : pictorial representation of the model which enhances visualisation of the model; the ability to change model parameters interactively during simulation; availability of data produced by the model to MATLAB, where model identification and sophisticated plotting routines are provided.

Appendix A

A1. Meteorological data

Meteorological data recorded at the Aeropuerto Reina Sofia and ITER in Tenerife (Spain) were obtained from the CMZ Santa Cruz Tenerife. Complete data were available for the 6 years 1987-1992.

The data consisted of monthly values for:

Maximum temperature (^{o}C)

Minimum temperature (^{o}C)

Total hours of sunshine (insolation) (h)

Average wind velocity (km h^{-1})

Dry bulb temperature (^{o}C) at 7.00, 13.00, 18.00 h local time

Relative humidity (%) at 7.00, 13.00, 18.00 h local time

Cloud cover at 7.00, 13.00, 18.00 h local time.

These data were used to generate the consistent set of hourly values, required by the simulation model for the months of June and December 1987 using the following methods.

A.1.1 Global radiation

The hourly global radiation received on a horizontal surface at a given latitude was predicted using the method developed by Bailey [1987]. This uses semi-empirical formulae to estimate:

i) Monthly extra-terrestrial solar radiation

ii) Monthly radiation integral at the earth's surface

iii) Hourly global radiation integral

Mean values for the monthly extra-terrestrial radiation on a horizontal surface, H_o *[MJ* m^{-2} *day*$^{-1}$*]*, were obtained using the equation of Duffie and Beckman [1974].

$$H_o = I_{SC}\,(\tau/\pi)\,[1 + 0.033\cos(2\pi N/365.24)]\cos\lambda\,\cos\delta\,(\sin\omega_S - \omega_S\cos\omega_S) \qquad (1)$$

where τ = length of the day *[s]*

I_{SC} = solar constant *[1353 W* m^{-2}*]*

N = Julian day number

The sunset hour angle [rad] is given by

$$\omega_S = \arccos(-\tan\lambda\,\tan\delta) \qquad (2)$$

where λ is the latitude [rad].

The solar declination δ *[rad]* is given by

$$\delta = \sin(23.45\pi/180)\sin[2\pi(N+284)/365.25] \qquad (3)$$

The average monthly global radiation received at the surface of the earth was calculated using the modified Angstrom relationship reported by Knight, Klein and Duffie [1991]

$$Hs = Ho\,(a1 + b1\,(S/Z'))\qquad(4)$$

where S = number sunshine hours for the month [h]

Z' = day length [h] [$360\,\omega_s/(15\,\pi)$]

$$a1 = -0.27 + 1.75(S/Z') - 1.34(S/Z')^2$$

$$b1 = 1.32 - 2.93(S/Z') + 2.30(S/Z')^2$$

The average hourly global radiation received on a horizontal surface was obtained using the equation given by Pereira and Rabl [1979]

$$I = Hs(\pi/\tau)((a_2+b_2\cos\omega)[(\cos\omega-\cos\omega_s)/((\sin\omega-\omega\sin\omega_s)]\qquad(5)$$

where ω = angle [rad] relative to solar noon $(=2\pi t'/\tau)$

$$a_2 = .409 + 0.5016\sin(\omega_s - 1.047)$$
$$b_2 = .6609 - 0.4767\sin(\omega_s - 1.047)$$

The diurnal variation in global radiation for 6 months is shown in Figs. A.1 and A.2.

A.1.2 Air temperature

The diurnal variation was obtained using the method proposed by Parton and Logan [1981] and evaluated by Wann *et al.* [1985]. This uses a truncated sine

function to predict the temperature during the day and an exponential function at night. In principle the parameters of the model can be estimated using the five temperature values (maximum, minimum, and values at 7.00, 13.00 and 18.00 GMT). However as the model consists of two discontinuous functions, one during the day and one at night, and because the three air temperatures available were measured during the day, fitting the exponential at night was problematic. Consequently the following method was used [Wann *et al.*, 1985].

A.1.2.1 Mathematical model for air temperature

Suppose that the maximum temperature occurs between sunrise, tr, and sunset, ts, and that the minimum temperature occurs in the early morning. Then the time of the maximum temperature is given by

$$tx = 0.5\,(tr + ts) + \alpha \qquad (1)$$

where α is the time difference between the occurrence of tx and midday. Similarly, the time of the minimum temperature is

$$tn = tr + \beta_0 \qquad (2)$$

where β_0 is the time difference between tn and sunrise. Furthermore,
The first inequality ensures that the minimum temperature occurs before the time of maximum temperature. The second inequality expresses the assumption that the maximum temperature occurs before sunset. For given maximum and minimum temperatures, and sunrise and sunset times, the model

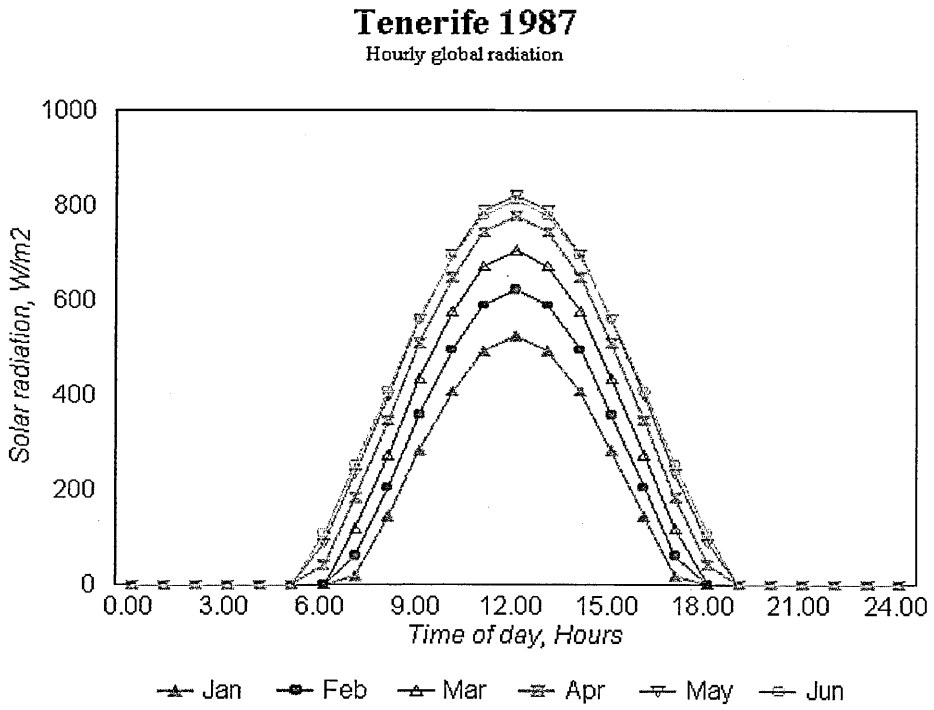

Fig. A. 1 Diurnal variation of global solar radiation January-June

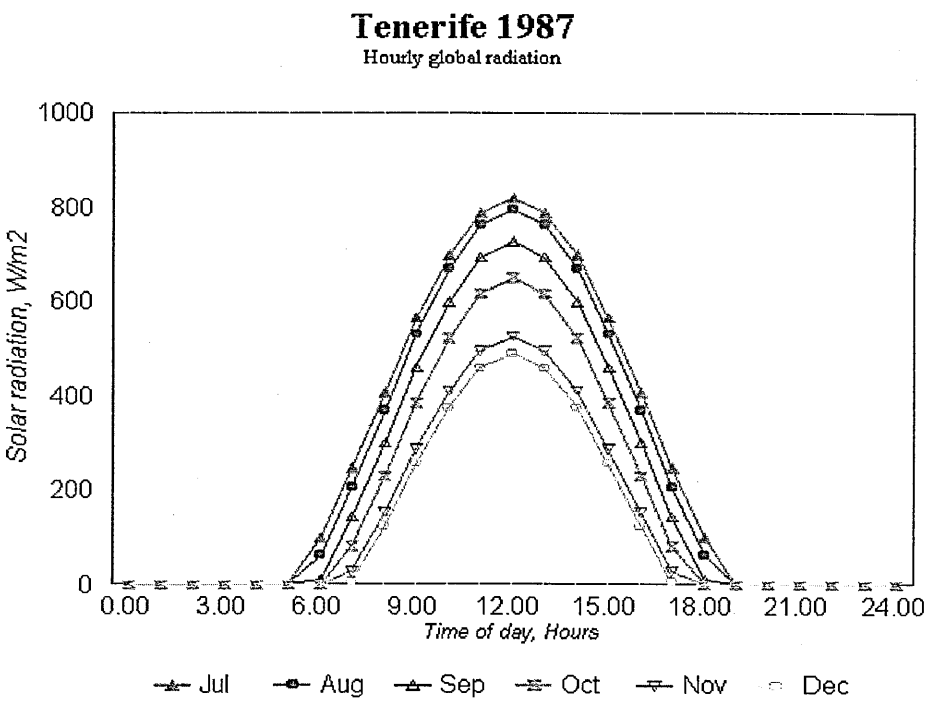

Fig. A. 2 Diurnal variation of global solar radiation July-December

$$0.5(ts-tr) + \beta_0 < \alpha < 0.5(ts-tr)$$

of Parton and Logan calculates the temperature Ta(t') at time t' according to the following equations:

$$Ta(t') = Ta+(Tx-Tn)\sin[(\pi(t'-tr-\beta_0))/(1 + 2(\alpha-\beta_0))] \quad (3)$$

for $tn \leq t' \leq ts$

and

$$Ta(t')=Tn+[Ta(ts)-Tn][\exp[-(\gamma_0(t'-ts))/(24-1+\beta_0)] \quad (4)$$

for $ts \leq t' \leq tn$

In the above equation tn is the time of the minimum temperature, $Ta(t')$, for the next day. The day length L is calculated as ts - tr and γ_0 is a decay parameter which determines the rate of temperature change from sunset to tn of the next day.

Note that equation 4 is substantially different to that given by Parton and Logan [1981] as it has been modified to allow for the exponential decay to the minimum temperature.

The original attempts to solve Equations 3 and 4 for α, β_0 and γ_0 using temperatures at 07:00, 13:00 and 18:00 hours proved unsuccessful because the values at 07:00 and 13:00 were inconsistent with the maximum and minimum temperatures.

As the latter pair was considered the more important of the sets, the parameters β_0 and γ_0 were fixed at zero and unity respectively [Bailey, 1987]. Setting $\beta=0$

means the minimum temperature occurred at sunrise. The curve fitting was carried out using the corrected Gauss-Newton method for the solution of non-linear least squares problems, which was available as a computer library
program NAG Library [1996]. The representations of the temperature for three months are shown in Fig. A3. The predicted diurnal temperature variation for the twelve months is given in Figs A4 and A5. These curves correctly represent the maximum and minimum temperature.

A.1.3 Humidity

Relative humidity values averaged over the days of each calendar month were available for 07:00. 13:00 and 18:00 hours. These values were used with the corresponding values of average air temperature to calculate the air moisture content. These data exhibited a much less pronounced diurnal cycle than the relative humidity data. A cubic spline was fitted to the three data values for each month and used for interpolation. The root mean square deviation between the observed and fitted values over the year was 0.000002 kg/kg.
The representations of the air moisture content for three months are shown in Fig. 6, a good fit between the predicted and measured air moisture content is obtained except for the month of September 1987. The diurnal variation predicted by the spline function for each month is shown in Fig. 7 and 8. We can note that there is a big variation of the moisture content of the air during the months of September and October 1987, which suggests there may be errors in the meteorological data records.

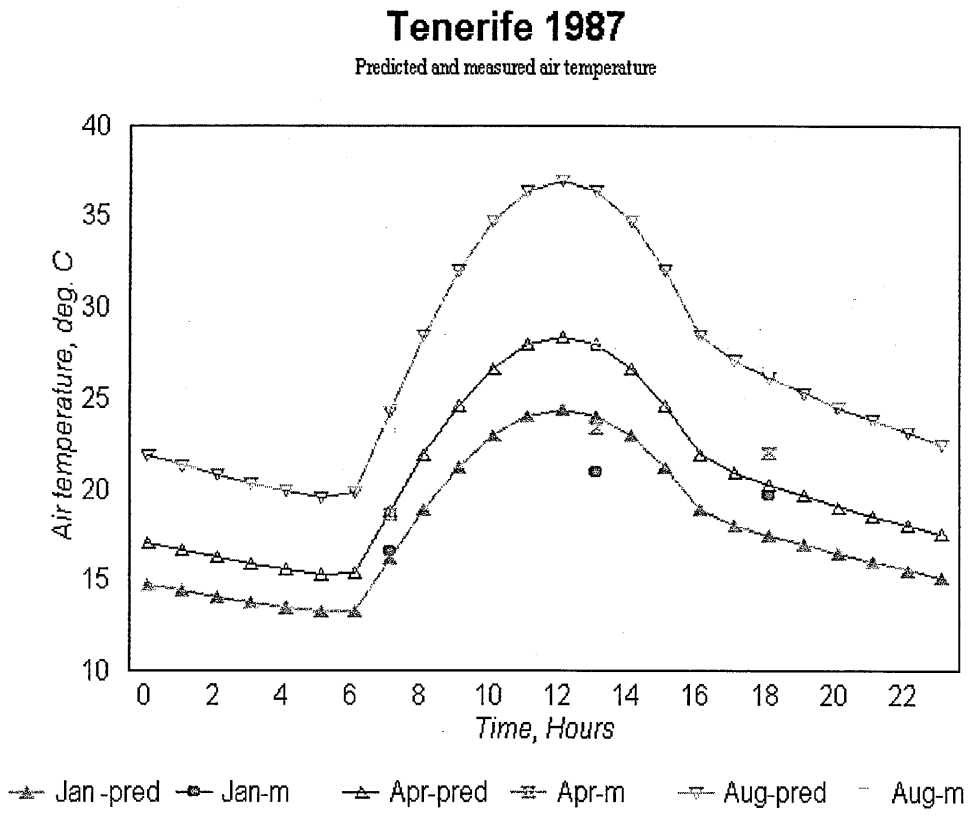

Fig. A. 3 Comparison of modeled and measured air temperature

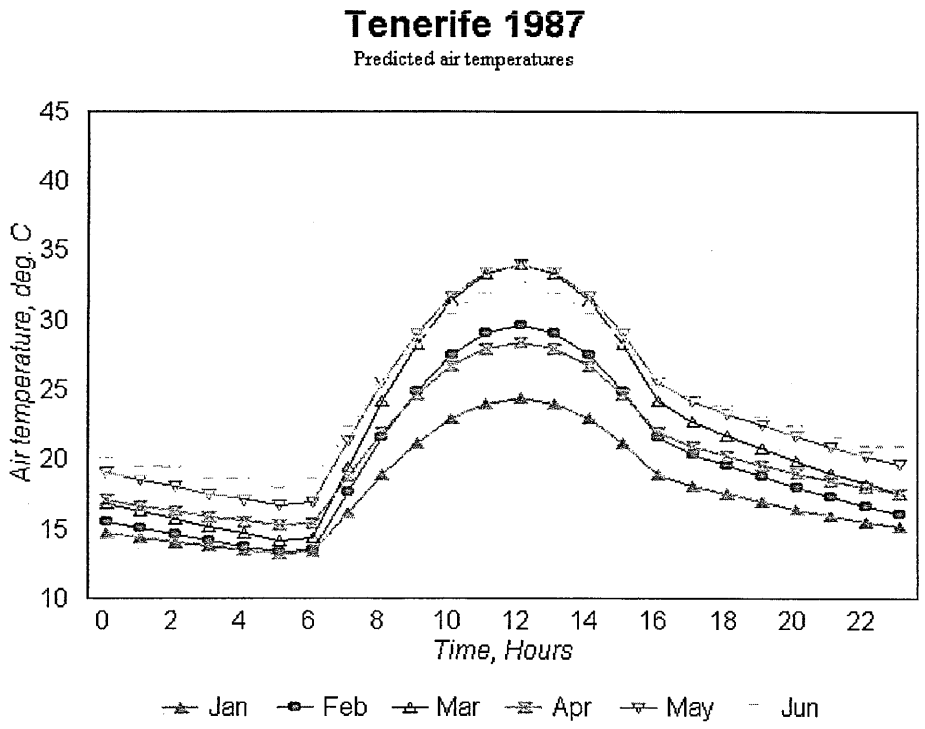

Fig. A. 4 Diurnal variation of air temperature January-June

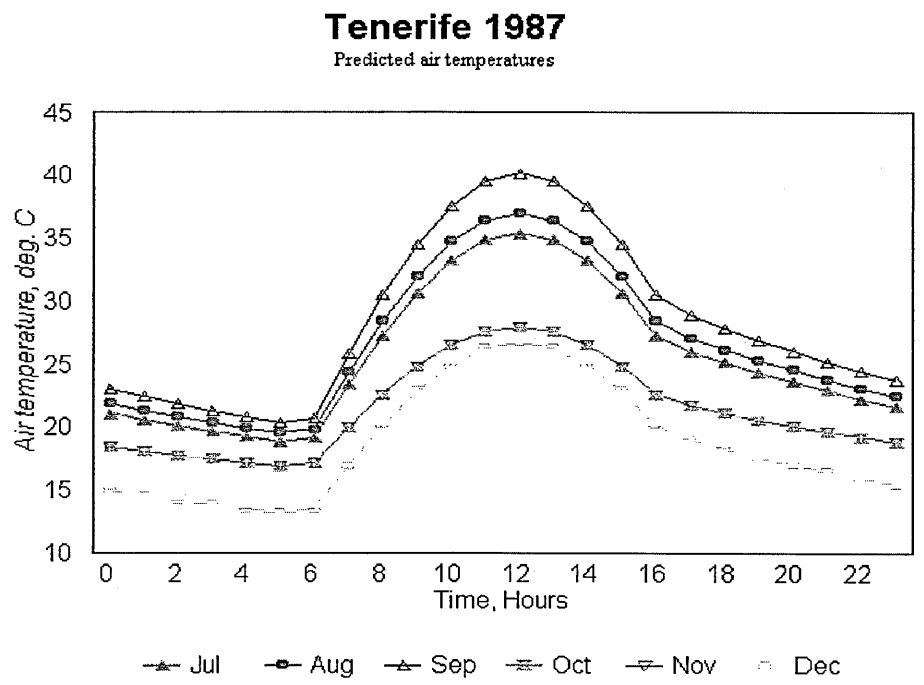

Fig. A. 5 Diurnal variation of air temperature July-December

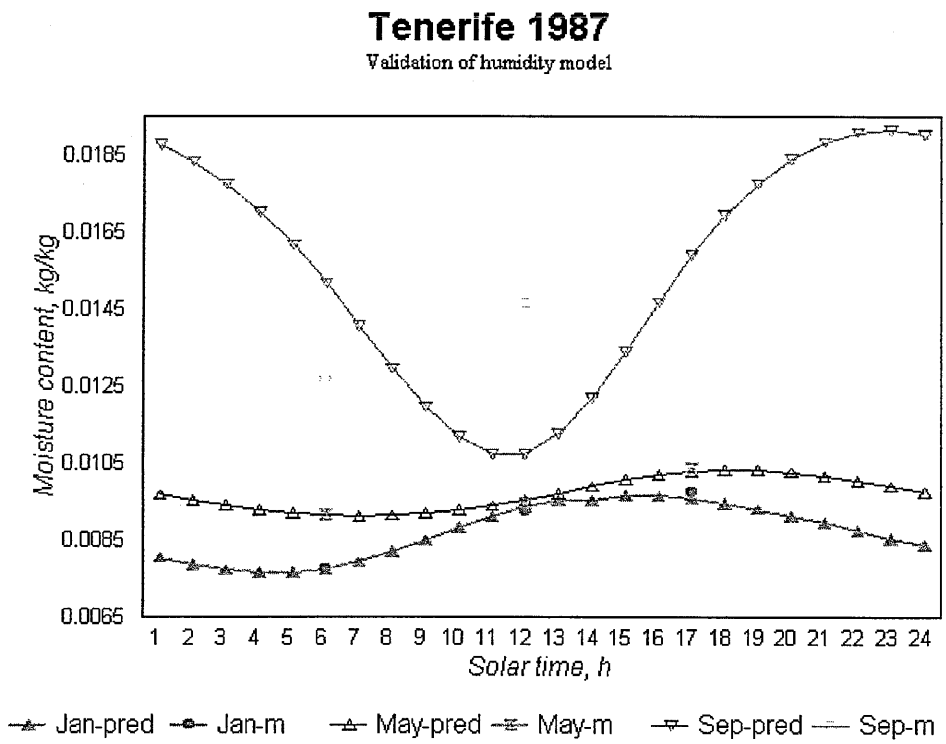

Fig. A. 6 Comparison of modeled and measured air moisture content

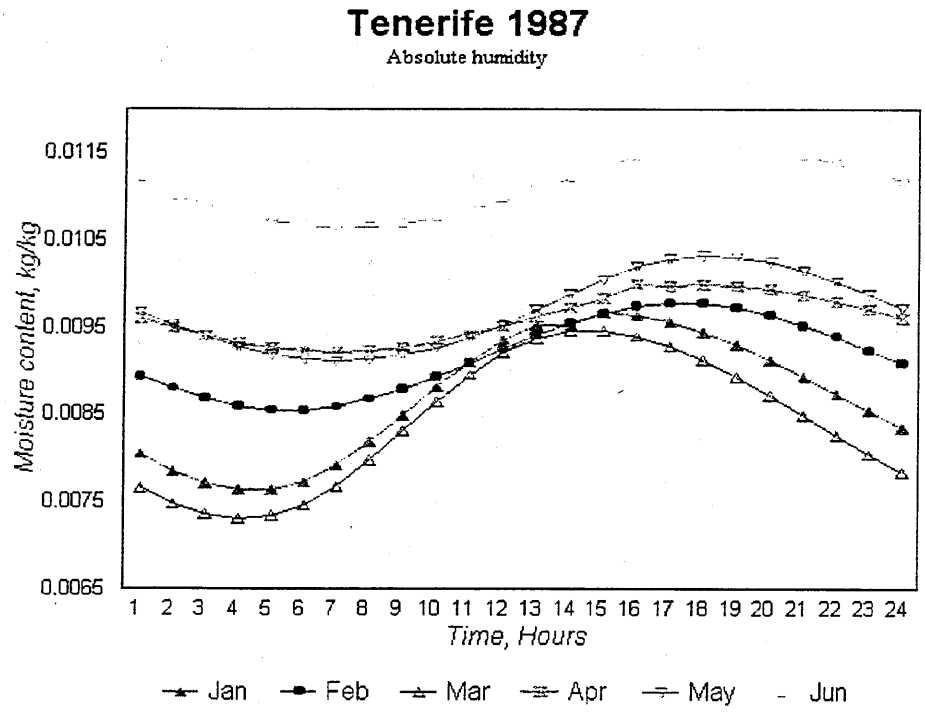

Fig. A. 7 Diurnal variation of air moisture content January-June

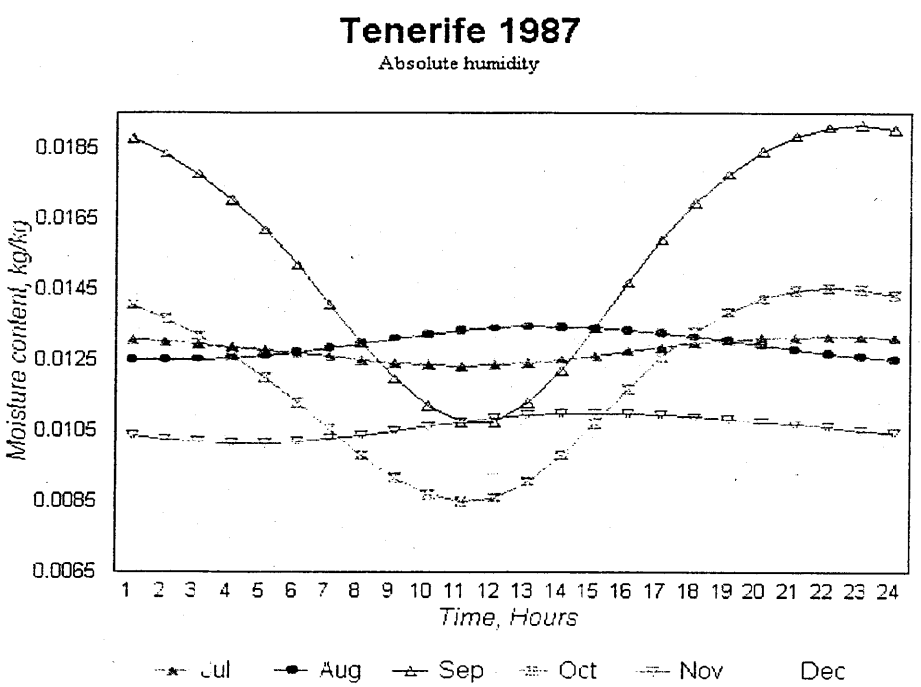

Fig. A. 8 Diurnal variation of air moisture content July-December

Appendix B

B.1 Greenhouse parameters

ó = 5.669E-8	Stefan-Boltzman constant
P = 1013	Atmospheric pressure (mbar)
CO2E = 350.	Ambient CO2 concentration (ppm)

Radiation exchange properties

ER = 0.7	Emissivity - roof
EF = 1.0	Emissivity - floor
SEFF = 0.0	Efficiency of selective absorber
ABR = 0.07	Sol abs - roof layers
ABF = 0.8	Solar absorbency - floor
ROG = 0.2	Solar reflectance - floor
ROC = 0.12	Solar reflectance - dense crop
TAUSR= 0.24	Solar transmitance- roof
TAULR= 0.0	Infrared transmitance - roof
KS = 0.48	Solar ext coef - crop
KL = 0.64	Infrared ext coef - crop
REFLR= 0.15	Reflectance of roof

Radiation shape factors

RSFRS= 0.89	Roof to sky
RSFCR= 1.0	Crop to roof
RSFFC= 1.0	Floor to crop
RSFCS= 1.0	Crop to sky
RSFFR= 1.0	Floor to roof
RSFFS= 1.0	Floor to sky

Thickness of elements (m)

SR = 0.001	Roof
SRC = 0.045	Roof cavity
SIA = 4.5	Greenhouse height
SC = 0.005	Crop
SP = 0.045	Diameter heating pipes
SF1 = 0.01	Top or 1st floor element

SF2	= 0.02	2nd floor element
SF3	= 0.04	3rd floor element
SF4	= 0.08	4th floor element
SF5	= 0.16	5th floor element
SF6	= 0.32	6th floor element
SF7	= 0.64	Lowest or 7th floor element

Geometric factors of greenhouse

AR	= 1.13	Relative roof to floor area
CDG	= 1.0	Characteristic dimension (m)
AHOUSE	= 216	Plan area of house (m2)
LHOUSE	= 12	Length of house (m)
Z	= 2	Pad height (m)

Crop factors

CROP	= 1	Crop or no crop, 0 or 1
LAI	= 2.00	Leaf area index
CDC	= 0.035	Characteristic dimension of leaves
STRMIN	= 82.0	Minimum stomatal resistance
AC	= 1.0	Relative crop to floor area
ALPHA	= 0.0101	Leaf light utilisation factor (mgCO2/J)
RD	= 0.18	Dark respiration (mgCO2 m-2 s-1)
TAUL	= 0.15	Leaf transmission coefficient

Specific heat capacity (Jkg-1K-1)

CPR	= 840.0	Roof
CPIA	= 1008.0	Air
CPF	= 840.0	Floor
CPC	= 4190.0	Crop
CPW	= 4190.0	Water

Density (kgm-3)

DR	= 2600.0	Roof
DF	= 1500.0	Floor
DC	= 998.0	Crop

Thermal conductivity (W m-1K-1)

KF	= 0.275	Floor
KR	= 1.0	Roof

System parameters

BETAH= 0.05	Air speed in house rel. to wind speed
BETAR= 0.27	Air speed in roof rel. to wind speed
EFF = 0.85	Efficiency of the condenser
VINF = 0.000	Infiltration rate (m3 m-2 s-1)
MSEA = 0.00325	Seawater flow rate in roof (kg/m2.s)
KCOND= 240	Condenser heat transfer coefficient (W/m2K)
ETA = 0.80	Efficiency of evaporative cooling pad1
ETAP = 0.80	Efficiency of evaporative cooling pad2
ACOND= 2500	Area of condenser (m2)
MWAT= 0.0117	Mass flow water in condenser(kg/m2s)
APAD2 =500	Surface area of the condenser (m2)

B.2 **Temperature Dependent Properties of Air**

(Temperature is specified in K)

Density [kg m^{-3}]

$\rho = 1/(2.8329\ 10^{-3}\ T)$

Thermal Conductivity [W m^{-1} K^{-1}]

$k = (7.8\ 10^{3})\ T+2.69\ 10^{3}$

Latent Heat of Evaporation [J kg^{-1}]

$\lambda_0 = 10^3\ (2500.77-2.36\ (T-273.15))$

Saturated Vapour Pressure [mbar]

$e_s = 10^3 \exp (65.832-8.2\log (T) + .005711\ T-7235.4/\ T)$

Rayleigh Number

$R_a = 9.89\ 10^9 \exp [-(T_1+T_2)/128.88]\ |T_2-T_1|\ L^3$

where T_1 and T_2 denote the temperature of two surfaces separated by a distance L (m).

Psychrometric Constant [mbar C^{-1}]

$\gamma = .646+.00064\ T$

Appendix C SIMULINK model

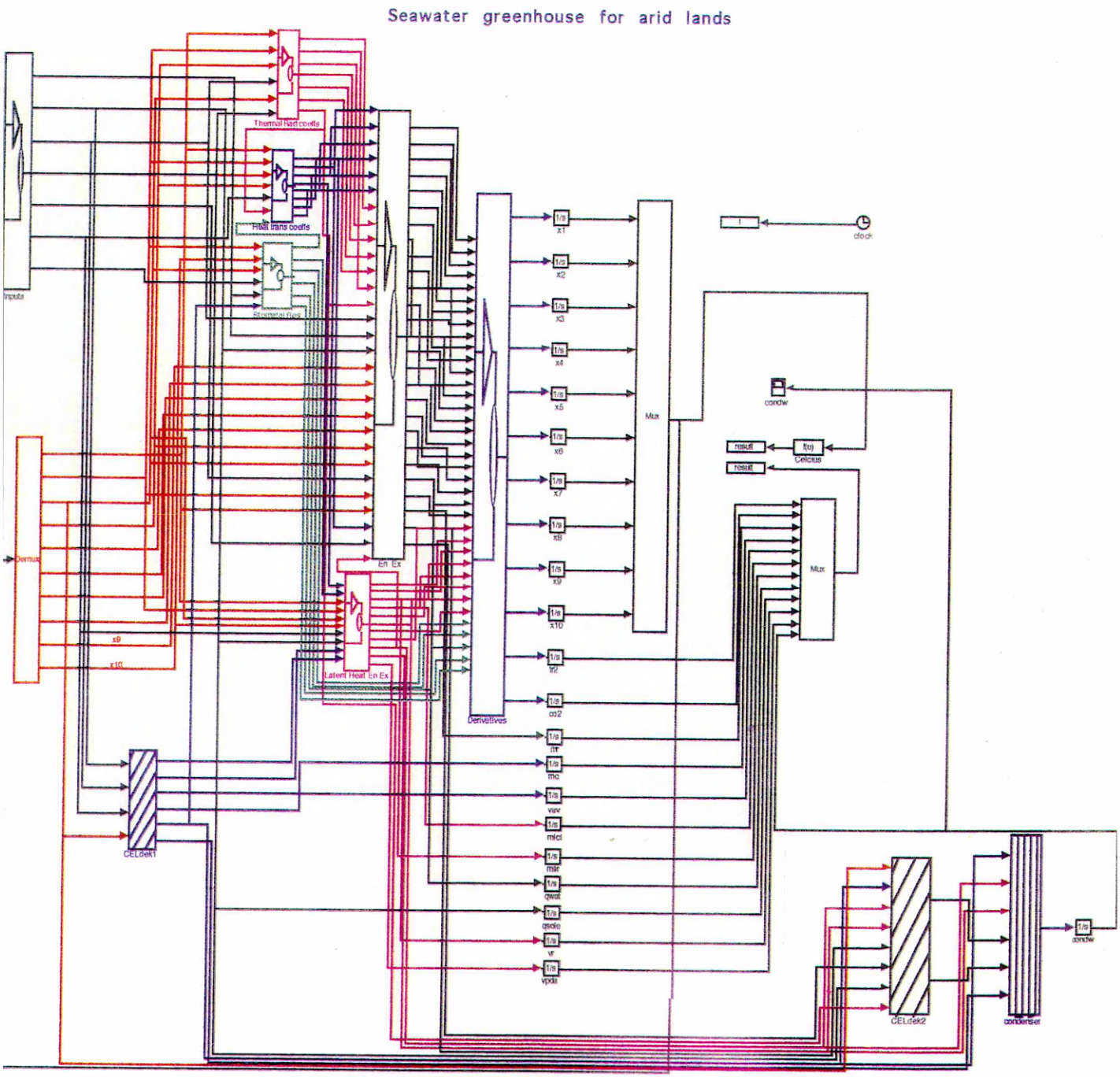

C.1 SIMULINK model diagram

Appendix D

trilite®
GRP SHEET

TRILITE G.R.P. ROOFLIGHT SHEETING AND DOUBLE SKIN FACTORY ASSEMBLED INSULATING ROOFLIGHTS

FUNCTION
Trilite translucent corrugated glass fibre reinforced polyester sheets and double skin insulating rooflights permit admission of diffused daylight into all buildings with corrugated roofing and cladding materials. Double skin Factory Assembled Insulating Rooflights permit high levels of energy conservation to be achieved, and reduce condensation.

AUTHORITY
The following documents determine how Trilite may be used:
The Building Regulations 1985, 1990
The Building Standards (Scotland) Regulations 1981, as amended 1982, 1984, 1986, 1987.
Building Regulations (Northern Ireland) 1990
The Rules of the Fire Office's Committee and the Fire Office's Committee of Ireland 1984.

IDENTIFICATION
Indelible printing near to the edge of each profiled sheet identifies the material and the fire performance.

COMPOSITION
Trilite sheets are manufactured from polyester resins containing U.V. inhibitors, fire retardants and processing additives with a glass fibre reinforcement and a protective polyester film bonded to both surfaces. Components used in assembling F.A.I.R. are not prescribed.

APPEARANCE
Translucent colourless corrugated sheeting with a high gloss surface showing the fine random texture of the reinforcing glass fibre and resin composite.

REINFORCEMENT
Standard weight Trilite contains 450g/m² glass fibre reinforcement. Selected profiles are available with 600g/m² and 900g/m² glass fibre reinforcement as specification or application conditions dictate. Rooflights with 375g/m² reinforcement can be used only under very limited conditions.

THICKNESS
Sheet of standard weight has a nominal thickness of 1mm.

DIMENSIONS
Profile dimensions correspond to those of the metal or fibrous cement profile matched. Trilite rooflight sheets to suit fibrous cement sheets are available in common stock lengths: otherwise rooflight sheets are manufactured to customer specified lengths. The maximum length of a Trilite F.A.I.R is always dependent on profile and type of F.A.I.R. being considered.

TOLERANCES
Length: sheets less than 5m: -0, +10mm
sheets over 5m: -0, +15mm
Width: ± 5mm

LIGHT TRANSMISSION
(BS4154 Appendix D)
Natural translucent Trilite.
single skin - in excess of 80%
double skin - in excess of 65%
triple skin - in excess of 53%

LIGHT DIFFUSION
(BS4154 Appendix C)
Natural translucent Trilite
• Classification II Moderately diffusing
Opal White tinted Trilite
• Classification I Very heavily diffusing

SHADING COEFFICIENTS
Natural translucent Trilite - 0.83
Opal White tinted Trilite - 0.51

TENSILE STRENGTH
91-93MN/m² BS2782 Method 320c.

FLEXURAL STRENGTH
170-180MN/m² BS2782 Method 320c.

HARDNESS (BARCOL)
40-50

BOLT SHEAR STRENGTH
In excess of the requirements of BS4154 Appendix A.

DEFLECTION UNDER LOAD
Profiles listed in BS4154 exceed the performance requirements of Appendix B.
Performance is assessed to a limiting deflection of span/70.

THERMAL CONDUCTIVITY (K)
0.15W/m°C

THERMAL TRANSMITTANCE (U)
5.7W/m² for single skin rooflights
2.8W/m² for double skin rooflights
2.0W/m² for triple skin rooflights

COEFFICIENT OF LINEAR EXPANSION
22 x 10⁻⁶/°C

EFFECTS OF HEAT
Trilite does not soften at high temperatures or become brittle at low temperatures. Trilite may be used in situations where temperatures are in the range -20°C to +80°C.
Some discolouration may occur at temperatures above 65°C but this will not significantly affect transmitted light.

WATER ABSORPTION
Less than 0.20% AV. 24 hours immersion at 23°C.

BIOLOGICAL
Resistant to micro-organisms, fungi and insects.
Cleaning with mild detergent solution will remove organic materials.

CHEMICAL RESISTANCE
Trilite is resistant to a large number of chemicals: exceptions are strong solvents, and concentrated acid and alkali solutions. For advice on specific chemicals contact the technical department.

COMPATIBILITY
Trilite may be used in conjunction with any other traditional construction material.

DURABILITY
The life span of Trilite is largely determined by the environment in which it is located. Generally a correctly fixed sheet in an area with moderate industrial pollution will have a life expectancy in excess of twenty years.

MAINTENANCE
The general condition of Trilite rooflights and the security of fixings and sealants should be checked periodically as part of the overall maintenance programme for the structure into which they are incorporated. Remove any dirt from rooflight surfaces with a mild detergent solution. Short term repairs to small holes and cracks may be effected using polyester resin and fibreglass mat, the surrounding rooflight surface having been previously thoroughly abraded and cleaned.

WIND LOADING/SPAN
Trilite rooflight sheets and double skin Factory Assembled Insulating Rooflights cannot be assumed to have in all circumstances span capabilities comparable to those of other roofing materials in conjuntion with which they are used. Refer to the technical department with details of individual rooflight profiles and intended site conditions.

FIXING
Extensive guidance is given in BS5427 1976. Minimum fixing requirements are given in the Rooflight Profiles Manuals 1 & 2. Detailed fixing information for individual situations is available from the technical department.

References

Abbott, S. and Brundett, E., 1981, 'A method for modelling light levels in greenhouses using an effective transmittance matrix', paper No 81-235, ASAE, St. Joseph, MI, PP. 21

Acme Corp., Engineering and Manufacturing Corporation, 1980, 'The Greenhouse Climate Control Book', Muskogee, OK.

Agarwal, K. and Verna, V.V., 1977, 'Thermal characteristics of glazing and shading materials', Building and environment, 12, pp. 55-62)

Akhtamov. R.A., Achilov, B.M., and Kakharov, S., 1978, 'Geliotekhnika', 14, No 2, 1978, pp. 47-48][Tinaut, D., Echaniz, G., Ramos, F.,'Materials for a solar still greenhouse', Optica Pura y Aplicada, pp. 11-59

Albright, L.D., 1991, 'Production solar greenhouses', Solar Energy in Agriculture, vol. 4, PP. 213-229, edited by Parker, B.F, Elsevier

Aldrich, R.A., Downs, R.J., Krozek, D.T. and Campbell, L.E., 1983, 'The effect of environment on plant growth', in: Ventilation in agricultural structures, Hellickson, M.A. and Walker, J.N. (Eds.), ASAE Monographs. ASAE, St Joseph, MI , pp. 217-256

Aussenac. D., Domenech, S., and Enjalbert, 1978, M., Ing. Quim., Madrid, 9. no 101

Bailey, B.J., September 1975,' Infra-red and optical properties of some plastic materials used in greenhouses', Departemental note No DN/G/616/2105, Silsoe Research Institute, Wrest Park, U.K.

Bailey, B.J., 1978, 'Application of Plastic Screens in Glasshouse Environmental Control', Conf. Advances in the Use of Plastics in Agriculture, Horticulture and Produce Distribution, British Agric. and Hort. Plastics Assn., Silsoe

Bailey, B.J., 1987, 'The evaporative and refrigerative cooling of greenhouses at Icarda', Vol 1, Contract report CR/242/87/8318a, Silsoe Research Institute, Wrest Park, Silsoe, Bedford, MK45 4HS, UK

Bailey, B.J., 1991, 'The environment in evaporatively cooled greenhouses', Acta Horticulturae, 287, pp. 111-118

Bailey, B.J., 1993, 'Seawater greenhouse project', Vol 1, Contract report CR/523/93/8269, Silsoe Research Institute, Wrest Park, Silsoe, Bedford, MK45 4HS, UK

Bailey, B.J., 1997, internal report (not published), Silsoe Research Institute, Wrest Park, Silsoe, Bedford. MK45 4HS, UK

Baille, A., Aries, F., Baille, M. And Laury, J.C., 1985, 'Influence of thermal screen properties on heat losses and microclimate of greenhouses, Acta Horticulturae, 174, pp. 111-118

Bolto, B.A., Pilkington, N.H., Weiss, D.E., Sharples, P.M., Stephens, G.K., and Wade, K.O., 1978, Progr. Water Technol., 9, pp. 911-922

Borner, H., 1965, 'Uber den warme und stoffubergang an umspulten einzelkorper bei uberlagerung von freir und erzwungener stromung', VDI (Ver. Deut. Ing.), Forschunggsh No 512

Bot, G.P.A., 1983, 'Greenhouse climate: from physical processes to a dynamic model', Ph.D. Thesis, Agricultural University, Wageningen, The Netherlands.

Boulard, T., Baille, A., Mermier, Vilette, 1991, ' Mesures et modelisation de la resistance stomatique foliaire et de la transpiration d'un couvert de tomates de serre', Agronomie (11), pp. 259-274

Bloemer, J.W. Irwin, J.R. and Eibling, J.A, 1965a, paper presented at the international solar energy society annual meeting, Phoenix, AZ

British Standard, 1965, BS1339:' Definition, formulae and constants relating to humidity of the air

Businger, J.A., 1963, 'The glasshouse (greenhouse) climate' in: Van Wijk, W.R. (Editor), Physics of plant environment, North-Holland, Amsterdam, pp. 277-318

Brown, E.M., 1939, ' Equipment for the growing of plants at controlled temperatures', Plant Ohysiol., 1939, 14, p. 517

Brownell, J.R., 1983, ' Solar greenhouse designs', Department of plant science and mechanised agriculture, California State University, Fresno

Breuer, J.J.G. and Picknies, 'Greenhouse climate control', pp. 183, Editors Bakker, J.C., Bot, G.P.A., Challa, H. And Van de Braak, Wageningen Pers.

Busch, G., Militzer, K.E., Scubert, M. and Wiss. Z., 1978, Tech. Univ. Dresden, 27, pp. 1251-1254

Bustany, S.T.. Harriot, P. and Wiegandt, H.F., 1979, AIChE J., 25, PP. 439-446

Byk, S.SH., and Fomina, V.I., Zh. Fiz. Khim., 1978, 52, pp. 1306-1308

Canham, A.E.. 1962, "Shading glasshouses with liquid films", Electrical Research Association

Carpenter. W.J., and Willis, W.W., 1957, ' Comparison of low pression mist, atomised fog, and evaporative-fan-and-pad systems for greenhouse cooling and plant response', Proc. Am. Soc. Hort. Sci. 70, 490-500

Chalabi, Z.S., and Bailey, B.J., 1989, 'Simulation of the energy balance in a greenhouse', Divisional note D.N. 1516, AFRC Silsoe Research Institute, Silsoe, U.K.

Chalabi, Z.S. and Bailey, B.J., 1991, 'Sensitivity analysis of a non-steady state model of the greenhouse microclimate', Agricultural and forest meteorology, 56,pp. 111-127

Ching. Y.Q., Bailey, B.J., Thompson, A.K. and Stenning, B.C, 'Predictions of condensation of tomatoes', Proceedings 1st IFAC/CIGR/EURAGENG/ISHS workshop on control applications in postharvest and processing technology (CAPP'95), Ostend, Belgium 1-2 June 1995. 51-56

Cohen. Y., Stanhill, G., Fuchs, M., 1983, 'An Experimental Comparison of Evaporative Cooling in a Naturally Ventilated Glasshouse due to Wetting the Outer Roof and Inner Crop Soil Surfaces', Agric. Meteorology, 28, pp. 239-251

Colburn, A.P., 1933, Trans. Am. Ins. Chem. Engrs, 29, 174

Collares-Pereira and A. Rabl, 1979, 'The average distribution of solar radiation-Correlations between daily and hourly insolation values', Solar energy, 22. pp. 155-164

Cockshull. K.E. and Hughes, A.P.,' The effects of light intensity at different stages in flower initiation and development of chrysanthemum morifolium. Annals of Botany, 35, 142, pp. 915-926

Critten, D.L.. 1983 'A computer model to calculate the daily light integral and transmissivity of a greenhouse', Journal of Agricultural Engineering Research, 28

Crool, J., February 1994, 'Design calculations for stressed skin, box girder, roofing for seawater greenhouse', Individual report. University College London

Crowe, C.S.. Zdenek, F.F. and Johnson Drillers, 1977, J. 49, No 6, pp. 6-8

Damagnez. J.. 1976, 'Need and design for a solar greenhouse', UK-ISES conference Solar Energy in Agriculture, Reading

Frangoudakis. A., Papadakis, G. and Kyritsys, S.,1988, 'Radiation exchange calculations in enclosures composed of boundary walls partly transparent at long wavelengths', Int. J. Solar Energy, 6, 221-234

Garg, S.K., Gomkale, S.D. and Datta, R.L., 1966, 'Use of solar energy for production supply and water disposal', at CPHERI, Nagpur, India, 19-20

Garrison, K. *et al.*, 1968, 'Freon-12 hydrate desalting process', Res. Develop. Progr. Rept., No 368, Office of saline water, U. S. Dept. Interior, August 1968

Garzoli, K., 1971, ' A comparison of glasshouse cooling methods', Australian Refrigeration, Air conditioning and Heating, 1971, Vol. 25,2,46-50

Garzoli, K.V. and blackwell, J., 1981, 'An analysis of the nocturnal heat loss from a single skin plastic greenhouse', Journal of Agricultural E ngineering Research, 26, pp. 203-214

Gebhart, B, 1961, Heat transfer, Mc Graw-Hill

Giacomelli, G.A., Giniger, M.S., Krass, A.E. and Mears, D.R., 1985, 'Improved Methods of Greenhouse Evaporative Cooling', Acta Horticulturae, 174

Goldseels, V.E. van der Stuyft and Avermaete, U. (eds), 1986, 'New perspectives for energy savings in agriculture, Solar Energy R&D in the European Community, Series H, 2. D. Reidel Publishing Co,

Gomkale, S.D, 1968, 'Review of of the first conference on water desalination in India', Desalination, 4(1), 131-134

Goto, S., Sato, N., Teshima, H., Sep. 1979, Sci. Technol., 14, No 3, pp. 209-217

Grass, A.J. and Hosseinzadeh-Dalir, A., 1994, 'Simple theoretical modelling and wind-tunnel testing of air flow regime through the greenhouse', University College London, Department of Civil and Environmental Engineering, progress report No 3, EEC contract No AIR-CT-920508

Gray, H.E., 1948, 'Summer Cooling of Greenhouse', New York State Flower Growers Bull., 33, 8

Grober, H. and Erk, S., 1961, 'Fundamentals of heat transfer', 3rd edition, McGraw Hill Book Co.

Hand, D.W., 1988, 'Effects of atmospheric humidity on greenhouse crops, Acta Horticulturae, 229, pp. 143-158

Helfferich, F., 1962, Ion exchange, Mc Graw-Hill, New York,

Hellenic Technologies, 1993, 'Wind-tunnel of the seawater greenhouse for arid lands', progress report No 2, EEC contract No AIR-CT-920508

Hendrickson, H.M. and Moulton, R.W. , 1956, ' Research and development of processes for desalting water by freezing, Res. Develop. Progr. Rept., No 10, Office of saline water, U. S. Dept. Interior

Hirsch, M., 1927, 'Die Trochentechnil, Springer, Berlin

Horiguchi, I., 1978, 'The variation of heating load coefficient for a greenhouse and overall heat-transfer coefficient through plastic film', J. Agric. Meteorol. Tokyo, 26, pp. 197-207

Hougen, O.A., 1934, Ind. Eng. Chem., 26, 1173

Howe, E.D., 1974, 'Fundamentals of water desalination', Marcel Dekker, inc. New York

Ichiki, T. and Asawa, T., , 1977, Asahi Garasu Kenkyu Hokuko, 27, No 2, pp. 115-121. C.A. 89, 217173

Idso, S.B. and Jackson. A.D., 1969,'Thermal radiation from the atmosphere'. J. Geophys. Rev.74: 5397-5403

Jolliet, O.J., Gay, J.B., Bourgeois, M., Danloy, L., Bretton, T., Mantilleri, S.. Reist, A. And Moncousi, C. , 1985, 'Solar gains and thermal rejects by ventilation', Acta Horticulturae, 174, pp. 127-134

Jolliet, O.J And Bailey, B.J., 1990, 'Modelling of water uptake, transpiration and humidity in greenhouses, and of their effects on crops', J. Of Agr. Eng. Research

Kanthak, P., 1970, 'Der einfluss von heizungssystemen mit unterschiedlichem strahlungsanteil auf das klima und den warmehaushalt von hallenbauten mit grossen glassflachen, speziell von gewachshausern', Fortschritt-Berichte der VDI Zeitschriften, serie 6, No. 28, VDI-Verlag GmbH, Dusseldorf

Kimball, B.A.. 1974, 'Simulation of the energy balance of a greenhouse'. Agric. Meteorol., 11, PP. 243-260

Kirsten, W.. 1973, ' Natural radiation in glasshouses as a function of their form and orientation and the nature of their covering', Dissertation accepted for degree of Doctor of engineering in the technical University of Hanover

Kleshchunov. E.I., Kleshchunov, A.I., Ermakov, V.B. and Tr. Krasnodar, 1976, Politekh. Inst., 72, pp. 17-20, -C.A. 89, 1978, 48706]
Knight K M: Klein, S A and Duffie. J A. 1991, 'A methodology for the synthesis of hourly weather data', Solar Eneray, 46(2). 109-120.

Korolev, A.K.. Kuznestov, G.A.. Boshok, N.I., Bogdanovich, V.B., Levchenko. A.A., 1978, V.I. Tyrin (Nek. Vopr. Sovrem. Elektrokhim. Kinet. [1976] 127-132, -CA 89 [1978] 48705

Kozai, T. and Kimura, M., 1977, 'Direct solar light transmission into multi-span greenhouses', Agricultural meteorology, 18

Kozai, T., Sase. S and Nara, M., 1980, 'A modelling approach to greenhouse ventilation control'. Acta Horticulturae, 106: 125-136

Leach, D. J.,1959, ' A study of greenhouse cooling', PhD Thesis, Cornel University

Leung, P.S., 1979, Sep. Sci. Technol., 14, pp. 167-174

Light Works Ltd, 1994, progress report No 2, EEC contract No AIR-CT-920508, 2a Greenwood Road, London E8 1AB, UK

Light Works Ltd, 1995, progress report No 3, EEC contract No AIR-CT-920508, 2a Greenwood Road, London E8 1AB, UK

Lof, G.O.G., 1980, final on consultant contract of Feb. 1, 1961. Including progress report for Jan-March 1962. Unpublished report to office of saline water. Washington. DC., Solar distillation. In: K.S. Spiegler and A.D.K. Laird (Editors), principles of desalination, part B (2 nd edition). Academic Press, New York, pp. 679-723, 1980)

London, A.L., and Kays, W.M., 1958, 'Compact heat exchanger', Mc Graw-Hill. 12-15

Luft, W. and Froechtenigt, J., 1981, 'Solar energy controlled-environment agriculture in the USA and Saudia Arabia', SERI/TP-270-1465, 1981]

Levchenko, A.A. and Tyrin, V.I., 1976, Net. Vopr. Sovres. Elektrokhim. Kinet. 1, pp. 127-132,-C.A., 89, 1978, 48705

Mac Neil, M. M., 1962, 'An experimental glasshouse with some control of the environment', J. Agric. Engng. Res. 7, 1962, 221-3

Malik, M.A.S., Tiwari, G.N., Kumar, A. and Sodha, M.S. 1982, 'Solar distillation', Pergamon Press, Oxford

Marshall, L.C., Eversole, H.O., Hess, A.J. and Went, F.W., 1948, 'The technical features of greenhouse air conditioning', Refrig. Engng., 55, p. 151: p. 269

McAdams, W.H., 1954, 'Heat transmission', 3rd edition, McGraw-Hill, New York,

McCree, K. J., 1971, 'The action spectrum, absorptance and quantum yield of photosynthesis in crop plants', 1971, Agric. Meteorol., 9:191-216

Merkel, F., 1925, 'Verdunstungskuhlung', VDI Forschunsheft, 275, Berlin

Monteith, J.L., 1973, 'Principles of Environmental Physics', Edward Arnold Ltd., London.

Montero, J.I, Short, T.H., Curry, R.B., and Bauerle, W.L., 1981, ' Influence of evaporative cooling systems on greenhouse environment', Am. Soc. Agric. Engng., paper no. 81-4027

Morris, L.G., Vanstone, F.H., and Wells, D.A., 1958, 'The Limitation of Maximum Temperature in a Glasshouse by the Use of a Water Film on the Roof', J. Agric. Engng Res., 3, pp. 121-130

Morris, L.G., 1970, 'Plant environment and environmental control in protected cultivation', Proc. 18th Int. Hort. Congr., Tel Aviv, 1970, (5), 41-47

Morris, L.G. and Winspear, K.W., 1971,'The control of temperature and humidity in glasshouse by heating and ventilation', Inst. Agr. Eng. Symposium on Agricultural Engineering, Silsoe

Moustafa, S.M.A. and Brusewitz, G.H., 1979, 'Solar Energy', pp. 141-148

NAG library. 1996, NAG Fortran library manual, NAG Ltd, Wilkinson house, Jordan Hill road, Oxford, OX2 8DR, UK

Nisen, A., Mai 1979, 'Transparence aux rayonnements des materiaux de couverture des serres et abris consequences horticoles', P.H.M. revue horticole, 197

Norov, E.Z.H. Achilov, B.M. and Odinaev, A., 1978,'Geliotekhnika', 14, No 1, PP. 61-62

ODA report. 1996, 'Water resource management and desalination options for small communities in arid and semi-arid coastal regions (Gaza)', RYEA\18655007\Fina\Issue01

Okada. M.. 1980, 'The heating load of greenhouse, convective heat transfer coefficients at the inside cover surface of a greenhouse as influenced by heating pipe positions', Journal of Agricultural Meteorology. 35, pp. 235-242

Parker. B.F.. 1991, 'Solar Energy in Agriculture', Vol. 4, Elsevier

Parker. R.O. and Treybal, R.E., 1960, 'The heat and mass transfer characteristics of evaporative coolers', Chem. Eng. Prog. Symp. Ser, 57(32). 138

Parkhurst. D.F. Duncan, P.R., Gates, D.M. and Kreith, F., 1968, 'Wind-tunnel modelling of convection of heat between air and broad leaves of plants. Agricultural Meteorology, 5:33-47

Parton, W. J. and J. A. Logan, 1981, 'A model for diurnal variation in soil and air temperature', Agricultural Meteorology, 23, pp. 205-216

Paton, A.C. and Davies, P, 1996, 'The seawater greenhouse for arid lands', Mediterranean Conference on Renewable Energy Sources for Water Production, Santorini, Greece, 10-12 June 1996

Pozin. G.M.. 1971, 'Solution of the system of heat balance equations for hothouses in unsteady regime', Appl. Solar Energy, 7 (2), pp. 52-61

Rosenberg. N.J., B.L. Blad and S.B. Verma., 1983, 'Microclimate - The biological environment', Second edition, John Willy and Sons Inc, New York. NY.455 pp

Rosa, R.. 1988, 'Solar and thermal radiation inside a multi-span greenhouse'. J. Agric. Engng. Res., 40, 285-295

Seginer, I. and Leav, N., 1971], 'Models as tools in greenhouse climate design'. Technion research No. 150-085, Israel ministry of agriculture

Selcuk. M.K.. 1970, 'Use of digital computers for the heat and mass transfer analysis of controlled environment greenhouse', Env. Res. Lab., University of Arizona

Selcuk, M.K., 1971, 'Analysis, design and performance evaluation of controlled environment greenhouses', Trans ASHRAE, 8, PP.21-72

Serodio, R., 1977, 'An energy balance study of glasshouse cooling with special reference to physical modelling', PhD thesis, University of Reading

Short, T.H. and Breuer, J.J.G., 'Greenhouseenergy demand comparisons for the Netherlands and Ohio, USA', 1985, Acta Horticulturae, 174, PP. 145-153

Silverstein, S. D. 1980, 'All Season Thermal Control Greenhouse Glasses with Selective Transmission of Photosynthesis Active Radiation', Solar Energy Materials, 4, pp. 47-65

Sodha, M.S.. Nayak, J.K., Tiwari, G.N. and Kumar, A., 1980b, 'Double-basin solar still', Energy conversion and management, 1980b, 20:23

Skvortsov, N.G., Kolosova, G.M., 1978, Zh. Fiz. Khim,, 52, pp. 1763-1765, C.A. 89. 1978, 185741]

Spatz, D.D. and Friedlander, R.H., 1978, 'Water Sewage Works', 125, No 2, pp. 36-40

Spiegler, K.S.. and Laird, A.D.K. , 1980, 'Principles of desalination', Part A and B, Second Edition, Academic Press, New York

stanghellini, C, 1987, 'Transpiration of greenhouse crops, an aid to climate management', Ph.D. dissertation, Agricultural University, Wageningen, the Netherlands

Stanghellini, C. and Van Meurs, W.TH.M., 1992, 'Environmental control greenhouse crop transpiration', Journal of Agricultural Engineering Research, 51, pp. 297-311

Stubstad, J. Quinn, W.F. and Yen, Y.C., 1978, AIChE Prepr., 17 th Nat. Heat Transfer Conf., pp. 188-198, C.A. 88, 9008

Tabor, H.Z., 1978, 'Impact of Sci. In Soc.', 28, pp. 339-348

Takakura, T., 1967, 'Predicting air temperatures in the greenhouse (1)', J. Met. Soc. Japan, 45 (1), pp. 40-52

Takakura, T., Jordan, K.A. and Boyd, L.L., , 1969, 'Dynamic simulation of plant growth and environment in the greenhouse', Winter Mt. Am. Soc. Agric. Eng., Chicago, IL, pap. No. 69-942, pp. 57

Takakura, T., 1974, 'Artificial climate' in: Mihara, Y. (Editor), Agricultural Meteorology of Japan. University of Tokyo Press, pp. 126-153

Tantau, H. J., and von Zabeltitz, Chr., 1974, 'Greenhouse heat requirement depending on different heating systems, Proceedings XIX

International Horticultural Congress, International Society for Horticultural Science, Warsaw

Tezuka S., 1972 'Performance of aqueous-film-type packing of cooling tower', Trans. JSME, 38, 2648-2655

Tinaut, D., Echaniz, G. and Ramos, F., 1978, 'Materials for a solar still greenhouse', Optica pura y aplicada, 11:59

Treybal, R.E., 1981, Mass-Transfer operations, third edition, McGraw-Hill

Trickett, E.S. And Goulden, J.D.S., 1958, 'The radiation transmission and heat conserving properties of glass and some plastic films', J. Agric. Engng. Res., 3 (4), 1958, pp. 281]

Unsworth, M.M. and Monteith, J.L., 1975, " Longwave Radiation at the Ground - Angular Distribution of Incoming Reflection ", Q.JI.R. Met. Soc., 101, pp. 1-13

Van Bavel, C.H.M., Damagnez, J. and Sadler, E. J., 1981, ' The fluid-roof greenhouse energy budget analysis by simulation', Agricultural Meteorology, 23:61-76

Van Bavel, C.H.M. and Damagnez, J., 1978, 'A simulation model for energy storage and savings of a fluid-roof solar greenhouse', Acta Hort. 76

Veenman, A.W., 1978, Desalination 27, 21-39

Verhaegh, A.P., 1980, 'The influence of insulation techniques on crop production and profitability in the Dutch glasshouse industry', Acta Hort., 115, pp. 453-466

Walker, J.N., 1965, 'Predicting temperatures in ventilated greenhouses', Trans. Am. Soc. Agric. Eng., 8, pp. 445-448

Wang, X.A., 1982, 'An experimental study of mixed forced and free convection heat transfer from a horizontal flat plate to air', J. Heat Transfer, 104. 139-144

Wann, M., Yen, D. and Gold, H.J., 1985, " Evaluation and Calibration of three Models for Daily Cycle of Temperature ", Agr. Forest Met.,34, pp. 121-128

Went, F.W., 1957, 'The experimental control of plant growth', Vol. 17, Chronica Botanica Company, Waltham. Mas. U.S.A.

Williams, V.C. *et al.*, 1968, 'Development of propane hydrate desalting process', Res. Develop. Progr. Rept., No 373, Office of saline water, U. S. Dept. Interior, August 1968)

Winter, E.J.. 1955, 'A forced ventilation system for cooling small glasshouse compartments', Ammu. Rep. Nat. Veg. Res. Sta., Wellesbourne. p. 43

Wood, R.W.. 1909, 'Note on the theory of the greenhouse', Phil. Mag., p. 319

Younis, M.A. Darwish, M.A. and Juwayhel, F., 1993, 'Experimental and theoretical study of a humidification-dehumidification desalting system', Desalination. 94(1993), 11-24

Zubets, N.N.. Bedyukh, G.A., Anishchenko, I.A., Cherevkov, V.V., Kuznestov, Levchenko, A.A., and Kozolev, A.K., 1978, Net. Vopr. Sovres. Elektrokhim. Kinet. 1, 1976. pp. 116-120,-C.A., 89, 48703

Zubets, N.N.. Lavrova, Z.D., Vorontsov, E.S., Shatalov, G.A., Kuznestov, N.A., Boshok, N.A., and Kozolev, A.K., 1978, Nek. Vopr. Sovres. Elektrokhim. Kinet. 1, 1976. pp. 120-126,-C.A., 89, 48704